Design and Advanced Manufacturing of Aircraft Structures using Friction Stir Welding

Sérgio M. O. Tavares
July 2011

A dissertation submitted to the Faculty of Engineering of the University of Porto
for the degree of Doctor of Philosophy in Leaders for Technical Industries
of the MIT-Portugal Program

Supervisor

Paulo M.S.T. de Castro
Faculdade de Engenharia da Universidade do Porto, Portugal

Co-Supervisors

Thomas W. Eagar
Massachusetts Institute of Technology, USA

Marco Pacchione
Airbus Operations GmbH, Germany

Jorge F. dos Santos
Helmholtz-Zentrum Geesthacht Centre for Materials and Coastal Research, Germany

Pedro Vilaça
Instituto Superior Técnico, Universidade Técnica de Lisboa, Portugal

Abstract

Aeronautical transportation, as all other transportation sectors, is facing new challenges, aiming at lower environmental impact, more technological innovation and greater economical efficiency. The demand for the reduction of pollutant emissions and operational costs, and at the same time, for increasing aircraft dispatch reliability and comfort of the passengers, puts more pressure on the development of new design solutions and concepts for air transportation systems.

More efficient and environmentally friendly transportation systems require increasingly lighter structures. New materials and new production processes are constantly emerging or are in continuous development in order to improve their efficiency in different ways as reducing their environmental impact or reducing the life-cycle costs through, for instance, structural weight reduction or reducing manufacturing costs. However, this implementation poses tough challenges due to the complex and multi-disciplinary approach required for the assessment and evaluation of its impact in the design, development, manufacturing, operation and maintenance, and disposal of those structures.

The case study chosen to be examined in this research is an emerging joining process for metallic structures, friction stir welding, object of large interest by aeronautical companies of commercial aircraft and aerospace. The development of new design concepts and the understanding of the effects of replacing previous joining processes, taking into account distinct technological and economical aspects during the product and process development, creates opportunities for a better acceptance of this technology. This research aims to contribute to an analysis of the process of infusion of new technologies for manufacturing of aeronautical structures.

Aeronautical structures continue to use extensively riveting as the joining processes for their structural parts. However, from an efficiency and Lean point of view, these joints can be much more simple and lighter.

For instance, if the joints are simply butt joined it is possible to eliminate thousands of fasteners, overlap areas and sealants which are applied in most of aircraft joints. The replacement of these riveted joints by other advanced manufacturing technologies, as friction stir welding, can bring weight and cost savings with a simplified design of the airframe, leading to Leaner manufacturing processes.

The application of friction stir welding as a joining process for aircraft structures is analyzed in a multi-perspective framework taking into account the requirements and drivers in new product development in aeronautics. Several new concepts were developed to help the infusion of this process and to create value to the final product, components and parts.

The analyzed process is confined to metallic joints, which compete with composites materials; therefore its application in future generations of aircraft structures depends upon the trends that will prevail. Nevertheless, this process creates an opportunity to make more efficient joints and the obtained results can be extrapolated for many other applications. The approach adopted can be extrapolated and extended for other manufacturing processes in aeronautical engineering, improving the adoption of new manufacturing processes.

Resumo

Os atuais desafios sociais têm exigido aos construtores de sistemas de transporte um menor impacto ambiental, mais inovação tecnológica e produtos economicamente mais eficientes. No setor aeronáutico este fenómeno tem-se traduzido na necessidade de redução de emissões e de custos operacionais e ao mesmo tempo no aumento da fiabilidade através do desenvolvimento de novas soluções tecnológicas.

A utilização de estruturas mais leves e mais eficientes faz parte destas novas soluções que o setor aeronáutico tem adotado, através do uso de novos materiais e conceitos reduzindo o peso específico da estrutura. Esta redução terá impacto na vida completa da aeronave uma vez que reduz os custos operacionais e as emissões de gases estufa. No entanto, a adoção de novas soluções neste setor é complexa requerendo uma abordagem multidisciplinares para uma correta avaliação do impacto na conceção, desenvolvimento, fabrico, operação, manutenção e fim de vida destas estruturas.

O caso de estudo analisado ao longo desta tese é um processo emergente para ligações estruturais, soldadura por fricção linear, que tem sido objecto de grande interesse por diferentes empresas aeronáuticas e aeroespaciais por possibilitar a otimização das ligações estruturais. O desenvolvimento de novos conceitos estruturais com esta tecnologia requer a análise de todos os aspetos associados à substituição do processo anterior, tendo em conta aspetos tecnológicos e económicos de forma a reduzir o risco de implementação e proporcionar uma melhor aceitação do novo processo. Esta tese visa contribuir para uma análise mais alargada da aplicação deste processo no fabrico de estruturas aeronáuticas.

A rebitagem ainda é o processo de excelência para unir as partes estruturais em aeronaves; no entanto, em termos de eficiência, estas ligações podem ser mais simples e mais leves com a aplicação de novos processos de ligação. Estas estruturas usam milhões de rebites e juntas sobrepostas que não adicionam valor, e que, substituídas por ligações

topo a topo levam a uma grande simplificação das ligações e reduções de peso. O processo de soldadura por fricção linear é uma alternativa para a substituição da rebitagem nestas estruturas, produzindo ligações mais simples e eficientes.

A aplicação da soldadura por fricção linear como processo de ligação de estruturas aeronáuticas é analisada ao longo desta tese numa perspetiva multidisciplinar, tendo em conta os diferentes requisitos atuais para o desenvolvimento de novos produtos em aeronáutica. Alguns novos conceitos serão desenvolvidos e analisados ao longo desta tese de forma a suportar a incorporação deste processo em futuros projetos de novas estruturas, adicionando assim valor acrescentado ao produto final.

Apesar de este processo estar confinado a estruturas metálicas, que atualmente competem com estruturas em materiais compósitos, a sua aplicação irá depender nas tendências de seleção de materiais. No entanto, este processo tem múltiplas vantagens, podendo ser aplicado em outras estruturas que não as aeronáuticas A abordagem adotada ao longo deste estudo poderá ser extrapolada ou complementada para outros processos de fabrico na indústria aeronáutica, melhorando e reduzindo o risco da sua adoção.

Kurzfassung

Der Lufttransport, so wie auch alle anderen Transportsektoren, steht neuen Herausforderungen gegenüber, die auf eine geringere Umweltbelastung, mehr technische Innovation und größere ökonomische Effizienz zielen. Das Verlangen, Verschmutzung und laufende Kosten zu reduzieren, und zur selben Zeit, die Zuverlässigkeit und Pünktlichkeit des Flugzeuges und den Komfort der Reisenden zu verbessern, erhöht den Druck neue Designlösungen und Konzepte für Lufttransportsysteme zu entwickeln.

Effizientere und umweltfreundlichere Transportsysteme benötigen verstärkt leichtere Strukturen. Neue Materialien und Fertigungsverfahren erscheinen ständig oder werden kontinuierlich weiterentwickelt um ihre Effizienz auf andere Weise zu steigern, wie durch die Reduzierung des Umwelteinflusses oder eine Reduzierung der Kosten innerhalb ihres Lebenszyklus, zum Beispiel durch Gewichtsreduzierung der Struktur oder durch Reduzierung der Produktionskosten. Diese Implementierung führt zu großen Herausforderungen bedingt durch ihre Komplexität und wegen des benötigten Multi-disziplinären Ansatzes um ihren Einfluss auf Design, Entwicklung, Fabrikation, Betrieb, Wartung und Entsorgung auswerten und beurteilen zu können.

Das für diese Forschung ausgewählte Anwendungsbeispiel ist eine noch junge Fügetechnologie für metallische Strukturen, Reibrührschweißen, welche sich hohen Interesses bei den Kommerziellen Luft- und Raumfahrt Unternehmen erfreut. Die Entwicklung neuer Designkonzepte und das Verständnis des Effektes der Ersetzung bestehender Fügeverfahren, wenn man technologische Eigenheiten und ökonomische Aspekte während der Produkt- und Prozessentwicklung mit einbezieht, kreiert Möglichkeiten für eine höhere Akzeptanz dieser Technologie. Diese Forschungsarbeit Zielt auf einen Beitrag zur Einführung des Einführungsprozesses der Produktion neuer Technologien für Luftfahrtstrukturen an.

Luftfahrtstrukturen setzen nach wie vor verstärkt Nietverfahren als Fügetechnologie für strukturelle Bauteile ein. Diese Verbindungen können

jedoch vom Blickpunkt der Effizienz und Schlankheit stark vereinfacht und leichter gemacht werden. Zum Beispiel können durch eine Stumpfstoßverbindung tausende Nieten, überlappende Regionen und Dichtmittel, welche in den meisten Strukturverbindungen in der Luftfahrtbranche vorhanden sind, eingespart werden. Das Ersetzen dieser Nietverbindungen mit anderen Produktionstechnologien, so wie Reibrührschweißen, kann zu Kosten- und Gewichtseinsparungen führen, mit einem vereinfachten Design der Flugzeugzelle, was wiederum zu einem schlanken Produktionsprozess führt.

Die Anwendung von Reibrührschweißen als Fügetechnologie in Luftfahrtstrukturen wird aus mehreren Blickwinkeln betrachtet, und bezieht Notwendigkeiten und Treiber mit ein. Mehrere neue Konzepte für die Einführung dieses Verfahrens wurden entwickelt um Mehrwert beim Endprodukt, bei den Komponenten und bei den Bauteile zu erschaffen.

Der analysierte Prozess beschränkt sich auf metallische Fügeverbindungen, welche mit Verbundwerkstoffen konkurrieren; deshalb hängt ihre Anwendung in den Flugzeugstrukturen der nächsten Generation auch von den Trends die sich durchsetzen werden ab. Das hier gezeigte Verfahren kreiert jedoch Möglichkeiten um effizientere Verbindungen zu schaffen, und die Ergebnisse können auf viele andere Anwendungen extrapoliert werden. Das angewandte Verfahren kann auch auf andere Produktionsprozesse im Luftfahrt-Ingenieurwesen erweitert werden, und somit die Adoption neuer Produktionstechniken verbessern.

Acknowledgements

During the years of this project a large cooperative effort took place in several locations, giving me the privilege to interact, to work and to learn with highly talented and dedicated people, with whom I accumulated invaluable knowledge and experience in a huge diversity of subjects and making possible the writing of this thesis.

First and foremost, I gratefully acknowledge my supervisor, Prof. Paulo T. de Castro from Faculty of Engineering of the University of Porto, Portugal, for his continuous supervision and support. I really appreciated his accessibility and contributions to make this research experience stimulating and motivating.

During the time that I spent at my home University, Faculty of Engineering of the University of Porto I want to sincerely acknowledge my colleagues Valentin Richter-Trummer and Pedro Moreira, with whom I had insightful discussions and engaging research work. The support of Prof. Pedro Camanho in the material selection review is also acknowledged. The conversations with many other colleagues at the working open space are also recognized, including Daniel Peixoto, Roberto Miranda, Albertina Medeiros, Dimitra Ramantani, Stanislav Stoykov, Raul Campilho, Filipe Chaves, Carlos Sousa and many other graduate students at FEUP. The support of Prof. Miguel Figueiredo, Rui Silva, José Almeida, Albino Dias and Pedro Alves in the experimental work is also acknowledged.

The discussion about the process analyzed along this research was improved with the multiple conversations with Prof. Pedro Vilaça from *Instituto Superior Técnico* (IST) of Technical University of Lisbon, Portugal. Thank you for all support, discussions, advices and lessons during these years. The availability to use the experimental welding equipment at IST was fundamental to broaden this research and to acquire valuable knowledge about the process depicted along this work. I would also like to express my gratitude to Telmo dos Santos for the conversations at IST and at GKSS about multiple topics related to the studied process and about non-destructive techniques and for providing specimens that were tested along this research. I would like to thank Bruno Emílio for the laboratorial support at IST in the production of multiple specimens.

A research period which took place at Massachusetts Institute of Technology (MIT), USA, gave the opportunity to interact with brilliant individuals and research groups. I'm greatly indebted to Prof. Thomas Eagar to accept me in the Welding and Joining Lab

and for his valuable, constructive and inclusive comments about this research. I would like to thank Brian Hohmann for the time spent in multiple discussions and experiments allowing a more comprehensive investigation, with interaction between different institutions to perform experimental trials including JENTEK, Sonoscan and Center for Nanoscale Systems at Harvard University. I would like also to thank the laboratory colleagues Yu Watanabe and Daniel Pressl among other members of the laboratory, including Jeri Hill. The contribution of Prof. Joel Clark in the cost analysis is also gratefully acknowledged. During this time, I also thank the MIT-Portugal staff at MIT for their support: Prof. Robin Lemp, Prof. Jeremy Gregory and Gerri Powers and all other students of MIT-Portugal at MIT during this period.

I would like to acknowledge Dr. Jorge dos Santos, head of the Solid State Joining Processes Department in the Helmholtz-Zentrum Geesthacht Centre for Materials and Coastal Research in Geesthacht, Germany, for the opportunity to participate in one of the most advanced research groups in friction stir welding. Throughout that time, I had the opportunity to learn and discuss many issues about this technology and to interact with remarkable persons, some of them: Arne Roos, Rudolf Zettler, Luciano Bergmann, Cesar Olea, Marco Tier, Matthias Beyer, Ivan Moroz, Marcelo Borges, Sérgio Amâncio, Morelia Renteria, Volker Leiser, Marcelo Beltrão, Robson Brzostek, Tonilson Rosendo, Cintia Mazzaferro and Jose Mazzaferro, André Abibe, Pedro Oliveira, among others.

The opportunity to carry out an internship in the civil aircraft manufacturing leader, Airbus, contributed also remarkably to this work and for my experience, allowing to bridge the investigated topics and their applications in real structures. I want to sincerely acknowledge Marco Pacchione and Hartmut Ostersehlte for their supervision at Airbus and for their support, dialogues and lessons during this time. I would like to thank all people from Engineering Design Metal Technology Germany at Airbus, including Andre Walter, Matthias Knuewer, Freerk Syassen, Gerhard Tempus, Solvejg Jansen, Jens Hackius, Jordan Nicole, Jens Gebur, Christian Engel, Kai Thormann, Guenther Volkmann, Karl-Heinz Ruediger, Knut Juhl, Nicole Preuschoff, Maurits Ijpma, Helge Decho, Metin Cengiz, Sparenborg Keno and Daro Krummrich among others.

The participation of industrial companies, OGMA, TAP Maintenance and Engineering and Embraer is also acknowledged. Their participation since the beginning of this project allowed me to align the research directions towards more practicable approaches and a better understanding of the limitations in the application of new manufacturing processes. At OGMA, I would like to acknowledge Prof. Mário Almeida Santos, Pedro Rodrigues, Deodato Cardoso and José Ribeiro. At TAP-ME, I would like to acknowledge Nuno Soares, João Silva Carvalho and Pedro Ornelas, and from Embraer, the interactions with João Taborda and the technical interest demonstrated by Hugo Resende, Paulo Cesar Giarola, Lucio Fortes and Fernando Ferreira Fernandez are also acknowledged.

The emergence of this project and this Ph.D. was possible due to the MIT-Portugal Program. I would like to thank Prof. Manuel Heitor, Prof. Paulo Ferrão, Prof. António Torres Marques, Prof. António Cunha, Prof. Manuel Freitas, as well as Prof. Francisco Pires, Prof. Mihail Fontul, Prof. Ricardo Simões and Prof. Luís Rocha, among others, for the functioning of the program. I also gratefully acknowledge the funding source that made my Ph.D. work possible, *Fundação para a Ciência e a Tecnologia* of the Portuguese Government, through PhD scholarship SFRH/BD/35143/2007. Parts of my doctoral research were developed in the context of the European Union projects: DaToN - "Innovative Fatigue and Damage Tolerance Methods for the Application of New Structural Concepts" (n. 516053) and COINS - "Cost Effective Integral Metallic Structure" (n. 30825), both of the 6th EU Framework Programme for Research and Technological Development (FP6), priority thematic area Aeronautics and Space. The participation in the first project was through the partner IDMEC-FEUP, whereas in the second was through the partner GKSS.

Finally, I would like to express my gratitude to my family, friends and a special mention to Angela for their encouragement, support and patience and for helping me going through all these years.

Contents

List of Figures

List of Tables

List of Acronyms

AD²	Advancement Degree of Difficulty
AMI	Acoustic Micro Imaging
BM	Base Material
CAEP	Committee on Aviation Environmental Protection
CE	Concurrent Engineering
CFRP	Carbon Fiber Reinforced Polymer
CS	Certification Specifications
DaToN	Innovative Fatigue and Damage Tolerance Methods for the Application of New Structural Concepts
DFA	Design for Assembly
DFM	Design for Manufacturing
DFMA	Design For Manufacture and Assembly
DFX	Design for X
DOC	Direct Operating Cost
DoD	The United States Department of Defense
DOE	Design of Experiments
DSM	Design Structure Matrix
EASA	European Aviation Safety Agency
EBW	Electron Beam Welding
ESA	European Space Agency
FAA	Federal Aviation Administration
FAR	Federal Aviation Regulation

FCG Fatigue Crack Growth

FEM Finite Element Model

FMEA Failure Mode and Effects Analysis

FSW Friction Stir Welding

HSM High Speed Machining

IACS International Annealed Copper Standard

ICAO International Civil Aviation Organization

IPPD Integrated Product and Process Design

IVHM Integrated Vehicle Health Management Systems

JAA Joint Aviation Authorities

JAR Joint Aviation Requirement

LBW Laser Beam Welding

LCC Life Cycle Costs

LEFM Linear Elastic Fracture Mechanics

MEW Manufacturer's Empty Weight

MWM Meandering Winding Magnetometer

NASA National Aeronautics and Space Administration, U.S.A.

NDT Non-Destructive Technique

NPD New Product Development

PWHT Post Welding Heat Treatment

QFD Quality Function Deployment

SIF Stress Intensity Factor

SHM Structural Health Monitoring

SZ Stirred Zone

TIES Technology Identification Evaluation and Selection

TMAZ Thermo-mechanically Affected Zone

TRIZ Theory of Inventive Problems Solving

TRL Technology Readiness Level

TWB Tailor Welded Blanks

TWI The Welding Institute

USAF United States Air Force

VCCT Virtual Crack Closure Technique

XMT X-ray Computed Microtomography

List of Symbols

$\mathbf{A}$	Crack or damage area
$\mathbf{a}$	Half crack length
$\mathbf{c}$	Sound speed constant
$\mathbf{C}$	Cost
$\mathbf{E}$	Modulus of elasticity (Young's modulus)
$\boldsymbol{E_p}$	Photon energy
$\mathbf{f}$	Frequency
$\mathbf{G}$	Energy release rate
$\boldsymbol{G_I}$	Energy release rate, mode I
$\boldsymbol{G_{Ic}}$	Energy interlaminar fracture toughness, mode I
$\mathbf{h}$	Plank's constant
$\mathbf{K}$	Stress intensity factor
$\boldsymbol{K_{max}}$	Maximum stress intensity factor
$\boldsymbol{K_{min}}$	Minimum stress intensity factor
$\boldsymbol{K_{res}}$	Residual stress intensity factor
$\boldsymbol{K_c}$	Fracture toughness
$\boldsymbol{K_{Ic}}$	Plane strain fracture toughness
$\boldsymbol{K_t}$	Stress concentration factor
$\mathbf{N}$	Number of cycles
$\mathbf{P}$	Applied load
$\mathbf{R}$	Stress ratio ($\sigma_{min}/\sigma_{max}$)
$\boldsymbol{R_{eff}}$	Effective stress ratio
$\mathbf{U}$	Strain energy release rate
$\mathbf{W}$	Weight

$\boldsymbol{\delta}$	Eddy current penetration depth
$\boldsymbol{\lambda}$	Wavelength
$\boldsymbol{\mu}$	Material magnetic permeability
$\boldsymbol{\rho}$	Density
$\boldsymbol{\sigma}$	Nominal stress
$\boldsymbol{\sigma_c}$	Material electrical conductivity
$\boldsymbol{\sigma_{max}}$	Maximum stress
$\boldsymbol{\sigma_{min}}$	Minimum stress
$\boldsymbol{\sigma_{UTS}}$	Ultimate tensile strength
$\boldsymbol{\sigma_{YTS}}$	Yield tensile strength

Chapter 1

Introduction

The design of new civil aeronautical systems meeting the latest requirements and goals of the different stakeholders requires large advances in the different subsystems. New propulsion fuels and systems, new structural concepts and new materials are examples of different subsystems that will be developed during the next years in order to achieve a more efficient air transportation, with lower ecological footprint. The theme of this dissertation is just a tiny part of the air transportation system, although it may have an impact in achieving these goals.

1.1 Motivation

Successful new aircraft for civil aviation require higher or, at least, equivalent reliability than the previous products, while at the same time they should be more efficient and less expensive. Aircraft are sometimes exposed to a longer than forty years' service life, their efficiency becoming a crucial factor for the competitiveness of the aeronautical companies. Efficiency is correlated with the operational costs, where the major variable is fuel consumption; therefore all weight reductions are in order to reduce this variable. The structural weight is a considerable part of the total aircraft weight and each kilogram saved in the structure corresponds to a large cost saving at the end of the product life cycle. The structural weight is reduced by applying new materials with better properties or by introducing new structural concepts.

The topic of this thesis is linked to the application of a new advanced manufacturing process that originates new design concepts and can optimize the way joints between structural parts are done. Large weight savings can be achieved with the application of the process studied along this research. Moreover, simplifications in the manufacturing and assembly processes during the joining of the different aircraft structural parts can also be achieved. Furthermore, these are inherent advantages that had been identified and are

commonly associated to the application of the integral joining processes in aeronautical structures.

The replacement of riveted structural connections by welded joints is not consensual and obvious due to the complexity of the industrialization of welding processes for aluminium alloys avoiding potential defects, and due to structural issues that can compromise structural integrity.

This thesis was motivated by the advances achieved in new structural joining processes to replace riveting in civil aircraft, with focus in friction stir welding since this is the most promising welding process for light metals that can fulfill all requirements of safety critical structures.

Different topics about the infusion of this process were chosen for the present research taking into account the critical aspects that can compromise or restrict its application in primary structures. Many research efforts concerning the application of friction stir welding in aeronautical structures were already performed. Nevertheless, a number of important aspects regarding the impact of the technology replacement were not yet exhaustively treated, originating an extra motivation for this work.

The knowledge accumulated in the early phases of new product development (concept development and detailed design) paves the way to efficiently improve complex products, since higher costs are incurred to perform changes or to rectify details that were not completed understood and developed. Figure 1.1 illustrates the importance of the developments in the early stages in order to avoid unexpected problems that could compromise the new engineering system or product success.

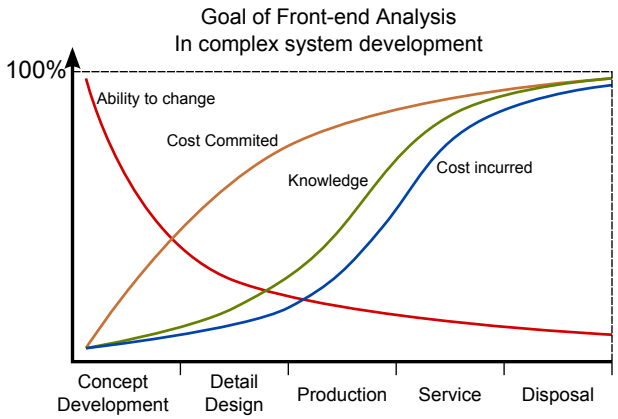

Figure 1.1: Importance of the right decision at the early stage of the product life cycle.

1.2 Problem Statement and Research Questions

The adoption of a new manufacturing process in aeronautics faces many challenges, as in the case dealt with in the present thesis, affecting the primary structures' design, with many repercussions that require a nearly full product development, or at least, re-engineering of the different parts. As aircraft have become increasingly complex the evaluation of all advantages and disadvantages should be scrutinized in detail in order to avoid not well-grounded or uncompleted conclusions.

The research done along this project has been driven by a major research question that condenses the topics investigated:

- Is friction stir welding of structural joints a potential alternative to riveted joints in aeronautical primary structures?

A precise answer to this question needs to address a huge amount of multidisciplinary topics due to the complexity associated with the full understanding of the process behavior and of the required design changes. In addition, any design change requires large interactions between different stakeholders related to aircraft. The major stakeholders are pointed out in Figure 1.2, with their major responsibilities which should be considered in the development or modification of any product, component or process that can modify the product behavior during its complete life-cycle.

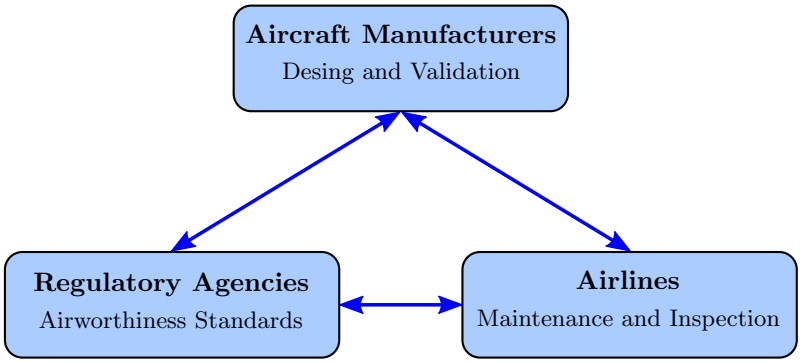

Figure 1.2: Aircraft stakeholders, required interactions.

Nevertheless, this research question is characteristically technical and specific to a detail in the overall structure. Looking in a holistic way to aircraft, it can be considered that the change of a joining process does not have a large impact in the design of the fuselage. Nevertheless, new joining processes have implications in structural design, in manufacturing, in assembly, in maintenance operations and at the end of the product life cycle, in the disposal. This thesis attempts to answer some of the questions involved in these implications, principally in the structural design and the implication in manufacturing and assembly.

Riveting continues to be applied extensively in aeronautical structures, being the major joining processes for their structural parts, although, from an efficiency point of view, these joints can be much more light. For instance, if the joints are butt joined this can eliminate thousands of fasteners, overlap areas and sealants. The replacement of riveted joints by other advanced manufacturing technologies, as friction stir welding, can bring weight and cost savings with a simplified design of the airframe and resulting in Leaner manufacturing processes.

1.3 Research Sites and Industrial Liaisons

The investigation concerning multiple aspects of the application of a new joining process was made possible due to the interaction between different universities, research institutes and industrial collaborations giving a multidisciplinary approach of the problem. The major intervenients in this research were:

GKSS is presently identified as Helmholtz-Zentrum Geesthacht, in Geesthacht (Hamburg, Germany). The department of *Solid State Joining Processes* has large know-how and research capability in solid state welding processes, with emphasis in the friction stir welding. A period of seven months was spent there for mechanical characterization of welded joints in aluminium lithium materials for aeronautical applications. New concepts were also analyzed, as the fracture mechanics behavior of tailor welded blanks, for structural optimization.

OGMA *Indústria Aeronáutica de Portugal* is a Portuguese specialist aviation company founded in 1918, dedicated to maintenance and production of aircraft parts for OEMs and first tiers supplieers. This organization represents today a major part of the Portuguese aviation industry, and is one of the oldest aviation production companies in the world. The interaction provided some useful discussions about the feasibility of the use of friction stir welding in small components or structural parts and opportunity for short term internships to understand the difficulties associated to the application of new advanced manufacturing processes.

TAP ME *Transportes Aéreos Portugueses* - Maintenance and Engineering is the part of TAP Portugal in charge of maintenance of the TAP entire fleet and of providing maintenance services to third party customers. The collaboration with a maintenance center through meetings and short term internships gave know-how for a better understanding of the aircraft life-cycle and concerning the requirements for the maintenance of aircraft structures. Opportunities to apply this joining process in repair operations were identified, that can avoid the replacement of damaged structures by completely new ones and reducing the time required for these operations.

Embraer is an aircraft manufacturer in São Paulo, Brazil that produces commercial (single aisle), military and executive aircraft. Embraer demonstrated interest in this investigation due to the potential of the joining process application in its structures.

FEUP *Faculdade de Engenheria da Universidade do Porto* were the headquarters of this project, where a substantial part of the work was done.

IST-UTL *Instituto Superior Técnico of the Universidade Técnica de Lisboa* Through the welding group that owns a FSW dedicated system, it was possible to perform welding trials in different configurations for their mechanical characterization and assessment.

MIT *Massachusetts Institute of Technology*, Cambridge, MA, USA, with a stay of six months, where it was possible to study the implications of non-destructive inspection in the application of welded joints in aeronautical structures. The investigation involved two companies with new techniques that were tested to verify if they can guarantee adequate inspection of welded defects or cracks originated during the life cycle. In addition, a preliminary cost analysis and comparative assessment with other joining technologies was done.

Airbus is a leading aircraft manufacturer, that has been following the emergence of FSW and has been developing research regarding to the application of this process in its structures. An internship of six months took place in its sites in Bremen and Hamburg, Germany, where the technology transfer and development of concepts for application this joining process during the assembly were investigated.

1.4 Dissertation Synopsis

The research done along this project covered different aspects related to the application of new manufacturing process for structural primary parts. Figure 1.3 presents and correlates the major topics that were addressed along this research and are presented in this thesis.

This dissertation is organized in nine chapters, including the introduction and conclusion. This first chapter introduces the work that was developed and that will be described along the following chapters, taking into account the scope of this thesis. The motivation, the problem statement, the research question and the different institutions involved along this work are described in this chapter.

The framework of this dissertation is the adoption and infusion of a new advanced manufacturing process in aeronautical civil sector. Chapter 2 describes how innovation and adoption of new technologies take place in this sector, with a brief introduction about the technology evaluation as the technology readiness levels and risk assessment tools. The new

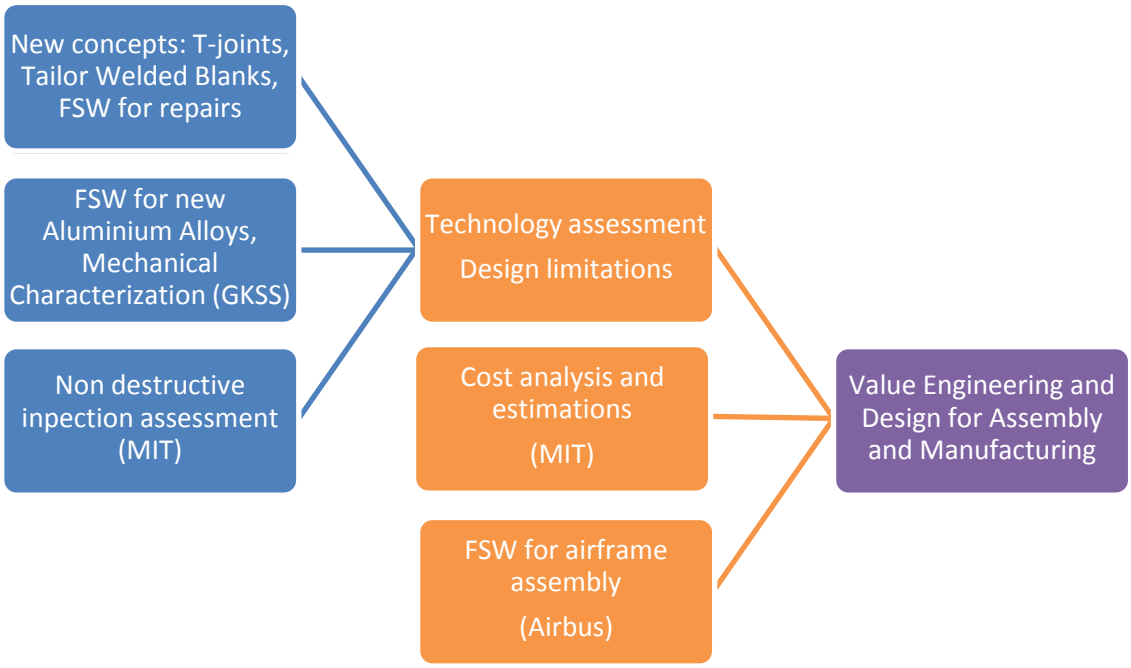

Figure 1.3: Relation of the dissertation topics.

product and process development is aeronautics is also reviewed discussing perspectives adopted by some of the major aircraft manufacturers.

The third chapter presents an overview of the master structure in a aircraft, the fuselage. The design philosophies adopted to design this structure are detailed and the major design drivers are discussed. An important characteristic in the design of these structures is the materials selection; a discussion about the last tendencies in materials for airframes will also detailed in this chapter. The joining processes, currently in use an in development will be discussed at the end of this chapter.

Chapter 4 describes the friction stir welding joining process. Characteristics, advantages and disadvantages will be presented along it. Mechanical properties of FSW joints of a new aluminium lithium alloy studied along this research will be detailed. The major defects that could occur with the application of this process will be discussed, presenting results obtained with different non-destructive techniques to detect root flaws in the friction stir welded joints.

Chapter 5 shows the structural design of reinforced panels, where the reinforcements were joined by FSW, in order to quantify the structural integrity. This study analyzes the application of numerical models to design reinforced structures taking into account fracture mechanics principles. The standard case of a crack growing between two stiffeners was modeled, considering residual stresses originated by the process, and the numerical results were successfully compared with experimental results.

Chapter 6 presents new concepts in aeronautical and aerospace structures that have been developed along this research. In the scope of this thesis, an alternative joint configuration for reinforced joints will be described, including its characterization. In addition, tailored welded blanks joined by FSW will be characterized. A new concept of this process will also be described that can simplify its application in lengthy joints. The application of this process for aeronautical repairs will be also discussed.

Chapter 7 presents a weight and cost analysis review with focus in the aircraft structures and their impact in the life-cycle costs. A comparison of the weight savings and manufacturing between FSW and a manual and automatic riveted joints is developed, giving a preliminary quantification of the advantages to be expected with this new joining process.

Chapter 8 introduces the impact of the application of friction stir welding from the manufacturing and assembly points of view. A model of a quality function deployment using the Cross analysis is described for a wider comparison considering different variables. The potential engineering value added by the replacement of riveted joints by FSW joints is analyzed considering the major aircraft design drivers.

Finally, Chapter 9 points out some of the major conclusions of this research, makes some recommendations for the application of FSW by different aircraft manufacturers and proposes areas for further research and development from the knowledge acquired along this study.

Chapter 2

Technology Adoption in Aeronautics

Commercial aviation has been experiencing a sustained growth and it is foreseen that between 2010 and 2029 the airline traffic will grow at a rate of 5.3% and the cargo traffic at 5.9%, [2]. At these rates, in 2029 the airline traffic will increase approximately 170%. This growth will require a large increase of the world fleet size, which is foreseen to double in 2029 (according to Airbus the fleet size in 2029 will be 29,050 representing a growth of 104%, [3]). The demand of new aircraft will be composed by the increase of the fleet size and by the replacement of older or less efficient aircraft. According to Boeing, the total demand of new aircraft will be about 30,900 new aircraft for the period of 2010-2029, [2]. In order to earn part of this demand, manufacturers need to introduce at the right time and at the right price new competitive products with higher efficiency.

Civil aviation, as other transportation sectors, has been experiencing along its history vast improvements in efficiency and effectiveness. These improvements have been following different objectives due to the diverse market needs along the time. At the beginning of the aviation era, this sector was driven by "Faster, Higher and Farther" goals in order to take the advantages of the air transportation to medium and long range travels. The "Faster, Better and Cheaper" (FBC) drivers emerged after the Cold War due to the increased resources scarcity and due to the globalization and massification in the sector. More recently, "Quieter, Cleaner and Greener" or "More Affordable, Cleaner and Quieter", [4], have been trying to replace the "Better, Faster and Cheaper" drivers due to the impact of the transportation in the environment changes, which should be reduced drastically in order to achieve more sustainable transportation systems. For instance, the European Union has been concerned with the impact of aviation in the global environment, and aims to achieve several goals for 2020 proposed by the Advisory Council for Aeronautics Research in Europe originating the Clean Sky initiative, [5]. This initiative has the ambition to reduce the perceived noise to one-half of the actual values, and aims at 50 % reduction in CO_2 emissions and 80% nitrogen oxide (NO_x) emissions by 2020, [5]. International organizations, as the Committee on Aviation Environmental Protection (CAEP), have also

been concerned with minimizing the aviation's effects on the environment regarding to emissions and noise, [6].

Undoubtedly, safety is the major concern, overriding any design driver. Historically, the main motivation for safety improvement was economical, linked to insurance companies policies, and not an intrinsic social requirement. Nowadays, all aeronautical systems require to be airworthy, which means that they are required to guarantee safe conditions during all the flight phases. All aircraft and related systems comply with necessary requirements so that the aircraft flies in safe conditions and the allowable limits are respected during all phases (i.e. maximum weight or maximum speeds), [7].

Several civil aviation authorities have strict regulations to guarantee the airworthiness of all civil aircraft that fly in their domains. The International Civil Aviation Organization (ICAO) is the international agency that regulates and ensures the safety in international civil aviation, with directives that all members are obligated to follow. ICAO members in addition established local authorities with their own standards and regulations, although in the accordance with ICAO Annexes, [8]. Two of the most relevant civil aviation regional authorities are the Federal Aviation Association (FAA) in the USA and the European Aviation Safety Agency (EASA) in the European Union. EASA has been replacing the Joint Aviation Authorities (JAA) that emerged in 1970 in order to harmonize the airworthiness standards in the European Community, [9]. Both authorities are active in the regulation of the sector in order to improve the safety and reliability of air transportation. The standards of FAA, Federal Aviation Regulation (FAR)'s and of JAA, Joint Aviation Requirement (JAR)'s that have been replaced by EASA Certification Specifications (CS), are divided in sections related to different activities of the air transportation, as the FAR part 25 or EASA CS-25 that comprises the airworthiness standards for transport airplanes (as Airbus A320 or Boeing 737). Each transport airplane type requires a certification according these specifications before any commercial flight. In order to keep these certifications up to date, when design changes occur, amends can be issued to promote technology adoption by the constructors and to face the constant technological evolutions, [10].

The efforts by the civil aviation authorities and by the aeronautical companies has been resulting in a reduction of the number of accidents, Figure 2.1a, and a fatality risk similar to the natural death, Figure 2.1b. Due to these accomplishments, nowadays civil air transportation is one of the most safe transportation system. Nevertheless, there is still space for improvement in aviation safety. The European Union asked for advice from a group of experts about what should be the goals for the future regarding aviation safety in order to create a research agenda. The main defined targets regarding to the aviation safety were, [11]:

- Reduce to zero hazards of on-board, in-flight and hostile actions;
- Reach 100% capability to avoid or recover from human error;

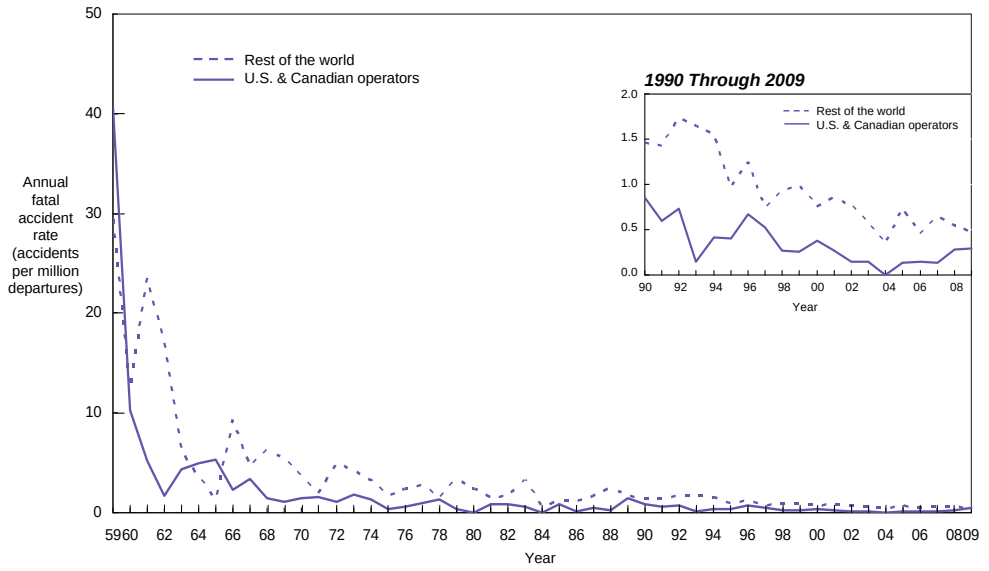

(a) Aeronautical accidents rate, [12]

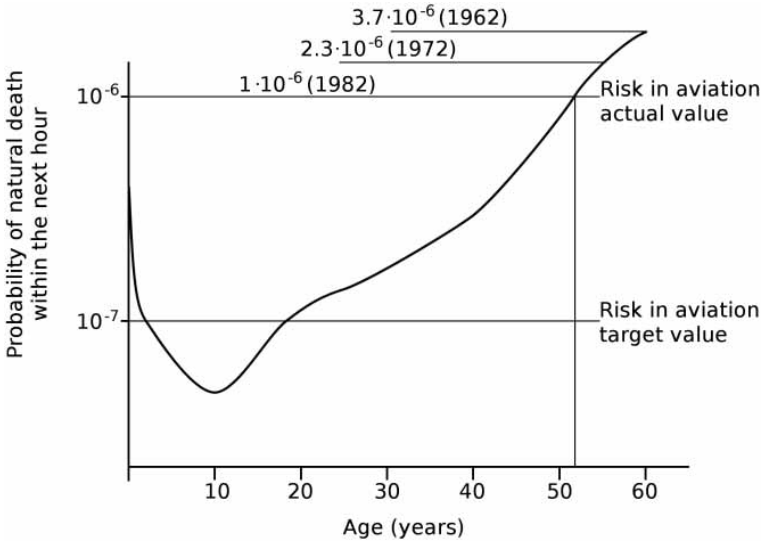

(b) Probability of death within next hour, [13].

Figure 2.1: Safety improvements and targets.

- Reduce accident rate by 50% in the mid term and 80% in the long term;
- Mitigate damage in survivable accidents.

Behind the assumption that the safety must be maximized for all aircraft and the severity of the aeronautical certification, the economical point of view should be also considered in order to achieve an economically viable product. Figure 2.2 shows schematically a theoretical trend of safety as a function of cost. A 100% safe airplane is unrealistic, although it is certainly possible to invest indefinitely in safety, improving it. For instance, it is possible to invest indefinitely in the design of redundancies of the airplane systems

improving the safety, however the improvement will be very low compared with the increase of cost. A trade-off between cost and safety is always required in order to have and economically feasible product. Aircraft designers as well as airline operators have to find a compromise between economy and safety. The aeronautical certification takes this fact into account specifying differences between airworthiness certification for transport airplanes and for normal, utility, aerobic and commuter airplanes (FAR and EASA CS-25 and, FAR and EASA CS-23, respectively), [7]. Nevertheless, all aeronautical sector keeps being driven by cost, as observed by Murman *et. al.*, [14]. It is observable that the main advances over the years in this sector have been been focused into reduction of the global costs, increasing simultaneously reliability and performance.

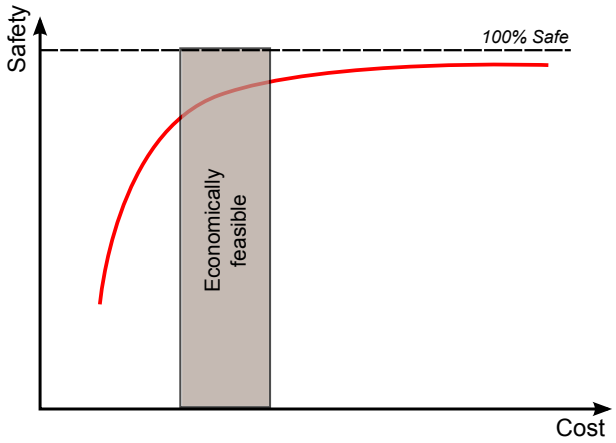

Figure 2.2: The safety and cost trade-off.

More recently, environmental protection is part of the concerns of civil aviation authorities and ICAO. The main focus has been the noise and the emissions limitations in aircraft. The first certifications are from EASA with the CS-34 regarding to Aircraft Engine Emissions and Fuel Venting, [15] and CS-36 regarding aircraft noise [16].

One drawback of these regulations is the increasing time to market and cost for new aircraft or for re-engineering existing aircraft or even for adoption of new technologies in existing products. This fact could be considered a barrier for higher innovation rates since it represents a obstacle for new players, mainly due to the high initial capital investment. It also represents an obstacle for the existing manufacturers due to the resources required for each new product development. Nevertheless, innovation in aeronautical sector has similar characteristics to innovation in many other industrial sectors as automotive, electronics or informatics.

Utterback, [17], pointed out that innovation in the major assembly industries follows a pattern composed mainly by three phases: fluid phase, transitional phase and specific phase. The development of a new innovative product begins with a fluid phase followed by high uncertainty about the final product, its processes and the market reaction. During

this stage, a large amount of patent applications usually occur to protect innovations and the larger product design changes (often customized), takes place. This initial phase is also linked to the emergence of many startups. If that new product is successful after this initial phase a new dominant design emerges and a new phase takes place, transitional phase. At this phase the innovation is more related to the processes than to the product, however product changes can occur to satisfy new consumers' needs. The production process becomes more rigid and at a large scale. The last stage, the specific phase, is mainly defined by a production of a very specific product at a high level of efficiency. E. Murman, [14], defends that the aeronautical sector is deeply in this phase due the reduction in public investment by the governments after the Cold War, forcing the new product development to be "cheaper". Nonetheless, opportunities for innovation are possible, as:

1. Incremental product technologies, to improve product productivity and quality;
2. Process technology;
3. Technological innovations that present superior product substitutes.

These three opportunities are almost correlated with the three drivers "Better, Cheaper and Faster". The incremental product technologies are generally concerned with new productivity concepts and philosophies as collaborative designing, Lean manufacturing and Six Sigma strategies that results in "Better" products. The innovation in processes technologies, as automation or faster manufacturing processes, which increases the production massification and reduces the product cost -"Cheaper"- and the technological innovations that can present superior product substitutes can move the product forward, responding to the market demand quickly, "Faster" than the competitors.

The aeronautical sector has been taking advantage of the innovation opportunities related to the specific phase. For instance, incremental product technologies had been used by Boeing to develop and produce the Boeing 777, as concurrent engineering during the product development, [18], total quality management, and Lean practices tools, [19]. Technological innovations were also constantly adopted by the large civil aircraft manufacturers. Very recently, the adoption by Bombardier in the new CSeries of new turbines from Pratt & Witney with Geared Turbofan technology is an example of technological innovation presenting improved efficiency, [20].

Technological innovations which present higher performance products can occur in different ways. A frequent scenario is the distinction between sustaining and disruptive technologies proposed by Christensen, [21]. Figure 2.3 illustrates the performance of disruptive technologies compared with the sustaining technologies and with the customer's expectations. Generally the companies follow the path of sustaining technologies, starting in the lower markets and moving to the high end markets making their product with more options, more capable and more expensive. When a new technology emerges with potential to replace previous products, it may become a disruptive technology depending on the

potential of acceptance in the market. These technologies usually have inferior performance than the competitors, even to satisfy the low end market requisites. Nonetheless, they can be simpler and less expensive attracting part of the low end market, and subsequently, taking advantage of the technology potential, are able to improve the product creating added value in a faster way compared with rival products. The performance path of disruptive innovations can have distinct configurations. Figure 2.3 shows two examples, where one of them requires more time to emerge than is the case of highly complex products.

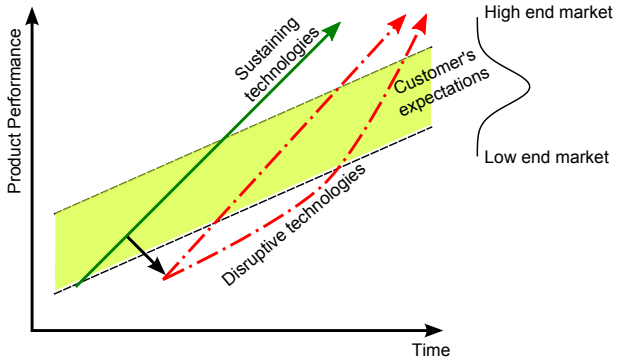

Figure 2.3: Performance of disruptive technologies and sustaining technologies.

Examples of recent disruptive technologies in civil aircraft are the fly-by-wire control systems and composites materials, [22]. The identification of disruptive technologies is not always consensual and the word disruptive can be misleading. In order to have a more explicit classification, Schmidt and Druehl [23] segmented the qualification of disruptive innovation in three different segments:

Disruptive Innovation Firstly the new product aims at the low end of the existing market and then progresses upwards;

New Market Disruption Creates new products that satisfy low end market customers needs that were unaccomplished. These new products can open up a fringe-market (when the customer needs are slightly different) or a detached market (when the customer needs are very different);

Low End Disruption The new products are focused on low-end market in the moment that are launched.

In the aeronautical sector, "New Market Disruption" tends to be more common than disruptive innovation, however some products can have a complete disruptive behavior. The case of the A318 which originated A318 Elite (an executive corporate jet) could be considered an example of disruptive technology, among other examples that can be found in the sub-systems of the aircraft.

The future of innovation in aeronautics is highly unforeseeable. Nevertheless, prospective studies are always under way, with experts announcing their thoughts about what will be

the main innovations. For example, Kroo, [24], pointed out a macro view of the innovation in this sector for the coming decades, that will be focused in:

- Exploiting computational advances for high-fidelity simulation and multidisciplinary design;
- Removing the constraint that aircraft must be designed around pilots or passengers;
- Designing the system rather than the vehicle: collectives and systems of systems;
- Supersonic flight with acceptable sonic boom;
- Build to demand production systems.

Innovation in the subsystems might also have huge impact in the performance of final products, as the example of re-engineering operations to bring up to date new technological advancements. A recent case is the Airbus A320 series, that will have a re-engineered version, the A320 NEO series, [25], with new engines and sharklets improving in this ways its fuel efficiency in 15% without large design changes. The Airbus A320 aircraft project was developed more than 25 years ago and is still up-to-date and competitive due to the different re-engineering operations. The application of radical different new designs, materials or disruptive technologies is not always possible with these operations, requiring a clean sheet design of all aircraft.

The number of adoptions or diffusion of a technology commonly follows a curve with S shape, result of a cumulative normal distribution of the diffusion vs. time. This result was pointed out by Rogers in [26], being useful to perform forecasts. The aeronautical sector might be more technological driven than consumers' needs driven. This S-curve has also application in multiple domains, for instance it can also represent the product life cycle growth behavior or, in the scope of this investigation, the technology development over the time. Foster [27] discussed this development, assuming as the upper limit the physical limits intrinsic to the technology. Figure 2.4 shows this curve, illustrating the position of the emerging, developing and mature technologies phases. Emerging technologies have a slow development with high costs and high uncertainty about its success and capabilities due to the knowledge impediments. The development phase is linked to the application of the technology into products and the beginning of the industrialization. At this phase a fast development is commonly observable without a significant increase of resources. In the mature phase, the technology advances slow down, with the investments in the development giving less reward.

2.1 Technology and Manufacturing Assessment

The adoption of new technologies in aeronautics, as in other critical safety systems, requires a very accurate evaluation of their behavior and of their interaction between all

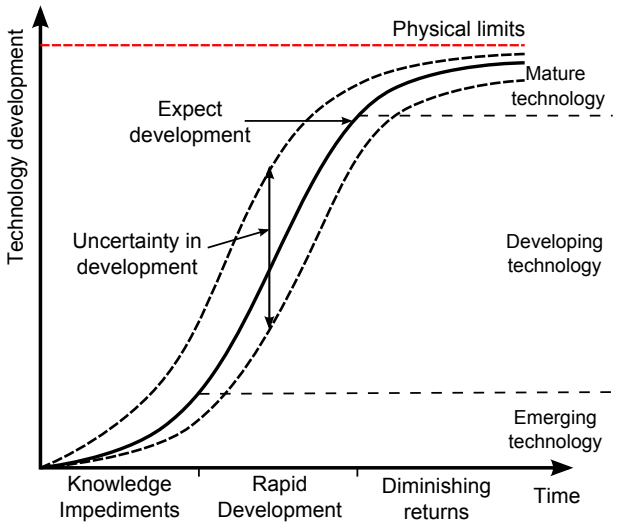

Figure 2.4: Technology development common behavior, S-Curve.

other subsystems. Technological assessment is essential for a successful infusion in the systems, preventing inaccurate evaluations. The infusion of unreliable technologies in complex systems can be very costly and time consuming due to all the corrective actions which will be required. Robinson *et. al.* [28], suggested that in order to improve the success of future aerospace programs and reduce the Life Cycle Costs (LCC), it is fundamental to use new technologies with some degree of maturity.

The maturity of technologies has been a concern for different agencies that work with complex systems. A quantitative technology assessment was developed in the 80's by Sadin at National Aeronautics and Space Administration (NASA) for a more effective technology transfer, [29]. This assessment is based on technology readiness levels, that at that time, was composed by 7 levels and was created to provide a base for mutual understanding of one technology between research and management. In 1995, Mankins from NASA presented a modified version of these Technology Readiness Level (TRL)'s scale, composed by 9 levels, [30]. This scale has been adopted by different organizations and governmental agencies as The United States Department of Defense (DoD) or European Space Agency (ESA), [31]. These 9 TRL's are summarized on Table 2.1, based on the definitions proposed by DoD, [32].

The deployment of technologies as a function of time also follows the S-Curve behavior until its complete development. The greatest endeavors are during the early TRL's and the last TRL's, however unanticipated problems or inaccurate TRL evaluation can force the development to diverge from this behavior. Considering a product that is being updated along the time with different technologies, as illustrated in Figure 2.5, the maturation of each technology has different time scales and the impact of it in the product performance

Table 2.1: Technology readiness levels description.

TRL	Definition
1	Basic principles observed and reported
2	Technology concept and/or application formulated
3	Analytical and experimental critical function and/or characteristic proof of concept
4	Component and/or breadboard validation in laboratory environment
5	Component and/or breadboard validation in relevant environment
6	System/subsystem model or prototype demonstration in a relevant environment
7	System prototype demonstration in an operational environment
8	Actual system completed and qualified through test and demonstration
9	Actual system proven through successful mission operations

will be also diverse. The upper limit, as expected, is a technology readiness level equal to 9, nevertheless, some technologies can be dropped during its development if it is concluded that they do not yield added value to the product or due to incompatibilities that cannot be solved. Examples of these developments are easily found in the aeronautical sector, as the case of the turbine development. For the same level of complexity and the same amount of resources, the time required to achieve the last TRL's levels has been currently reduced due the application of new product design techniques as the application of numerical and computational tools.

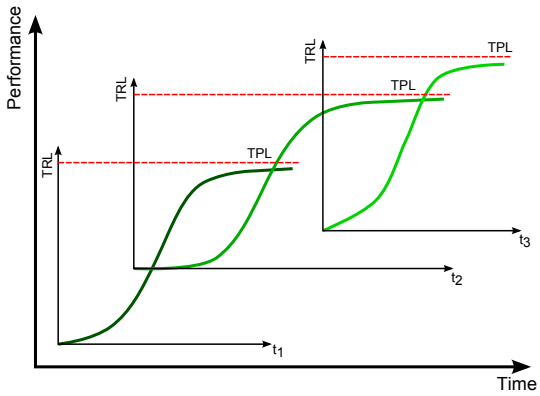

Figure 2.5: Product performance and the development of its technologies.

Boeing developed the TRL's scale not just for its own products but also for processes and for analyses and simulations (numerical and computational models) in order to have a higher level of control and more accurate risk assessment in its different projects. Table 2.2 summarizes this classification in the context aircraft development.

Table 2.2: Technology readiness levels for products, processes and analysis/simulations, [33].

	TRL	Product	Process	Analysis/Simulation
Implementation	9	Actual System "Flight Proven" Through Successful Mission Ops.	Actual Process Proven Through Successful Operation by Program	Actual Models in Use by the Community
Validation and Certification	8	Actual System "Flight Qualified" Through Test and Demo	Actual Process Completed and "Qualified" Through Test/Demo	Actual Models are validated against "Flight Qualified" data
	7	System Prototype Demonstration in an Operating Environment	Prototype Process Demo in a Program Environment	Prototype Model Validated Against Flight-Test Data
Demonstration	6	System/Subsystem Prototype Demo in a Relevant Environment	Process Prototype Demo in a Relevant Environment	Model Validated Against Relevant Ground-Test Data
	5	Component Validation in Relevant Environment	Beta Version: Key Elements Validated in Relevant Environment	Model Components Evaluated Against Relevant Data
Development	4	Component Validation in Laboratory Environment	Alpha Version: Key Elements Validated Against Benchmark	Tools Assembled into Package and Tested Against Hand Calcs.
Providing feasibility	3	Critical Function of Characteristic Proof-of-Concept	Alpha Version: Operational in a Test Environment	Data Flow Diagrams, Tools Collection and Familiarization
	2	Technology Concept and/or Application Formulated	Requirements Document Approved by Customer	Methods and Algorithms for Similar Systems Identified
Basic Research	1	Basic Principles Observed and Reported	Current Process Documents and Potential Savings Identified	System Characterized and Tool Needs Defined

The TRL's scale has been also expanded for different domains in order to comprise other phases of complex products life cycle. Examples of these scales are: Manufacturing Readiness Levels, [34], which gives an assessment of the maturity of a part from the manufacturing point of view; Software Readiness Levels for evaluation of software development; Human Readiness Levels for assessment of human skills to perform the required tasks related to product; Integration Readiness Levels, [35, 36], which is a metric to measure the integration degree and its maturity between the different technologies when they interact; and System Readiness Levels, that measure the state of development of a system taking into account the different assessments mentioned above, [35]. Figure 2.6 illustrates how these different readiness levels metrics are correlated, based on Sauser *et. al.*, [37]. The system readiness level is evaluated from the technology readiness levels (TRL_1, TRL_2 and TRL_3), from the human readiness level, from the software readiness level and from the integration readiness level (IRL_1, IRL_2 and IRL_3), $SRL = f(TRL_i; IRL_j)$, giving a comprehensive assessment of the system development, including in a probabilistic way [38].

These tools have been supporting the risk management in the development of new aircraft or in the re-engineering of actual aircraft due to their complexity. Additional tools can help the estimation of the risk taken in the adoption of technologies and reduce the uncertainty in the early stages of TRL's. For instance, the Advancement Degree of Difficulty (AD^2) allows to estimate the costs, the schedule and the risk when it is required to develop a technology from the present state to the readiness level required for a proper infusion into the system, [39].

Technology Identification Evaluation and Selection (TIES) is another methodology that gives a deterministic evaluation of the technologies taking into account the uncertainty

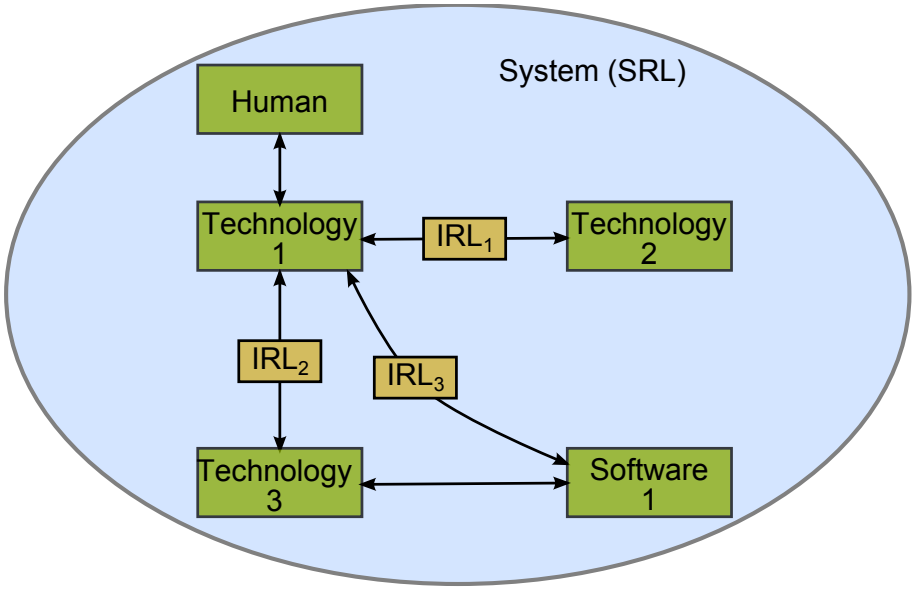

Figure 2.6: System readiness level, interrelation between technology, human and integration readiness levels.

associated with immature technologies in aeronautical systems, [40]. Mavris *et. al.* evolved this method from 7 steps, [40], to 9 steps, [41] comprising:

1. Problem definition
2. Baseline and alternative concepts identification
3. Modeling and simulation
4. Design space exploration
5. Determination of system feasibility/viability: probability of success
6. Technology identification
7. Technology evaluation
8. Population of the Pugh evaluation matrix
9. Technology selection

In each of these steps tools are proposed to identify or to evaluate the different variables. For instance, in step 6, technology identification is proposed to create a compatibility matrix between the other technologies of the system, to identify incompatibilities. Subsequently, a technology impact matrix points out the benefits and obstacles of the different prospective technologies. This matrix takes into consideration the foreseen technology development, based on the S-Curve, Figure 2.4, the present technology readiness level, Table 2.1, and subjective opinions from expert panels, [42].

Another technology infusion assessment in aeronautical systems design is proposed by Smaling and de Weck, [43], with the concept of "Fuzzy Pareto Frontier" and the Technology Invasiveness index (a scalar index that measures the disruption caused by infusion of new

technology in the system) applying Design Structure Matrix (DSM) for global system interactions representation. NASA has also been developing other technology assessment tools based on real options, a business management assessment tool, to valuate the risk and uncertainty of technology development taking into account costs and schedule, [44]. This tool is more focused in technologies with low maturity (TRL$\leq$ 6) that are associated to higher uncertainty. The algorithm of this tool is based on stochastic models for each technological attribute and on option value of the technology with Monte Carlo simulations, assessing the technology real option valuation.

2.2 Product and Process Development

Structured New Product Development (NPD) is imperative for all aeronautical parts to satisfy all requirements of all players involved in the life cycle of an aircraft. There are two main organizational structures of traditional NPD, *(i)* from the marketing point of view, which is mainly composed by 6 to 8 steps (idea generation, idea screening, concept development and testing, marketing strategy, business analysis, product development, test marketing and commercialization), [45, 46], and *(ii)* from the design point of view, generally composed by 6 phases presented in Figure 2.7.

Figure 2.7: Generic product development process proposed by Ulrich and Eppinger, [47].

In the aeronautical industry, due to the complexity of the products and due to the distinct customer requirements, the product development steps are slightly different with additional stages. Figure 2.8 shows the product development structure disclosed by [48] of a generic aircraft development, divided in three major groups: configuration development, detail design and product support. In the configuration development and detail design, very specific project goals are defined in order to meet the design requirements. These requirements can be very complex since they should aggregate airplane performance, safety, reliability, maintainability, subsystems properties and performance, and many others, [48]. Linked to the different phases of the NPD process, milestones are established that identify the successful accomplishment of the different phases.

Two examples of practical NPD processes by large civil aircraft manufacturer are presented here. Figure 2.9 presents schematically the product development process at Bombardier, [49]. In this process it is visible that the different business processes are more juxtaposed for a more concurrent and parallel development and the number of milestones increase to identify clearly the different product development achievements.

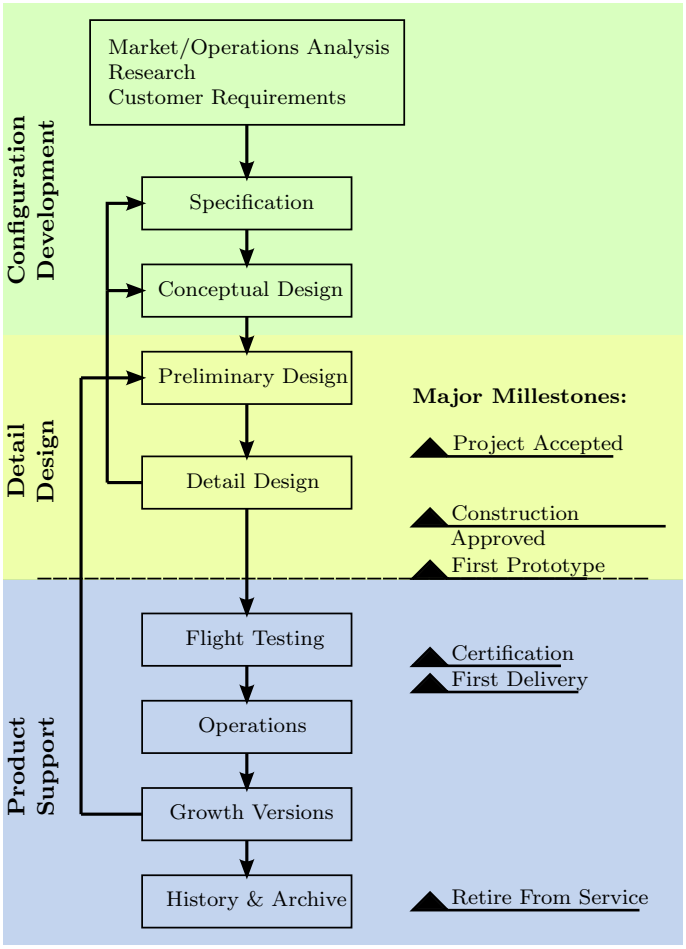

Figure 2.8: Aircraft design process, [48].

The common and structured NPD cycle at Airbus is presented in Figure 2.10 and is the baseline for all Airbus programs, [50]. This structure is composed by five major phases: feasibility, concept, definition, development and series. These phases are schematically presented sequentially, although Airbus has been also adopting concurrent engineering approaches where these phases occur in parallel. In this case, 14 milestones were defined, where in the M6 milestone, after the commitment with customers, it is decided to move forward or not to proceed with the project. All different areas must interact with common and well defined objectives and targets, for a more successful and efficient aircraft development.

The development of new processes (as manufacturing processes) requires a different approach than the one used in the product development, due to the different objectives and requirements, although they can be compared based on their targets. Figure 2.11 presents schematically an example of differences between the process and product development and the interactions between the two different approaches. In the case of the development of a new manufacturing process for aeronautical parts, additional steps might be required in

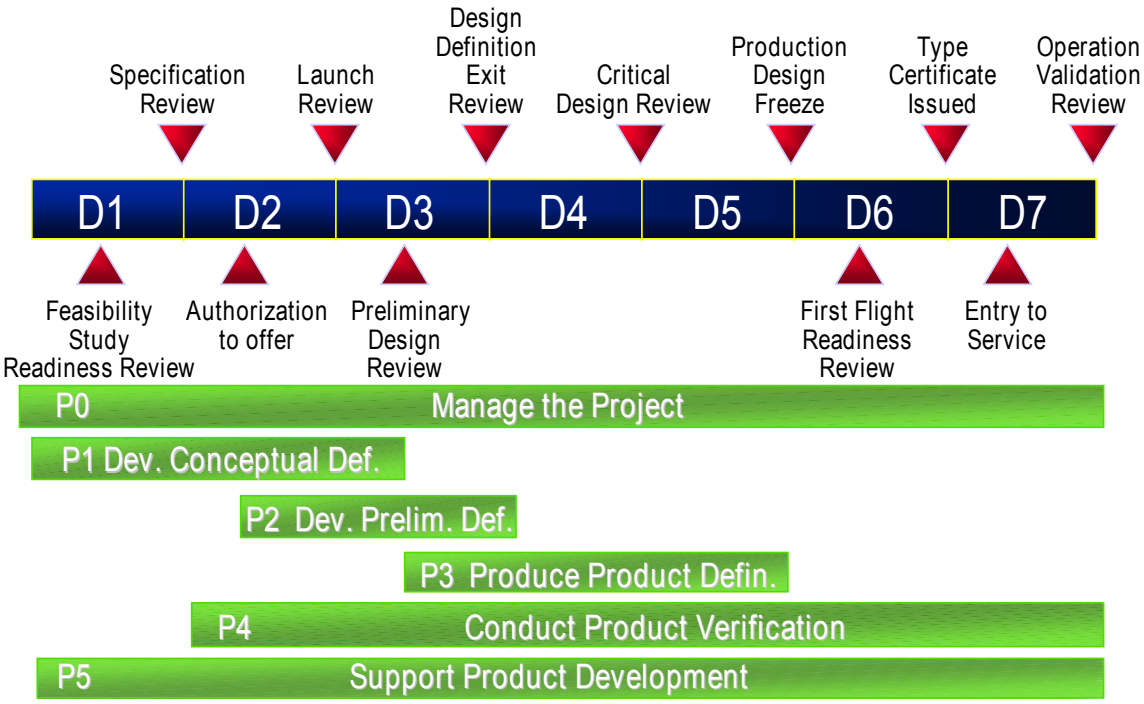

Figure 2.9: Product development in aeronautical context, [49].

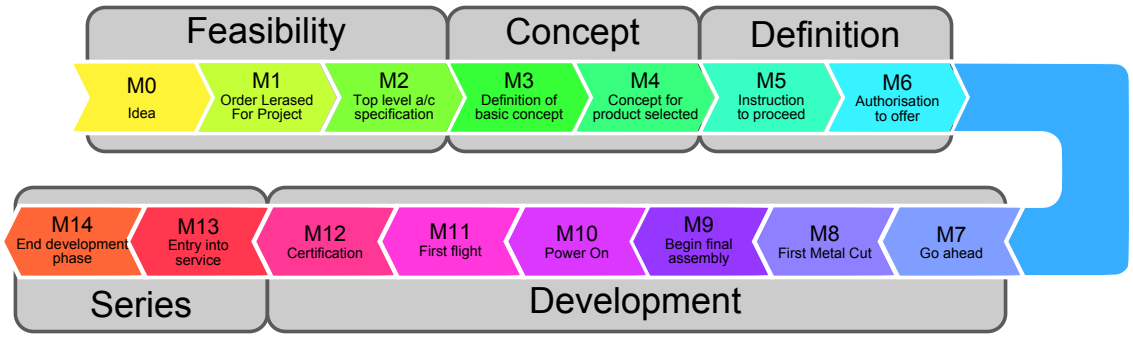

Figure 2.10: Aircraft design process at Airbus, adapted from [50].

order to fulfil all aeronautical requirements not only from the design point of view, but also from economical, product life cycle and assembly points of view.

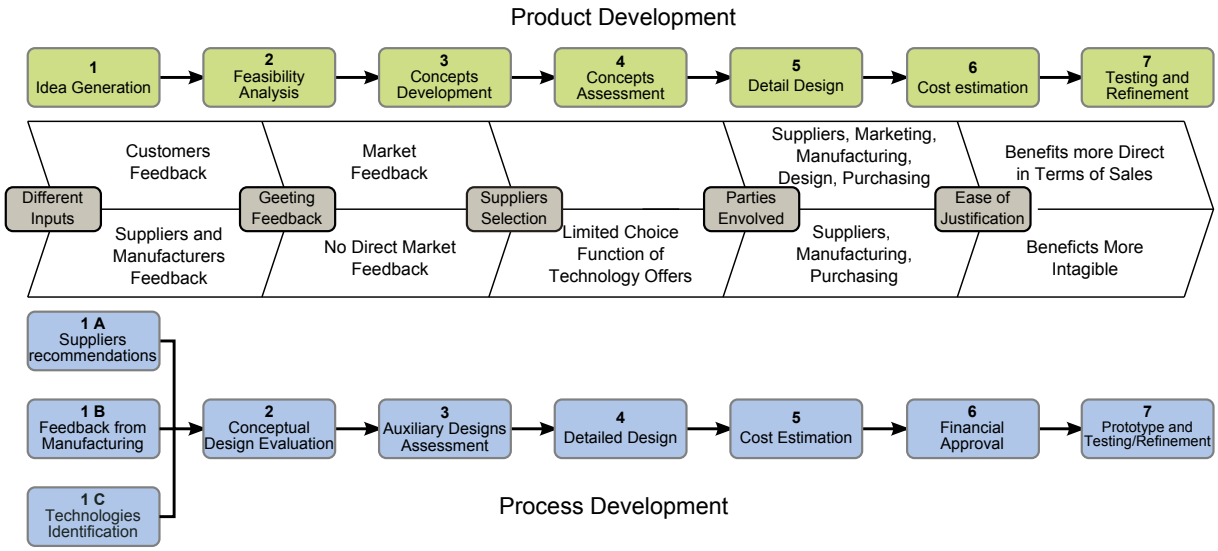

Figure 2.11: Product and process development.

Chapter 3

Design of Aeronautical Structures - Fuselage

Civil aircraft are complex engineering systems, mainly composed by structures and systems. Aircraft structures comprise fuselage, wings, landing gears and many other smaller structures; aircraft systems include electronic, hydraulic, mechanic and propulsion sub-systems. In the case of aircraft structures, they can be divided in different groups according to their repercussion in the aircraft safety[1]. A generic division comprises always primary, secondary and tertiary structures, although the definition of each division is done by each aircraft manufacturer. For primary structures, the FAR Advisory Circular 25.1529-1 uses the definition "structure that significantly contributes to the carrying of flight, ground, or pressure loads", [51]. For the other groups the airworthiness authorities do not provide a definition. In military aircraft, the aircraft battle damage repair manual of United States Air Force (USAF) presents a detailed description of these groups based on the reparability in defense contexts, [52, 53]. Based on this division, a general description of each of these structural aircraft groups was created:

Primary structures are the structures that are critical to the safety of the aircraft. They need to support most of flight and weight loads and without them the aircraft could not sustain the structural integrity. Wingbox, wings, fuselage frames and landing gear are examples of primary structures.

Secondary structures are structures which in case of failure would affect the aircraft operation but will not cause its loss. These structures transfer loads to the primary structures. When compared with the primary structures, they are more damage tolerant since they can hold on greater damages without requiring repair.

Tertiary structures are nonessential structures with no impact in the aircraft airworthiness when completed damaged. Most of the times, it is not imperative to repair or replace these structures. Some internal doors, pylons and some interior panels and parts are examples of these structures.

[1] Multiple divisions are found in the literature, as in the structural repair manuals of civil aircraft, however the adopted division was found to be the most comprehensive.

Aerodynamic and special components are parts with functions essential to the aircraft controllability and performance as the aerodynamic control or pressurization, but their main design objective is not their strength but other properties. Radome and engine nacelles are examples of these structures.

Repair restrained structures are structures for which repair is usually unfeasible; therefore when damage occurs they should completely replaced. Complex forgings or machined parts that can be found in the landing gear are examples of these structures.

The application of new structural design concepts in primary and secondary structures requires extra concern due to their importance in the aircraft safety. Examples of these new structural concepts are the application of new materials or new joining processes, since the design concepts need to take into consideration all structural loads and environmental conditions during the complete life-cycle.

The structural engineering design might be done in different modes and philosophies. According to the official certification regulations, as the FAR parts 23 and 25 [54, 55], for aeronautical structures, three design philosophies evolved:

Safe-life design: the structure is designed to withstand, without catastrophic failure, the repeated loads of variable magnitude expected in service throughout its operational life. The "safe-life" concept involves a point in the aircraft life-cycle, typically expressed in hours or in flight cycles, when the structure is replaced or removed, preventing any development of fatigue cracks or corrosion degradation.

Fail-safe design: the structure is designed to retain a minimum residual strength after a damage or a partial failure of a principal structural element. This design philosophy usually involves a safe-life component or primary structural element, and a redundant or backup structural element. This fail-safe design is often considered a redundant design or a multi-load path design, which in case of failure still allows a safe flight and landing.

Damage tolerant design: the structure is designed to display a minimum residual strength for a further period of service, after being subjected to the regular service conditions, which accumulates structural degradation due to fatigue loading, corrosion and accidental damages. This design philosophy involves scheduling of regular structural check-ups using non-destructive techniques which examine detectable damages. If any damage outside of the design limits is detected, the structure is repaired and the residual strength is recovered.

Figure 3.1 illustrates these design concepts based on operation time. This figure illustrates that safe-life design presents lower safety coefficients, that in unforeseeable conditions can to lead catastrophic failures or lower life in order to prevent any fatigue

damage. Due to this reason, it is infrequently applied in aeronautical structural parts since it represents higher costs for the part replacement or due to the extra weight to have the same strength as the other philosophies. Fail-safe design presents also short life cycle, since the structure is designed to retain a required residual strength for a period of unrepaired service after the failure or partial failure of a principal structural element, [56]. With this philosophy the structure is designed to have lower stresses than the material fatigue strength, during its service. The redundancy used in this design philosophy might penalize the structural weight and life-cycle costs; however it is required in order to ensure the structural integrity in extreme conditions. Damage tolerant design gives the compromise between weight and strength. If the structure can withstand damages of a given size and for a specified period without repair, this can improve the specific weight of the structure, since no extra mass is required to increase its strength. If these damages are detected and repaired, the original structural residual strength is restored. This design procedure has been refined along the years, [57] and nowadays is applied intensively in most of the civil aircraft components, during the complete life-cycle with regular check-ups, being feasible to extend their life indefinitely, [57]. The damage tolerant design is applied intensively in airframes with high interest of manufactures and regulatory agencies, as FAA which published a handbook composed by two volumes to support a more accurate design with this concept, [58, 59].

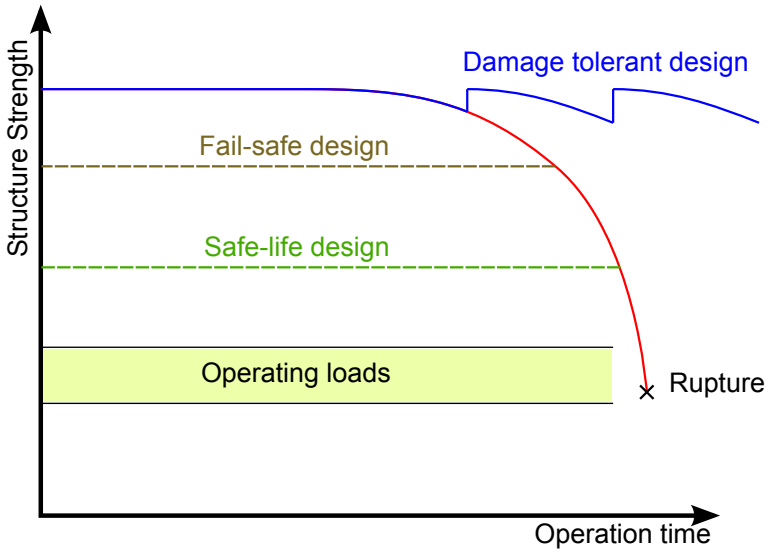

Figure 3.1: Aircraft structural design philosophies.

The damage tolerant design adoption can be improved using a deeper control of the structure with active sensors that monitor the structure behavior during the aircraft service. Maintenance operations become only necessary when anomalies are detected and better scheduling of preventive maintenance will be possible. This technique has been labeled Structural Health Monitoring (SHM) and is part of a Integrated Vehicle Health

Management Systems (IVHM), [60], firstly adopted by Boeing in its 777 aircraft. The application of SHM techniques has been explored extensively by Boeing and Airbus due to the application of composite materials in the fuselage, for a better control of the material behavior during the aircraft operation. The idealistic application of SHM would involve all structural parts. However, it should be taken into account that the complexity and costs will increase, further to weight penalties when the systems mass is higher than the structural weight savings. Figure 3.2 presents an example of how Airbus is thinking in these systems and illustrates how complex the sensor network can be if it aimed to monitor all structural parts, [61].

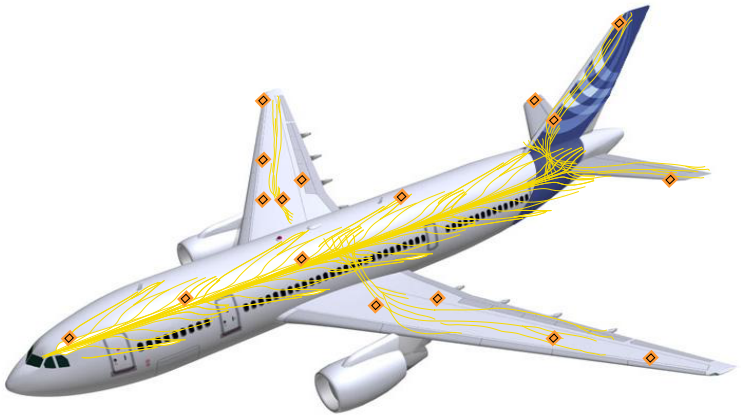

Figure 3.2: Structural health monitoring concept by Airbus, [61].

3.1 Damage Tolerant Structures and Reinforced Fuselage Panels

As the aircraft structures require the lowest weight configurations with enough strength to support all operational loads with high reliability, the structural configurations are deeply optimized. The major focus of this dissertation is the fuselage, chosen because it is the largest structure, composed mainly by primary parts and the one with the most demanding design requirements. It is also considered the main structure in the aircraft, since it holds crew, passengers and cargo.

Truss, monocoque, and the semi-monocoque are the solutions found for the design of this structure. Truss or framework types of construction have wood, steel or aluminum tube, or other cross sectional shapes which may be bolted, welded, bonded, pinned, riveted or machined into a rigid assembly. The vertical and diagonal cross-members are arranged to withstand both tension and compression loads. This type of fuselage has been in use for about 80 years, [62]. It is a very strong structural concept and of relatively light weight (high specific strength). Both the monocoque and semi-monocoque fuselage structures use

their skin as an integral structural or load carrying member. Monocoque (single shell) structure is a thin walled tube or shell which may have rings, bulkheads or formers installed within. It can carry loads effectively, particularly when the tubes are of small diameter. The stresses in the monocoque fuselage are transmitted primarily by the strength of the skin. As its diameter increases to form the internal cavity necessary for a fuselage, the weight-to-strength ratio becomes more efficient, and longitudinal stiffeners or stringers are added to it. This progression leads to a semi-monocoque fuselage, which depends primarily on bulkheads, frames and formers for vertical strength, and longerons and stringers for longitudinal strength. Semi-monocoque is the most popular type of structure used in aircraft nowadays, composed of a long tube shape with a large number of longitudinal reinforcements (stringers) and circumferential reinforcements (frames) which carry all stresses, [63].

As an example, a semi-monocoque fuselage configuration of the Boeing 737 is presented in Figure 3.3, with the indication of the major structural parts of these components.

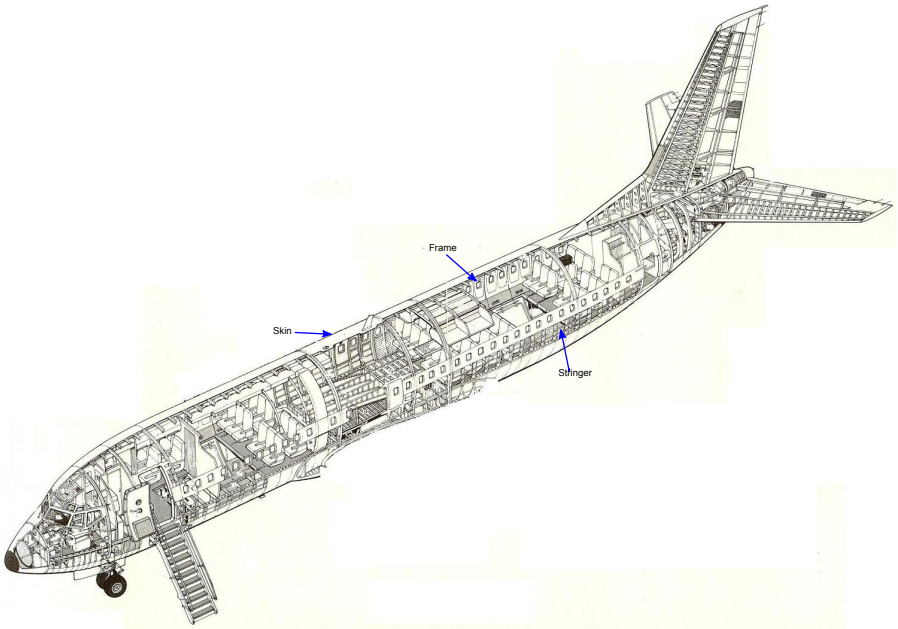

Figure 3.3: Semi-monocoque fuselage of a Boeing 737. (Source: *FlightGlobal*)

The fuselage structure is required to withstand multiple loads. During flight these loads promote mainly tension stress in the upper parts, shear stress on the fuselage laterals and compression stress in the bottom. These stress conditions are promoted by the cabin pressurization and by the fuselage bending. During the aircraft taxing the top and bottom stresses are inverted, but with lower amplitude due to the absence of pressurization. Fuselage materials need to have high specific strength, high specific Young's modulus, good

fatigue properties and toughness and corrosion resistance. The material fracture toughness is often the higher limitation in the structural design of the components in tension, [64].

The manufacturing of the fuselage in large aircraft is done through the assembly of the reinforced panels, that already have assembled the skin, stringers and frames. The design of these reinforced panels can vary as a function of their position in the aircraft, since the loads are different in each point of the aircraft. This allows to adopt different materials and cross sections for the reinforced panels, tailoring its strength and giving opportunity for better optimization.

3.2 Materials Selection

The material selection is one major driver in the aircraft design, considering that it will stipulate the processes (joining, manufacturing and assembly) that will be involved. The traditional fuselages are based on aluminium alloys, a material that has been used since the last century. In aeronautics, the most widely used aluminium alloy is the AA2024 that was introduced by Alcoa in 1931 and supplied as an alclad sheet with good corrosion resistance. However, a new tendency for the use of composite materials started to emerge firstly in military applications and has now reached the major civil aircraft constructors for medium and long-range civil aircraft. The most recent examples of composite materials application at a large scale in airframes are the Airbus A350 XWB that is foreseen to fly in 2013 and the Boeing 787 that is going through its testing program for final certification expected during 2011. For instance, in the Airbus A350 XWB, [65], 52% of airframe materials are composites, to be compared with, for example, the Airbus A320 that has 65.5% of aluminium alloys and 12.5% composite materials, [66]. The titanium percentage has been also growing, since some aluminium parts need to be replaced by titanium parts due to the galvanic corrosion with composite materials and for a higher thermal expansion compatibility. This trend, presented in Figure 3.4, implies a significant change in the global characteristics of the fuselage.

The decision to select composite materials as the main material for airframe material, instead of aluminium alloys, is not consensual and represents a radical innovation, when compared with other alternatives. Since the aircraft is a complex system, many different variables are not easily quantified and measured, as the material behavior during the life cycle, the impact of the environmental conditions, the real maintenance costs and many other variables. In addition, the costs forecasting with new materials is difficult, since the variation of materials' quotations during the complete project extension (more than 20 years in the case of civil aircraft) is unpredictable in the early phases. The adoption of aluminium as main material in airframes had also presented problems; the structural

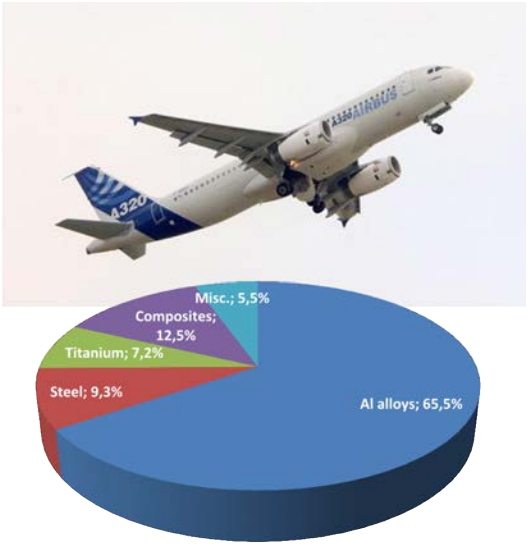

(a) Airbus A320, 1988

(b) Boeing 787, 2011

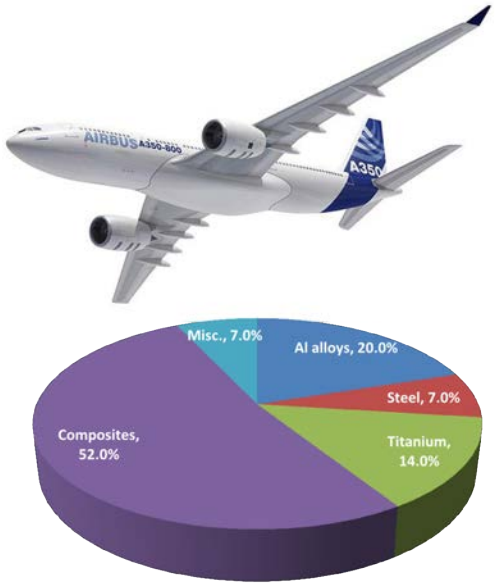

(c) Airbus A350 XWB, 2013

Figure 3.4: Evolution of the materials percentage in the airframe.

behavior including fatigue aspects was not completely understood, which led to several casualties as de Havilland Comet or the Aloha Boeing 737 accidents, [67].

The development of advanced aircraft airframes is currently one of the important improvements and challenges of the air transportation sector. In the development of primary structures, the industry started to investigate smart solutions and smart structures with intelligent characteristics, [68]. The use of these solutions requires innovative materials allied to optimized designs. The prospect materials require clear technology readiness level valuation, with well understood mechanical properties and mechanical behavior and with well stabilized manufacturing processes, which means that only mature materials (technological ready) are suitable for primary and secondary structures. Taking into account the mature materials for airframes, presently, three main materials groups are applied:

- Aluminium alloys
- Fibre reinforced composites
- Fibre metal laminates

The aluminium alloys, the carbon fiber reinforced polymers and the GLARE (a fiber metal laminated) are, inside of these groups of materials, the materials that that have been applied to produce airframes, as a result of their lightweight and high specific strength (static and dynamic).

For better decisions on the best materials and processes selection, the largest number of variables during the design phase should be considered, for a wide-ranging and more complete comparison. As regards material selection, Vermeulen and van Tooren, [69], analyzed the performance of different aerospace materials summarizing that the fatigue damage growth and residual strength are the main design drivers for a fuselage. The major fatigue properties of materials suitable for fuselages were examined, estimating the specific weight taking into account material toughness and damage tolerant properties. Commonly, the static strength is applied to assess materials in terms of specific weight; however the static strength is not a primary property for the engineering design of an airframe. Due to the different fatigue behaviors of these materials, direct comparison of their properties is not realistic since their failure is based in different phenomena.

3.2.1 Aluminium Alloys

Aluminium alloys have been the dominant material for airframes since the 1940s, at that time because of their strength-to-weight ratio or their specific strength and reasonable costs, [70]. After the first applications in aeronautics, Alcoa developed a higher strength alloy by increasing the alloys content and developed new heat treatments creating the most popular aircraft aluminium alloy, AA2024 with heat treatment T3 that is still in use in

most aeronautical structures. Corrosion in the Al alloys was a concern in these applications, and in order to improve the corrosion resistance the Alclad concept was created consisting in the application of a small layer of pure aluminium that has good corrosion resistance and protects the aluminium alloy structure.

Aluminium alloys still represent a competitive solution as a material for airframe structures. However, they are challenged by composite and hybrid materials with higher specific strengths. In order to face this competition the aluminium alloys producers increased the R&D activities to improve the properties of their alloys. Figure 3.5 shows the evolution of two different types of aluminium alloys optimized for the application in skin and stiffeners of the airframes. For the skin the main mechanical property is the fracture toughness (noted in the cited reference as Kapp) and for the stringers the main property is yield strength (TYS in Figure 3.5). It is noticeable that until the middle of 1990s, no significant evolution took place. Facing the competition of composites, the producers invested in the R&D of new alloys and improvements of 40% higher fracture toughness and 20% higher tensile strength were achieved.

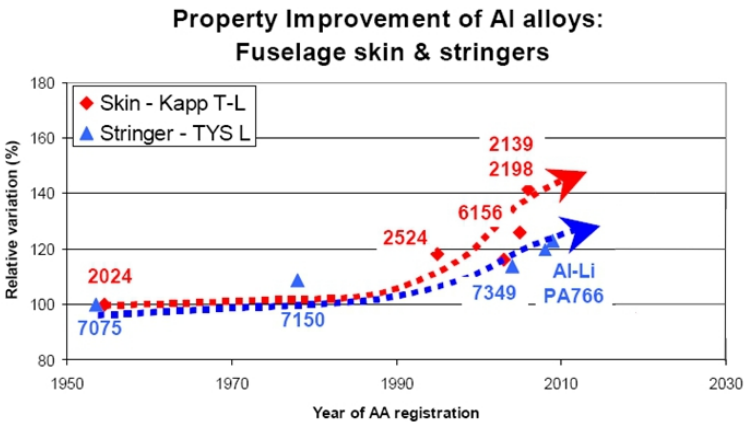

Figure 3.5: Aluminium alloys evolution regarding to the fundamental properties, [1].

Aluminium-lithium alloys are examples of currently successful materials (for instance, the alloys AA2195 and AA2198). Lithium (Li) is less dense than the aluminium, 0.53 kg/m^3 compared to 2.7 kg/m^3, reducing the density of the alloy and improving the mechanical properties. Nonetheless, pure lithium is not abundant on earth, its extraction is very expensive and its application in electrical batteries inflates its price, making these alloys costly. Due to the high material cost, the cost benefit for airframes is low. Nevertheless, these alloys are already applied for space applications since in these application the weight costs are higher. Beginning in the later 1990s, these Al-Li alloys, have been applied in different aerospace structures, as in the Space Shuttle external tanks, where the Al-Li alloys AA2195-T8 was used in order to reduce the total weight and enable the shuttle to

carry out more payload, [71]. The Airbus A350 XWB will use Al-Li for some frames of the fuselage (whereas the skin and stiffeners will be in carbon fibre reinforce polymer), [72].

Scandium-reinforced aluminium is another new type of aluminium alloy, under development, with interest for aeronautical primary and secondary structures due to its mechanical performance. These alloys are stronger than other high strength alloys, having a significant grain refinement, and exhibit a good resistance to corrosion, [73]. Some of these alloys are developed by Alcoa, as the alloy C557 and AA7X11 that NASA is developing for the Hypersonic-X fuel tanks, [74]. In this case the price is also high, due to the scandium scarcity, [75]. Aluminium-beryllium alloys have also interest in airframe structures, due to the lower density of the beryllium (1.85 kg/m^3) and the high stiffness of these alloys, although its strength still lower that the Al-Li alloys, [76] and the application of beryllium could generate health problems.

An additional new type of aluminium alloys which are emerging recently are the aluminium-copper with vanadium patented by Alcoa, [77]. Although the alloy density is similar to the common alloy AA2024, these new alloys have improved combined mechanical properties. One of the limitations in the development of new aluminium alloys is the difficulty in the improvement of one property without degradation of another one.

3.2.2 Fibre Reinforced Composites

Fibre reinforced composites materials are composed primarily by fibres, as glass fibres, carbon fibres or others, impregnated in a matrix that transfers the stresses between the reinforcing fibres. This matrix can be made by different types of polymeric resins such as epoxy or polyurethane. The most attractive composite material, widely used in aeronautical primary and secondary structures, is the Carbon Fiber Reinforced Polymer (CFRP). Structures designed with this type of material present an attractive alternative to structures using the more conventional materials due to its high specific strength (ratio of strength per density) in compression and tension, good thermal conductivity and dielectric constant, good toughness and wear properties, [78]. Drawbacks are manufacturing and processing costs, low damage tolerance properties, [79], difficulty in the inspection and in repair, dimensional tolerances and less knowledge about the material behavior in service during its life cycle.

Nevertheless, CFRPs are an increasingly popular material for aeronautical applications; their percentage of application in airframes is growing significantly and it evolved to be the main material in some new civil airframes, as shown in Figure 3.4. Early applications of these materials were found in military aircraft and in a few parts of civil transport aeronautical structures. Progressively, they have been applied in civil aircraft with continuously growing weight percentage of civil airframes, as exhibited in Figure 3.6.

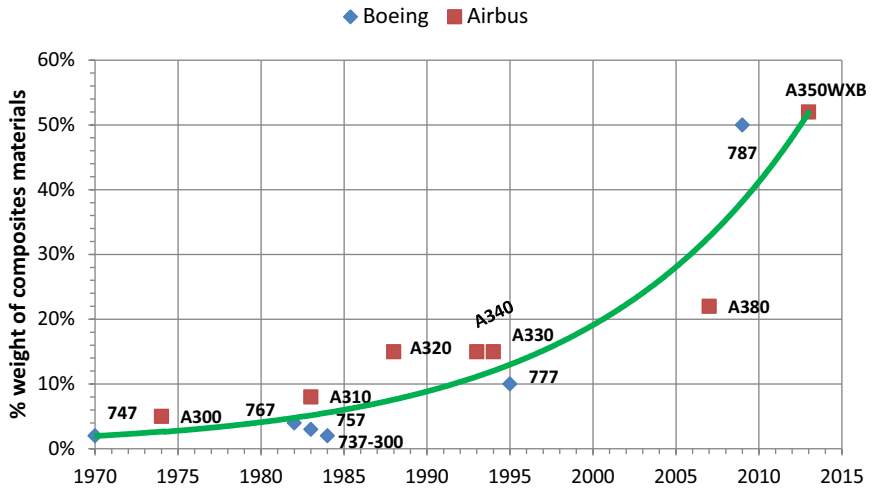

Figure 3.6: Carbon fiber reinforced composites evolution.

The major progress of these materials in the civil airframes is in the new Boeing 787 (Dreamliner), with a fuselage entirely in CFRP materials, [80]. The solution adopted by Boeing represents a dramatic shift from traditional airframe philosophy and creates a considerable number of new challenges. This solution was selected by Boeing in order to achieve the goal of 20% less fuel consumption per passenger compared with the Boeing 767 or the Airbus A320, but the weight saving, changing the technology from aluminium to CFRP will be 3% or less due to modifications in the initial design according different sources, although just after the final design will be possible to estimate the real weight savings.

Further advantages have been possible with the replacement of aluminium alloys by CFRPs such as reduction in the number or parts (rivets and other fasteners to join the stiffeners to the skin), an expected reduction in the maintenance costs in 30%, the increase of the passenger comfort and Leaner manufacturing processes, [81].

Airbus adopted the same approach in materials selection as Boeing in order to improve the efficiency of its twin aisle long range aircraft. The A350 XWB, presently in design and development phases, will use intensively composites in primary structures, (52% of the airframe weight), Figure 3.4. The fuselage design approach is distinct from the one used in the Boeing 787. Boeing uses a monolithic barrel construction. The barrel is constructed integrally, where the composite strips are applied to a spinning barrel using multiple robotic tapes laying heads, [82]. In the design of the Airbus A350 XWB fuselage, each barrel is composed by four reinforced panels in CFRP, (4 shells concept: top, bottom and laterals), each one attached to metallic frames, in aluminium-lithium alloy or in titanium. The A350 XWB fuselage is a hybrid solution (skin, doublers, joints and stringers are in CFRP) that will save weight via optimization of the fibre lay-up and thickness of the different skin

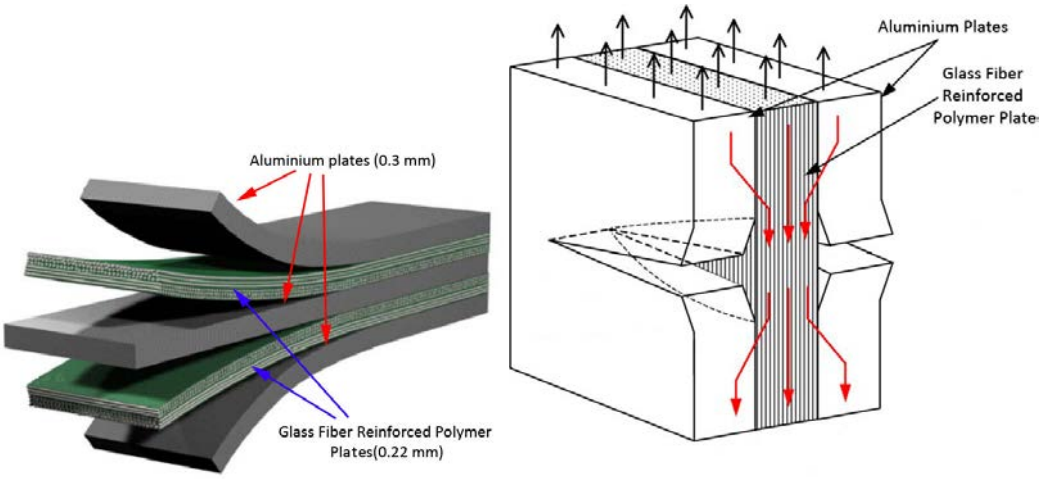

(a) Glare concept, example of 1.4 mm thick sheet, [87]

(b) Glare crack bridging, [88]

Figure 3.7: Glare (glass-reinforced aluminium laminate) concept.

panels, which can be tailored to the local load requirements of each individual airframe part, [65].

3.2.3 Fibre Metal Laminates

Fibre metal laminates are hybrid materials developed focusing on aeronautical applications, particularly for fuselages. The development of these materials started in 1945, with cooperation between Delft University and Fokker in the Netherlands. The material concept consists on aluminium sheets bonded to sheets of embedded fibres, [83]. After few years of product development, a patent with the concept of fibre metal laminate was submitted in 1982, [84]. Firstly, ARALL (aramid aluminium laminate) composed by aluminium plates and tough aramid fibres was used to improve the specific strength, protecting the fibre/epoxy layers by aluminium in order to allow water permeation. This material presented drawbacks concerning fatigue behavior and was ten times more expensive than the aluminium. After some research it was demonstrated that the weakness of this material was the difficulty of adhesion between aramid fibres and epoxy resin since the fibres can easily split, [85]. Therefore, several other alternatives were studied. Carbon fibres are not suitable material to combine with aluminium plates, due to the galvanic corrosion; however glass fibres, while still being a strong material, do not interact with aluminium. In this way, a new fibre metal laminate with aluminium and high strength glass fibres, denominated Glare, glass-reinforced aluminium laminate, was developed and patented in 1991, [86].

Figure 3.7a shows schematically the Glare concept; with the orientation of the glass fibre it is possible to optimize the structure. The University of Delft demonstrated that this type

of material presents an exceptional fatigue resistance as a result of the crack bridging effect of the glass fibres in the cracks located in the aluminium plate, as represented in Figure 3.7. Some of the fatigue properties are also improved compared with the fibre reinforced composites, mainly the damage tolerance to the low-energy impacts, an important issue in fibre reinforced composites. A recent application of Glare is in the upper fuselage shell of the Airbus A380 offering 15-30% weight savings over aluminium panels with improvement in fatigue properties, [89]. Taking advantage of the mechanical characteristics of this material, the application of Glare panels on this aircraft is done mainly in the upper fuselage part, Figure 3.8, since the major stress in these areas are tensile stress.

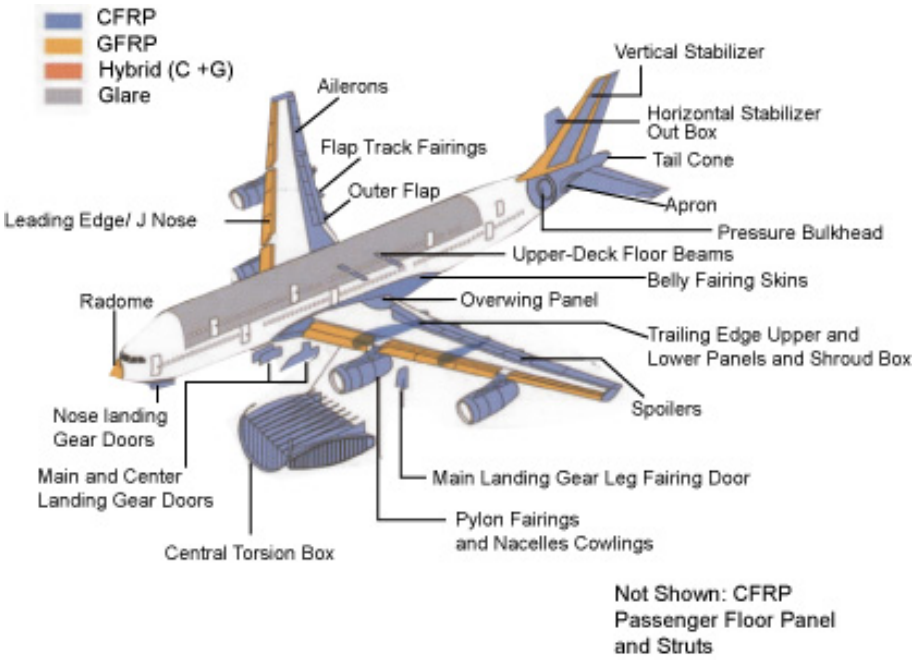

Figure 3.8: Glare panels in the Airbus A380, [90].

3.2.4 Materials Comparison

Most of failures in structures occur due to fatigue, inclusively, some structural engineers indicate that 80% to 90% of all structural failures are due to fatigue, [91]. In aircraft structures most of the parts are subject to cyclic loads and the fatigue behavior of the components is an important issue, considered during the design phase using damage tolerant philosophies. The damage tolerance criterion is used for structures subjected to dynamic loads and assumes that the structure is tolerant to flaws with a maximum size defined during the design phase. These flaws and damages are controlled by periodic inspections during the life cycle of the structure using non-destructive inspections. The maximum flaw

size and the growth rates are estimated previously in order to guarantee the structure's safety safety evidence supported by analyses.

The fatigue life of structural components can be decomposed in three distinct phases. The first phase is characterized by the appearance of the flaw. This flaw can be a result of fatigue of the structure or be generated by an external damage source. A second phase is related to the stable and slow growth of the crack under the fatigue loads. Depending on the stress state in the crack tip and the properties of the material, the structure can tolerate thousands of cycles before the flaw reaches a critical value. The third phase corresponds to the failure of the structure, which in the case of thin shells (as found in fuselages) is associated to a R-curve residual strength behavior before the complete rupture.

Figure 3.9 represents the different phases for a component subjected to high cycle fatigue. These modes are interconnected, nevertheless crack growth can occur without nucleation and the fracture of the structure can occur without previous crack growth.

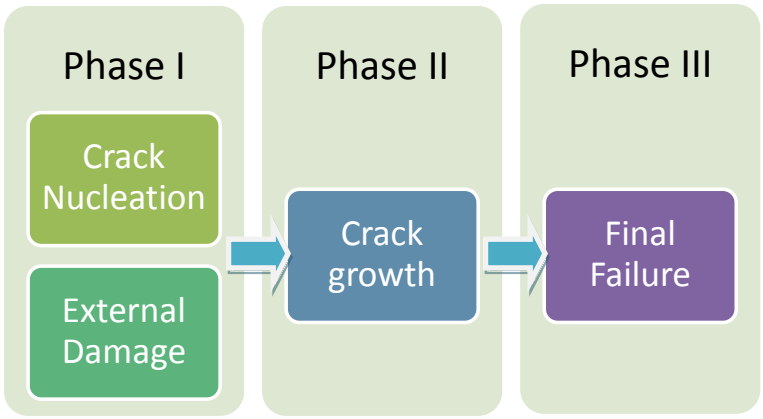

Figure 3.9: Phases in the fatigue life of a component.

The materials presently applied in fuselages have distinct fatigue crack propagation behaviors, as presented in Figure 3.10. With these different behaviors, it is not reasonable to carry out direct comparisons of the materials based on the fatigue performance. In the case of composite materials, different modes of fracture can occur as delamination between layers, internal delamination, matrix cracks and fibre fracture. These modes are linked to distinct crack propagation behaviors. Nevertheless, it is feasible to make comparisons with equivalent damage scenarios.

Composites fatigue also presents a strong non-isotropic nature, where each layer presents different properties in different directions. These materials require a multi-layer layout to be comparable with isotropic materials, although it creates opportunity for structural strength optimization in the different directions using multiple layers.

matrix cracks as result of the cyclic loading[10]. Especially, when maximum allowable strains
ng used.
clear and general accepted method or approach has been found to predict the fatigue behavior of
s. The variety in possible composite materials (fibers, matrix systems, lay-ups) induces a large
l responses to cyclic loading, which seem to prohibit a general approach to describe the fatigue
licity of crack lengths being the dominant damage parameter in monolithic metals has confused
n their attempt to determine a method based on a single damage parameter. A single damage
t make any sense for the
multiple damage modes in

tigue response of composite
not the design driver, static
ecially the small strain to
the allowable stresses
signer should be aware that
es in the structure might
ctural properties in time.
ct is incorporated in the
gn by knock down factors.
to their overall degradation
cracking and delaminations,
structure is usually not an
ue damage exceeds the
ral degradation due to
ctural usage, components
ed. Metals however, show

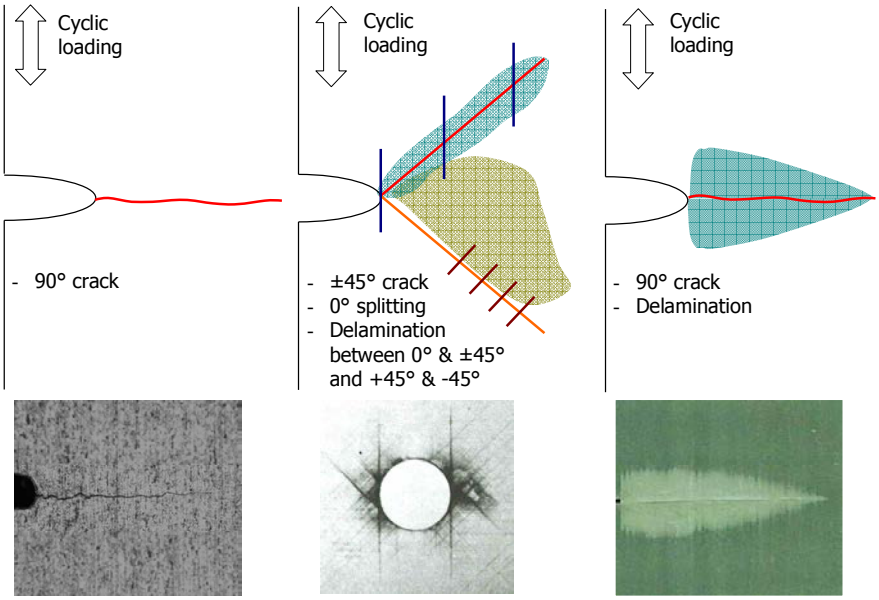

Figure 5. Illustration of fatigue damage modes in metals, fiber reinforced polymers and fiber metal laminates

Figure 3.10: Fatigue crack propagation modes for metals, fibre reinforced composites and fibre metal laminates, respectively, [92].

Crack Nucleation

Crack nucleation is a phenomenon that occurs in ductile materials when exposed to cyclic loads above a minimum value, function of their properties. The crack nucleation in fatigue is associated to the slip of grains. Slip lines appear at early stages of fatigue, and with the continuation of application of cyclic loads these slip lines broaden into bands in which fatigue cracks ultimately form, [93]. Fatigue strength characterization is done with standard specimens that are tested under constant cyclic loading, usually below the yield strength, measuring the number of cycles until the complete failure. The standard representation of fatigue strength is commonly done with SN (or Wöhler) curves where the stress amplitude or the maximum stress is represented as a function of the number of cycles. Two different factors are generally considered for these curves, the load ratio ($R = \sigma_{min}/\sigma_{max}$) and stress concentration factor (K_t).

Figure 3.11 shows two SN curves, with the fatigue strength in ksi, of the common aluminium alloy AA2024 with heat treatment T4, for different load ratios and for two stress concentration factors (K_t=1 and K_t=3.4). It is noticeable that the notch with a stress concentration factor equal to 3.4 reduces significantly the fatigue strength of the material.

SN curves for carbon fibre reinforced polymers present a slightly different behavior with lower fatigue strength drop, as shown in Figure 3.12, since this material is less sensitive to the crack nucleation phenomena. This is one of the advantages of composites compared

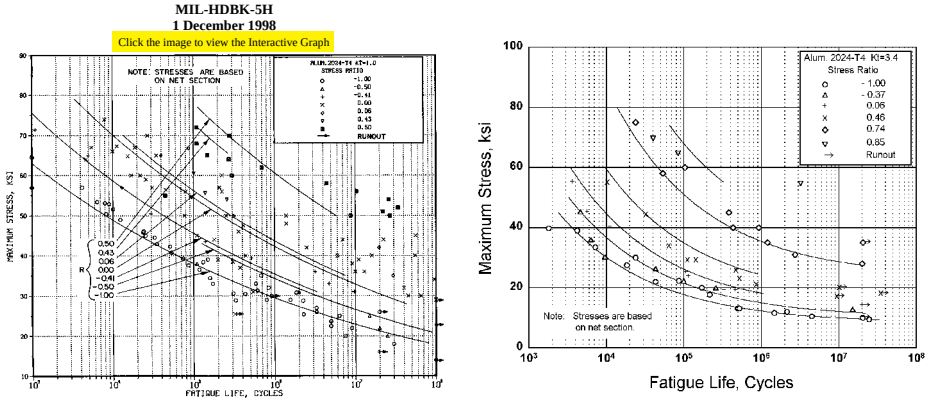

(a) Stress concentration factor $K_t = 1$ **(b)** Stress concentration factor $K_t = 3.4$

Figure 3.11: SN curves in ksi, for different load ratios and two stress concentration factors, [94].

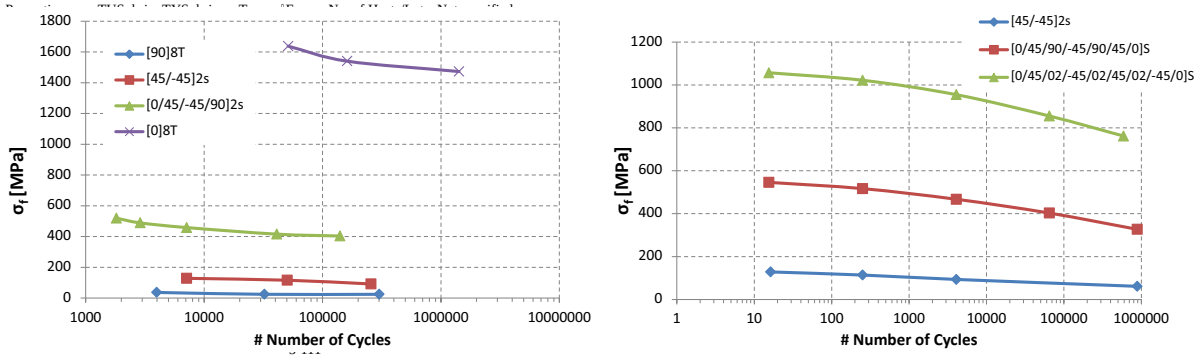

(a) Unidirectional layers **(b)** Comparison with multi directional layers

Figure 3.12: SN curves for CFRP in different configurations, [95].

with aluminium alloys and with other lightweight metals. Figure 3.12 presents SN curves for different configurations of fibre orientation, which has a significant influence in the fatigue strength. Combining different layers orientations it is possible to design structures in order to obtain higher resistance to the fatigue.

Regarding Glare materials, the fatigue nucleation is induced by the aluminium layers reducing the fatigue strength. Figure 3.13 shows a comparison of the SN curves between the Glare and the aluminium alloy AA2024-T3. Stresses in Glare are related to the overall applied stresses as well as to the stresses in the aluminium layers.

Fatigue Crack Growth

The stage linked to stable crack propagation, where the crack grows progressively up to a certain limit preceding final rupture, follows crack nucleation. This stage has significant importance in damage tolerant design, since the crack growth rate is an estimation of

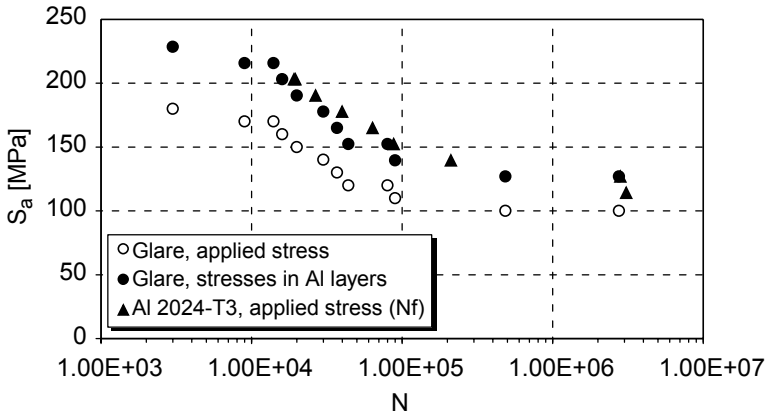

Figure 3.13: SN curves for Glare and comparison with the aluminium alloy AA2024-T3, [96].

the tolerance of the material in the presence of damages or cracks. The damage tolerant design of a structure estimates the maximum number of cycles (or the remaining life) that the structure can withstand after detection of a defect. This is done using the material characterization, particulary da/dN vs. ΔK curves, which measure the crack propagation rate (a is the crack length, N is the number of cycles and ΔK is the amplitude of the stress intensity factor, function of the load amplitude, geometry of the structure and crack size). Figure 3.14 presents, schematically, the typical shape and behavior of the curves and their comparison for metals and brittle materials as composite materials. The metallic materials have advantage in this point and that is the main reason why these materials are called damage tolerant materials.

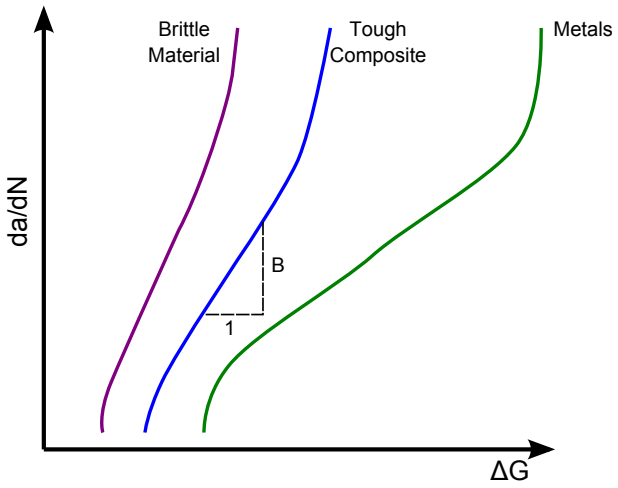

Figure 3.14: Typical da/dN curves for different groups of materials.

The stress intensity factor (K) concept and the amplitude of this factor ($\Delta K = K_{max} - K_{min}$) are used to characterize crack growth rates (da/dN) mainly in metals, considering linear elastic principles, since that the plasticity in these phenomena is negligible

in must of the fatigue life. The Linear Elastic Fracture Mechanics (LEFM) philosophy is applied in most metal structures due to this fact, contributing to a better estimation of the fatigue life. In fibre reinforced composites, the plasticized area in front of the crack tip has influence in the crack growth and needs to be considered for a correct fatigue life estimation. In fibre reinforced composites and in fibre metal laminates the crack growth rate curves are presented as function of dA/dN (where A is the crack or damage area) and energy release rate (G). Nevertheless, the stress intensity factor can be converted in energy release rate considering LEFM assumptions, and for plane stress (as the case of thin shells) can be estimated by:

$$G = \frac{K^2}{E} \tag{3.1}$$

where E is the Young's modulus of the material. For metal alloys a database with different curves of da/dN for different conditions is provided by Southwest Research Institute, NASGRO, [97]. Figure 3.15 shows the da/dN curves for the same alloy considered above, AA2024. These curves correspond to several experimental tests for different load ratios and the continuous lines are best fits to the experimental points using the NASGRO law. Figure 3.16 shows experimental points of a delaminated CFRP HTA/6376C carbon/epoxy

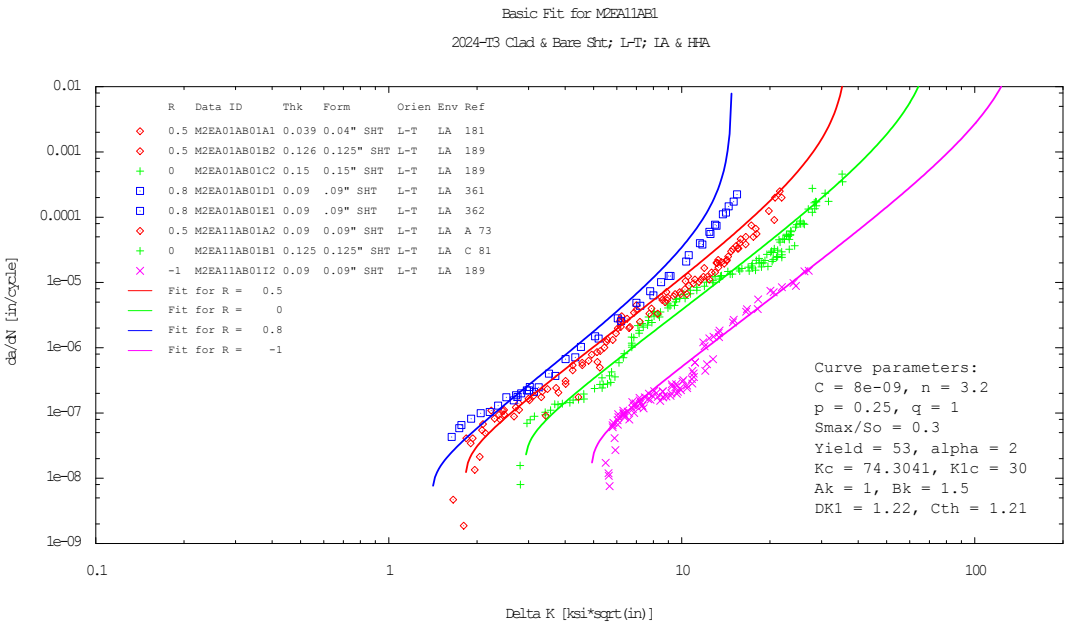

Figure 3.15: Crack growth curve, da/dN, for AA2024-T4, at different load ratios, [97].

material and one curve of a numerical method and other curve with a curve fitting of a Paris law. At the horizontal axis the energy release rate is normalized by the fracture toughness of the material in mode I. Due to the anisotropy of composite materials the crack propagation is analyzed in different directions and in different modes of crack tip deformation, tension (mode I), shear in plane (mode II) and shear out plane (mode III).

Shim *et. al.* in [99], measured experimental da/dN curves of cracked Glare 3-6/5 panels

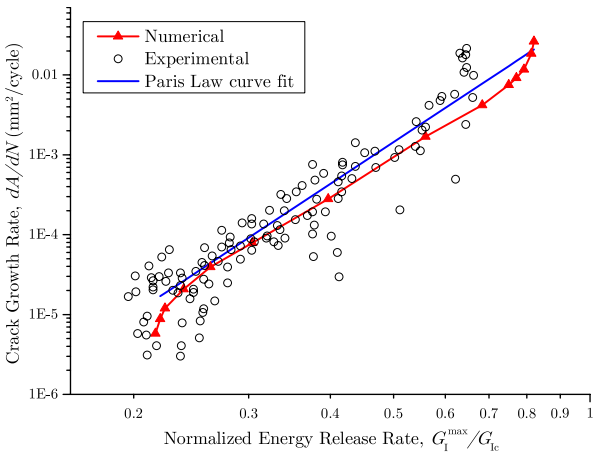

Figure 3.16: Crack growth curve, da/dN, for CFRP HTA/6376C, numerical, experimental and Paris law curve fitting, [98].

composed by 6 aluminium sheets and 5 glass fibre sheets ($[Al/0/90/Al/0/90/Al/90/0/Al]$). The experimental results were evaluated for three different stress range with maximum stress 80, 100 and 120 and with a load ratio $R = 0.05$ ($R = \sigma_{min}/\sigma_{max}$). Figure 3.17 presents the experimental data points measured. It is noticeable that the da/dN values are nearly constant with the increase of the stress intensity factor. This is one of the main advantages of Glare materials, since they tolerate high damage size with small reduction in the structural integrity, being a good material for damage tolerant design. Considering the different da/dN data and converting K to G with equation 3.1, plane stress formulation, and considering a reference of 1 mm thick aluminium sheet in order to convert da/dN to dA/dN, the different crack growth curves can be compared. Additionally, to take into account the material density for elucidation of the weight penalty for equivalent crack growth rates, a specific energy release rate (G/ρ) was used to compare the different materials. This comparison is presented in Figure 3.18. As expected, CFRP presents the lower damage tolerant properties and the Glare presents lower crack propagation rates for higher energy release rates. Nevertheless, the experimental data found in literature for Glare do not include the crack growth rates in the threshold area, possibly due to the difficulty of measuring the crack/damage length in this type of material.

Despite the lower damage tolerant properties of the CFRP, the adoption of these materials is due to the higher strength properties (static and fatigue), as noticeable in Figures 3.11 and 3.12. As explained above, the CFRP is still a less understood material when compared to the aluminium alloys, and it is expected that the most predominant damage is due to external impacts causing delaminations contrasting with metallic structures, where critical damage is mainly due to fatigue. Therefore, several types of uncertainties have

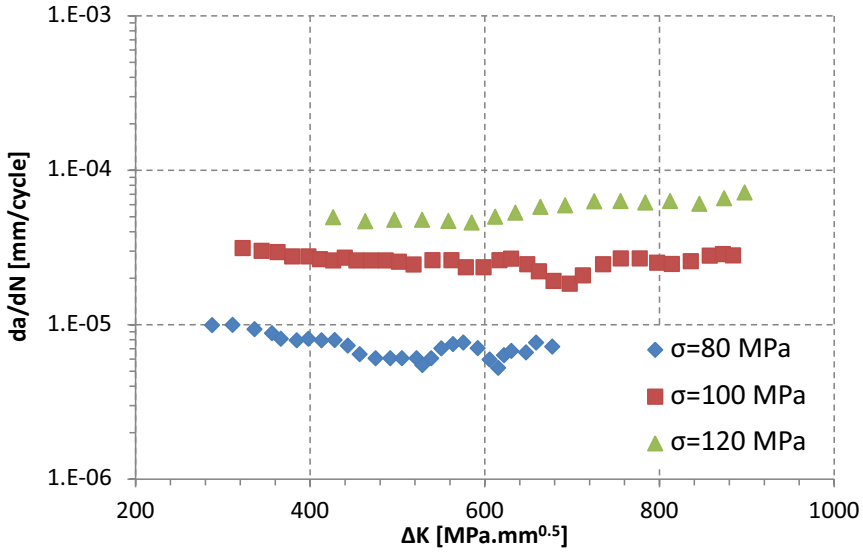

Figure 3.17: Experimental fatigue crack growth rates for Glare-3, under maximum stresses of 80, 100, and 120 MPa, [99].

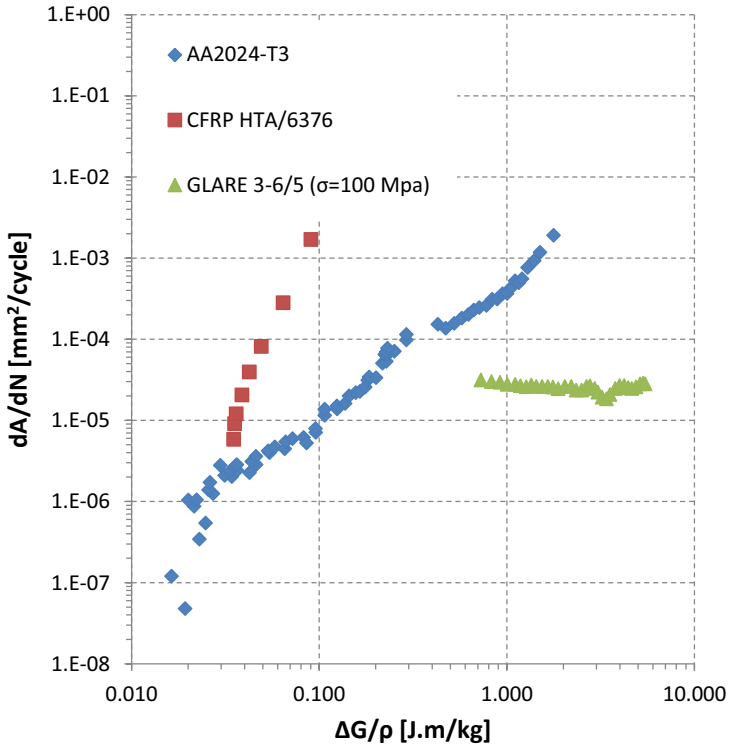

Figure 3.18: Comparison of fatigue crack growth curves for different materials.

been identified and compared in damaged aeronautical structures. Table 3.1 lists several of these uncertainties in the structural aeronautical design with aluminium alloys and CFRP, based on the reliability damage tolerant design research done by Lin *et al.*,[100].

Table 3.1: Damage uncertainties in metals and composites in aeronautical structures.

	Fatigue damage, metal	**Impact damage, composites**
Type of uncertainty	Predominantly: fatigue crack	Predominantly: external impact damages
Location of uncertainty	Predominantly: stress concentration locations	All structure, mostly on exposed partss to impacts
Size of uncertainty	Limited to the non destructive techniques, although the design accepts it and can be stopped.	Created instantly, then usually doesn't grow.
Predictive methods	Well developed, the fatigue life can be predicted with reasonable accuracy	Poor prediction due to lack of appropriate statistical data
Inspection interval	Predominantly: should be enough to detect any crack before to reach a critical size	Uncertain: no deterministic criteria to follow

3.2.5 Material Tendencies

At short term it is foreseeable that the main structural materials used will still be aluminium alloys, CFRP's and fibre metal laminates (mainly Glare). The tendency for growth of percentage of CFRP materials in fuselages is not definitive, due to the last events in the Boeing 787 development regarding to the possible speculated weight penalties [101], manufacturing control as in the horizontal stabilizers, [102] and several safety concerns about the behavior of these materials under service, [103]. The structural solutions adopted in the next generations of aircraft will be a function of the success in the application of the CFRP in the Boeing 787 and in the Airbus A350 XWB. This possible success will be function of the real total life cycle cost (including manufacturing and maintenance), the material behavior in operation and weight savings that can be achieved. A full understanding of these variables will be possible only after some years of service with this option. Nevertheless, new aluminium alloys, as Al-Li mentioned above, are serious candidates for fuselage. For instance, Bombardier chose Al-Li alloys for the next medium range aircraft (C-Series). The Al-Li alloy that will be used, will be perhaps AA2099 or AA2199 from Alcoa or the AA2198 from Alcan (Rio Tinto), with improved fatigue strength, toughness and corrosion resistance, allowing to reduce the structural weight (it is speculated 25% of weight savings), [104]. An optimal solution is tailored fuselage composed by multiple materials taking advantage of their best properties, without an increase of the

manufacturing costs. During the early stages of its development some of these materials present enhanced properties, and will be also prospective candidates to be used in primary and secondary aeronautical structures. Three groups of potential disruptive materials that Boeing has been watching closely are the low density intermetallics, the nanomaterials and morphable materials, [33]. In a long term, Noor *et al.*, [105] suggested that the major advances for new structural technologies for aerospace systems can be grouped into six categories:

- Smart materials and structures
- Multi functional materials and structures
- Affordable composite structures
- Extreme environment structures
- Flexible load-bearing structures
- Computational methods and simulation-based design

According to the mentioned authors, [105], regarding fuselage structures of sub-sonic aircraft smart, multi-functional and affordable composites structures are the most important groups of materials. Computational methods and simulation-based design will also provide better solutions in the design of fuselage primary structure since more detailed models can be calculated and the model refining will be easier, giving a better and faster understanding of the structural and material requirements required for an optimal structure. The multiphysics models will also take into consideration more materials properties in the design, allowing a wide understanding of the structure behavior in different conditions and environment.

3.3 Joining Processes

Joining processes are essential components of the manufacturing and assembly effort in most of engineered mechanical parts. For instance, data published in 2008 states that material joining technologies are responsible for approximately 7.1% of the manufacturing added value in the vehicle transportation sector in Germany, [106]. These joining processes are fundamental in the design and fabrication of large civil aircraft due to the semi-monocoque construction, requiring thousands of meters of structural joints in order to join all parts. Usually, these joints produce weakness points due to stress concentrations, areas exposed to corrosion and prone to manufacturing defects during the joining operations. From an idealistic (and from a Lean philosophy) point of view, structural joints should be avoided since they do not originate direct added value and they increase the structural weight. Also, the reduction of the number of parts is one of the guidelines of the design for assembly, to decrease the productions costs and lead times. Nevertheless, it is completely unfeasible to create large reinforced structures composed by just one piece. In addition,

from the manufacturing and assembly side, large structures can create difficulties in their manufacturing and in tolerance management, and from maintenance side, the replacement of parts is more unsuitable. Three main joining processes are used to join the structural aeronautical parts: fastener joining, bonding and welding, fastener joining being the predominant process.

3.3.1 Fastener joining

Fastener joining is widely used to manufacture aeronautical structural joints due to a number of advantages: it is a low cost process which does not require highly skilled operators; it can join entirely dissimilar materials, it does not change material microstructure, it does not require special joint preparations, and structural parts can be disassembled an replaced without damaging the remaining parts. In addition, this joining method allows material physical discontinuity, i.e., the damage propagation through the joint may be arrested due to the absence of a continuous material path.

Hundreds of different kinds of rivets and fasteners can be found in a single aircraft due to the different structural and aerodynamics requirements. Along the airframe joints, the countersunk head rivets or the blind head rivets are the most common rivets, although more complex geometries can be found, [107]. The countersunk head rivets were essential in the fuselage skin in order to not deteriorate the aerodynamics. Hi-shear rivets are also common in the fuselage to improve the shear strength, where instead a solid shank is used a screwed collar. In situations of difficult access or for alignment of the joints, threaded fasteners are applied, as the Hi-Lok fasteners composed by a threaded pin and threaded locking nuts.

The application of these fasteners still is a labor intensive process, requiring specialized workers to perform the several tasks as hole drilling, countersinking, deburring, riveting, shaving and sealing, consistently. The aircraft manufacturers have been attempting to carry out this work automatically, however in some components this is difficult due to the physical access to both parts of the joints and due to the accuracies required, [108]. Nevertheless, automated riveting is being used successful and has been replacing the manual riveting in many parts, as the A380 wing box assembly at Airbus, [108], A320 wing panels, [109], presented in Figure 3.19a and in skin panels and covers, Figure 3.19b.

3.3.2 Adhesive Bonding

Early application of adhesive bonding were in primary aeronautical structures since the origins of the aircraft due to the use of wood parts. After the transition of wood to

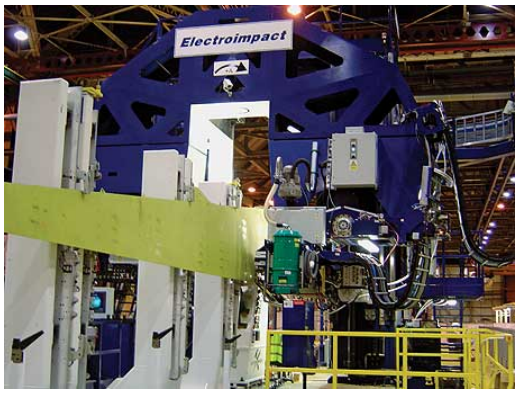

(a) Electroimpact rivet injector, [110]

(b) Skin panels automatic riveting (*Source: Brötje Automation*)

Figure 3.19: Automated riveting systems.

metals materials, bonding fall out of use. In 1941 a vinyl-phenolic adhesive was developed and was applied in the Havilland Hornet fighter for stringer-skin joints, [111].

The application of adhesives in primary structures has been found in metallic and non-metallic joints, as airframes joints joining the stringers to the skin in the fuselage and wings or the metallic sheets to the honeycomb cores (applied for instance in the elevators and spoilers), [112]. The joint strength under shear loading is satisfactory. However, in joints where the major stresses are tensile, adhesive bonding is avoided due to the possibility of peeling failures. The proclaimed advantages of the bonding joints are related to the integral joint (the joint is joined continuously), when compared with riveted joints: points of stress concentration are reduced, and in joints of two metallic parts, they do not contact due the adhesive layer, avoiding fretting, [113].

The most typical adhesives in aeronautical structural joints are based on the phenolic or epoxy resins with hot or cold cure. In the hot cure, the adhesive reaction is based on condensation reactions (as the Hexcel Redux adhesives) and in the cold cure, a catalytic reaction occurs to cure the adhesive, requiring a catalyst that is mixed with the adhesive (the most common in these group are the Araldite adhesives), [112]. The application of adhesives has been growing in the composite materials structures, as in the Boeing 787 where epoxy resins are applied to bond various laminates and fuselage parts, [114]. Figure 3.20 shows a picture of a fuselage barrel of the Boeing 787 where the composite stringers are co-bonded to the skin without fasteners can be observed.

The adhesives can be also applied as films and pre-impregnated to produce and join hybrid panels (as the aluminium composite laminates or GLARE). In critical applications, adhesives are applied together with other joining processes, as riveting or fastening, improving the joint strength by 1.5 to 2 times, and enhancing the joint reliability and

Figure 3.20: Fuselage structure of Boeing 787, stringers bonded to the skin.

durability, [115]. However, in these critical applications, the fasteners do not carry out loads and are used in order to have a damage tolerant joint, since in bonded joints it is difficult to apply non-destructive techniques to detect delaminations and kissing bonds.

When adhesives are exposed to extreme environments, their static and fatigue strength can be compromised. For instance, the humidity exposure of adhesive bonded aluminium structures can severely affect their performance, reducing its strength, [116]. In this study, Ashcroft *et. al.* showed also that in adhesive bonded composite structures the temperature has a considerable effect on mechanical strength and it was responsible for the failure in most of tested cases.

3.3.3 Welding

Welding is a joining alternative mainly applied in metallic structures, however it can also be used to join ceramic and thermoplastic polymer components. This process is widely applied in many different sectors due to the high joint efficiency without substantial weight penalty. This joining process can be easily fully automated and in most of applications is an inexpensive process when compared with the fastened applications. An important drawback is the disassembly of these joints since it cannot be done without the destruction of the weld, [117].

Its application in aeronautical structures is an attractive option since it allows joints with less stress concentration points and might be applied efficiently without overlapping the two joining parts (with a butt-joint configuration) reducing the joint weight. This weight reduction can have a small impact in the production costs, but has an huge impact in the life cycle costs. However, the application of welding process has been limited due to two major reasons: low crack arrest in welded joints compromising the structural integrity and

the weldability of the aluminium alloys used in the airframes. Several welding processes can now deal with the low weldability of the hardened precipitated aluminium alloys, although the low crack arrest persists and is an obstacle for massive adoption of this joining process.

Nevertheless, the application of the welding process has been growing to join metallic structures. Two examples of these applications are presented in Figure 3.21. Electron Beam Welding (EBW) has been adopted to join titanium parts in military aircraft, as in Lockheed Martin F/A-22, where GKN used EBW to join the different parts of the aft boom, Figure 3.21a reducing by approximately 75 percent the use of fasteners, [118]. Laser Beam Welding (LBW) has been used by Airbus to join the fuselage stringers to the skin in the A318, A340 and A380 eliminating thousands of fasteners. However, this application is confined to the lower panels of the fuselage since the stresses are mainly compression, being less exposed to fatigue cracks. These two welding processes are based on high concentrated energy beams which originate small heat affected zones and the distortion.

Other welding processes had been adopted by aeronautical manufacturers as the Gas Tungsten Arc Welding (GTAW), Plasma Arc Welding (PAW) or Variable Polarity Plasma Arc Welding (VPPA) and diffusion welding, but just for specific applications, [119, 120].

The joining process adopted in this research is based on different physic phenomena, since during the welding the material is not melted, improving in this way the joint strength as will be analyzed in the following chapters.

(a) Electron beam welding in F/A-22 titanium aft boom, [121]

(b) Laser beam welding at A380 stringers, [122]

Figure 3.21: Application of welding processes in aeronautics.

Chapter 4

Friction Stir Welding Process

The major obstacles to the introduction of welding processes in aeronautics were related to the loss of mechanical properties due to the large heat input, defect control (process reliability) and the impossibility to weld precipitated hardened alloys (as AA2024). Some of these issues are mitigated with the application of newer joining processes that require less heat input and are more trustworthy. Friction stir is the most appealing welding process in aeronautical structures since it has been shown to produce joints with excellent properties when applied to aluminium alloys.

4.1 Process

FSW is a breakthrough welding process, invented in The Welding Institute, UK, by W. Thomas, [123]. It is a solid-state (or a semi-solid) joining process which joins integrally plates or sheets, mixing them along a welding line without fusion. The main concept of this process is a non-consumable rotating tool that is inserted into the abutting edges of sheets or plates to be joined and traversed along the line of joint, Figure 4.1.

The welding tool for friction stir welding is elementary, composed just by a pin and a shoulder, Figure 4.2a, which can be integrated in a single piece. The shoulder applies most of the vertical load, generating most of the heat during the process due to the rotational friction between the tool and the plates and due to the linear movement of the tool. It also pushes the material in order to prevent the material uplift. The generated heat softens the material to a plasticized state (semi-solid state) around this tool, which combined with the material flux promoted by the rotation, forces the material blending of both parts, creating a joint without a fusion of the materials. Multiple shapes for the pin geometry can be applied to improve the material flux and the surface appearance. Several tool designs to optimize the final welding properties and parameters that attempt to quantify the material flux as swept volume to pin volume ratio, [124], have been developed,

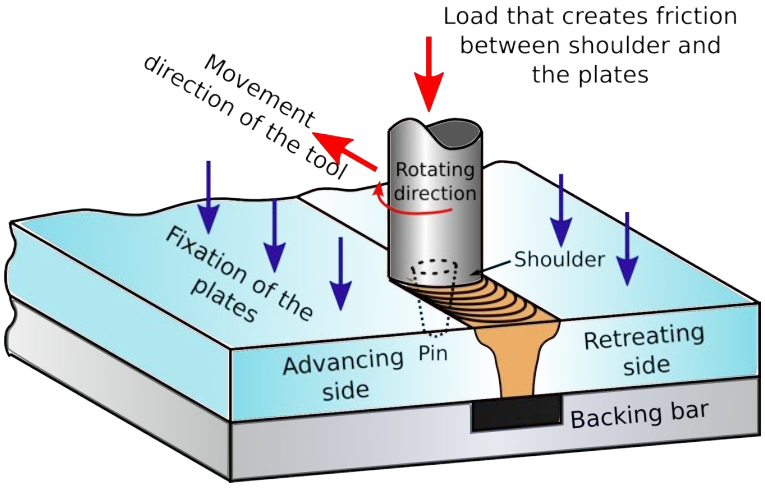

Figure 4.1: Friction stir welding process.

The vertical load and the torque applied by the tool results in horizontal loads in the plane of the plates and vertical loads that need to be reacted by external supports. The external support which holds the parts that will be welded are schematically represented in Figure 4.2b. The area behind the tool, under the plates, usually includes a removable part, since the pin tip might touch the bottom and damage this part. The distance between the pin tip and the bottom of the plates needs to be tiny[1] for complete welding of the plates. When instability in the tool position control occurs, or when the plate presents thickness variations, the contact between the supporting holder and the tool is likely. The backing bar, illustrated in Figure 4.2b, usually a removable part, is therefore an important part with higher hardness and wear resistance than the materials to be welded.

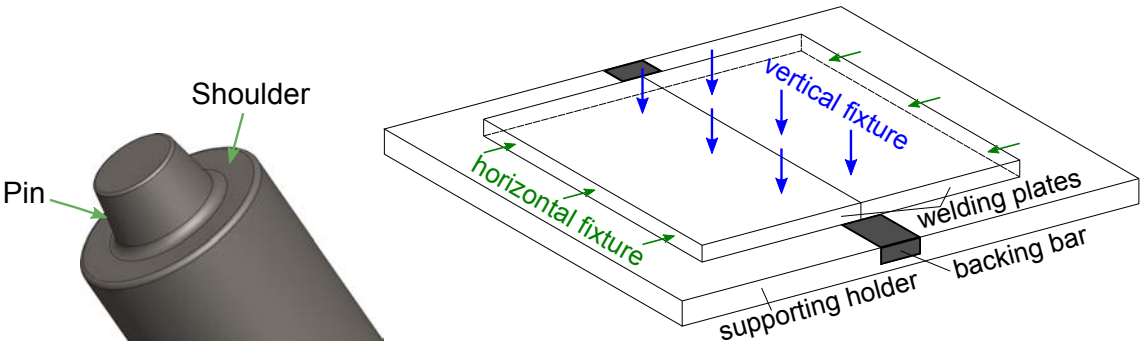

(a) FSW Tool **(b)** Clamping

Figure 4.2: Friction stir welding - tool and clamping.

[1]This distance is function of the tool, welding parameters and plates thickness, although 0.1 mm is a reference value for most of the situations.

One of the major limitations of this process is the reaction to the loads and torque applied by the tool in the work pieces, which restrains the applicability and portability of this process. The joint geometries conceivable with this process are illustrated in Figure 4.3. Typical configurations are butt-joints and overlaps joints, the others being variants of these two. These two configuration also have the advantage of not requiring special preparations (as the V shape required for butt-joints in fusion welding processes).

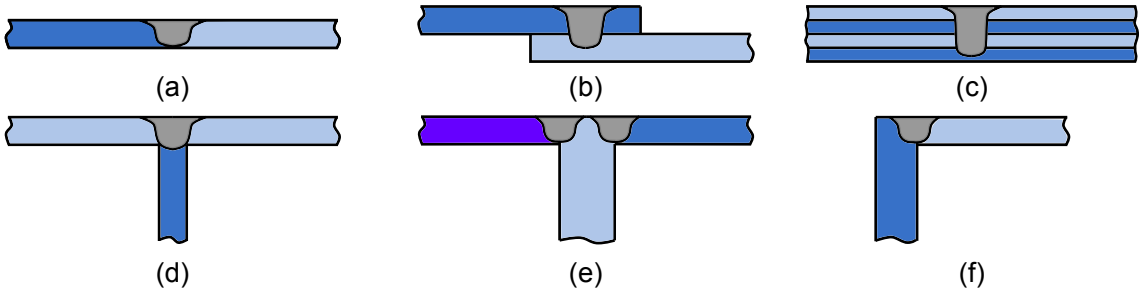

Figure 4.3: Friction stir welding - welding geometries.

When compared with other traditional welding processes, friction stir welding presents several advantages, some of which were described in two major books dedicated to FSW, [125, 126]:

Mechanical Benefits:

- Low welding distortion and good dimensional stability;
- Weldability in all aluminium alloys;
- Low residual stress;
- Low risk of cold cracking;
- Improved joint strength (static and fatigue);
- Weldability of dissimilar alloys and materials;
- No edge due to the filler material;
- Mechanized process;
- Good surface appearance;
- Leaner manufacturing process.

Economic Benefits:

- Improved materials use, no waste and possibility to welding plates with different thicknesses;
- Low energy consumption;
- Joint weight reduction (allowing fuel consumption reduction in transportation structures);
- Lower processing time;
- Reliable process (low defect rate);
- No consumables as filler materials or shielding gas.

Environmental Benefits:

- No shielding gases required and gases not released;
- Lower energy consumption in the process and during service;
- In most of the cases, does not require solvents for decreasing.

Nevertheless, the FSW process also presents some drawbacks and technical obstacles which might obstruct its implementation in some applications:

- Reaction to the process loads;
- Requires special fixture systems;
- Access to both sides of the working pieces;
- The beginning of the weld usually presents lower properties;
- The end of the weld has the keyhole;
- Limitations in the joint geometries, such as welding T corners;
- Tool control: distance between the pin tip and the backing bar;
- Root flaws along the welding line;
- Reduction of maximum elongation at break.

In most of the situations these drawbacks can be overcome with new concepts or modifications to the main principle. For instance, when the plates or the working plates are not completely flat, the tool should counterbalance the variation of the thickness, but keeping on the distance between the pin tip and the backing bar. This function can be done by reacting pin tools, where the pin position is controlled independently to the shoulder position.

4.1.1 Process Evolution

Friction stir welding has been experiencing a huge growth during the last 18 years with applications in multiple domains such as ship, automotive, train, aeronautical and aerospace structures. Figure 4.4 presents the number of filled and granted patents internationally, calculated by the author and based on the list of patents related to FSW published regularly by The Welding Institute (TWI), [127]. Analyzing the number of filled patents and granted patents, it is noticeable the considerable growth in the number of granted patents, still in expansion, although the number of filled patents has begun to stabilize, approaching to the upper part of a S curve, Figure 2.4. Nevertheless, this behavior needs to be confirmed along 2011, since the filled patents are not immediately public. However, in case this trend is confirmed, it might be motivated by two reasons: it may be due to the a possible decline of research and development resources focused in this process, or it may be due to the saturation of new solutions based on the friction stir welding principles.

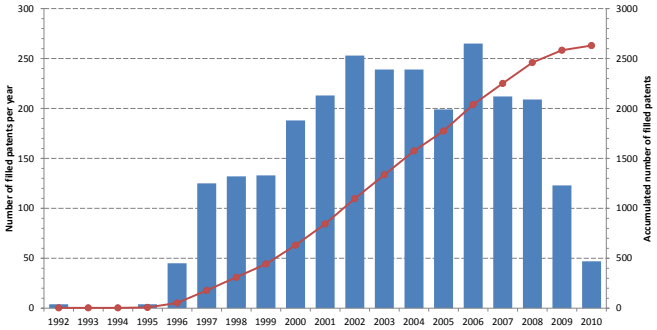

(a) FSW patents filled

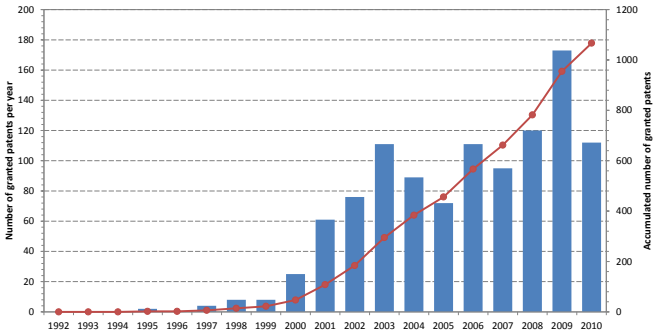

(b) FSW patents granted

Figure 4.4: Friction stir welding, number of filled and granted patents.

Most of these inventions are related to new concepts, new applications or new tools. One of the most significant advances was the bobbin or self reacting tool. This concept is presented and compared with the standard process in Figure 4.5. This concept does not require a backing bar, which is an interesting advance to weld parts with difficult access to both part sides in long welds. This concept was superficially described in the first FSW patent, [123], although other concepts had been developed as the ones by MTS Systems Corporation (USA), [128] or GKSS (Germany), [129] where the distance and load applied between the two shoulders can be actively controlled.

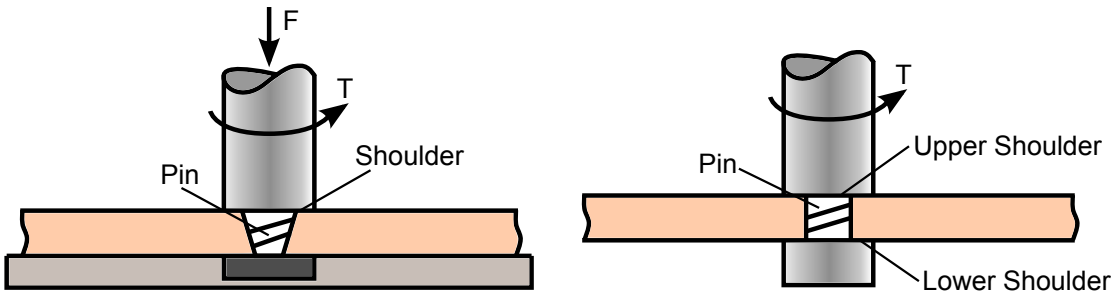

(a) FSW standard process **(b)** FSW bobbin tool

Figure 4.5: Friction stir welding standard tool vs. bobbin-tool.

The bobbin tool has been object of great interest in several companies and organizations, as at the NASA, USA, where two new concepts of self reacting tools were developed and patented. These two concepts are presented in Figure 4.6. The first concept, Figure 4.6a is a counter rotating bobbin tool composed by two shoulders that rotate in opposite directions. This concept has the advantage to react internally most of the forces and torques applied during the process. The lower shoulder presents a lower diameter than the upper shoulder, in order to balance the torque promoted by the pin. The second concept is a gimbaled bobbin tool, where one or both shoulders are gimbaled, allowing to the shoulders different tilt angles between the pin. This concept allows to handle slopes in the workpieces' surfaces in an easier way and it is also able to weld plates with different thicknesses, as sometimes it is required.

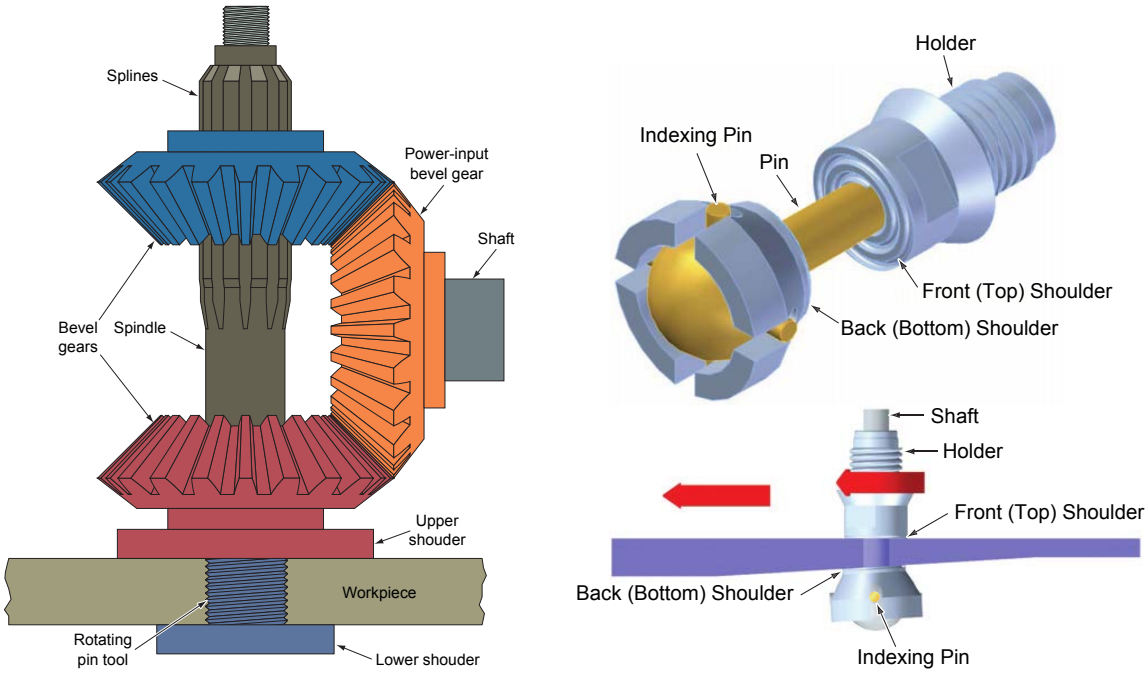

(a) Counter rotating bobbin tool, [130] **(b)** Gimbaled bobbin tool, [131]

Figure 4.6: Friction stir welding, bobbin tools variations.

FSW has been experiencing a fast spread to other domains outside of its initial purpose due to its ability to change, repair or improve material properties. Figure 4.7 shows schematically current variations of the original FSW process based on presentation by Burford and Widener, [132]. These FSW variations can be applied in different circumstances to manufacturing structural parts in a straightforward and effective way.

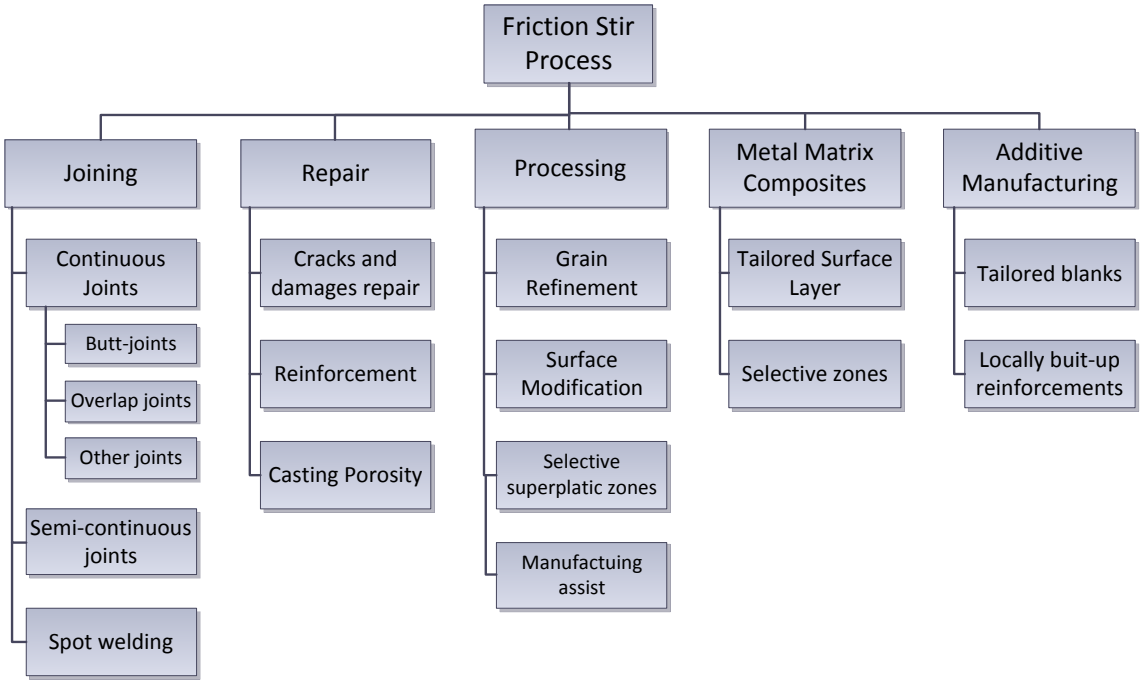

Figure 4.7: Friction stir process applications and developments.

4.1.2 Applications

The range of applications that adopted friction stir welding has been growing in multiple domains. The development of this process for different materials has supported this growth. Figure 4.8 is based on the Burford and Widener presentation, [132], and shows some of typical materials and respective applications currently are reported in the literature. Most of these applications are linked to aluminium alloys, as a result of the process readiness and reliability in aluminium alloys joining. Precipitation hardening (pptn) aluminium alloys (mainly 2XXX and 7XXX series) have low weldability with conventional processes due to the hot cracking phenomenon, making them impracticable for structural parts when high strength joints are required.

From the structural design point of view, the most essential property of a joint is its strength. For this reason, a quantitative evaluation of a friction stir weld based of the Base Material (BM) strength is commonly adopted. This assessment gives the efficiency of the joint, comparing its ultimate tensile strength or yield tensile strength with the corresponding properties of the base material. Considering the efficiency of ultimate tensile strength (UTS), this is calculated as:

$$Efficiency[\%] = \frac{\sigma_{UTS_{FSW}}}{\sigma_{UTS_{BM}}} \times 100 \tag{4.1}$$

Results for the classical Al alloy AA2024 showed that FSW can achieve efficiencies of about 98% in the transverse direction (transverse to the rolling direction) without post heat treatments or other post processing, [133]. In the Khaled extended review about friction stir welding, [134], some results from the literature for the alloy AA7050 are reported, showing that an efficiency of 96% was achieved for the ultimate tensile strength and 93% for yield tensile strength for a weld in rolling direction (lamination orientation) and tested in transverse direction.

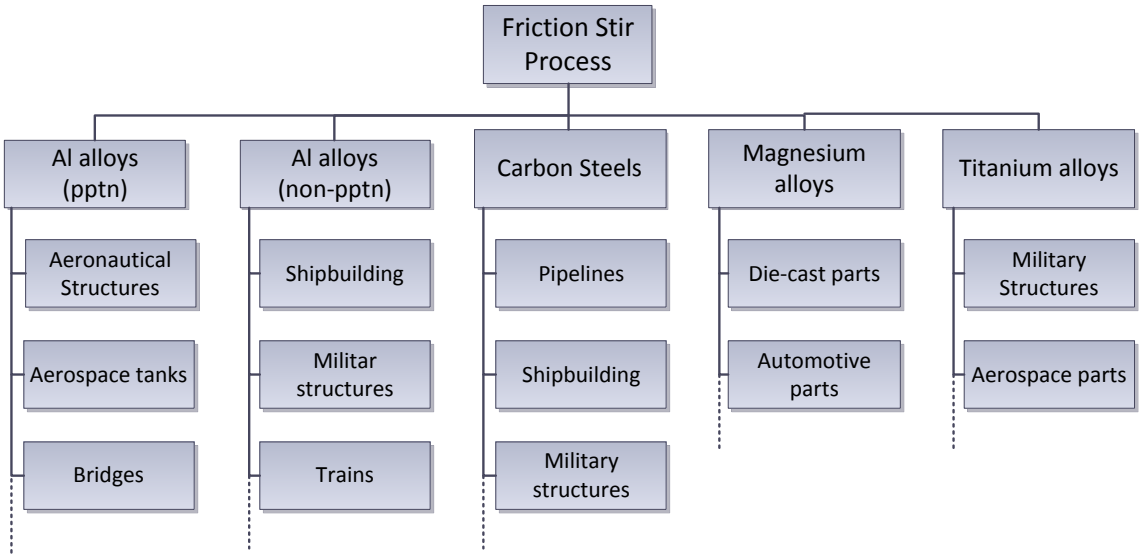

Figure 4.8: Friction stir process, materials and applications.

The number of structural parts manufactured with magnesium alloys has been growing during the last years (about 20% per year, higher that any other metal, [135]). This growth is related to the interest of the automotive industry, since Mg is an abundant material in the earth and has low density (about 1.74 g/cm^3), making the structures more efficient. However, Mg alloys have low weldability to be welded by fusion processes, limiting their application in automotive manufacturing. Johnson and Threadgill, [135], tested the application of FSW in four different magnesium alloys, achieving excellent results in the three cast alloys (AM50, AM60 and AZ91), with efficiencies nearly 100%. The wrought Mg alloy (AZ31) present lower efficiency due to the loss of heat treatment in the welding area, that might be recovered by post heat treatments. Weldability of magnesium alloys with aluminium alloys has also been demonstrated in several research works. Zettler *et. al.*, [136], showed that friction stir welds of AA6040 to AZ31 can have strength efficiencies higher than 80% without post processing operations.

The application of FSW to other materials has been increasing, with some peculiar applications as the case of low-carbon steel for pipelines. A portable orbital welding machine was been developed for this purpose, capable of welding the complete circunference in a

single-pass for a butt-joint configuration, [137]. Sound welds were obtained for different low-carbon steel as X65, X80, and X100. The joining of titanium alloys with FSW has been also investigated with promising results. Lienert, [138], demonstrated welds of Ti-6Al-4V with about 950 MPa of yield strength and 1030 MPa ultimate tensile strength (corresponding to nearly 95% of efficiency), however with a substantial reduction of the elongation at break. The major obstacle in welding of these materials is the temperature required to mingle the pieces, requiring tools with high thermal strength. For this purpose several tools with new materials have been developed. Refractory metals (tungsten, molybdenum, tantalum, niobium, and hafnium-based), [139], polycrystalline cubic boron nitride (PCBN) and polycrystalline diamonds (PCD) materials, [140], are materials that have been developed in order to make possible the welding of these high temperature materials, including the mentioned titanium and steel alloys, but also nickel alloys as the Inconel 600, [141].

Presently, a large number of companies are using the FSW process to join materials in a variety of sectors achieving interesting results. One of the first products that took advantage of the FSW process was a small business jet aircraft, the Eclipse 500. This aircraft has most of the airframe parts joined by FSW. The FSW process was applied to join integrally stiffeners and frames to the skin panels by lap welding. The skin areas which will be welded have pockets previously machined or chemically milled for reinforcement of the welded joints and reduction of the panel weight. The airframe skins that are welded include the cabin, aft fuselage, and wing skin panels. The most difficult technical challenges, compared with rivetted solutions, were related to the distortion control, corrosion protections and the understanding of the material properties for the design. FSW allowed to join the different parts six times faster than automated riveting solutions and 60 times faster than manual riveting and with higher quality, [142]. The gantry system used by Eclipse Aviation is presented in Figure 4.9, where other rig pre-prepared with the skin and different parts to be joined is visible.

Boeing was also a pioneer in the application of FSW, starting to look at this process as early as 1997, through the Phantom Works project, in order to develop concepts for various aircraft structural parts, and also military and aerospace applications. Some of these concepts are in the market, such as the Delta II and Delta IV fuel tanks, since August 1999, [143], the Boeing C-17 cargo ramp and in Boeing 747-8 freighter barrier beam, [144]. In November 2010 Bolse, [145], pointed out that Boeing has produced more than 8,900 meters of friction stir weld without defects, mainly for Delta rockets, which have already done 73 missions using welded tanks. Concerning space applications, further FSW applications have been developed to join safety critical structures which require high reliability. NASA in association with Lockheed Martin replaced the joining process in the Space Shuttle External Tank from variable polarity plasma arc (VPPA) to friction stir welding since it was concluded that this replacement will originate more reliable joints and with higher strength, [146]. The Space Shuttle external tanks are not reusable, requiring

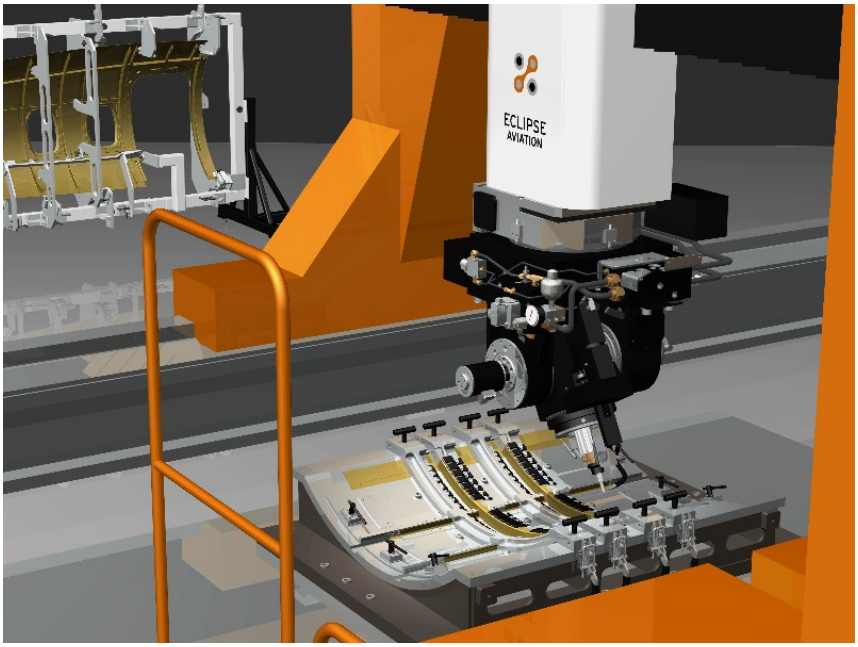

Figure 4.9: FSW gantry system at Eclipse Aviations. (Source: `http://www.plm.automation.siemens.com/en_us/Images/Eclipse-fsw_tooling_tcm1023-21267.jpg`)

new tanks for each mission. The first tank joined by FSW were ET-132, for the mission STS-128, was launched in August 28, 2009. In this tank and in the next one, ET-133, part of the longitudinal joints (in just two of the four hydrogen barrels) were welded by friction stir, using dissimilar aluminium lithium alloys AA2219 with AA2195. After these two proof-of-concept situations, in the remaining fuel tanks, all barrels (four liquid hydrogen tank barrels and a single liquid oxygen tank barrel) were produced with all longitudinal joints using FSW, [147]. Figure 4.10 shows two more applications of FSW in aerospace structural components. The NASA Orion crew module, Figure 4.10a, is part of the Constellation program, applies FSW to join the forward cone assembly and crew tunnel to the aft assembly, [148]. In this program, NASA also applies FSW to weld the upper stage of Ares I (a crew launch vehicle). This upper stage includes the liquid oxygen and the LH2 propellants tanks, done in Al-Li AA2195 plates, welded by FSW, [149]. Another space company that has been extensively applying FSW is the SpaceX, a new company in the space transport sector. It uses friction stir welding for the fabrication of the aluminum-lithium fuel tank of the Falcon 9, a cheaper spaceflight launch system. The circumferential joints are done using a bobbin-tool, solution similar to the adopted in space Shuttle tanks, and the longitudinal joints are done with the classical tool and backing bar, Figure 4.10b. The wall thickness varies between 1.6 mm up to 12.5 mm, [150]. The adoption of this processed allowed to speed up the manufacturing, the reduction of welding defects rate and a simple way to repair casual deficiencies.

(a) NASA Orion module (Source: `http://www.lockheedmartin.com/`)

(b) First stage of Falcon9 SpaceX tanks, (Source: `http://spacefellowship.com`

Figure 4.10: Application of FSW in aerospace structures.

4.2 Welds Characterization

Structural design for safety critical components, as the case of airframes, requires comprehensive characterization of the materials and joints properties. This characterization has to take into account a large amount of variables required for an accurate design in order to ensure the structural integrity during the different phases of the product life cycle. A mechanical characterization was performed during this research using a last generation aluminium-lithium alloy, with potential applications in aeronautical and aerospace components. This mechanical characterization was preceded by welding parameter calibration and comprised a program of experimental tests of welded joints. This work was performed at GKSS Helmholtz-Gemeinschaft Research Centre (now Helmholtz-Zentrum Geesthacht) in Geesthacht, part of Hamburg Metropolitan Region in Germany. The research performed was in the scope of a Cost Effective Integral Metallic Structure (COINS) project, part of the Sixth Framework Programme for Research and Technological Development of the European Union. The COINS project had the objectives of extending the application of integral metallic structure by friction stir welding with the industrialization of the state of the art of FSW technologies, and of developing new welding geometries and to create innovations in the design joints, [151].

4.2.1 Base Material

The aluminium-lithium selected to this material characterization was the AA2198. This alloy was developed by Alcan (presently Rio Tinto Alcan) and is part third generation of aluminium-lithium alloys, which are optimized Al-Cu-Li(-Mg-Ag-Zn) alloys. The best

known 3^{rd} generation Al alloys are the Weldalite alloys, developed by Lockheed Martin and applied to the Space Shuttle (comprising the alloys AA2196, AA2098, AA2050 and AA2195). The Weldalite 049 is the identical alloy applied in the Space Shuttle tanks, AA2195, and had high success since its high ultimate tensile strength of 713 MPa with a T8 temper, [152]. The composition of the AA2198, in weight percent, is presented in Table 4.1, according the Aluminium Association, [153]. This alloy presents a better balance between the maximum strength and toughness when compared with previous alloys.

Table 4.1: Chemical composition of AA2198 in (in wt.%).

Cu	Li	Mg	Ag	Mn	Zn	Fe	Ti	Si	Cr	Others	Al
2.9-3.5	0.8-1.1	0.25-0.8	0.10-0.50	0.5	0.35	0.1	0.1	0.08	0.05	0.15	Remainder

The Al-Li sheets used along this research were provided by Alcan Rio Tinto, and they were supplied with the heat treatment T851. This heat treatment is solution heat treated, followed by cold working and after an artificial aging. The cold working improve the nucleation of precipitates, decreasing the grain boundary precipitates and reducing the aging time required to achieve the highest strength. However, the highest strength in Al-Li alloys usually minimizes the toughness. A different aging process was developed by Curtis *et. al.*, [154], consisting in a low temperature underaging process (between 93°C and 150°C), giving a better combination of strength and fracture toughness properties. This aging process as been used in the Space Shuttle tanks, for the alloy AA2195.

A comparison of some relevant mechanical properties for different aeronautical and aerospace alloys are presented in Table 4.2 based on the references [97, 155, 156]. The base material used for the friction stir welds was characterized using tensile tests based on three specimens longitudinal to the lamination direction (L-T) and three transverse to the lamination direction (T-L). The tensile strength curves are presented in Figure 4.11. These two tensile curves demonstrates the differences of mechanical properties in both directions, there the L-T direction presents high strength and in T-L direction high elongation. The summary of the tensile properties is presented in Table 4.3 based on the average of the three specimens.

4.2.2 Welding Parameters

The friction stir welds were performed in a portal system developed at GKSS, Figure 4.12. A total of eight plates with dimensions of 300×500 mm were welded. The welding

Table 4.2: Mechanical properties comparison of different aluminium alloys.

	$\boldsymbol{\rho}$	$\boldsymbol{\sigma_{UTS}}$ **(L-T)**	$\boldsymbol{\sigma_{YTS}}$ **(L-T)**	$\boldsymbol{\varepsilon}$ **(L-T)**	$\mathbf{K}_{I_c}$
	$kg/m^3 \times 10^3$	MPa	MPa	%	$MPa\sqrt{mm}$
AA2024-T3	2.78	483	345	18	938.2
AA2098-T8	2.70	555	530	12	-
AA2195-T8	2.71	610	575	8.5	868.7
AA2198-T8	2.69	510	470	12	1390

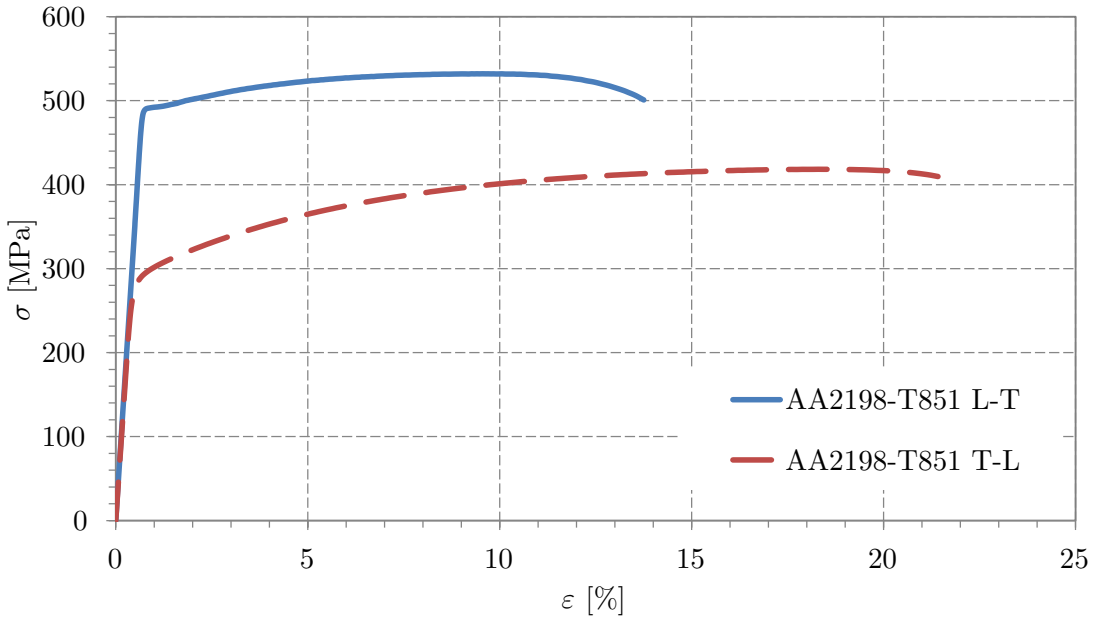

Figure 4.11: Tensile curves in L-T and T-L directions of AA2198-T851.

Table 4.3: Measured tensile strength values of AA2198-T851.

	$\boldsymbol{\sigma_{UTS}}$	$\boldsymbol{\sigma_{YTS}}$	ε
	MPa	MPa	%
AA2198-T851 (L-T)	532.3	491.2	14.0
AA2198-T851 (T-L)	416.5	288.2	20.6

parameters are presented in Table 4.4 obtained from previous optimizations at GKSS and by other partners of COINS project. The tool used in these welds was composed by a conical screwed pin with three facets and with 5 mm of diameter was used coupled to a shoulder with a diameter of 15 mm with one scroll and a radius convexity of 40 mm. From these welded plates, specimens for metallographic analyses, hardness measurements and tensile strength were cut.

Figure 4.12: FSW portal system at GKSS used to perform the AA2198-T851 butt-joints.

Table 4.4: Welding parameters AA2198-T851, butt-joints configuration.

Plate ID	Rotational Speed	Linear Speed	Load	Tilt Angle
	$[RPM]$	$[mm/sec]$	$[kN]$	$[°]$
COI[X]	600	5	8.5	0

4.2.3 Metallographic Characterization

The metallographic characterization of welded specimens is a common destructive procedure in friction stir welds in order to analyze the welded region and to check if the

welding parameters induce any internal defects. Correlations between these analyses and mechanical properties can be done, giving a deeper understanding of the welding procedures and parameters. For this characterization three samples of each plate were cut using an abrasive disc, in the beginning, in the middle and at the end of the weld. These samples were embedded in an auto-hardening resin, were polished and etched, immersing the sample during 30 seconds in a Keller's solution composed by 2ml of HF at 48%, 3ml HCl, 5ml HNO_3 and 190ml H_2O.

These specimens were observed using an optical microscopy with a digital camera. A couple of the results are presented in Figures 4.13 and 4.14. All the macrostructures observed do not present visible defects, except the beginning of weld COI8, Figure 4.14a. The uncompleted weld is due to the cut of the specimen being behind the beginning point of the weld. In these macrostructures a bright line in the bottom or in the top of some welds is visible, consisting of a line of precipitates, a defect in the base material. These defects did not change significantly the welds' properties. From these macrostructures, the different regions of the weld are also visible: the stir zone (SZ), the thermo-mechanical affected zone (TMAZ), the heat affected zone (HAZ) and the base material (BM).

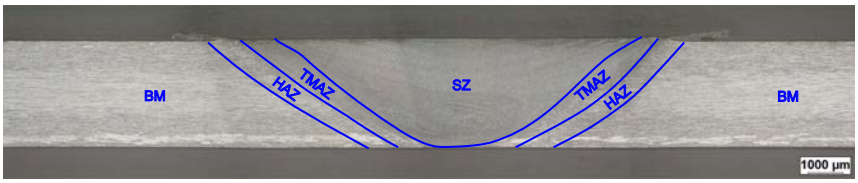

(a) Beginning

(b) Middle

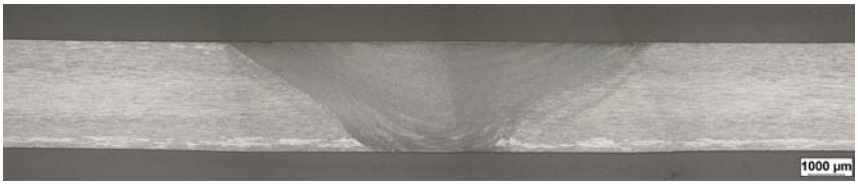

(c) End

Figure 4.13: Macrostructures of the AA2198-T851 FSW butt-joints, plate COI5.

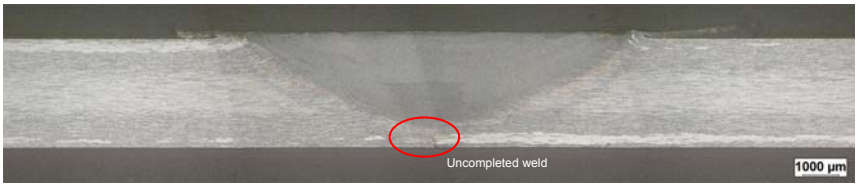

(a) Beginning

(b) Middle

(c) End

Figure 4.14: Macrostructures of the AA2198-T851 FSW butt-joints, plate COI8.

4.2.4 Mechanical Characterization

The determination of the optimum welding parameters (commonly called "sweet spot") is based on the mechanical characterization of welded specimens with different parameters. The common mechanical characterization at this stage is mainly composed by bending tests, tensile strength tests and microhardness measurements of the weld cross section. These tests give an indication on the choice of welding parameters that lead to defect-free welds. With a quantitative assessment and interpolations from the different points, it is possible to determine the ideal point to maximize the joint strength or other parameter.

The mechanical characterization done in the scope of this research didn't comprise the determination of the optimum welding parameters, since those parameters were agreed by the project COINS partners. Nevertheless, these results certify the properties of the final welding parameters, their mechanical properties and their variance.

Microhardness Measurements

The samples used for macrostructures were also used for microhardness measurements. These measurements were done in some specimens along three lines, one in the bottom, near the root of the weld, in the middle and in the top and with 0.5 mm distance between each indentation. A microhardness tester Zwick Roell ZHU MkII was used to perform

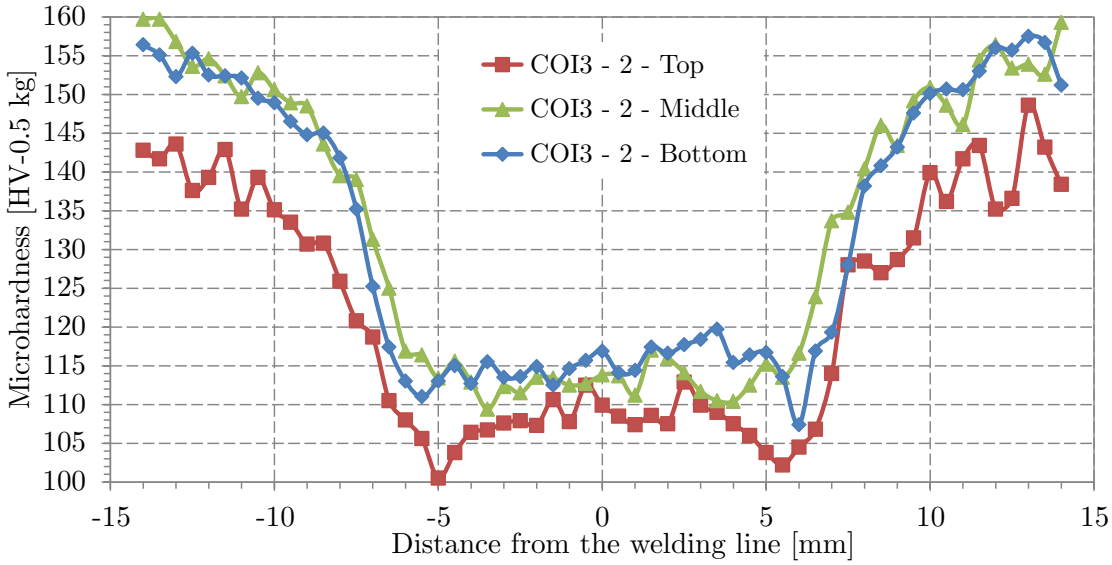

Figure 4.15: Microhardness of a cross section of the COI3 weld.

these measurements, applying a load of 0.5 kg in the indenter. The results for one of these measurements are presented in Figure 4.15. The hardness behavior in weld area is similar to the other aluminium alloys, with minimum values in the thermo-mechanical affected zone.

Tensile Tests

Three tensile specimens in accordance to the DIN 50125 standard were machined from each welded plate. These specimens are tested in a Zwick Roell static testing machine with a 100 kN load cell and a FOEPS 180 laser extensometer. The tests were performed in displacement control with a speed of 0.5 mm/min.

Table 4.5 presents the summary of the results obtained for these welds. These results are the average of the three specimens tested. L_0 is the initial gauge length, measured after the laser calibration, and E is the Young's modulus estimated from the elastic part of the tensile-strength curves. From these values the welds efficiency are estimated, compared with base material, using the equation 4.1 and using the measured strength values in T-L direction, since the welds were performed in the rolling direction. The values are very consistent between the different plates, demonstrating the reliability of this process. The efficiency yield tensile strength (σ_{YTS}) and ultimate tensile strength (σ_{UTS}), above 90% was achieved in all tests. The efficiency of the maximum elongation before rupture was above 40%, which it is a positive value in friction stir welds.

Table 4.5: Stress-strain values of AA2198-T851 FSW butt-joints.

Plate ID	L_0	σ_{YTS}	σ_{UTS}	ε	E
	$[mm]$	$[MPa]$	$[MPa]$	[%]	$[GPa]$
COI3	30.5	261.5	385.7	10.2	77.8
COI4	30.3	261.1	384.7	9.8	96.2
COI5	30.3	263.2	389.3	10.6	78.1
COI6	30.1	261.8	386.4	10.1	77.9
COI7	30.2	263.0	385.0	8.8	80.3
COI8	30.0	262.9	388.7	9.7	77.8
COI9	30.4	262.0	388.7	8.9	80.4
Average	**30.3**	**262.2**	**386.9**	**9.7**	**81.2**
STDV	**0.18**	**3.94**	**22.79**	**2.68**	**271.1**

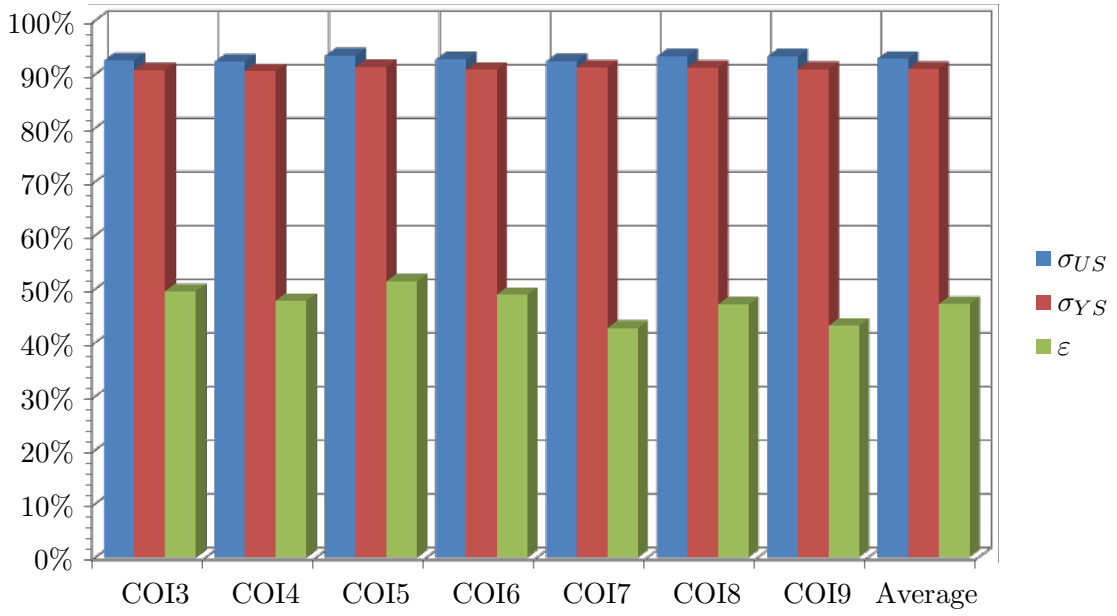

Figure 4.16: Efficiency of AA2198-T851 friction stir welds butt-joints.

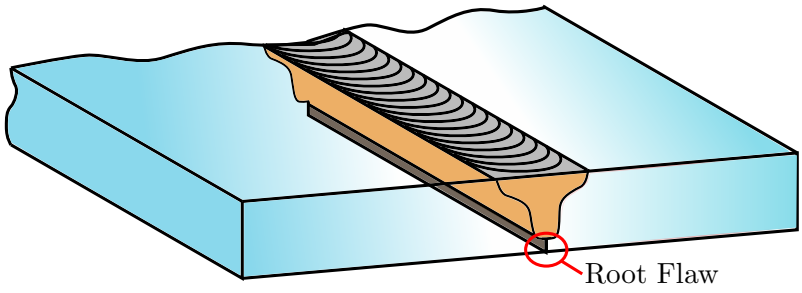

Figure 4.17: FSW root flaw.

4.3 Non-destructive Techniques for FSW Defects Detection

Despite the fact that FSW leads to low defect rates, the process needs to be controlled and the weld inspected to ensure that no defect is present that could compromise the structural integrity. FSW defects have several sources as too cold or too hot welds, tool geometry, tool positioning control, excess of impurities or oxides along the welding line and large gaps along the welding line. These sources can induce several defects as lines of oxides, tunnel effects due to the insufficiency of heat generation, "kissing-bond" defects due to low frictional force and low heat in the pin tip, and welding root flaws due to the lack of penetration of the pin instigated by the positioning control instabilities or fluctuations in the plates flatness, [157, 158, 159]. After an adequate determination of the welding parameters, most of these defects are 100% avoidable, with exception of the root flaws. In many cases it is not possible to ensure a constant thickness of the workpieces and the control, therefore the distance between the pin tip and the backing bar is not constant, resulting in root flaws when this distance is too high. In addition, the positioning control of the tool can experience perturbations creating occasional root flaws. Figure 4.17 shows schematically a weld with a root flaw. This type of defect has a high stress concentration factor that reduces considerably the fatigue life and the structural integrity, [160].

NDTs are routinely used to inspect aeronautical structures and are taken into account in early phases of the structure design given the close interplay of actual defects measurement, and damage propagation modeling used in damage tolerant design. Several types of NDTs are available to inspect different types of properties. The NDT techniques can be categorized into six main groups: visual, penetrating radiation, magnetic-electrical, mechanical vibration, thermal and chemical-electrochemical. Most of these techniques are based on the measurement of the structure reaction to a wave beam; thus these techniques can as well be grouped based on the operation frequency, giving some guidance about the maximum resolution of certain techniques. However, the major limitation usually lies in the sensor sensitivity in the measurement of the structure reaction to the beam. NDTs are classified as active or passive, [161]. In the active techniques, energy stimulus is fed

onto the structure and its response is measured, with variations to the normal behavior usually indicating that an anomaly is present. Examples of the active techniques are ultrasonics inspection, Eddy currents and X-rays. The passive techniques analyze the structure under its load environment or with a visual inspection of the surface, as example: visual inspection, liquid penetrant and acoustic emission, [162]. NDT technologies based on the electromagnetic phenomena and in the acoustic phenomena are the most interesting for friction stir welds, since they can penetrate through the structure and give an indication of the defect depth. Figure 4.18 shows the electromagnetic spectra and the framework NDT technologies that are based in the electromagnetic spectra. On this work, three different innovative active techniques were tested to detect defects in friction stir welded samples. The applied techniques have three different energy sources: ultrasounds, eddy currents and X-rays. All of them allow to look through the material thickness, enabling the detection of porosities and tunnel defects along the welding line.

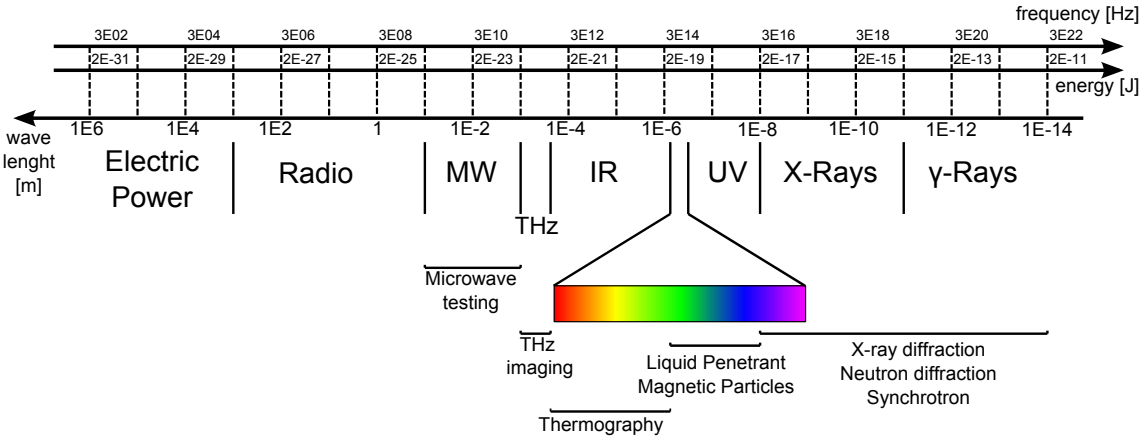

Figure 4.18: Non destructive technique spectrum based.

4.3.1 Scanned FSW Samples

Four AA2024-T3 friction stir welding samples were scanned with the three NDTs in order to determine their feasibility in the detection of root flaws in friction stir welds without special preparations or changes in the inspection equipment. Three of these samples have root flaws, one with 200 μm, other with 60 μm and other with oxides alignment along the weld line ("kissing-bond"). The fourth specimen is a regular welded without any defect. These samples were produced in the scope of the doctoral thesis of dos Santos, [163], where new eddy current probes were developed to detect root flaws in welded specimens in a more efficient way. During the tests, the scanned specimens did not have any indication about the type of defect or defect size, in order to not influence the final conclusions. Figure 4.19 shows the four samples examined and respective references.

(a) Sample A

(b) Sample B

(c) Sample C

(d) Sample D

Figure 4.19: Friction stir welds tested with NDT.

4.3.2 Ultrasonic Inspection: Scanning Acoustic Microscope

The application of sound waves to inspect components is an old technique. It is assumed that this principle has been applied since the beginning of metal casts production, where some disruption of the sound homogeneity on the object was associated to imperfections in the cast. However, the frequency of the sound that the human ear can hear is relatively low (roughly from 20 Hz to 20 kHz) and the variations in these frequencies are difficult to be detected by human ear for small defects. The correlation between the sound frequency and the wavelength is defined as:

$$\lambda = \frac{c}{f} \tag{4.2}$$

where c is the sound speed constant and λ is the wavelength. As example, in steels, a nominal value of sound speed is about $c = 4700m/s$, with the limits of frequency for human ear, the wavelengths that we can ear for steels corresponds λ=0.235 m, therefore defect sizes smaller that 0.1175 m could be completely imperceptible using the maximum frequency noticeable for the human ear. Other difficulty is the accuracy of the human ear, that only permits to detect considerable variations on the sound frequency. For smaller defects, acquisition systems that work at higher frequencies (ultrasounds) and which analyze small sound variations in order to have a higher accuracy are required.

Nowadays, several techniques apply the effect of sound propagation in the materials to analysis their structure.

Different ultrasounds techniques can be found in the market for different purposes. They are object of great current interest for structural aeronautical inspections. Several examples of these techniques are: Acoustical Interferometry, Laser Based Ultrasounds (LBU), Air Coupled Ultrasounds (ACU), Acousto-Ultrasonic (AU) and Acoustical Microscopy, [164]. Because they are emerging techniques with high potential application in aeronautics, it was deemed interesting to include in this thesis a comparative study of their performance when applied to FSW of aeronautical Al alloys.

In this work the acoustical microscopy technique, also known as Acoustic Micro Imaging (AMI), was applied to detect root flaws in the FSW specimens. This type of microscope takes advantage of high frequency ultrasounds, typically from 10 to 500 MHz, to generate images through the thickness. This technique is based on the pulse-echo effect, where short bursts of ultrasonic energy are introduced in the structure. These bursts cross through the structure thickness until they encounter a reflecting surface; at this point a echo is reflected and will be measured by a transducer, [165]. Through the application of ultra-high frequency ultrasounds, AMI enables to find and characterize physical defects as cracks, voids and porosity that occur during manufacturing or under normal component operation. Figure 4.20a shows schematically the C-Scan that was used in the tests and Figure 4.20b shows a piezoelectric sensor and transducer that was used in the acoustic microscope.

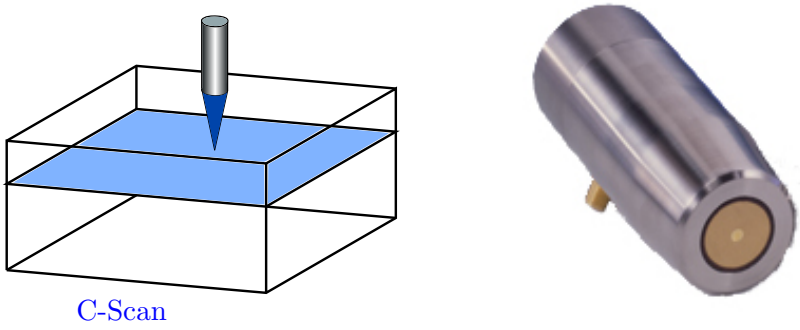

(a) C-Scan mode **(b)** Sonoscan transducer

Figure 4.20: Ultrasononic inspection through acoustic micro imaging.

The FSW specimens with different defect sizes were measured during this doctoral research using the last generation of acoustic micro imaging microscope, Sonoscan Gen5 C-Mode Scanning Acoustic Microscope, shown in Figure 4.21. Sonoscan is a manufacturer of scanning acoustic microscopes systems, that introduced in 1975 the worlds first commercially

acoustic microscope. These tests were done in the now extinct Sonoscan laboratory in Burlington, MA, USA.

Figure 4.21: Sonoscan scanning acoustic microscope.

Two different piezoelectric sensor transducers with different operating frequencies were used to measure these specimens. One with 50 MHz, with the capability to measure through the thickness, but with less resolution than higher frequency transducers. The other transducer, with a work frequency of 230 MHz, was focusing just below the back surface of the weld area and gating just past the echo from the top surface to collect information about the bulk material below this surface. A focal length of 0.375 in (9.5 mm) was used for all 4 specimens.

Scanning Acoustic Microscope Results

Firstly, a simultaneous scan was done with all specimens aligned. This analysis allows to have a global perception of the samples and limits for the probe focus and to clarify if with the probe frequency is capable to pass through completely thickness. Figure 4.22 and 4.23 shows the ultrasonic images focused on marked surface (shoulder surface) and on unmarked surface (bottom surface of the weld), respectively.

A detailed analysis of the samples is presented below. The detection of defects is based on the discovery of patterns, as discrete discontinuities along a line. In the case of

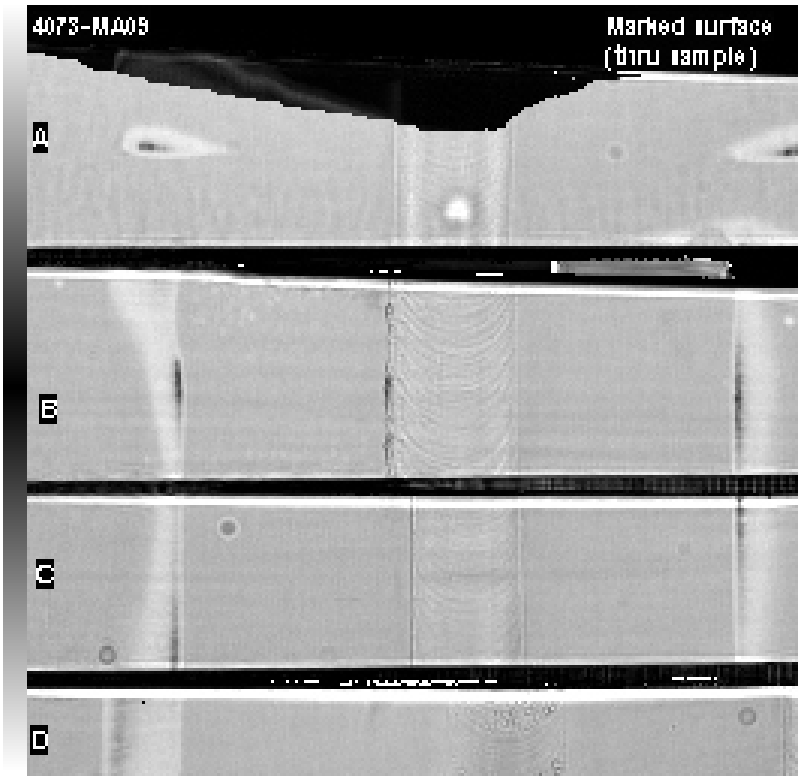

Figure 4.22: C-SAM at 50 MHz, focused on top of the weld, marked surface.

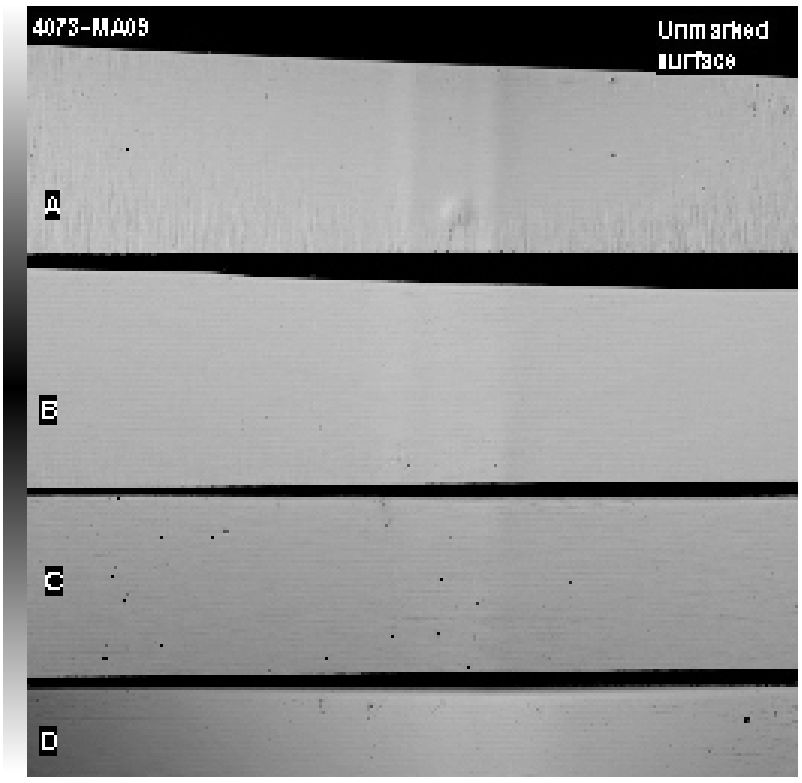

Figure 4.23: C-SAM at 50 MHz, focused on bottom of the weld, unmarked surface.

root flaws, they are expected to be detected by an alignment of spots, caused by waves deflection, along the welding line. Since a material discontinuity does not exist, this kind of defect is not straightforward to be detected.

For the first sample, with a frequency of 50 MHz it was demonstrated that it is possible to perform C-Scan along the complete specimen thickness (about 4 mm). Figure 4.24 shows two scans, one close to the back surface, Figure 4.24a, and other one close to upper surface, Figure 4.24b.

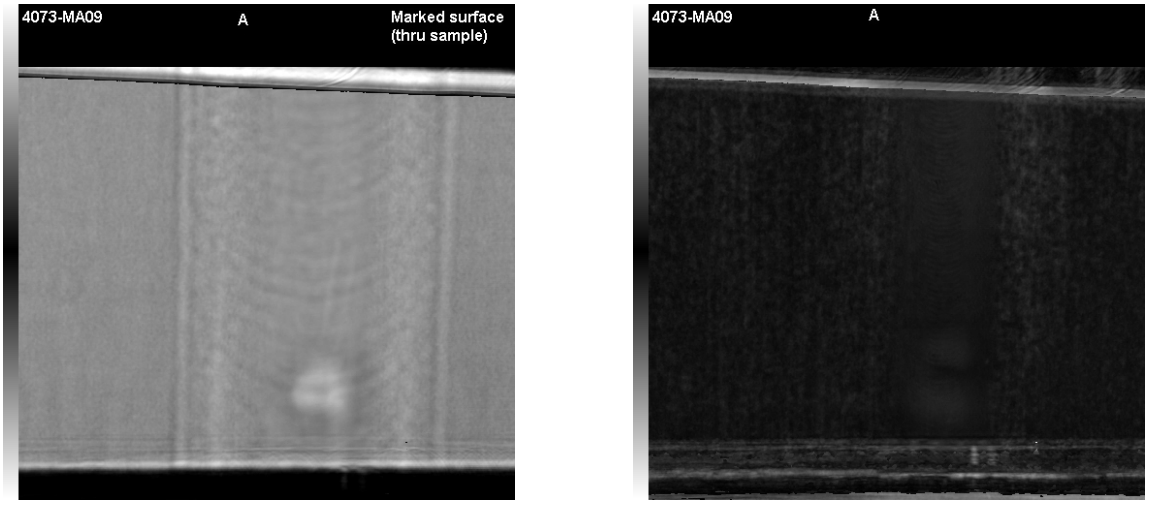

(a) Top surface **(b)** Back surface

Figure 4.24: Sample A, scanned with a probe of 50 MHz.

Figure 4.25 presents a more detailed analysis inside of the sample A, exhibiting several small porosities, which might also be noise. The exact position and depth of the porosity is possible to be determined from the spectrum using the velocity of the sound in aluminium and distance between the first punctual peak and the second peak.

Using a scan with a probe of 230 MHz, the resolution was significantly increased, however loosing the feasible depth that was possible to analyze. Nevertheless, since the region of defects is likely to be near to the surface, this probe might be advantageous for root flaws detection. Figure 4.26 shows the results for a scan done in the back surface (weld bottom). With these two probes it was only possible to discern small and disperse porosities that do not have a significant influence at the mechanical properties.

The scans made in the sample B with the 50 MHz probe are presented in Figure 4.27, one focused at the bottom and other in the top of the sample. Sizable defects were not detected at this frequency.

Figure 4.28 shows the scan the sample B with the 230 MHz probe and with a focus near to the upper surface (about 60 μm from the surface). In this figure aligned discrete dots

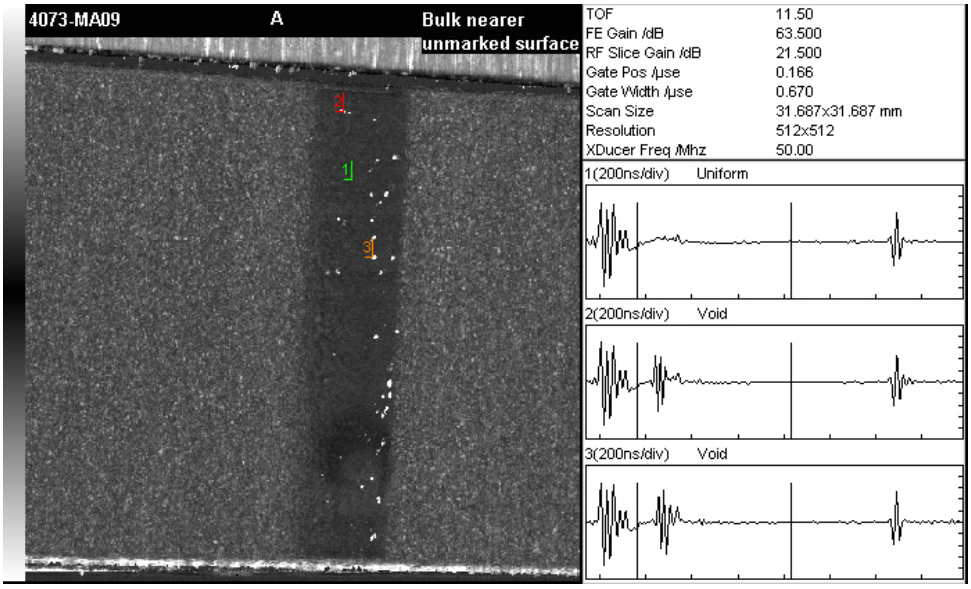

Figure 4.25: Sample A scan analysis of 50 MHz results at the weld root.

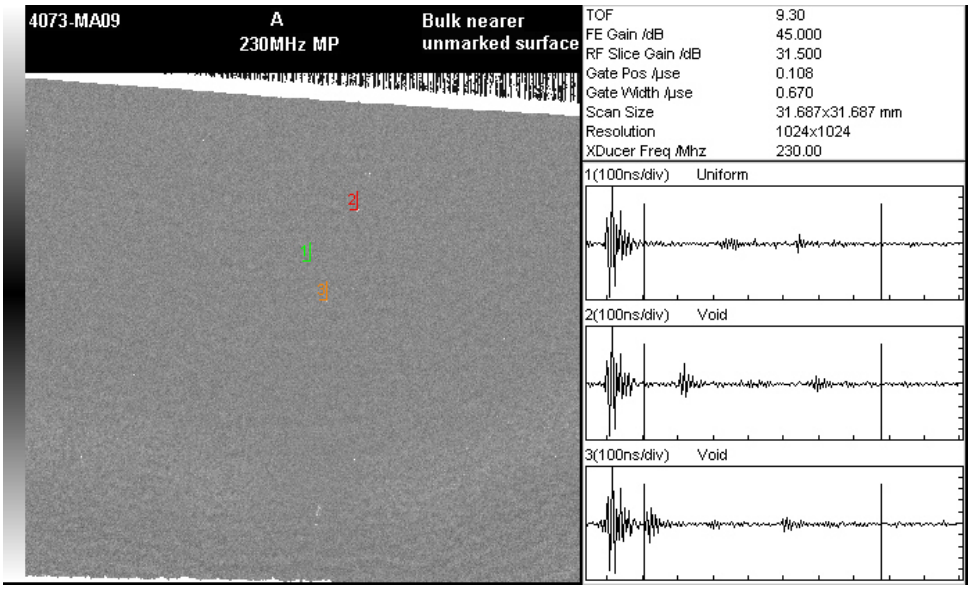

Figure 4.26: Sample A scanned with 230 MHz probe and spectrum analysis.

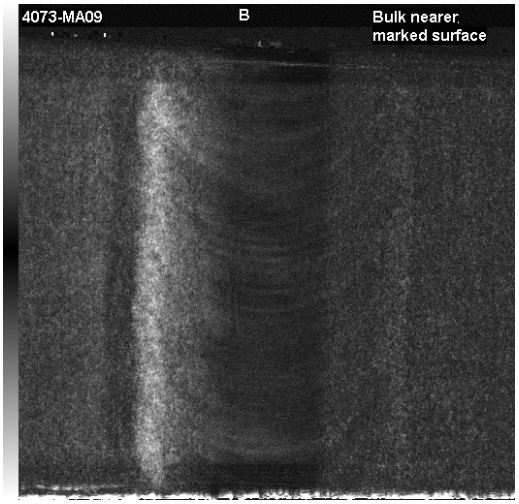

(a) Top surface

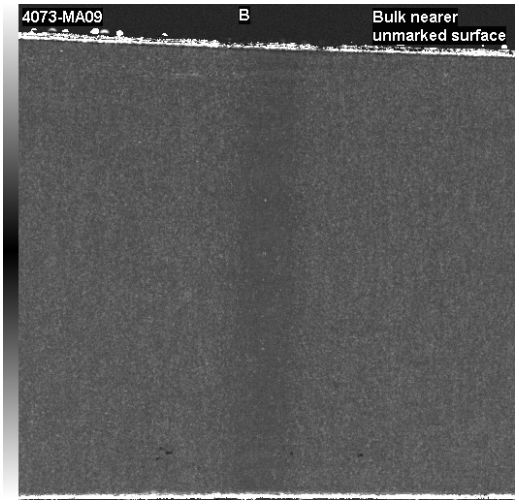

(b) Back surface

Figure 4.27: Sample B, scanned with a probe of 50 MHz.

along the weld line are visible. It is assumed that these aligned discontinuities correspond to a root flaw caused by an incomplete penetration of the pin during the welding. With the spectrum analysis presented in Figure 4.29 it is not possible to identify porosity depth, since the scale of 200 ns/div corresponds to about 1.2 mm/div (assuming the sound speed in aluminium of 6300 m/sec). However, it is expected that with some modifications of this Scanning Acoustic Microscope it will be feasible to identify these defects in a more effective way.

The scan with the 50 MHz probe of the sample C is shown in Figure 4.30. Only near the surface some imperfections or discontinuities are visible, which can be also caused by some noise during the measurement.

Figure 4.31 shows a higher resolution scan at the top of the surface. The scan gives a very regular image and no visible imperfections were detected at this plane.

The same procedure was adopted for the sample D, with one image near the bottom surface and another near the top surface, Figure 4.32. Figure 4.33 displays a scan of the interior of the sample near the top surface (60 μm), with the 230 MHz probe. No observable defects were also found in this specimen.

4.3.3 Eddy currents - Meandering Winding Magnetometer (MWM®) Results

Eddy currents (also known as Foucault currents) are electro-magnetic phenomena, associated to the inductive properties of alternating current. These currents are induced by electrical currents that flow in a circular path. They get their name from“eddies” that

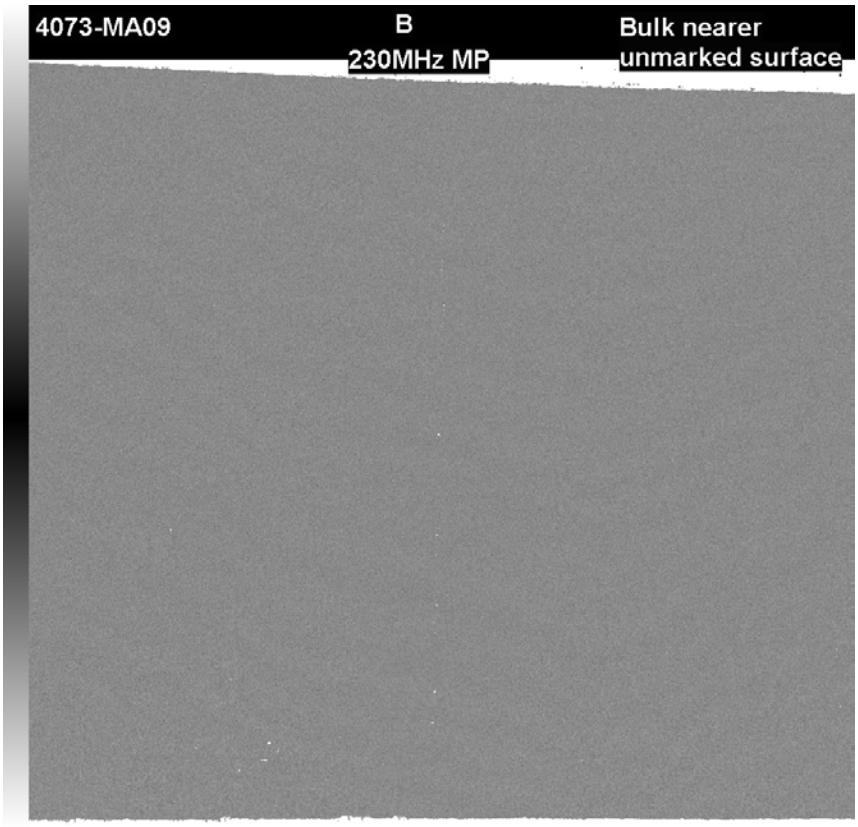

Figure 4.28: Sample B scanned with 230 MHz probe.

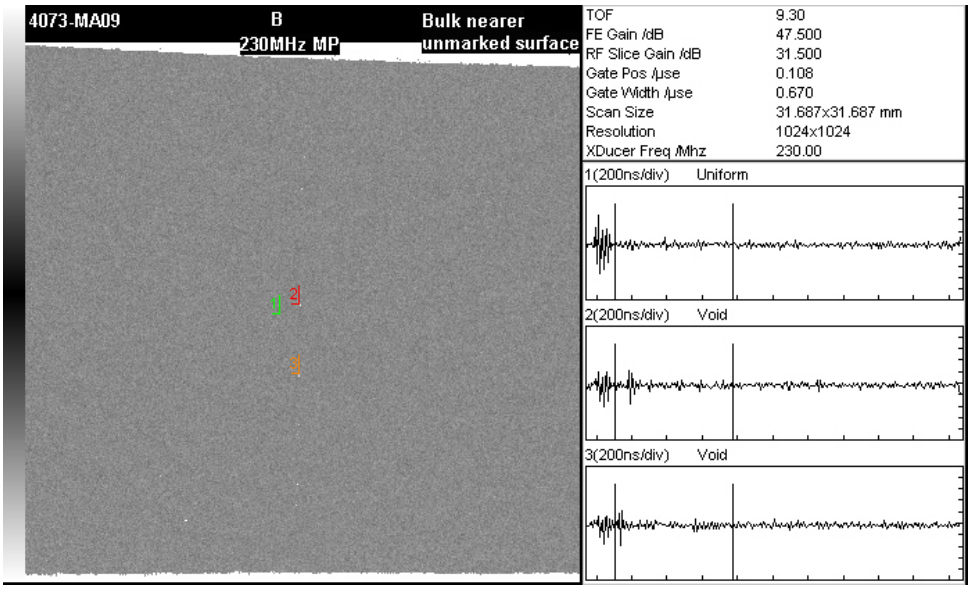

Figure 4.29: Sample B scanned with 230 MHz probe and spectrum analysis.

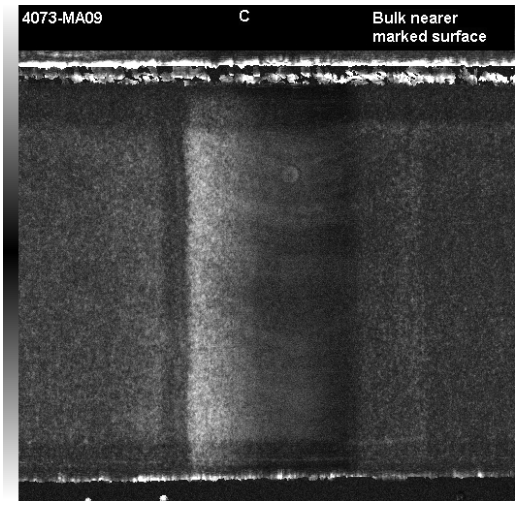

(a) Top surface

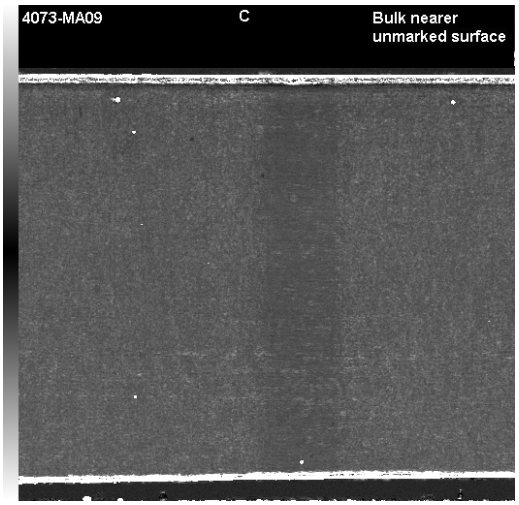

(b) Back surface

Figure 4.30: Sample C, scanned with a probe of 50 MHz.

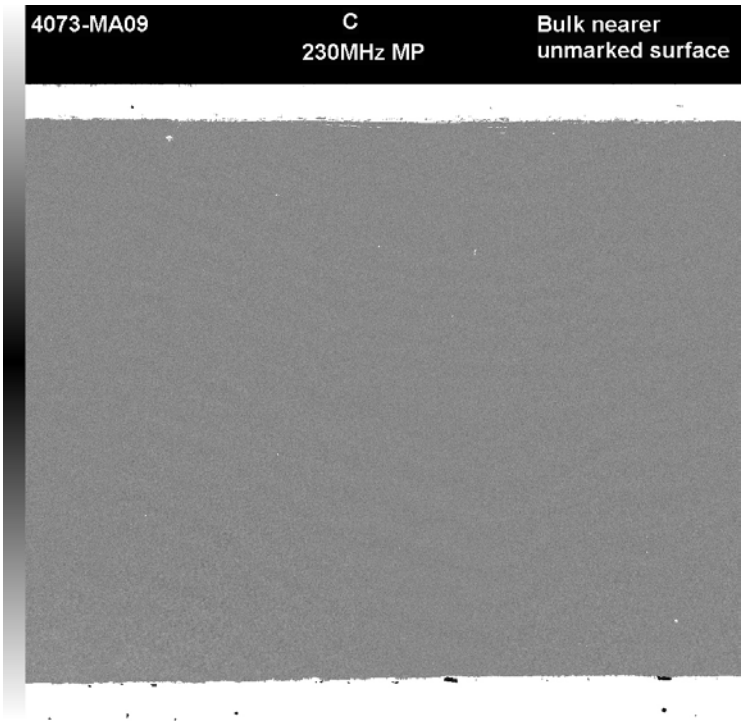

Figure 4.31: Sample C scanned with 230 MHz probe.

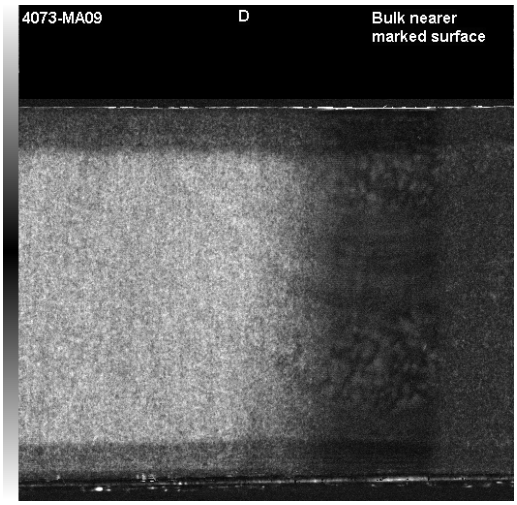

(a) Top surface

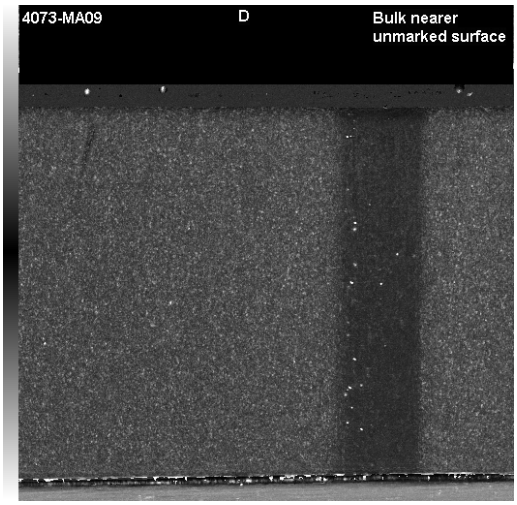

(b) Back surface

Figure 4.32: Sample D, scanned with a probe of 50 MHz.

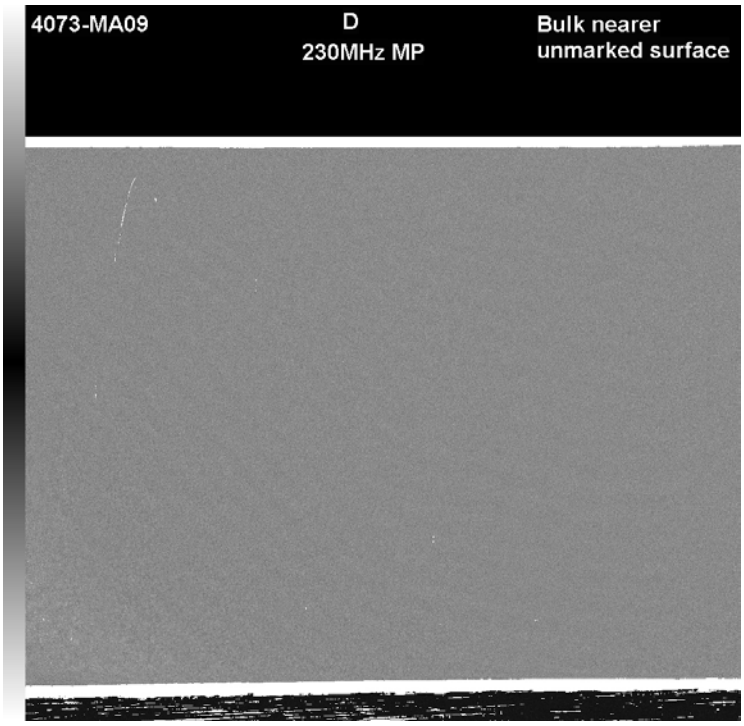

Figure 4.33: Sample D scanned with 230 MHz probe.

are formed when a liquid or gas flows in a circular path around obstacles when conditions are right. This effect is localized, where an electric current is induced in a conductive material by the magnetic field produced by a coil. This electric current also generates a magnetic field opposite in sense to the one from the active coil and reduces the inductance in the coil. When the distance between the target and the probe changes, the impedance of the coil changes correspondingly. This change in impedance can be detected by a bridge circuit. One of the limitations of the eddy currents is their penetration in materials with low conductivity. The maximum depth of the eddy currents can be defined by, [162]:

$$\delta = \frac{1}{\sqrt{\pi \mu \sigma_c f}} \tag{4.3}$$

where δ is the eddy current penetration depth, f is the frequency (Hz), μ is the material magnetic permeability and σ_c is the material electrical conductivity.

Since the electrical conductivity and magnetic permeability are a function of the material and its metallurgic properties, eddy current measurements can be used to sort materials even if the material was heat treated or aged. Its application in friction stir welds is advantageous due to its capability to verify the material structure in the welding zone. The application of this technique for root flaws detection was done using the Meandering Winding Magnetometer (MWM), which is a patented technology by Jentek Sensors, a company specialized in electromagnetic non-destructive techniques located in Waltham, MA, USA. MWM sensors are inductive sensors composed by two windings, a primary winding that generates a magnetic field and a secondary adjacent winding that gauges the changes in the magnetic field through the workpiece. In order to increase the scan area with one probe, Jentek developed arrays of these sensors allowing faster scans or even to measure more complex physical phenomena, as the torque in shafts, [166].

The application of their sensors in the detection of flaws in welded structures and to characterize weld integrity has been also developed by Jentek, where a first patent was issued in 2006 by Goldfine *et. al.*, [167]. The application of the MWM sensors in friction stir welds was done in the Space Shuttle tanks project, at Lockheed Martin and NASA, were this technology was tested to detect root flaws in welds of AA2195 with AA2195 and AA2219 with AA2195, with the minimum size of 0.75 mm, [168]. Grundy *et. al.*, [169] reported results with this technique in the detection of root flaws, kissing bond and planar type discontinuities, showing that this technique can be very effective.

The defects presented in the samples mentioned in [168] and [169] are greater than the ones present in the four tested samples in the present thesis, which require higher sensitivity. The results of C-scans at 3.981 MHz at the surface near the root and near to the top are presented in Figures 4.34, 4.35 and 4.36.

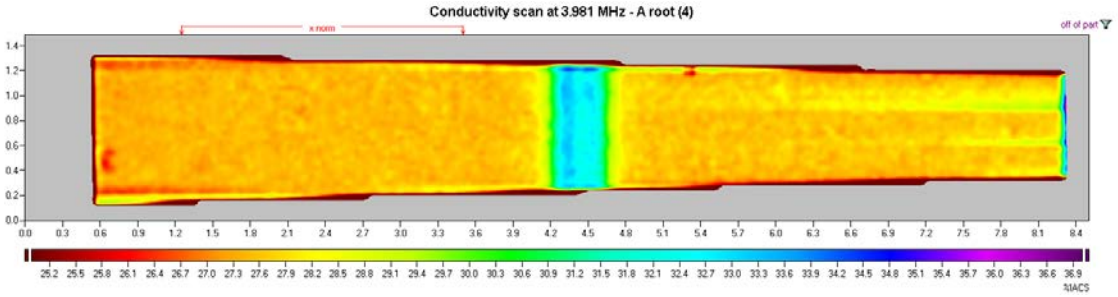

(a) Conductivity at root

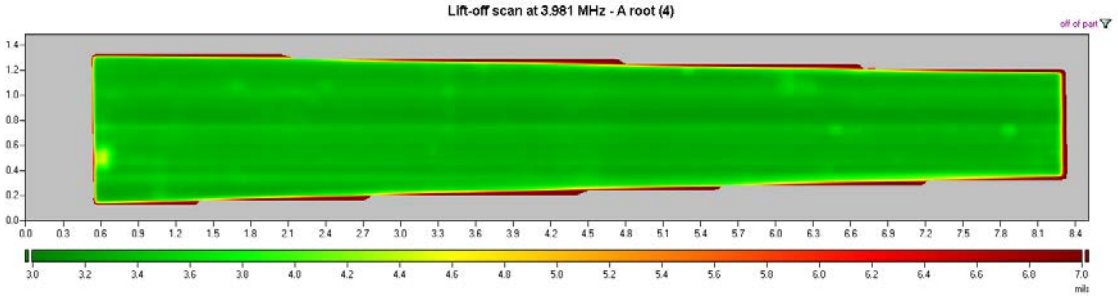

(b) Lift-off at root

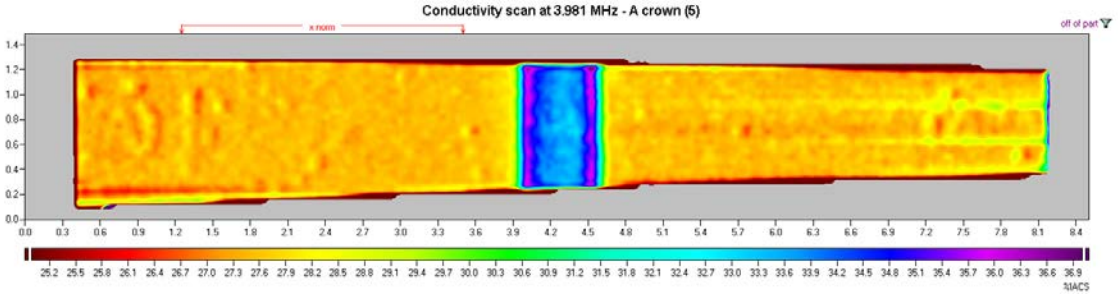

(c) Conductivity at top

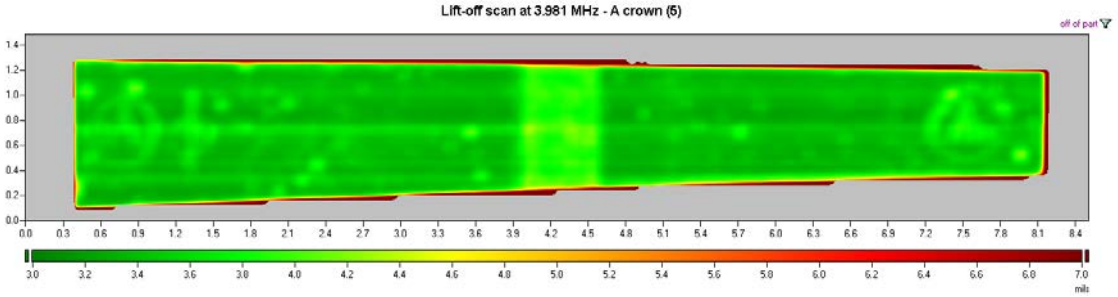

(d) Lift-off at top

Figure 4.34: Sample A, conductivity and lift-off scans at root and top of the weld.

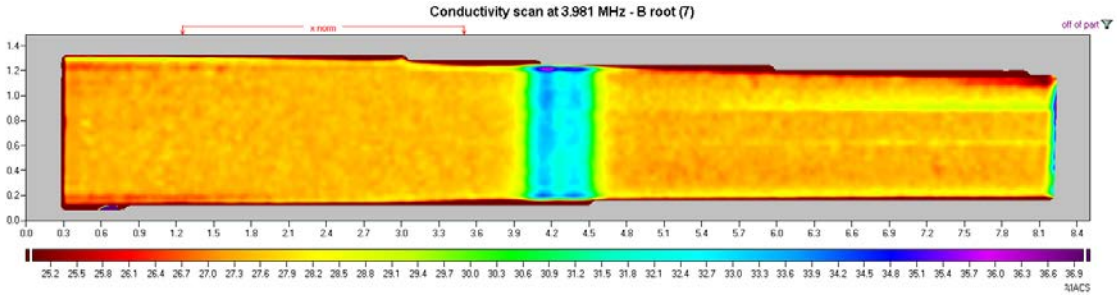

(a) Conductivity at root

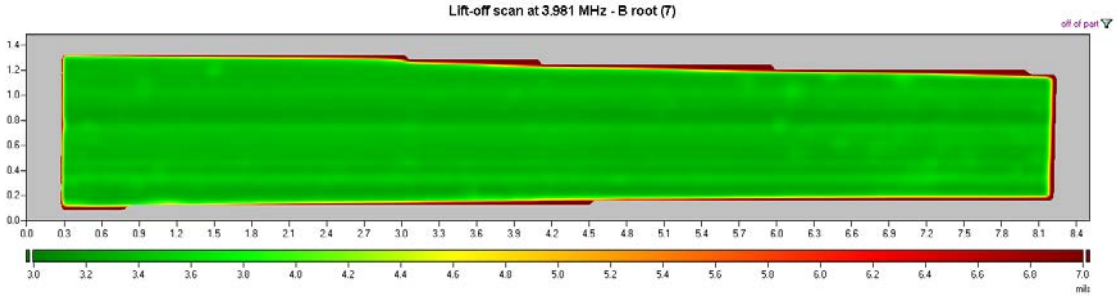

(b) Lift-off at root

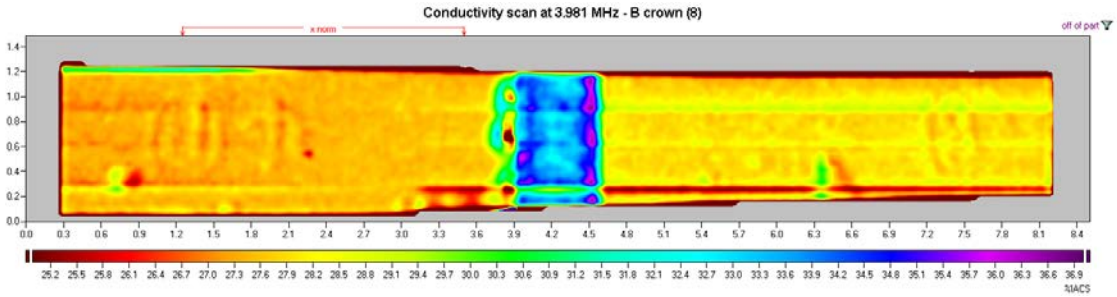

(c) Conductivity at top

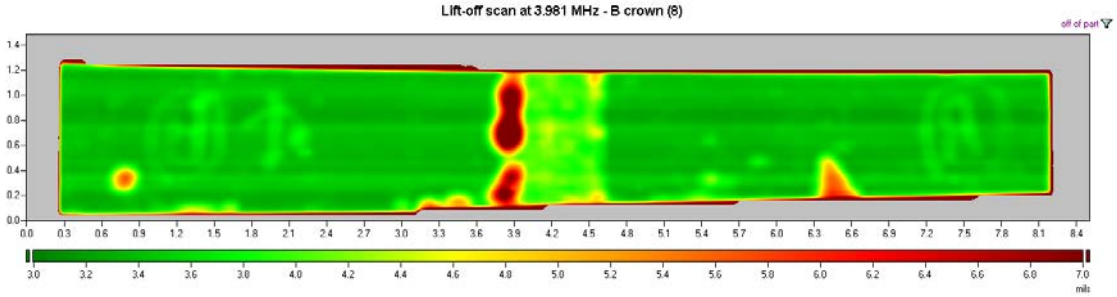

(d) Lift-off at top

Figure 4.35: Sample B, conductivity and lift-off scans at root and top of the weld.

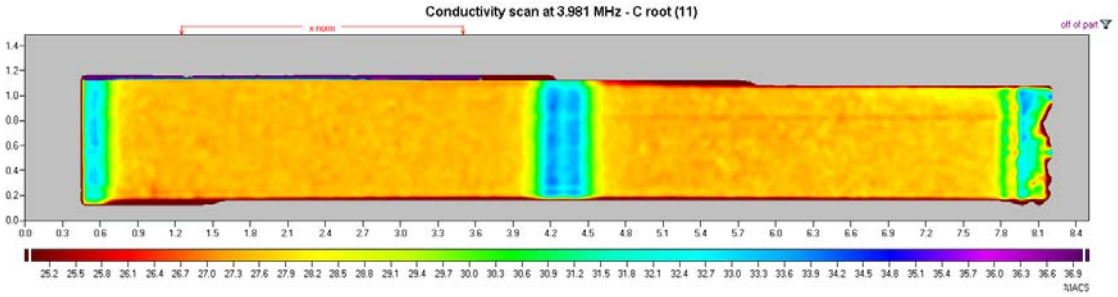

(a) Conductivity at root

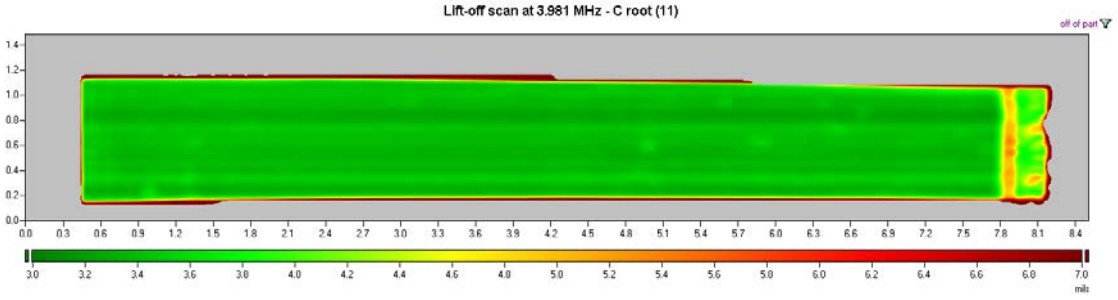

(b) Lift-off at root

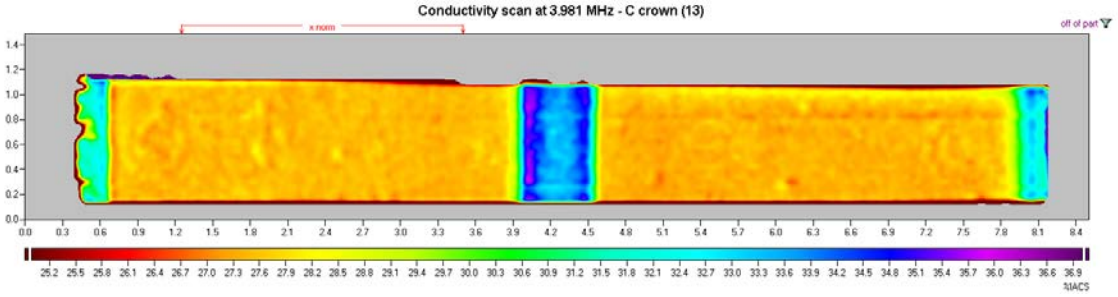

(c) Conductivity at top

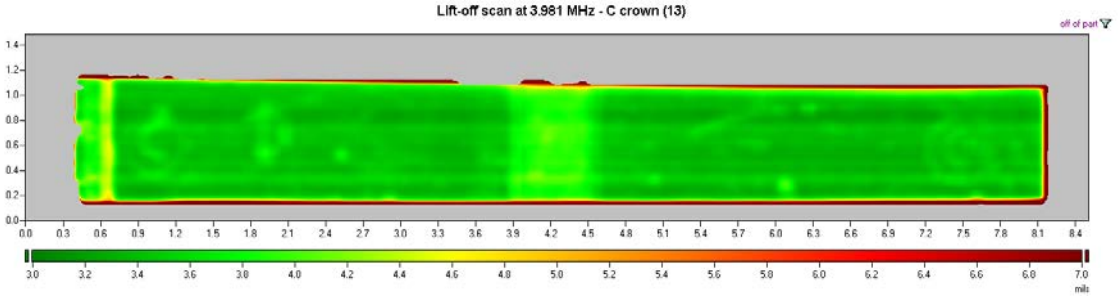

(d) Lift-off at top

Figure 4.36: Sample C, conductivity and lift-off scans at root and top of the weld.

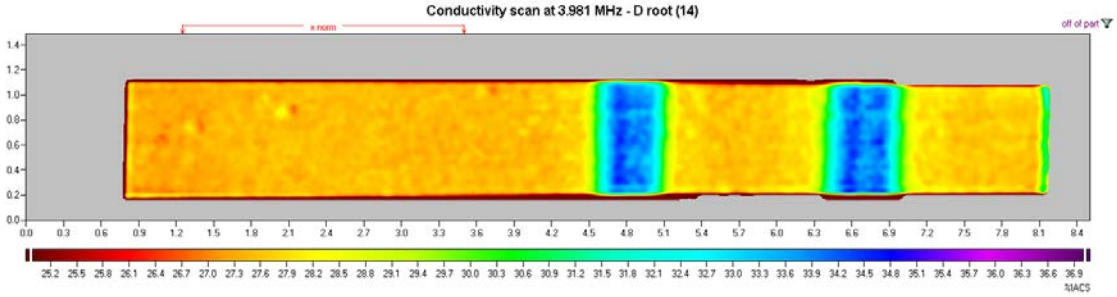

(a) Conductivity at root

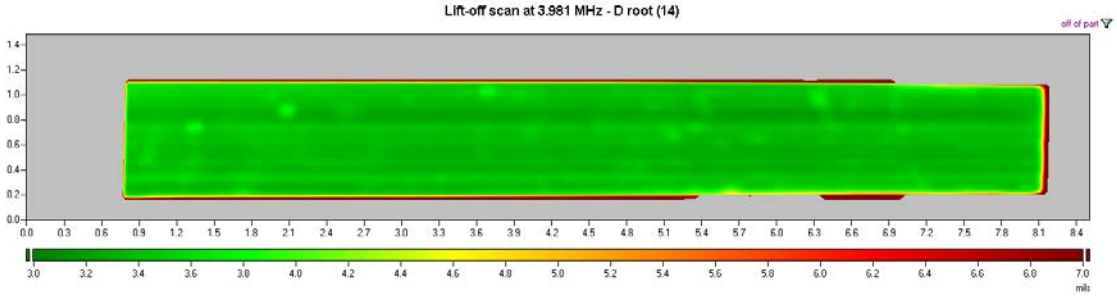

(b) Lift-off at root

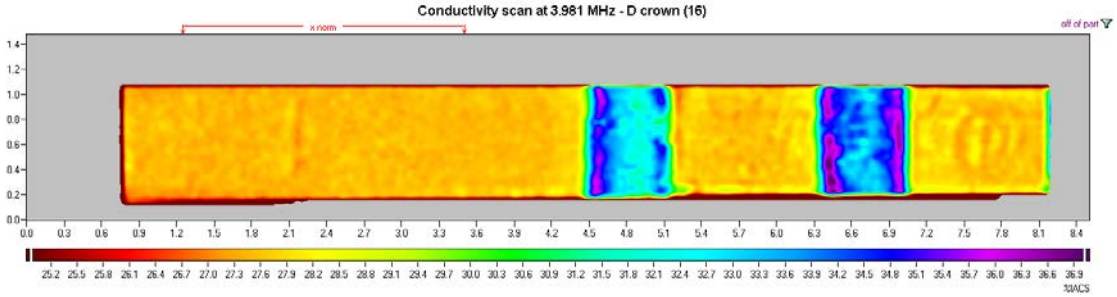

(c) Conductivity at top

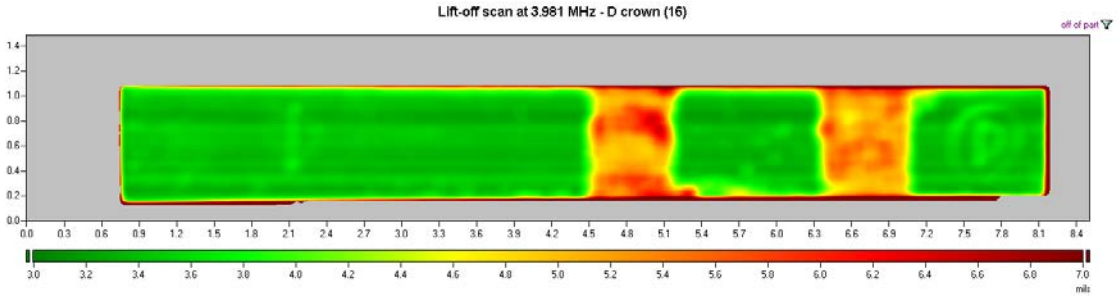

(d) Lift-off at top

Figure 4.37: Sample D, conductivity and lift-off scans at root and top of the weld.

The conductivity unit used in these measurements is based on the International Annealed Copper Standard (IACS), which is highly variable with the alloy composition and with heat treatment. For instance, pure aluminum has approximately a conductivity of 61% IACS and the alloys used in these tests (AA2024-T3) has a conductivity of 28.5%-32.5% IACS, [170]. The conductivity measured in the base material of the samples has values inside of this range. An interesting point is the increase of conductivity in the thermo mechanically affected and stirred zones, due to the loss of heat treatment and perhaps some of alloy elements.

From the conductivity contour maps, the same pattern appeared in the welded area for the four specimens, denoting that at this frequency enough resolution to detect the root flaws is not achieved. The sensitivity of this process could be increased with different probes or increasing the eddy current frequency, a option that was not feasible during these trials. The lift-off contour maps can also give an indication of superficial defects, however, observing the lift-off maps at the top, the weld striations are not completely defined, demonstrating insufficient resolution in the lift-off measurements in order to detect tiny defects at the surface. Nevertheless, for welding quality control, this technique is very promising, since different metallurgical and mechanical variables can be measured from one measurement, including residual stresses, [171].

4.3.4 X-ray Computed Microtomography

X-ray Computed Microtomography (XMT) or computed tomography is a nondestructive technique that uses the X-Ray source to produce 2D and 3D analysis through the tomography of an object. The source of X-rays is composed by electromagnetic waves, with short wavelengths (from 10^{-9} to 10^{-12} m) and with high energy:

$$E_p = hf = \frac{hc}{\lambda} \tag{4.4}$$

where E_p is the photon energy (J), h is the Plank's constant (6.626×10^{-34} J.s), f is the radiation frequency (Hz or s^{-1}), c is the speed of light (2.998 m/s) and λ is he wavelength of radiation (m).

Due the short wavelengths and high energy, this radiation can penetrate in most solid materials, crossing the objects. If on the other side a film or sensor records the radiation intensity after crossing the object, it is possible to have an image of the interior of the object. When the X-rays beam crosses a solid material, part of the energy is absorbed, attenuating the X-ray beam. This attenuation is function of the materials and its density allowing the measurement of the internal geometries. The relation between the attenuation and density can be calibrated allowing to detect materials properties, [172].

The XMT technique collects these X-Ray images from different directions and with these cross-sectional images the interior structure is reconstructed with software analysis. The conventional X-Ray images or films only give bi-dimensional information. This is a limitation for a non-destructive inspection, since the detected information is only for defects in the plane perpendicular to the source; in the case of a planar defect aligned with source, it will be invisible in these images. In the case of tomography, it allows the complete structure of an object to be scanned and examined, and allows to obtain the size, shape and location of internal feature or defects. However, it is a time expensive technique since that is required multiple scans to obtain the full 3D reconstruction of the scanned object.

This technique was applied in this work in order to understand if it can offer better resolution for root flaws and kissing bond detection or give more information about the weld region. The measurements were done at the Center for Nanoscale Systems at Harvard University (Cambridge, MA, USA), with a X-TEK HMXST225 equipment. This equipment is presented in Figure 4.38 and was mainly composed by a open source X-ray tube with a maximum resolution of 3-5 μm in reflection mode and 2 μm in transmission mode, Figure 4.39a and a Perkin Elmer 1621 X-ray panel with 2000×2000 pixels and size of 16 in $\times$ 16 in, Figure 4.39b.

Figure 4.38: XTEK tomography equipment with X-Ray source.

Due to the time required to perform each measurement, the procedure was tested just in the sample A. The area of the inspection was confined to the welded region of the specimen. The results are composed by 1800 tomograms, that were used to reconstruct a 3D model of the scanned area. Figure 4.40 shows two views of this reconstruction, with some degree of

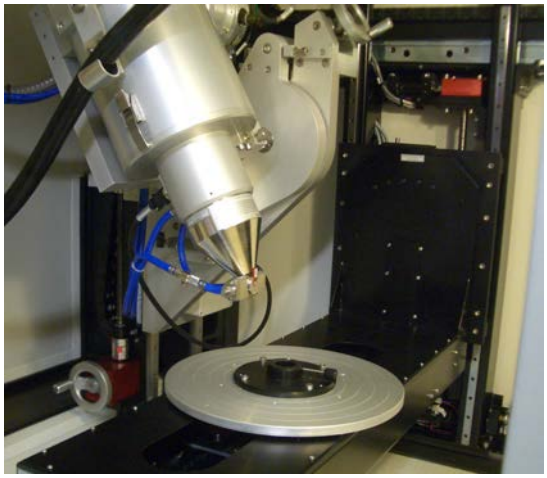

(a) Condenser and filter

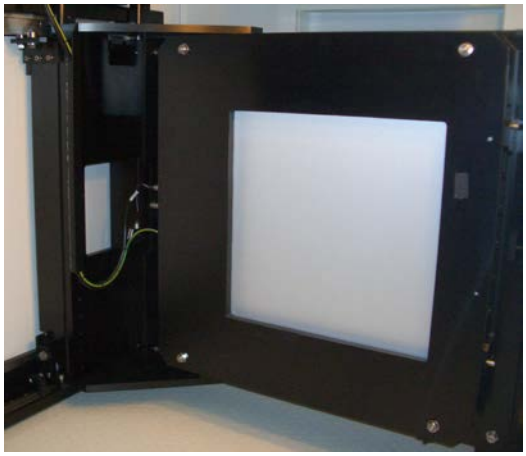

(b) Sensor

Figure 4.39: XTEK X-ray tomography, main components.

transparency to allow the visualization of the internal appearance. The software allows the application of different filters and refinement in the model, however major imperfections were not detected with this technique, even porosities that were detected with AMI. The increase of resolution in this technique might be possible using other sensor closer to the specimen.

From the top side (shoulder side), Figure 4.40a, FSW striations were not visible, even applying different image manipulations. It was concluded that, probably due to software limitations, surface contours could not be observed. The application of some degree of transparency in the tomograms makes the external shape discernible and when the transparency is removed the external surface still is not perceptible. It is assumed that since these images were obtained by the addition of the different tomograms it will be difficult to create a image just with the shell of the specimen. From the root side, and with higher brightness, the Figure 4.40b was obtained. In this case, a detailed representation of the surface was also not obtained, the identification of defects being difficult.

4.3.5 Results Discussion

The results obtained from the three NDTs demonstrated that the detection of root flaws and kissing bond defects is extremely difficult due to the absence of physical discontinuity that might disturb significantly a beam of energy. The most promising results were obtained with the acoustic micro imaging, since without special modification in the equipment and post-processing software, the detection of the bigger defect with about 200 μm was possible. This technique works at high frequency requiring a conductivity interface, which in this case was water, that could be a drawback.

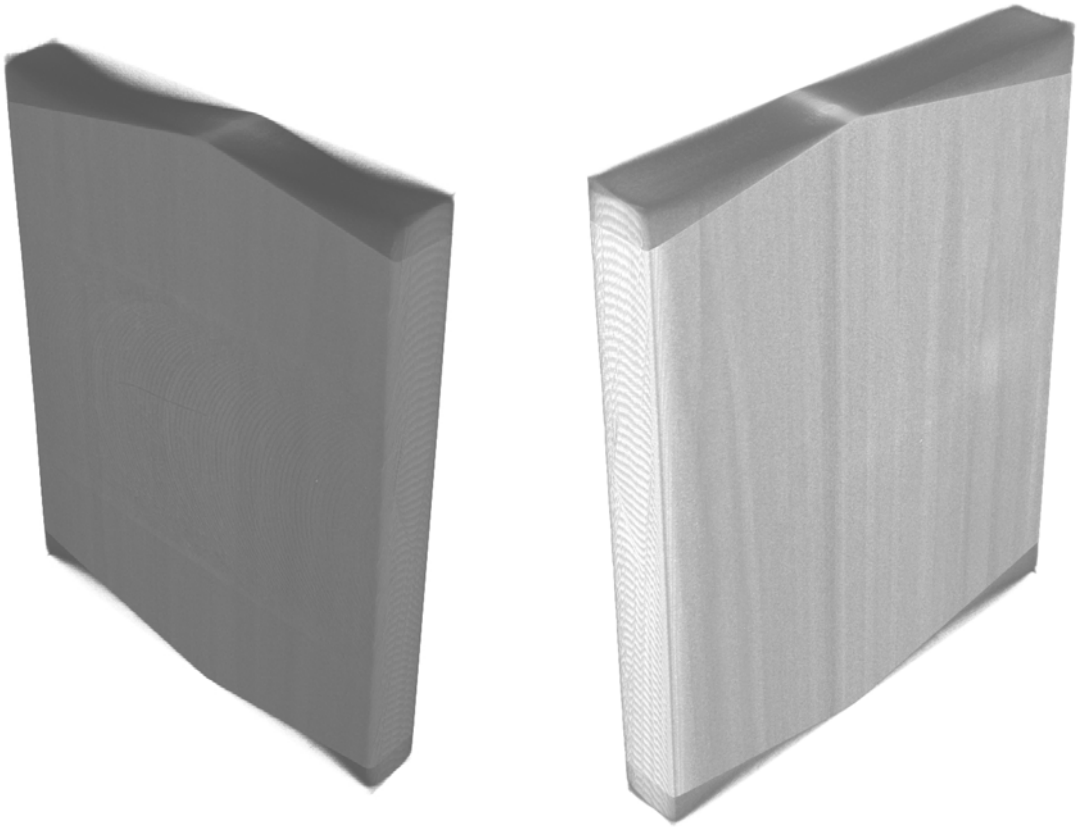

(a) Shoulder side **(b)** Root side

Figure 4.40: Computed tomography of the sample A.

The meandering winding magnetometer MWM technique can be promising if it is possible to improve its resolution, due to the fact that no evidence of defects was found in these analyses. This technique might be advantageous since it can give additional information about weld metallurgy and mechanical properties. The X-ray computed microtomography XMT did not exhibit advantages when compared with the two other NDT techniques. Possibly, when information along the complete thickness is required, or in welds with difficulty access, this technique can present advantages, however it is required to develop this technique with sensor panels with higher resolution.

The results of these techniques applied in the root flaws detection were summarized in Table 4.6. To the results obtained in the present research, were also added the results obtained by a new eddy current probe, IOnic probe, developed for friction stir welds by T. dos Santos in the scope of his doctoral thesis, [163]. It was pointed out that this probe detects root flaws up to 60 μm, with relative low frequencies (200-400 kHz). Compared to the MWM, a good improvement in the root flaws detection is found. With further developments, including multi array solutions to increase the scanned area and decrease the inspection time, this technique can be very competitive.

Table 4.6: NDT results comparison.

Technique	**Root flaw detection**	**Detection Speed**	**Portability**	**Major drawbacks**
Acoustic Micro Imaging	At least until 200 μm	Medium	Medium	Requires couplant between the probe and the workpiece
Meandering Winding Magnetometer	200 μm not detected	Very fast	High	Low resolution at this stage
X-ray Computed Microtomography	200 μm not detected	Low	Low	It is not portable and it is time consuming
Eddy Currents, IOnic Probe	60 μm is detectable	Low	High	It may be time consuming if is required to inspect all the weld

Chapter 5

Reinforced Panels Joined by Friction Stir Welding

Reinforced panels composed by multiples parts (as skin, stiffeners, frames, doublers and others), are the major structural components of an aircraft. Traditionally, most of these joints are riveted, as shown in Chapter 3. In order to optimize these panels from the manufacturing and operational points of view, new joining processes have been investigated to reduce structural weight without compromising the structural integrity during the life cycle of an aircraft. From the mechanical performance of friction stir welding process, analyzed in the previous chapter, this joining technique might improve these structures since it is possible to achieve joint efficiencies close to 100% and, if butt-joints configurations are used, it is possible to reduce the weight of the overlap areas. In the following sections, the impact of the friction stir welding application to join stiffeners is analyzed. The fatigue performance under cyclic loads representing pressurization cycles of cracked stiffened panels produced by different joining processes, including friction stir welding, is analyzed and compared. Numerical tools were also developed to estimate these phenomena considering different effects promoted by the welding of stiffeners. These tools were validated with experimental results and can be used for future design of panels welded by this process.

This work was done in the scope of the project Innovative Fatigue and Damage Tolerance Methods for the Application of New Structural Concepts (DaToN), of the Sixth Framework Programme for Research and Development of the European Union. This project aimed to develop new damage tolerance assessment tools for integral monolithic reinforced panels manufactured by FSW and comparing the results with two other different processes: High Speed Machining (HSM), and LBW. All these three processes lead to an integral joined structure design. Damage tolerance behavior of the reinforced panels is a crucial point when joining or manufacturing processes are replaced, limiting the application of new techniques. This project developed tools for the assessment of the damage tolerance of integrally stiffened structures, manufactured by HSM, LBW or FSW, and gave illustrative assessment as well as identified differences between the three manufacturing methods, contributing to find optimized structures, [173].

5.1 Differential and Integral Reinforced Panels

The integral and differential panels are two design options to produce reinforced structures using different joining processes. In the conventional solution, the parts that compose the structure are joined differentially (wich means that the joint is joined in discrete points with rivets, fasteners or screws), whereas in the integral solution the joints are integrally joined, *i.e.* the different parts are joined continuously, Figure 5.1a.

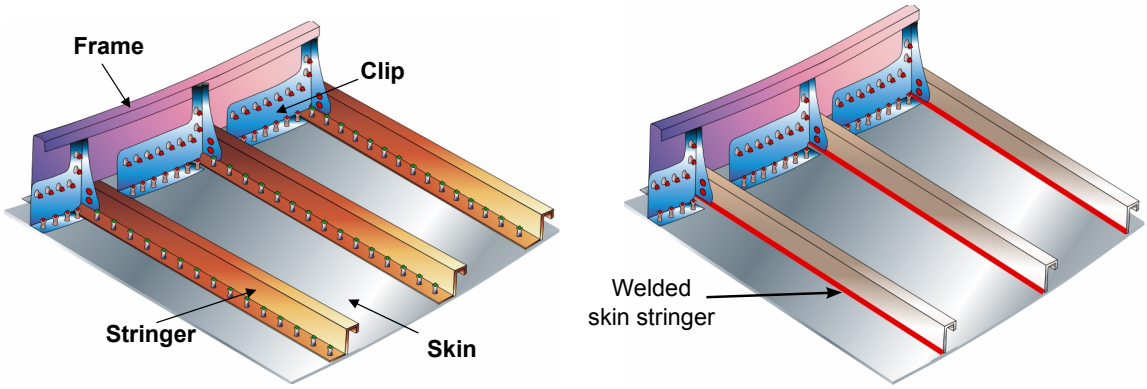

(a) Differential panel **(b)** Integral panel

Figure 5.1: Differential and integral panel, [174].

These integral panels have been the object of considerable interest by different aircraft manufactures and research organizations due to the possibilities to reduce manufacturing and operational costs, structural weight and complexity. An example of the research programs carried out is the Integral Airframe Structures (IAS) Program managed by NASA, where several techniques to create reinforced stiffened panels were investigated, [175]. In this program, it was pointed out that, compared to conventional riveting processes, the high-speed machining of an exemplary stiffened panel, from an aluminum plate, would yield a recurring cost savings of about 61%. In addition, the number of parts that compose the exemplary panel dropped from 78 to 7 parts for machined panels, a huge reduction. Figure 5.2 shows a cross section of a riveted joint, Figure 5.2a, and the alternative integral solution with the stringer welded, Figure 5.2b, pointing out the simplification and the advantage of integral joined solutions.

The transition from differential to integral design creates complex challenges because one main failure mode of these structures is associated to crack propagation and the integral solutions present less crack arrest features due to the continuous paths for crack growth. As identified in the IAS program, the major concerns and most important technical aspects in integral panels are their damage tolerance and fail safety, [176]. Due to this reason, this

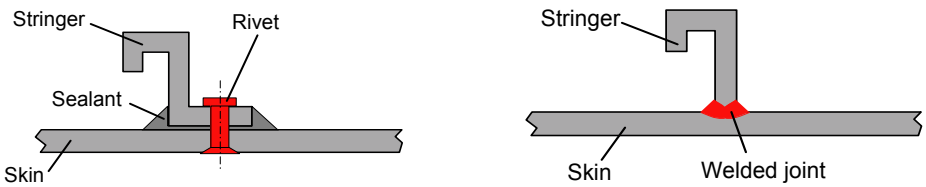

(a) Riveted stringer **(b)** Welded stringer

Figure 5.2: Riveted and welded stringer, [174].

topic was investigated in the scope of this doctoral research in order to create tools for a proper design of integral structures joined with FSW.

5.2 Numerical Design and Modeling

The application of integral design solutions in aeronautical structures requires a deep understanding of their mechanical behavior under cyclic loads during the aircraft service. As concluded above, integral joint design has a detrimental effect in the damage tolerance and fail safety, mainly due to the FCG behavior. An accurate modeling of the FCG behavior will help to understand and estimate the fatigue life and to perform engineering design calculations reducing the experimental testing required for aircraft structures.

The determination of FCG in stiffened panel is done in two main phases: the stress intensity factor is estimated as a function of the crack size, to characterize the stress state in the close neighborhood of crack tips, and, subsequently, the fatigue life is estimated using a FCG law. Several techniques can be used to estimate the SIF based on analytical solutions, empirical solutions and numerical solutions. Several DaToN partners used different techniques to estimate the SIFs that afterwards were compared in [177]. In the present research, FCG tests were modeled, aiming at the validation of a numerical virtual testing, where the determination of the FCG and fatigue life might be inexpensively carried out due to the massification of computational tools.

5.2.1 Panel Geometry and Manufacturing Processes

A straightforward geometry of a stiffened panel was used in this project, mainly composed by two straight stiffeners and with dimensions of 1000mm $\times$ 450 mm including a clamping area for testing. Figure 5.3 presents the geometry used as reference for this project. A central crack was applied between the two stiffeners to simulate a defect that under the cyclic loads will propagate until the final rupture. From this base geometry, panels manufactured using three different processes were tested. These stiffened panels

were produced using HSM, LBW and FSW. In the case of panels with stiffeners welded by LBW, two different configurations were used. Figure 5.4 shows a cross section of the different configurations used to weld the stiffeners to the skin. The two LBW configurations used gave information about distortion and about the structural integrity improvements if the stiffeners are not welded directly to the skin, Figure 5.4b, although this configuration requires previous machining operations to obtain the base of the stiffener.

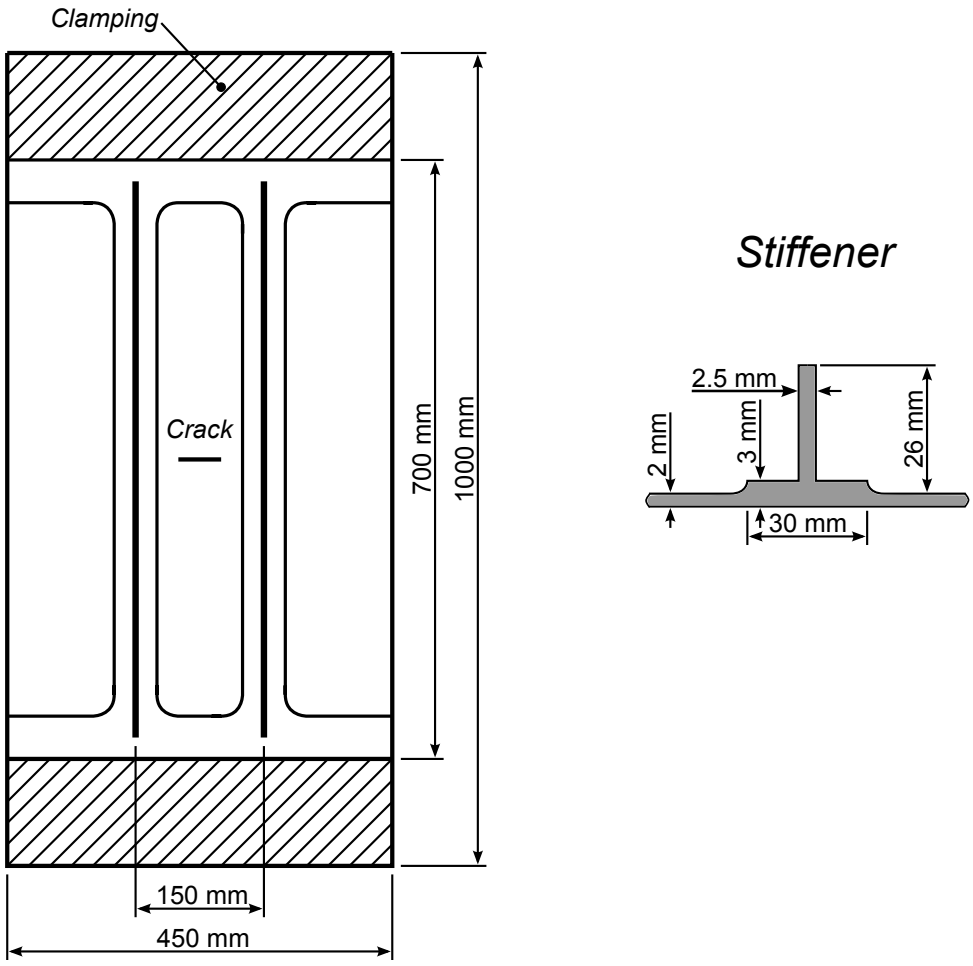

Figure 5.3: Geometry of the stiffened panel analyzed.

Besides the three manufacturing processes and joining configurations, different materials and heat treatment conditions were used to manufacture these panels. The aluminium alloys and heat treatments used in these stiffened panels were:

- AA2024-T3
- AA6056-T6
- AA6056-T4 and post welding treatment (PWHT) to T6 condition.

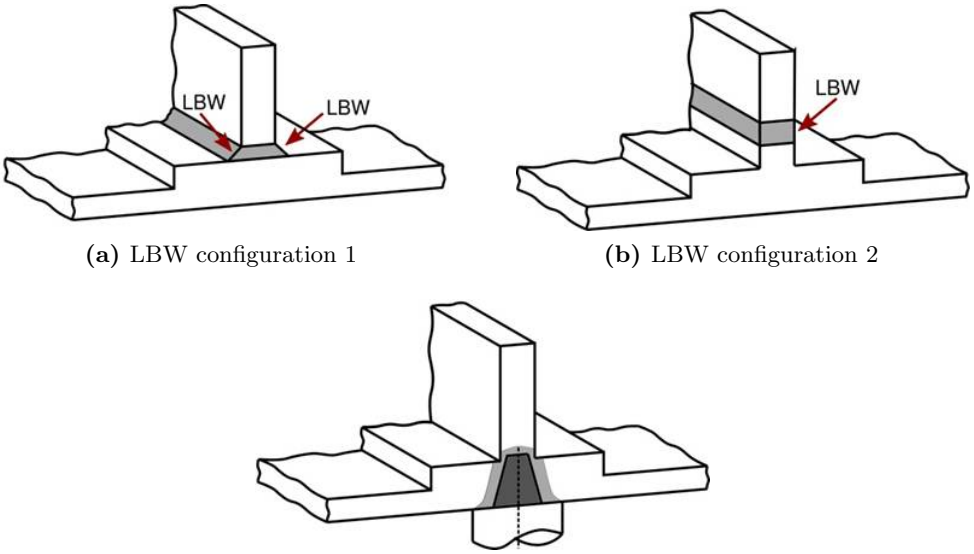

(a) LBW configuration 1

(b) LBW configuration 2

(c) FSW configuration

Figure 5.4: Welded stiffeners configurations.

For each configuration the specimens were tested in order to measure the crack growth, in the situation of an applied cyclic load for two different load ratios ($R = \sigma_{min}/\sigma_{max}$) with different maximum loads:

- R=0.1 $\rightarrow \sigma_{max} = 80$ MPa
- R=0.5 $\rightarrow \sigma_{max} = 110$ MPa

5.2.2 Finite Element Model

A Finite Element Model (FEM) was built to model and calculate the stress field in the cracked panels in order to estimate the stress intensity factors. The finite element (FE) solver used in this work was ABAQUS Standard, that permits to incorporate different phenomena as the residual stress fields and the stress redistribution during the crack growth. The mesh used in the FEM concerned half geometry due the symmetry of the stiffened panel and includes part of the grip system for a better simulation of load distribution. This mesh is composed by 3D solid elements, with fine refinement in the crack tip for better description of the stress field around it. This mesh was built with Femap, a specific tool to generate advanced finite element meshes, [178]. The mesh representing half of the stiffened panel is presented in Figure 5.5.

This mesh has at least two elements along the thickness in the thinnest section, in order to make it possible the computation of the stress intensity factor evolution along the thickness and a better description of bending effects. The elements used in this model

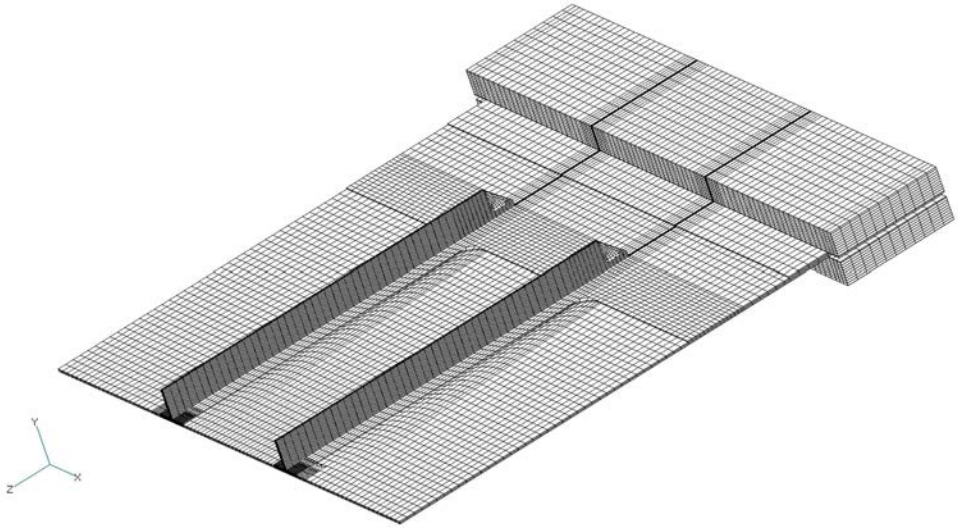

Figure 5.5: Finite element mesh.

are parabolic solid elements with 20 nodes. The numbers of fundamental variables in the model were:

- 230287 nodes;
- 47978 elements;
- 690861 variables (matrix dimension).

These FE models are solved in ABAQUS, using the C3D20 and C3D15 elements of the ABAQUS element library, [179]. Crack growth was simulated changing the boundary conditions along the theoretical crack growth line. For each crack length a step was created where the stress field in the specimen and the stress intensity factor in the crack tip were calculated. A total of 38 steps were used for each configuration.

5.2.3 Residual Stresses

Since the welding processes generate heat in the working pieces, the cooling gradients will generate residual stresses. These residual stress fields should be taken into account due to their influence in the global stress field in the loaded panel. These residual stresses were also considered in the FEM and were obtained by an experimental and destructive method. These measurements were done at the University of Pisa using the cutting method. The residual stresses were obtained by sectioning the panel, perpendicular to the stiffeners, and measuring the relaxation after the cut using strain gauges distributed along the cutting line, [180]. By using 62 strain gauge measurements on both sides of the panel and in the stiffeners very detailed information was possible to obtain a detailed information about the stress field.

In order to import the experimental residual stress measurements to the finite element models, an algorithm was developed to interpolate the residual stresses from the strain gauge points to the centroids of the finite element models, using the MATLAB v4 griddata function, [181]. Figure 5.6 shows the centroids of the first line of elements, the blue points, and the location of the strain gages where the residual stresses were measured, the red points.

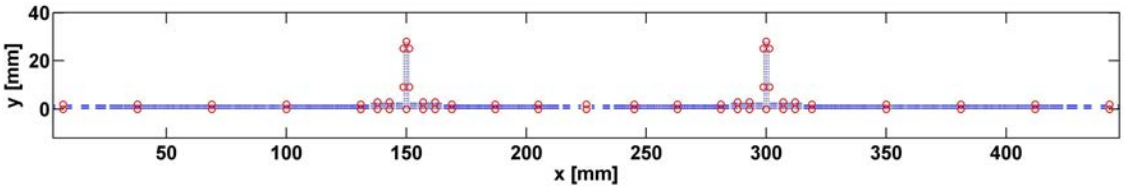

Figure 5.6: Interpolation of the experimental residual stress to the finite element model.

After the estimation of the residual stress in the centroids of the elements in the FEM, they were imported to the ABAQUS models as initial conditions. Figures 5.7 and 5.8 show contour maps with the initial stress field originated by the residual stress field. It should be pointed out that just the longitudinal residual stress were measured and just these were applied in the FEM. However, these longitudinal residual stresses are predominant and are the ones that have more influence in the crack growth phenomena.

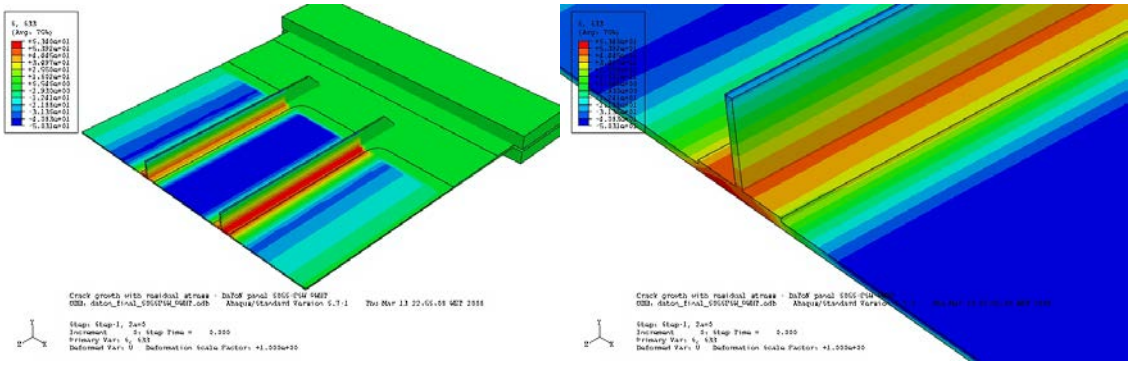

(a) General view **(b)** Detail

Figure 5.7: Initial residual stress state for the case of AA6056 FSW PWHT.

5.2.4 Stress Intensity Factor Determination

Several techniques might be used to calculate the stress intensity factors from the stress/strain field around the crack tip, [182]. For this purpose an energy technique based on Virtual Crack Closure Technique (VCCT) was applied, as it provides values along the skin panel thickness and it is an effective technique to estimate the SIF values in the

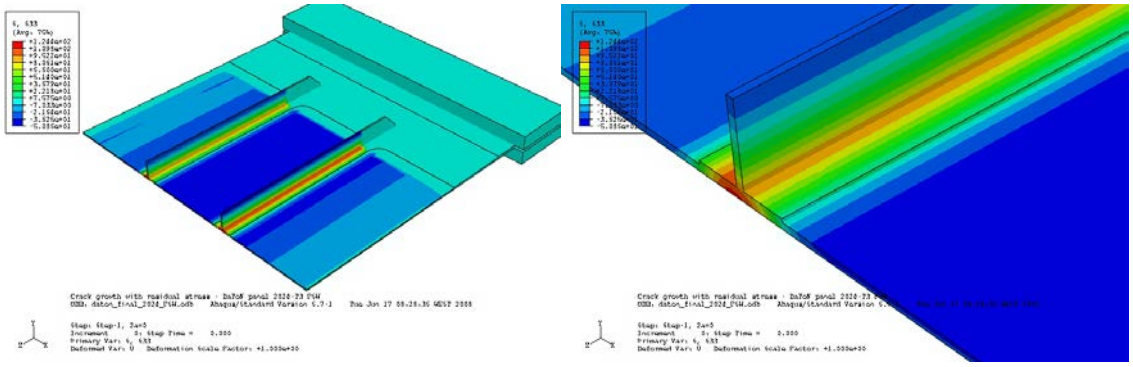

(a) General view **(b)** Detail

Figure 5.8: Initial residual stress state for the panels in AA2024-T3, welded by FSW

presence of residual stress fields. The J-integral approach was also considered but the algorithm presented in ABAQUS package presented difficulties in the convergence when the residual stress field is considered and when boundaries were in the vicinity of the crack tip. This issue is related to the contours that J-integral uses to estimate the energy release rate

Modified Virtual Crack Closure Technique

The VCCT was proposed by Rybicki and Kanninen in 1977, [183] in order to calculate the energy release rate (G) based upon the calculation of the strain energy release rate (U). From the energy variation when a virtual extension of crack length is imposed (Δa) the energy release rate can be approximated by the following equation:

$$G = \frac{\partial U}{\partial a} \approx \frac{U_{a+\Delta a} - U_a}{\Delta a} \tag{5.1}$$

The application of this concept in finite element models with cracks is done calculating the energy released during an infinitesimal crack growth. This energy (ΔE) can be calculated using the nodal loads that are required to maintain the crack increment closed ($\mathbf{f}$) and the displacement ($\mathbf{u}$) in the same nodes promoted by removing these loads:

$$\Delta E = \frac{1}{2}\left(\mathbf{f} \cdot \mathbf{u}\right) \tag{5.2}$$

The energy release rate is related to the energy release by the area (ΔA) created by the virtual crack extension:

$$G = \frac{\Delta E}{\Delta A} = \frac{\Delta E}{\Delta a \cdot t} \tag{5.3}$$

For plates with constant thickness t, this area is equal to $\Delta a \cdot t$. The energy release rate for each mode of fracture (mode I, II and III) can be determined by the decomposition of the Equation 5.2, using the nodal forces and nodal displacements in the direction that characterizes each fracture mode. The procedure requires two simulations, one to determine the reaction loads and another to determine the displacements, which can be a labor intensive and time consuming task in large finite element models.

A modified version of the virtual crack closure technique was presented by Krueger in 2004, [184]. This modified technique presupposes that the nodal displacements near the crack before and after a sufficiently small crack growth to a crack length of $a + \Delta a$, for nodes equidistant to the crack tip, are identical. This assumption allows a calculation of the energy release rate by using only the results from one finite element analysis for each crack length.

For 3D quadratic finite elements, the determination of the energy release rate using the modified virtual crack closure technique can be determined using the nodal loads and nodal displacements. However, it is required to consider different weights for the nodes being located on the mid-side of the element edge and on the corners of the element. For mode I, considering the notation presented in Figure 5.9, the equation used to determine the energy release rate for the node at the crack surface (node 3) is:

$$G_I = -\frac{1}{2\Delta a \cdot \Delta b}\left[F_{z_3}\left(u_{z_{1*}} - u_{z_1}\right) + F_{z_4}\left(u_{z_{2*}} - u_{z_2}\right) + \frac{1}{2}F_{z_6}\left(u_{z_{5*}} - u_{z_5}\right)\right] \tag{5.4}$$

F_z is the nodal force in the z direction, u_z is the displacement in z direction and Δa and Δb are the element dimensions.

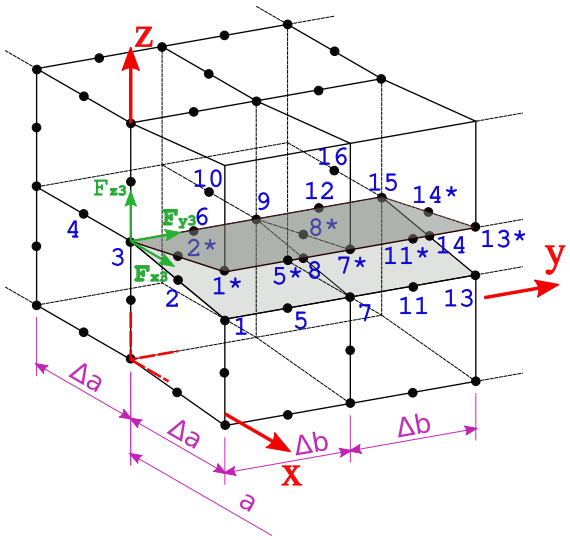

Figure 5.9: Annotation and node location for a quadratic solid elements.

For the nodes being positioned in the middle of an element edge, in this case node 6, this gives:

$$G_I = -\frac{1}{2\Delta a \cdot \Delta b}\left[\frac{1}{2}F_{z_3}\left(u_{z_{1*}} - u_{z_1}\right) + \frac{1}{2}F_{z_4}\left(u_{z_{2*}} - u_{z_2}\right) + \right.$$
$$\left. + F_{z_6}\left(u_{z_{5*}} - u_{z_5}\right) + \frac{1}{2}F_{z_9}\left(u_{z_{7*}} - u_{z_7}\right) + \frac{1}{2}F_{z_{10}}\left(u_{z_{8*}} - u_{z_8}\right)\right] \tag{5.5}$$

For the corner nodes inside the crack tip, in this case for the node 9, the energy release rate will be:

$$G_I = -\frac{1}{2\Delta a \cdot \Delta b}\left[\frac{1}{2}F_{z_6}\left(u_{z_{5*}} - u_{z_5}\right) + F_{z_9}\left(u_{z_{7*}} - u_{z_7}\right) + \right.$$
$$\left. + F_{z_{10}}\left(u_{z_{8*}} - u_{z_8}\right) + \frac{1}{2}F_{z_{12}}\left(u_{z_{11*}} - u_{z_{11}}\right)\right] \tag{5.6}$$

These three equations, 5.4, 5.5 and 5.6, are able to determine the evolution of the mode I stress intensity factor along the crack tip in thickness direction. Similar equations for the determination of SIFs in modes II and III can be derived from the above equations by exchanging the nodal loads and nodal displacements according to the associated mode of loading and can be found in [185].

5.2.5 Finite Element and SIF Results

Applying the modified virtual crack closure technique presented above, stress intensity factors were estimated for 37 crack lengths and for 8 models corresponding to different manufacturing states characterized by their residual stress field. In addition, since multiple elements along the skin thickness were used, the variation of the SIF along the thickness was determined, giving an indication about the crack front, the bending effect originated by the stiffeners and the effect of the non-symmetrical residual stress field along the thickness. At least two elements along the thickness were used in the thinnest part of the skin (2 mm). As these elements are parabolic, it is possible to determine the stress intensity factor for at least 5 points along the thickness. Figure 5.10 shows the results for the panels with stiffeners joined by FSW in AA6056-T6 and Post Welding Heat Treatment (PWHT) to T6, Figure 5.10a and in AA2024-T3, Figure 5.10b. These SIF values were obtained when a remote load equivalent to σ_{max} =110 MPa in the panel is applied.

Collecting the calculated stress intensity factors corresponding to 37 crack lengths and for different manufacturing processes and materials, the SIF variation with the crack size is obtained and presented in Figure 5.11.

In order to better recognize the impact of the residual stresses promoted by the different manufacturing processes and materials, the difference between the SIF for a panel without

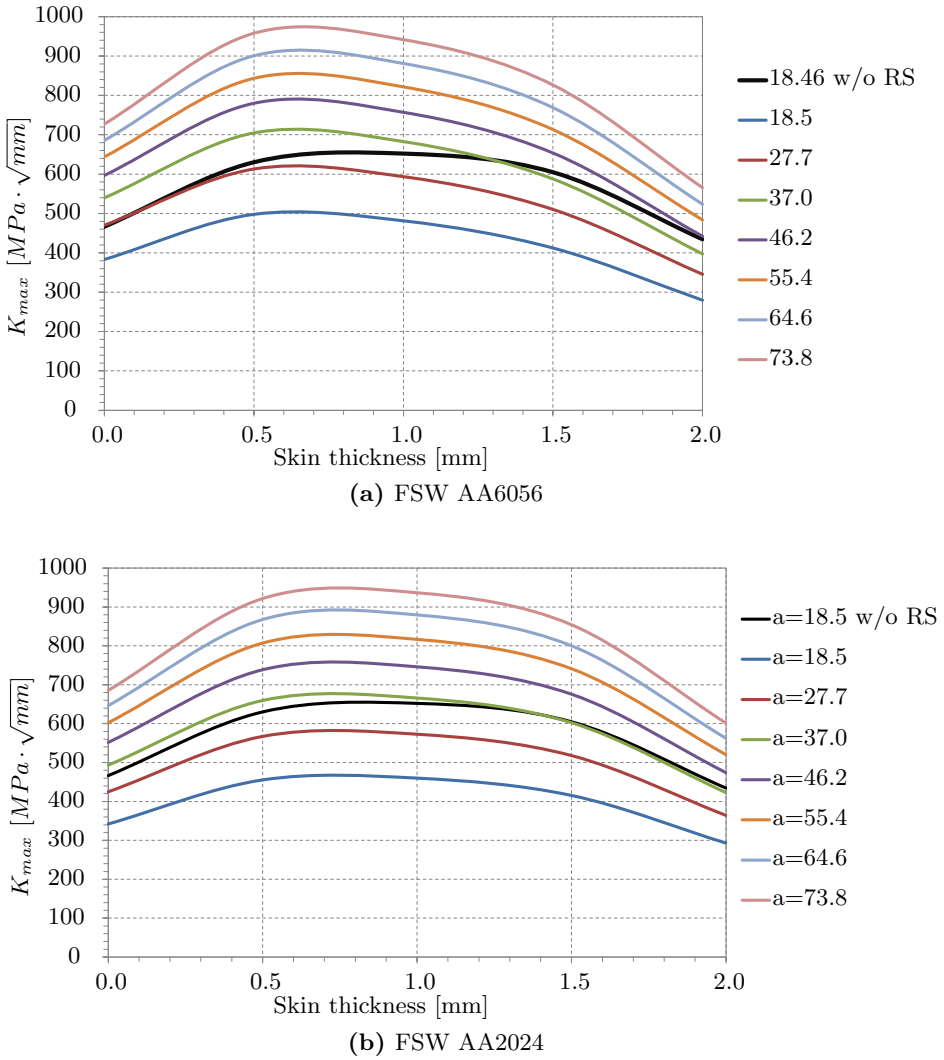

(a) FSW AA6056

(b) FSW AA2024

Figure 5.10: SIF variation along thickness, when applied a remote stress of σ_{max}=110 MPa.

residual stress[1] and the panel with residual stress, with the stiffeners welded, was calculated. This assessment is presented in Figure 5.12, using the SIF when a remote stress of σ_{max}=110 MPa is applied.

Figure 5.12 shows the impact of the residual stress field, which can increase or decrease the SIF in about 30%. The welded panels present lower SIF values for the small crack lengths, in the middle of the specimen of the specimen due to the compressive residual stress in this region. When the crack tip reaches the stiffeners the SIFs are higher than the reference without residual stress, due to the tensile residual stress. As concerns the different welding process and materials, it is noticed that the FSW process and the material AA2024-T3 induce higher compressive residual stress in the middle of the panel. Globally, the stiffened panel in AA6056 PWHT to T6 and joined by FSW process presents a good

[1]representing the stiffened panel that was produced by HSM

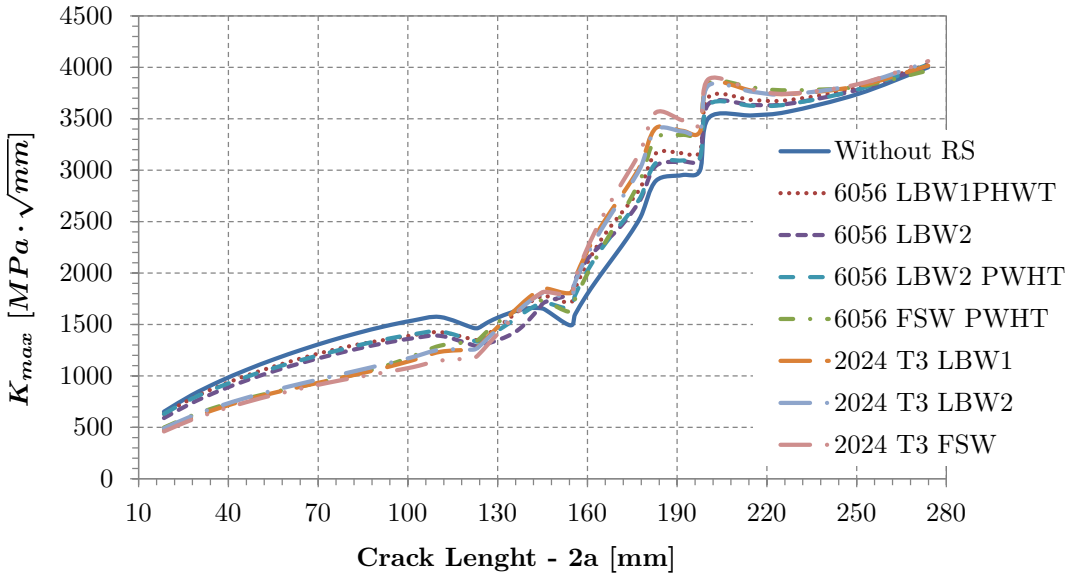

Figure 5.11: SIFs for the different manufacturing processes, when applied a remote stress of σ_{max}=110 MPa.

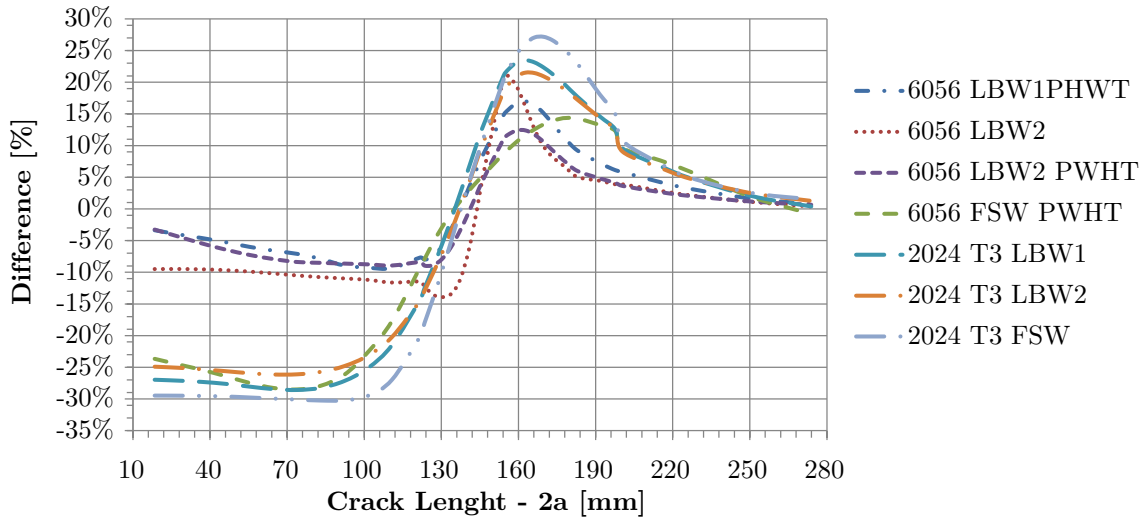

Figure 5.12: Residual stress impact in the SIF variation.

result, do to the lower SIF values in the stiffener region. The panels in the aluminium alloy AA2024-T3 have the higher differences, caused by a more severe residual stress field.

5.2.6 Fatigue Crack Growth

After the characterization of SIFs for the geometry, residual stress, remote load and defect considered, the fatigue crack growth determination and the fatigue life estimation,

when a panel has this initial defect, are possible. A number of laws may be used to predict the fatigue behavior. Since in this study the stiffened material is anisotropic aluminium alloy, linear elastic fracture mechanics assumptions are suitable to model the FCG and fatigue life.

The first FCG law was proposed by Paris in 1963, [186], defined as:

$$\frac{da}{dN} = C_P \Delta K^{n_P} \tag{5.7}$$

where a is the crack length, N is the number of cycles, ΔK is the stress intensity factor, C_P and n_P are material constants. The integration of the Paris law could give a good estimation of the fatigue life in the cases where the stress intensity factor is the linear part of the $log(da/dN)$ *vs.* (ΔK) (phase II of the FCG curve), and when $log(da/dN)$ is only function of the stress intensity factor and material constants. In the cases where the load ratio R at the crack tip is not constant, as in the presence of a residual stress field, the integration law should also reflect this value.

Forman in 1963, [187], proposed a more complete FCG law, including the effect of the load ratio (R) and the asymptote associated to the fracture toughness of the material (K_c), corresponding to the phase III of the FCG laws:

$$\frac{da}{dN} = \frac{C_F \Delta K^{n_F}}{(1-R)\, K_c - \Delta K} \tag{5.8}$$

where C_F and n_F are material constants for the Forman law, that can be estimated from the constants used in Paris law (C_P and n_P).

Another fatigue law suitable for fatigue crack growth in the phase II and that takes into account the influence of the load ratio (R), is the Walker law, [188]. This law introduces a exponent m_W in order to improve the accuracy of the growth rate dependence with the load ratio:

$$\frac{da}{dN} = \frac{C_W \Delta K^{n_W}}{(1-R)^{m_W}} \tag{5.9}$$

A more comprehensive FCG law based on previous laws, which includes the fatigue threshold and fatigue toughness effects, with a better fit for different load ratios is the NASGRO law, [97]:

$$\frac{da}{dN} = C_N \left[\left(\frac{1-f}{1-\mathrm{R}_{eff}} \right) \Delta K \right]^{n_N} \frac{\left(1 - \dfrac{\Delta K_{th}}{\Delta K} \right)^p}{\left(1 - \dfrac{K_{\max}}{K_C} \right)^q} \tag{5.10}$$

where C_N, n_N, p and q are empirically derived constants for the material, f is the crack opening function for plasticity-induced crack closure that has been defined as:

$$f = \begin{cases} \max\left(R, A_0 + A_1 R + A_2 R^2 + A_3 R^3\right) & R \geq 0 \\ A_0 + A_1 R & -2 \leq R < 0 \end{cases} \tag{5.11}$$

A coefficients are defined as:

$$A_0 = \left(0.825 - 0.34\alpha + 0.05\alpha^2\right) \times \left[\cos\left(\frac{\pi}{2}\frac{S_{\max}}{\sigma_0}\right)\right]^{1/\alpha} \tag{5.12}$$

where α is a plane stress/strain constraint factor, and S_{max}/σ_0 is the ratio of the maximum applied stress to the flow stress. And the other A coefficients are:

$$A_1 = \left(0.415 - 0.071\alpha\right)\frac{S_{\max}}{\sigma_0} \tag{5.13}$$

$$A_2 = 1 - A_0 - A_1 - A_3 \tag{5.14}$$

$$A_3 = 2A_0 + A_1 - 1 \tag{5.15}$$

NASGRO provides a material database with these constants for different types of materials, heat treatments and thickness. The fracture toughness values usually presented in the material databases are for the condition of plane strain fracture. However in thin plates the plane stress condition is predominant and for this condition the fracture toughness depends of the thickness. The following equation can be used to estimate the fracture toughness for thin plate, K_c, from the value of fracture toughness K_Ic:

$$\frac{K_c}{K_{Ic}} = 1 + B_k e^{-\left(A_k \frac{t}{t_0}\right)^2} \tag{5.16}$$

where

$$t_0 = 2.5\left(\frac{K_{Ic}}{\sigma_{YS}}\right)^2 \tag{5.17}$$

where t is the thickness of the plate, the constants A_k and B_k are presented in NASGRO database and σ_{YS} is the yield tensile strength of the material.

Regarding to the threshold stress intensity factor range, ΔK_{th} for the NASGRO law, it can be approximated by the following expressions:

$$\Delta K_{th} = \frac{\Delta K_1^* \left[\frac{1-R}{1-f(R)}\right]^{\left(1+R\cdot C_{th}^p\right)}}{(1-A_0)^{\left(1-R\cdot C_{th}^p\right)}}, R \geq 0 \tag{5.18}$$

and

$$\Delta K_{th} = \frac{\Delta K_1^* \left[\frac{1-R}{1-f(R)}\right]^{\left(1+R\cdot C_{th}^m\right)}}{(1-A_0)^{\left(C_{th}^p - R\cdot C_{th}^m\right)}}, R < 0 \tag{5.19}$$

where ΔK_1^* is calculated by:

$$\Delta K_1^* = \Delta K_1 \left[\frac{a}{a+a_0}\right]^{1/2} \tag{5.20}$$

where ΔK_1 is the threshold stress intensity factor range as $R \rightarrow 1.0$, C_{th} is an empirical fit constant with different values for positive (superscript p) and negative (superscript m) R ratios, and a_0 is a small crack parameter (typical value of 0.0015 inch or $\sim$0.04 mm).

Effective Load Ratio

A common approach used for incorporation of residual stresses effect on fatigue crack growth is based on the estimation of the effective stress ratio (R_{eff}) at crack tip. This approach can be described in detail by considering the specific cases of Walker or Forman equations in [189]. For instance, the Forman law to take consideration a residual stress field can be written as:

$$\frac{da}{dN} = \frac{C_F \Delta K_{eff}{}^{n_F}}{(1-R_{eff})K_c - \Delta K_{eff}} \tag{5.21}$$

where R_{eff} is calculated with the SIF without residual stress (K_{max} and K_{min} and the SIF due to the residual stress:

$$R_{eff} = \frac{K_{\min} + K_{res}}{K_{\max} + K_{res}} \tag{5.22}$$

and ΔK_{eff} is basically ΔK without residual stress as can be demonstrated by:

$$\Delta K_{eff} = K_{\max_{eff}} - K_{\min_{eff}} = (K_{\max} + K_{res}) - (K_{\min} + K_{res}) = K_{\max} - K_{\min} = \Delta K \tag{5.23}$$

Thus the effective stress ratio is the only term that considers the effect of residual stress. For this reason, Paris law cannot be used for such purposes, but at the same time any fatigue crack growth law that includes R could be applied using the effective load ratio at the crack tip. Figure 5.13 shows an example of the evolution of the effective load ratio, calculated from the stress intensity factors of the numerical models with residual stresses, in this case for stiffened panels produced with FSW in AA6056 and AA2024-T3, for the both load ratios. The effective load ratio at crack tip is much lower that the load ratio applied for most of crack growth length. In the case of the load ratio equal to 0.1, the crack tip has under compression stresses during most of the crack path length (until $2a \cong 130$ mm).

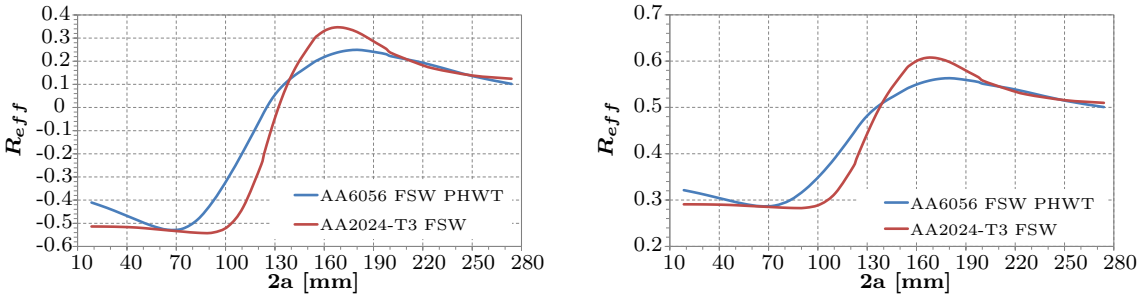

(a) R=0.1 **(b)** R=0.5

Figure 5.13: Variation of R_{eff} for the stiffened panels produced by FSW.

Fatigue Crack Growth Laws Constants of AA6056-T6 and AA2024-T3

The use of representative material data is one of the most important parts of a fatigue crack growth analysis in order to have an accurate estimation of the material constants. The material constants for the aluminium alloy AA2024 with heat treatment T3 are presented in NASGRO database, [97]. However, the AA6056 is a recent aluminium alloys and, for this alloy, data is not found in the databases. Due to these circumstances, experimental testing was done to measure these parameters. The local changes in the material heat treatment was not considered in these models, as in the LBW AA6056-T6 as welded panels it was not possible to define the real heat condition along the heat affected zone; however this only changes the crack growth condition at the welding line and not throughout most crack path.

To determine the FCG material parameters, experimental data was collected for 6056 aluminium alloy from different partners in DaToN project using standardized coupons that were machined from tested panels. A comparison of the FCG behavior of coupons machined from a block of 40 mm (used to manufacture HSM stiffened panels) and from plates used in the LBW and FSW panels are presented in Figure 5.14

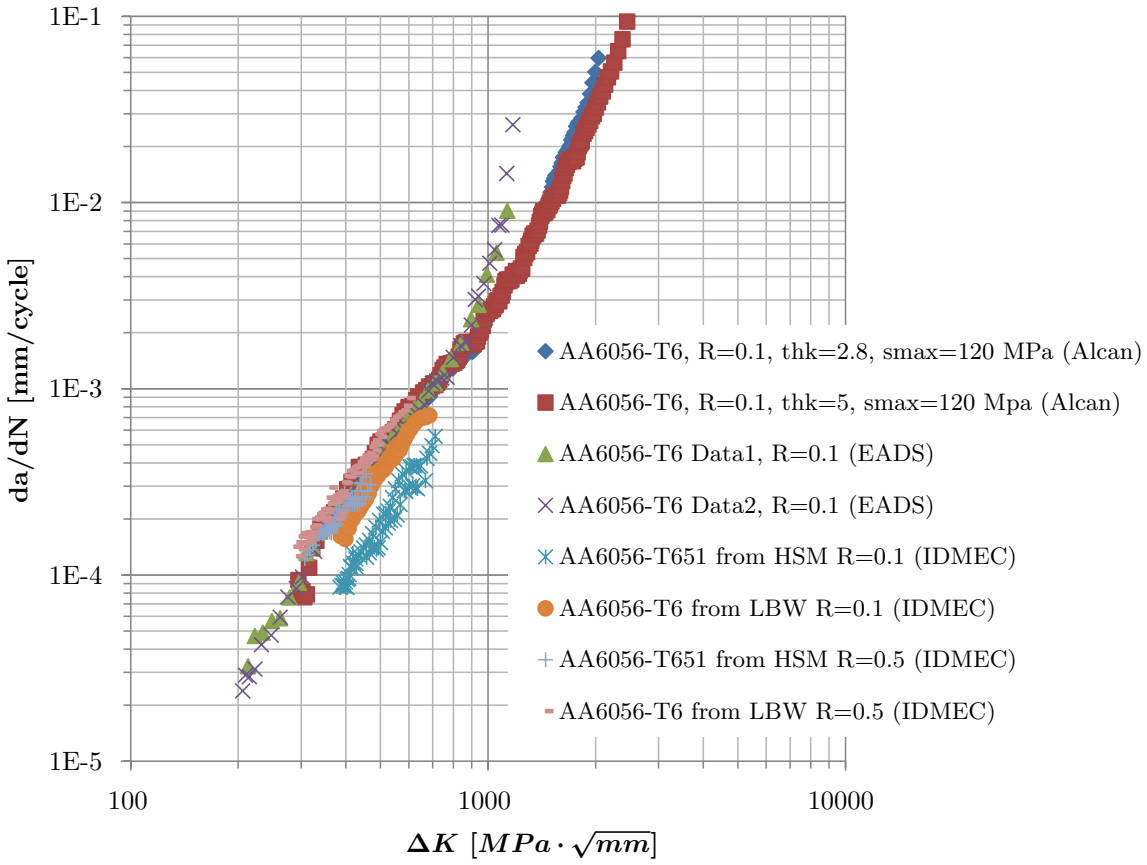

Figure 5.14: Experimental FCG points for AA6056-T6.

The FCG Forman law was applied to this case because good fits to the experimental data can be obtained with simple computational algorithms. Nevertheless, each set of experimental data could be fitted separately using a power law with their coefficients C_P and n_P being the parameters of the Paris law, [190]. Unfortunately, the best fits to the experimental data not always give the best predictions, [189]. The reason for this is that in all curve fitting procedures the same weight is given to each point in the experimental data, while it is known that points at low da/dN levels have a greater influence in the total fatigue life (most of the specimen life is spent during that period). The lack of physical meaning provided by mathematical procedures should be also balanced with engineering judgement in order to obtain a representative fit to the real problem. For Forman FCG law several fits were used by the partners in order to determine the best parameters aggregation leading to a reasonable description for the two load ratios, R=0.1 and R=0.5. The procedure used to determine the Forman constants was done linearizing the logarithmic values from experimental measurements for both load ratios:

$$\log\left(\frac{da}{dN}\cdot\left[(1-R)\,K_c-\Delta K\right]\right)=n_F\log\left(\Delta K\right)+\log\left(C_F\right) \tag{5.24}$$

Afterwards, the value n_F is determined using the least mean squares technique and the C_F value is determined using the minimization of the error between the Forman law and the experimental points. The achieved values that will be used for fatigue life estimation were:

C_F=2.9E-7
n_F=2.351
K_c=3000 $MPa\sqrt{mm}$

Figure 5.15 shows the two Forman laws curves using this parameters in the plot with the experimental points. Since the experimental data for the load ratio R=0.5 is scarce, an accurate fitting to several load ratios is limited. Nevertheless, these data have some variance due to the natural aging and fluctuations in the manufacturing processes.

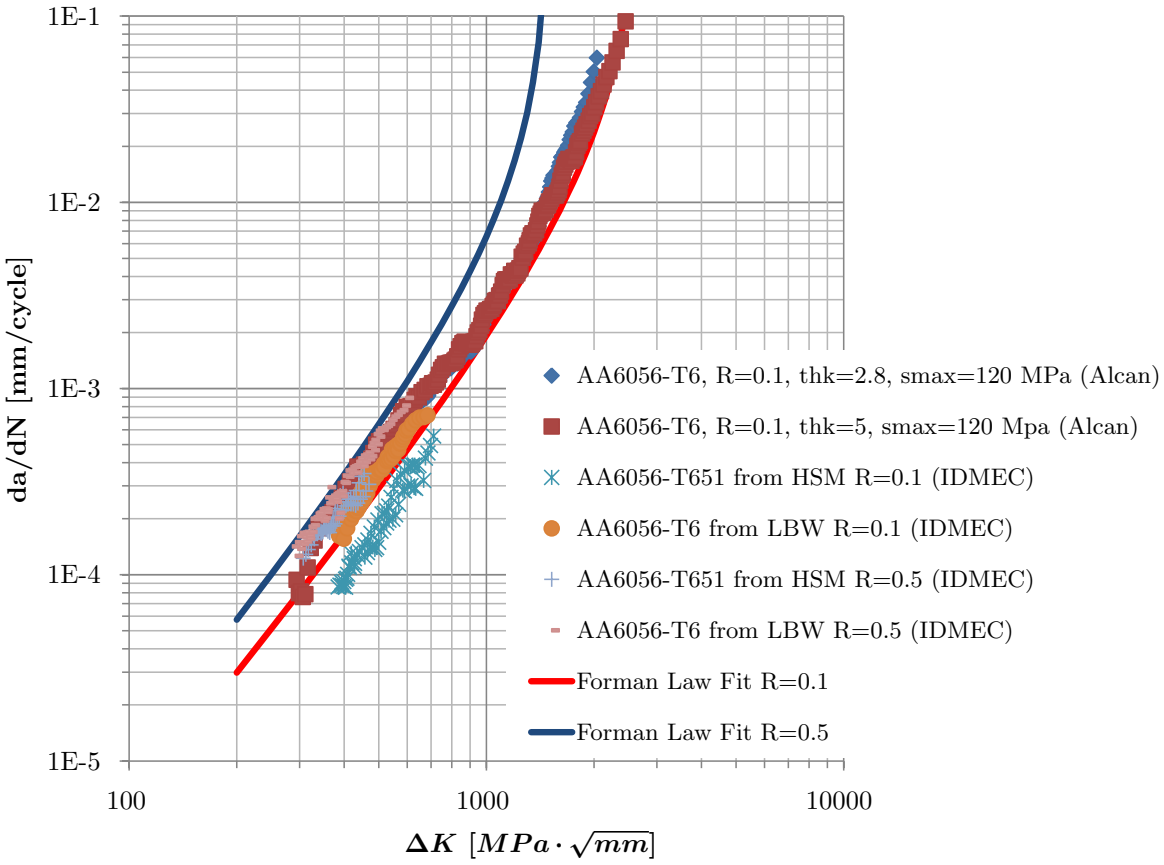

Figure 5.15: Forman law, constants fitting to the experimental data, AA6056.

For the alloy AA2024-T3 the fatigue properties were obtained from the NASGRO database. In this database two different calibrations are presented for the AA2024-T3 L-T. The calibration 11AB1 was used for the fatigue life estimation. Figure 5.16 shows the curves for 4 different load ratios and NASGRO equation fitting.

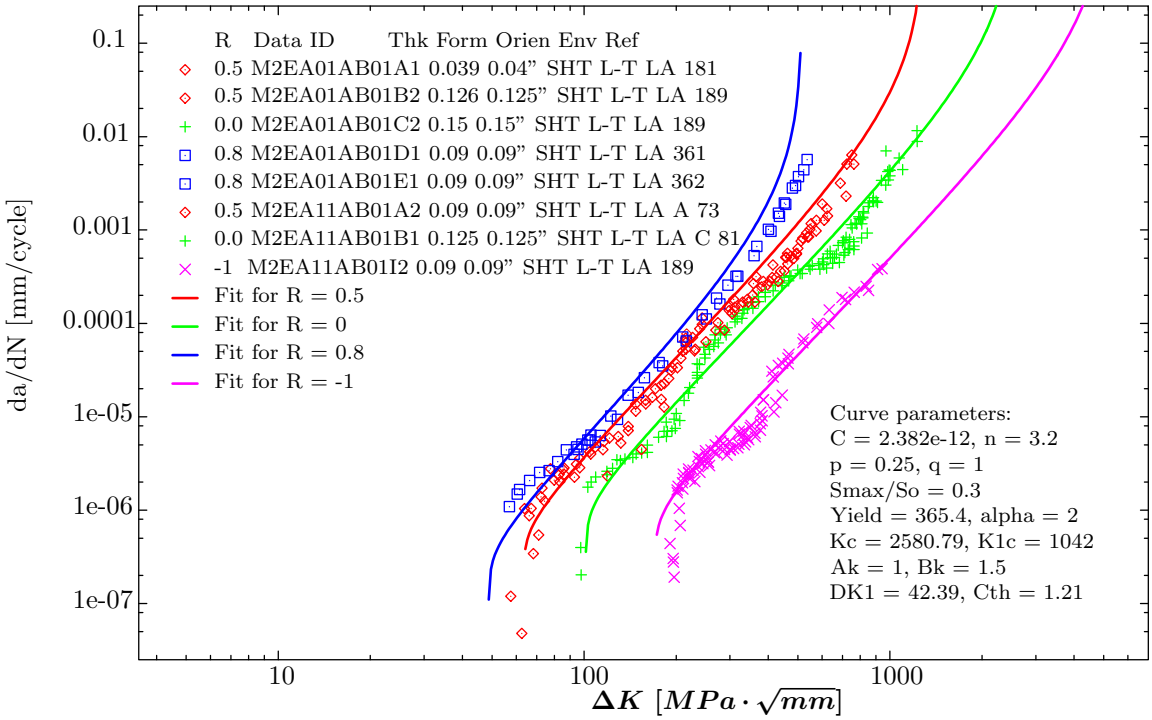

Figure 5.16: NASGRO law, curve fitting to experimental poitns.

5.3 Fatigue Life

The fatigue life of these two stiffeners panels, manufactured by the different process, will be calculated with FCG laws in order to study the viability to evaluate the fatigue life based on the residual stress field.

5.3.1 Numerical Results

With the stress intensity factors solutions calculated in section 5.2.5 and with the integration of the crack growth laws presented in section 5.2.6, the fatigue life of these stiffened panels was modeled. For this purpose algorithms that integrate the fatigue crack growth laws (Forman and NASGRO) considering the variation of ΔK and R_{eff} as functions of a were developed. The algorithms were built in Matlab applying numerical integration of the FCG and considering linear variations between the discrete points of $\Delta K(a)$ and $R_{eff}(a)$.

The results obtained for the different panels are presented in Figure 5.17 for the stiffened panels subjected to a maximum remote stress of σ_{max}=80 MPa and a load ratio of R=0.1 and Figure 5.18 for the panels subjected to a maximum remote stress of σ_{max}=110 MPa and a load ratio of R=0.5. The models without residual stresses represent the HSM panels,

since the manufacturing process does not generate considerable heat and the yielding is negligible, therefore the residual stress field is negligible. The fatigue life results of the stiffened panels in AA6056-T6 were obtained using the Forman law and the stiffened panels in AA2024-T3 were obtained with the NASGRO law and with the parameters presented above.

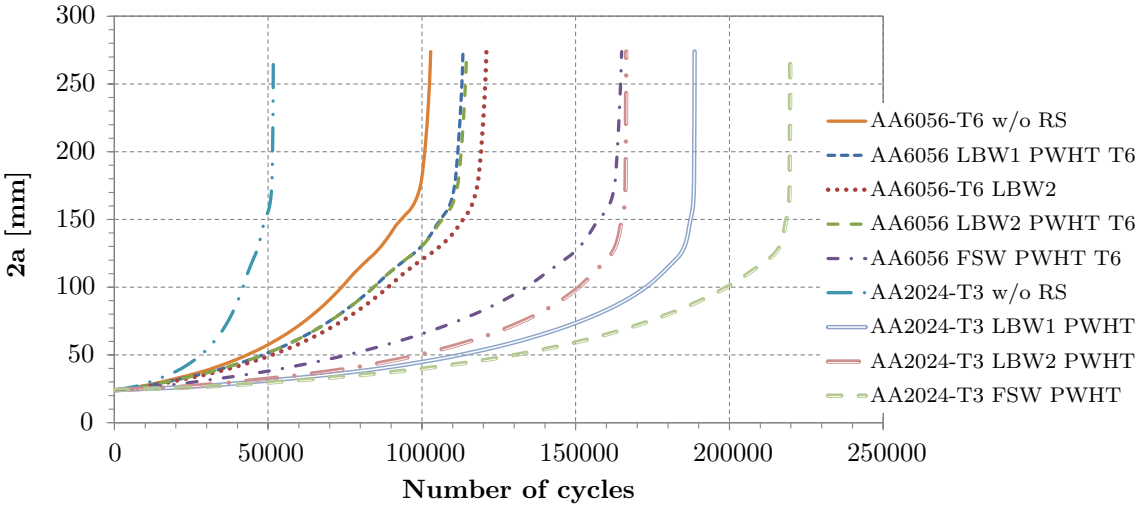

Figure 5.17: Modeled fatigue life for the load ratio R=0.1 and σ_{max}=80 MPa.

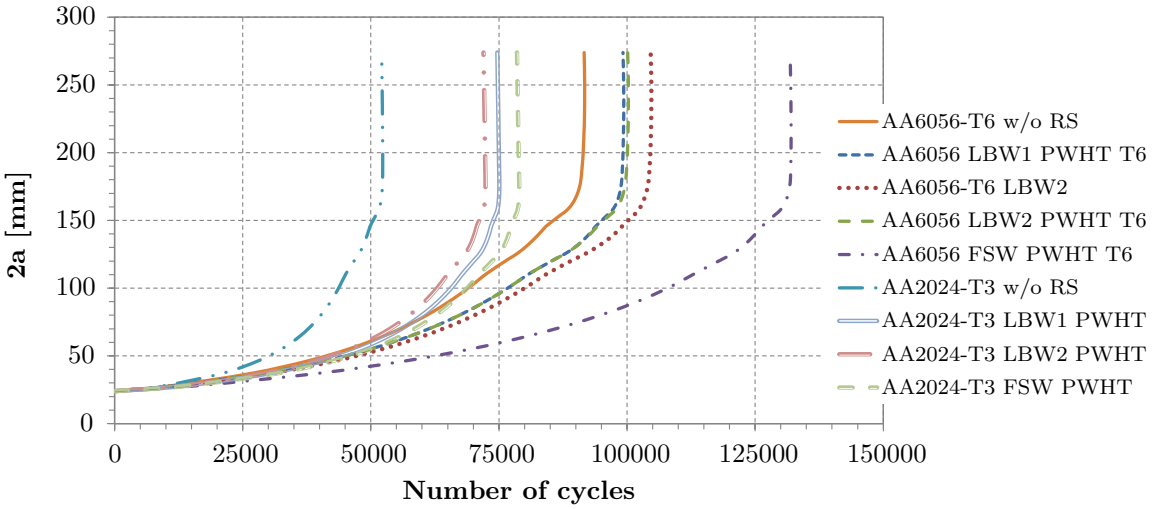

Figure 5.18: Modeled fatigue life for the load ratio R=0.5 and σ_{max}=110 MPa.

The stiffened panels manufactured by LBW have a significant increase of their fatigue life compared with the machined panels; however the FSW panels present the higher fatigue life. This fact is originated by the compressive residual stresses in the beginning of the crack and most of the remaining fatigue lives of these panels are in the small crack lengths (less than 100 mm). The fatigue life of the AA2024-T3 with a load ratio of R=0.1 presents

better fatigue life than the AA6056-T6. These results are due to the consideration in the NASGRO law of the crack closure effect for compressive residual stress, a effect that the Forman law does not take into account. Nevertheless, the AA6056-T6 material is more damage tolerant than the AA2024-T3, as it is observable from the fatigue life results for the load ratio R=0.5.

5.3.2 Experimental Comparison and Validation

As mentioned above, the fatigue behavior of each configuration was experimentally studied by different partners in the DaToN project in order to acquire a better understanding of the impact of the different manufacturing process to produce stiffened panels and to validated the numerical models. In Figure 5.19, a plot with the experimental results for panels in AA6056-T6 and tested with the load ratio R=0.1 performed by IDMEC at Porto, [191], is presented. It is perceptible that the manufacturing processes change significantly the fatigue life. In this case, the HSM gave the lower fatigue life while the LBW with the configuration 2 gives the higher fatigue life. However, fatigue life models have some dispersion inherent to the integration of the fatigue crack growth laws used. These are exponential laws, very sensitive to the material parameters.

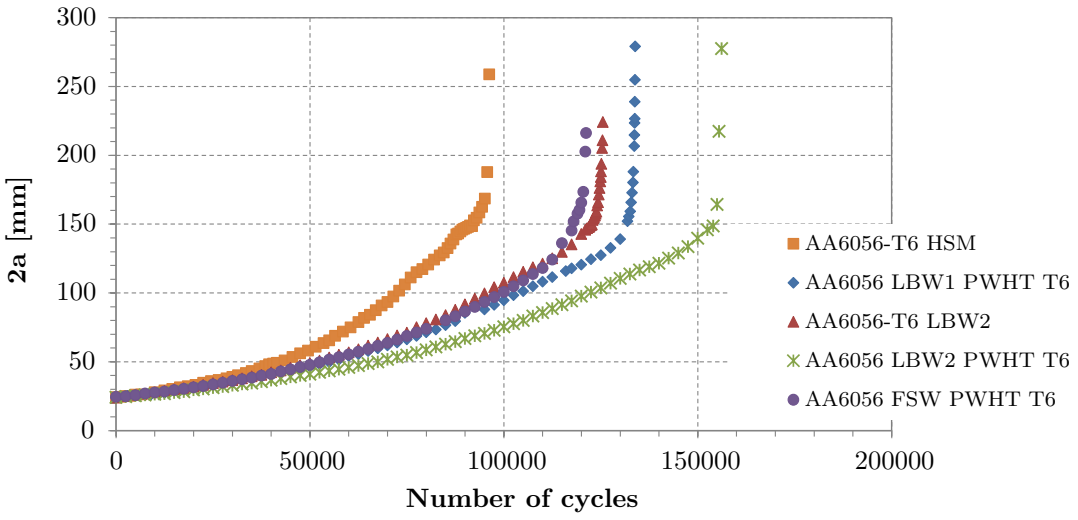

Figure 5.19: Experimental results from A6056-T6 panels tested at the load ratio R=0.1 and σ_{max}=80 MPa.

Comparisons between the experimental results and numerical models of the fatigue life for these stiffened panels were done for all manufacturing processes, HSM, LBW and FSW, for the two materials, AA6056-T6 and AA2024-T3 and for the two stress levels corresponding the load ratios R=0.1 and R=0.5.

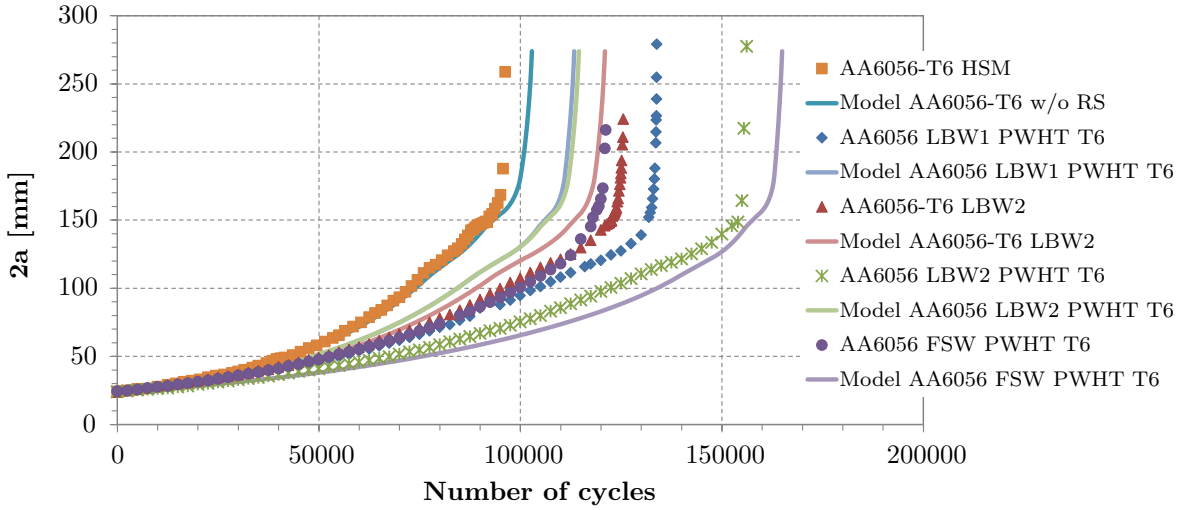

Figure 5.20: Fatigue life comparison for the A6056-T6 panels tested at the load ratio R=0.1 and σ_{max}=80 MPa.

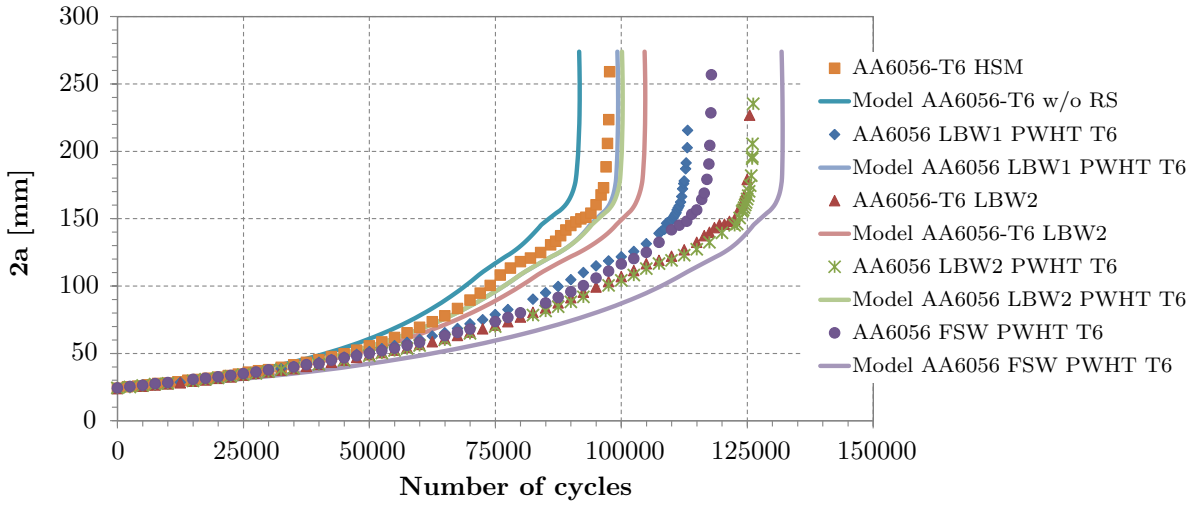

Figure 5.21: Fatigue life comparison for the A6056-T6 panels tested at the load ratio R=0.5 and σ_{max}=110 MPa.

Figures 5.20 and 5.21 shows the comparison for the case of AA6056 stiffened panels. Good convergence in the results was obtained for both load ratios. In LBW panels some divergence is observed, but in the fatigue life these differences are not significative due to the sensitivity of the FCG laws. For more accurate models, measurements of the material crack growth properties, locally, are required, and that is not feasible with non-destructive techniques.

The presented methodology can support the design of stiffened structures as in the optimization of the joining positions and geometry, and the estimation of maintenance

intervals for check-ups to prevent catastrophic failures. Accurate material properties are fundamental for fatigue life estimations, although these properties are function of the multiple variables, even the aging (due to the natural aging in aluminium alloys).

Chapter 6

New Friction Stir Welding Concepts

Since FSW is still an emerging technique, the development of new design concepts taking advantage of this process will help its adoption in many diverse applications. During this research, several new concepts that might contribute to the success of new structural solutions for aeronautical airframes were analyzed and developed.

T-joints and tailored welded blanks are two welding geometries that can provide wide flexibility and lightweight solutions for reinforced panels. FSW T-joints might reinforce joints along the welding line and join stiffeners and doublers to the skin. Tailored welded blanks allow an optimization of skin panels with capability to join parts with different thicknesses without weight penalties. Another concept that will be presented is a new procedure to react the forging force of the friction stir welding process with several advantages for long welds, avoiding root flaws and with lower drawbacks when compared with the bobbin tool concept. The application of FSW is also expandable to structural repairs, capable to repair cracked structures recovering the full integrity without the necessity of replacement of the complete part.

6.1 T-Joint Configurations

T-joint welding configuration is a type of geometry commonly found in diverse structures because it can increase significantly the inertia and strength of thin skins or plates without a significant increase in weight, which is particularly relevant in transport structures. This configuration is regularly used as reinforcement of aircraft airframes, in ships, trains and many other applications where the specific strength of the structure is especially important. This joint type can be obtained using many different manufacturing processes, as riveting, fastening, bonding or welding. This joint geometry can also be obtained using extrusion or machining, however the overall dimensions of components produced are limited due to the limitations of aluminium blocks for machining and due to the high extrusion forces and stability. Therefore, when large reinforced panels are needed, extrusion or machining are

not feasible solutions, being required the application of welding or other type of joining processes as riveting or adhesive bonding. FSW might therefore be used to achieve this geometry with several advantages. An intrinsic advantage is that an overlap area is not required to perform the joint as it is required in riveted and bonded joints. The application of welding processes to produce T-joints is very common procedure, where the web (the vertical element) is joined to the flange or plate (horizontal element) with the fusion of material in the corners of the T. However, this methodology cannot be used with FSW without special machining operations in the elements to create flat tangential surfaces along the weld line. A common alternative to join T-joints with FSW is welding from the opposite side, with the shoulder tangential to the upper surface of the frame element, and the probe crossing the frame and partially penetrating the web mixing the materials and joining both parts. However, the flux of material may be insufficient to mix the top web completely, and small cracks in the T corners are frequently found, [192].

Just a few studies are found in the literature concerning the application of the FSW process to the production of T-joints. Erbslöh *et al.* [193], report a study about T-joints in aluminium alloy AA6013-T4 and 4 mm thick plates. Plunging the tool through the skin and the stiffener, the effect of the backing plates shape in the T corners was analyzed. Another study related with this topic was done by Fratini *et al.* [194], where a comparison of the performance of T-joints obtained with metal inert gas welding, extrusion and FSW for the alloy AA6082 is presented. A study about T-joints produced using FSW, with A36 mild steel material was reported by Steel *et al.* [195]. In this study T-joints composed by flanges, 6 mm thick and a web with of 3 mm were joined with a polycrystalline cubic boron nitride material tool (comprised by a pin length of 7 mm and mm and a shoulder diameter of 25 mm). Difficulties to remove tunnel defects, even forcing the generation of chamfers were reported, although the major defect was the ligament interface defect requiring further investigations to improve the material flux and blend.

A new concept to weld T-joints with FSW was developed and studied in order to solve the problem of the unwelded material in the T corners and to improve the mechanical properties. Different alternatives to create T-joints with FSW are presented in Figure 6.1, some of them described in the Portuguese patent number 103867, [196]. When the web penetrates the flange, less material flow is required in order to promote the weld and it is easier to eliminate the cracks in the T corners without special operations. Another advantage is the tool (or probe), which can have a larger diameter and lower height, therefore being more robust.

An investigation, focused on the solution where the T is composed by three elements and the web is inserted in the two parts of the flange, 6.1a, was performed and published in [197]. This option was selected because it opens the possibility to reinforce plates simultaneously with the welding operations, without special machining of the plate edges

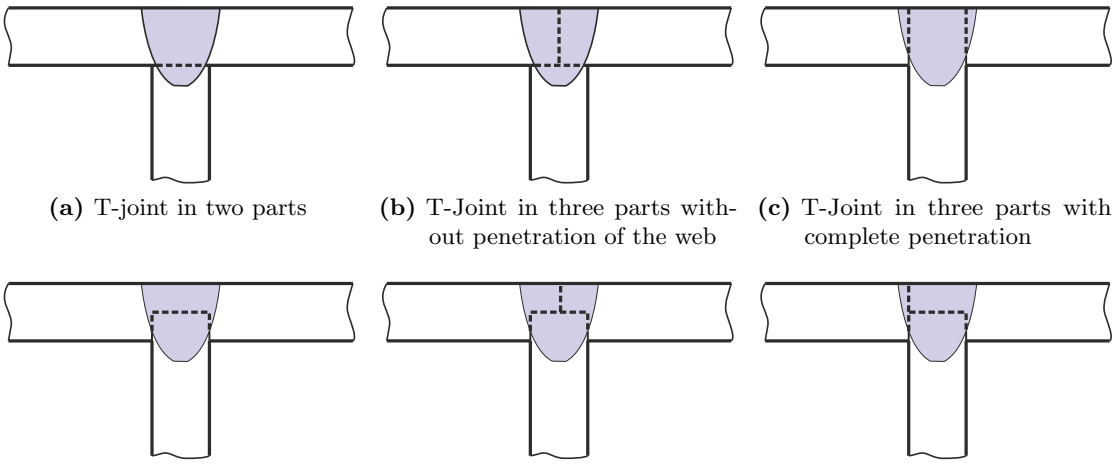

(a) T-joint in two parts

(b) T-Joint in three parts without penetration of the web

(c) T-Joint in three parts with complete penetration

(d) T-Joint in two parts with partial penetration

(e) T-Joint in three parts with partial penetration

(f) T-Joint in three parts with partial penetration

Figure 6.1: Design solutions to produce T-joints by FSW

(as in Figures 6.1d, 6.1e and 6.1d). Indeed, the fabrication of a large uniform thickness flat plate out of n smaller plates, requires (n-1) weldments; using the T configuration described (Figure 6.1c), the same number of weldments creates a reinforced structure at reduced cost. A preliminary study of this configuration was presented in references [198, 199], where T-joints, with the material AA6082, were produced without cracks and with reasonable mechanical properties.

In many applications, the reinforcement (in this case, the T web) requires higher strength and the skin or the T flange requires higher toughness because it is subjected to the initiation of defects and other damage during the product life. In this study the AA6056-T4 alloy, with good toughness, is used in the flange and AA7075-T6 alloy, with high strength, is used in the web. The chemical composition, in weight percentage, of these three alloys is presented in Table 6.1.

Table 6.1: Chemical composition of the welded aluminium alloys, (in wt%), [200].

	Si	***Mg***	***Cu***	***Mn***	***Fe***	***Zn***	***Zr***
AA6056	0.7-1.3	0.6-1.2	0.5-1.1	0.4-1.0	<0.5	0.1-0.7	0.07-0.2
	Zn	***Mg***	***Cu***	***Cr***	***Si***	***Fe***	***Mn***
AA7075	5.1-6.1	2.1-2.9	1.2-2.0	0.2-0.3	<0.4	<0.5	<0.3

6.1.1 Experimental Procedure

The cross section of the T-joint geometry welded in these tests is shown in Figure 6.2. The plates were cut and welded longitudinally to the rolling direction. Specimens welded with AA7075 have a 3.2 mm thick web.

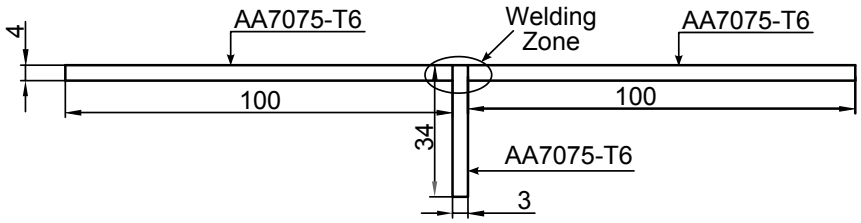

Figure 6.2: Dimensions of the cross section of welded T-joint geometry.

The welds were performed at Instituto Superior Ténico, in Lisbon, Portugal. A dedicated FSW ESAB Legio 3UL machine, Figure 6.3a, under vertical downward force control, was used to make these welds, Figure 6.7b. All the specimens were welded along the workpieces lamination direction with a planar scrolled (2 spiral striates) shoulder, which enabled a null tilt angle. The shoulder diameter was 19 mm for the T-joints and 15 mm for the butt joints. The probe length was about 4 mm in all the welds and the shape was selected in order to promote a complex random visco-plastic material flow in the stirring zone. The probe geometry for the T-joints was threaded on a conical body whose diameter ranged from 8 mm (top) to 6 mm (bottom) including 3 vertical helicoidal channels. The probe shape for the butt joints was cylindrical M5 threaded with 3 conical facets.

(a) ESAB LEGIO 3UL FSW equipment.

(b) T-joint welding.

Figure 6.3: T-joints welding, equipment and process.

In all T-joint welds, the rotation speed was 1120 rpm and the travel speed was 200 mm/min with a vertical downward force in the range of 7000 to 7500 N. The process

parameters implemented for the equivalent butt joints were a rotational speed of 800 rpm, a travel speed of 200 mm/min and a vertical downward force of 6500 N.

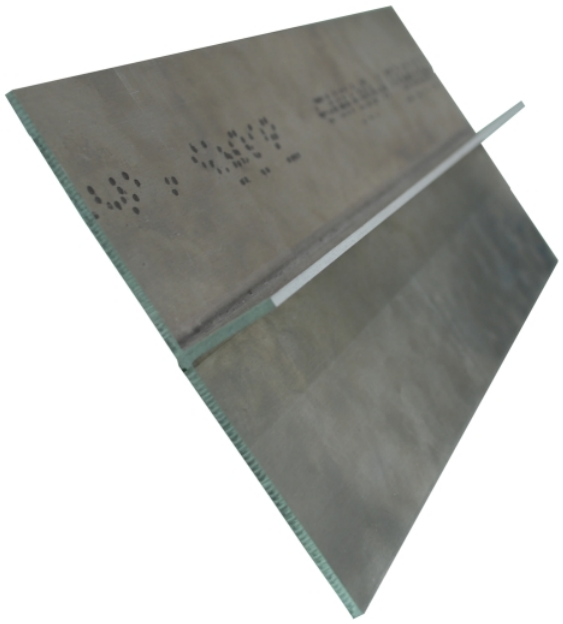

Figure 6.4: T-joint friction stir welded specimen.

Specimens for mechanical characterization, residual stress measurement and metallographic analysis, were produced from the welded samples to test the integrity of the joint and of the welding parameters.

Mechanical Characterization

The mechanical characterization consisted of tensile, fatigue and bending tests. The tensile tests were done in accordance with ASTM E8M standard, [201]. Stress-strain curves were also obtained for base materials AA6056-T4 and AA7178-T6 in order to compare and control the base material properties. These tensile tests were performed on a MTS servo-hydraulic machine. The tensile strain was measured by a clip gage with a gage length of 25 mm and the specimens were loaded under displacement control at a speed of approximately 1 mm/min. The measured tensile properties for the base materials AA6056-T4 and AA7178-T6 are presented and compared with literature results in Table 6.2.

Stress strain curves were measured for welded specimens in the butt joint and T joint configurations transversally to the weld line. At least three tensile specimens for each combination were produced. The results were compared with those of the AA6056-T4 base material perpendicular to the rolling direction (the same direction of the weld). Figure 6.5

Table 6.2: Mechanical properties of base materials.

	σ_{YTS} [MPa]	σ_{UTS} [MPa]	ε [%]	E [MPa]
Literature AA6056-T4 LT, [202]	240	316	23	–
Literature AA6056-T4 LT, [203]	230	330	32	72000
Measured AA6056-T4 LT	257.8	352.9	30	77469
Measured AA6056-T4 TL	234.3	335.5	20.5	68000
Literature AA7178-T6 LT, [200]	548	607	10	71700
Measured AA7178-T6 LT	618.9	658.2	17.6	63321
Literature AA7075-T6 LT, [200]	503	572	11	71700

shows the engineering stress-strain curves for the different conditions. The reduction of toughness is noticeable as a result of the reduction of elongation at fracture for the welded joints, particularly for the T-joint configuration due to the blend of the harder material into the joint. The averages of the mechanical properties measured are presented in Table 6.3

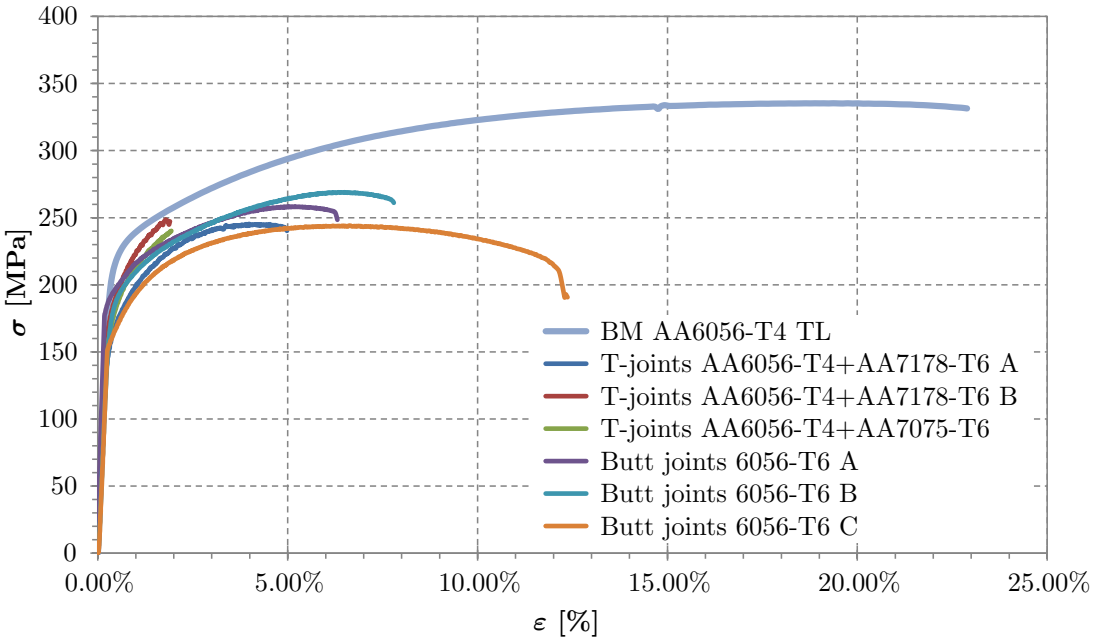

Figure 6.5: Stress strain curves of the friction stir welded specimens.

The efficiency of the yield strength, of the ultimate strength and of the elongation at rupture compared to the base material is presented in Table 6.4. Similar efficiencies between the butt and T-joints show that the stress-strain values were not strongly affected

Table 6.3: Static strength properties of the welded specimens.

	σ_{YTS} [MPa]	σ_{UTS} [MPa]	ε [%]	E [MPa]
FSW AA6056-T4	179.6	257.6	8.81	70587
FSW T-joints				
AA6056-T4+AA7178-T6	179.7	247.5	5.07	70806
AA6056-T4+AA7075-T6	180.2	245.1	1.89	69338

by the welding of the reinforcement. The efficiency of the elongation at rupture decreased in the T-joint, due the lower elongation of the AA7075-T6 base material compared with the AA6056-T4 and due to the recrystallization in the joint.

Table 6.4: Weld efficiency compared to base material properties.

	σ_{YTS} [MPa]	σ_{UTS} [MPa]	ε [%]
AA6056-T4 TL (reference results)	220.3	335	21.4
Butt-Joint FSW AA6056-T4	179.6	257.6	8.81
Efficiency	81.50%	76.90%	41.10%
FSW T-joints AA6056-T4+AA7075-T6	180.2	245.1	1.89
Efficiency	81.80%	73.20%	8.80%
AA6056-T4+AA7178-T6	179.7	247.5	5.07
Efficiency	81.57%	73.88%	23.69%

Most fractures in the tensile tests occurred in the heat affected zone, as shown in Figure 6.6, demonstrating a good weld performance with defect free corners of the T. Nevertheless, some specimens broke in the corners, where a lack of penetration of the probe during the process was noticeable.

The bending tests were performed in accordance with the ASME standard for welding and brazing characterization, [204], with three contact points. The setup and rollers diameter are schematically represented in Figure 6.7a. Theses tests were done on a MTS servo-hydraulic machine, where the punch is moved with a loading speed of approximately 7 mm/min and the test was finished when the specimen is completely bent.

These bending tests were performed to the welded specimens and to base material specimens in order to compare the bending resistance. During these tests the punch force and displacement were recorded. This type of test gives useful information about the

Figure 6.6: T-joint friction stir welded specimen.

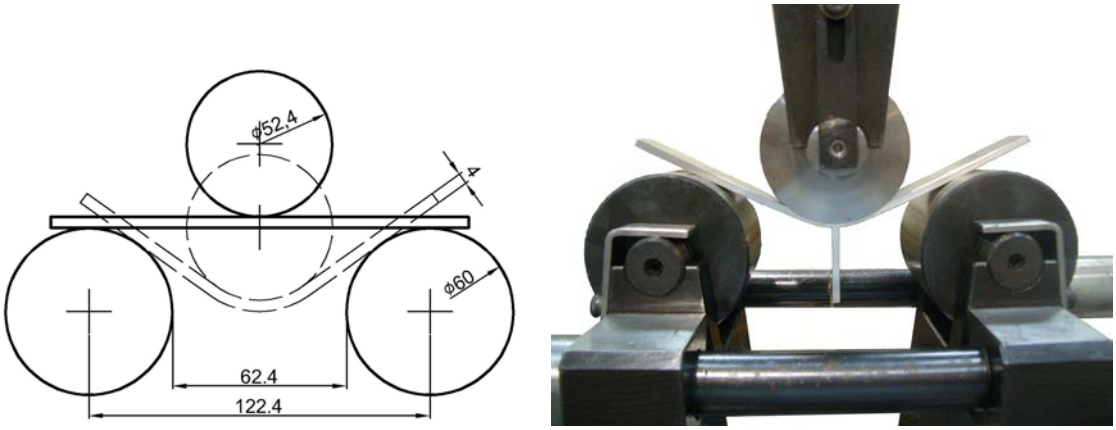

(a) Dimensions **(b)** Setup

Figure 6.7: Bending tests, dimensions and setup.

integrity in the weld root from the information about the energy absorbed by the specimen along the test, which is compared with to the base material. The data recorded for these tests are represented in Figure 6.8 for the base materials AA6056-T4 and AA7178-T6, for the butt joints AA6056-T4 and for the T-joints AA6056-T4 with AA7178-T6 and one test for AA6056-T4 with AA7075-T6. The AA7178-T6 presents a higher energy of deformation, due to the higher strength. The butt joints did not present root defects during the tests and their behavior is similar to the AA6056-T4 base material. It is noticeable that the T-joints present some root defects in the corners of the T. These defects are visible in displacement vs. load curves when the load decreases quickly as the specimen loses its integrity. The load is recovered after 45 mm of displacement but at this point the bending stresses in the weld root are low. This load recovery is related to the specimens bending strength outside the welding area.

Fatigue behavior was analyzed carrying out fatigue tests comparing T-joints, butt-joints and base material. These tests were done in accordance with the ASTM E466, E467 and E468 standards, [205, 206, 207]. All these experimental tests were performed on a MTS

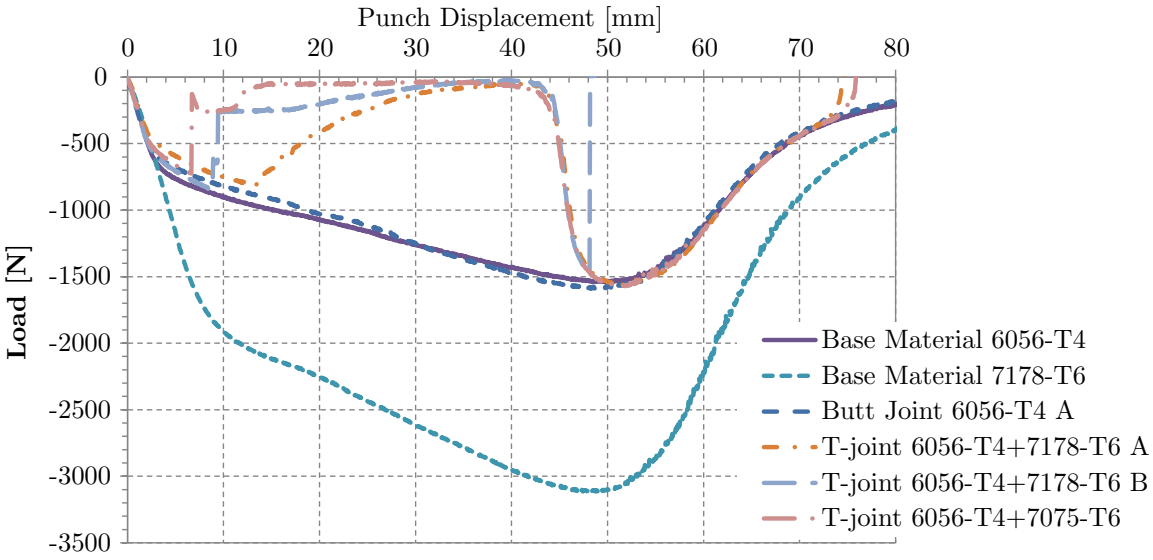

Figure 6.8: Bending tests, punch load *vs.* displacement.

servo-hydraulic machine. Fatigue tests were performed using butt and T-joint specimens in order to compare the fatigue performance. All the fatigue specimens were tested with a load ratio (R) of 0.1 at different stress levels and the cyclic loads were applied at a frequency of 10 to 16 Hz, depending on the maximum load. The maximum stresses applied in these tests were in the range of 70% to 110% of the yield strength of the base material. The results were compared with the behavior obtained for the base material AA6056-T4 and with FSW butt joints also made of AA6056-T4. The results are compiled in Figure 6.9. A reduction of fatigue strength of the FSW T-joints and FSW butt joints is noticeable when compared to the base material fatigue strength. This fact can be correlated to the reduction of toughness in these welds (low elongation after rupture). A reduction of the heat input during the process could increase the toughness but then, the strength of the welds would possibly also decrease. If higher fatigue strength is needed, post weld heat treatment can be used in order to obtain better fatigue properties.

Metallurgical Analysis

A straightforward metallurgical analysis was performed in order to discern how the different aluminium alloys mix during the welding. This analysis includes a comparison with equivalent FSW butt-joints for a better understanding of the dissimilar materials joints. Due to the stirring and heat promoted by the FSW process the uniformity of the hardness profiles and the microstructure in terms of Al phases, grain size and grain orientation was changed.

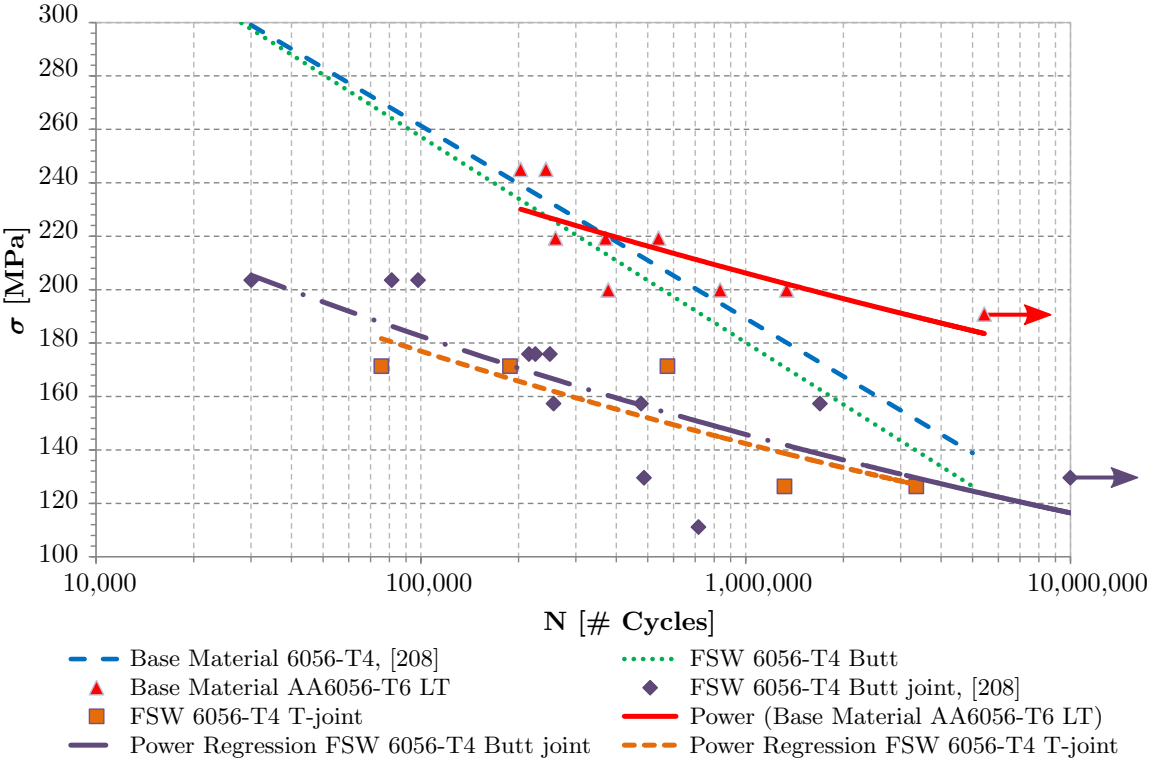

Figure 6.9: Bending tests, punch load *vs.* displacement.

The information about the hardness variation along the weld may give a better perception about the phenomena involved in this process and about the causes of loss of strength compared with the base material. Microhardness fields were measured in three specimens, one butt joint and two T-joint specimens. 51 measurements were carried out for the butt joint, and 69 measurements were performed for each T-joint. In all cases more dense data acquisition was made in the area of the nugget and Thermo-mechanically Affected Zone (TMAZ). In Figures 6.10 and 6.11, the microhardness fields are represented on a black area, which corresponds to the total area of the specimen used in the measurements. In Figure 6.10, corresponding to the butt joint, hardness losses along the limits of the weld are visible, associated with the TMAZ.

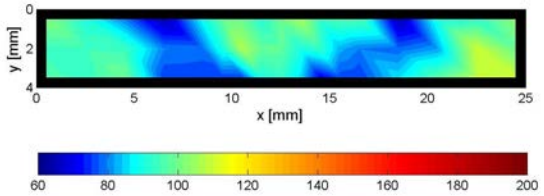

Figure 6.10: Microhardness field of the butt joint AA6056-T4, HV-100gf.

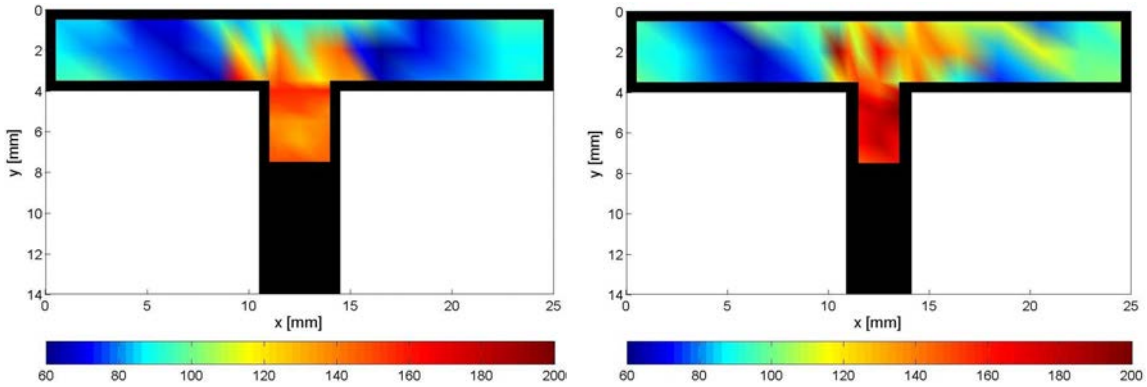

(a) T-joint AA6056-T4+AA7178-T6 **(b)** T-joint AA6056-T4+AA7075-T6

Figure 6.11: Microhardness fields of the T-joints, HV-100gf.

Figures 6.11a and 6.11b show similar patterns of hardness distribution for the T-joint 6056-T4+7178-T6 and for the 6056-T4+7075-T6, respectively. The difference in hardness of the web and flange materials is clearly observed, as expected. A decrease of the hardness in the TMAZ is shown, whereas the nugget area presents a quite irregular pattern, which can be attributed to the non homogenous mixture of the materials. The trends above could be more refined, in case a denser mesh of measurement points was used.

Furthermore, a metallographic characterization of the welded joint was performed, comprised of a macrographic analysis, a microstructure analysis. For the macro- and microstructures an 8% concentration of hydrofluoric acid (HF 8%) was used for the chemical etching of the dissimilar joint. As The skin material is AA6056 with the T4 heat treatment (T4 - solution heat treated and naturally aged at 20°C for 5 to 10 days), and the reinforcement material is AA7075 in the T6 temper (T6 - solution heat treated and artificially aged). After welding, the artificially aged alloy locally loses its temper due to the relatively high process temperatures reached in the nugget zone. Numerical models presented by Colegrove and Shercliff, [209], show that for the AA7075-T7351, the peak temperature during the process can be close to the solidus temperature. In the case of AA7075, the friction stir welding promotes an in situ quenching which in some cases can result in an increase of the mechanical properties, [210], however this local quenching in AA6056 does not seem to be beneficial, as demonstrated by the loss of elongation.

In Figure 6.12 the macrostructure from a cross section of the butt joint AA6056-T4 and locations that will be detailed in the following microstructural analysis are shown. It is visible that the stirred zone is small revealing that the weld had low heat input, reducing in this way the impact of heat in the material transformation. No visible defects as porosities were found in the butt welds.

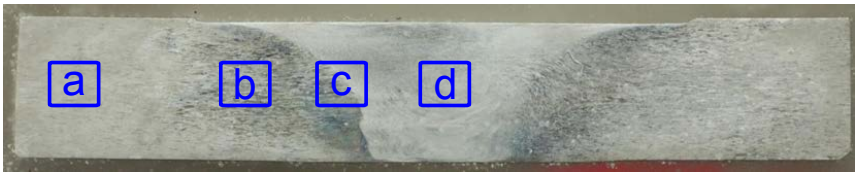

Figure 6.12: Macrostructure of the FSW butt joint AA6056-T6 and microstructure locations.

Microstructures from the different zones of the macrastructure were analyzed in Figure 6.13 for the different zones of a FSW weld: base material, TMAZ, Transition Zone (TZ) and the Stirred Zone (SZ), for the respective locations which are given in Figure 6.12.

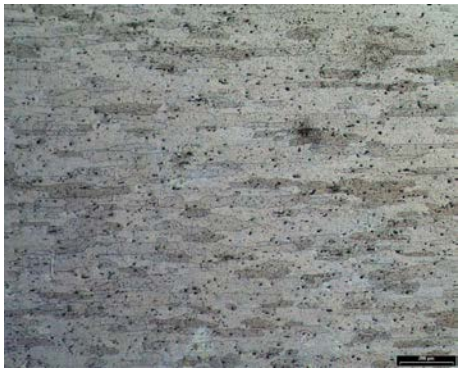

(a) Base material

(b) TMAZ

(c) Transition TMAZ-SZ

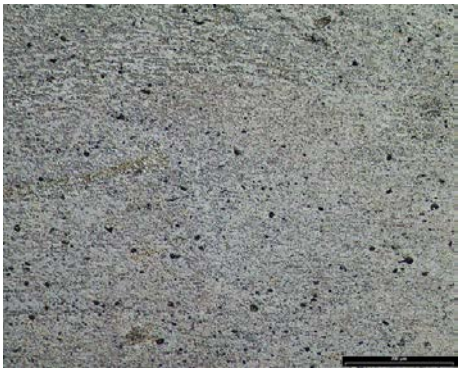

(d) SZ

Figure 6.13: Microstructures of the FSW butt joint AA6056-T6.

In Figure 6.14 and Figure 6.16 the macrostructures of the cross sections in the welding area of a FSW T-joint are presented for the two T-joints configurations. Several microstructures were taken in the locations marked in these figures for a more detailed analysis, Figures 6.15 and 6.17.

As can be seen in the microstructures of base materials, see Figures 6.15a, 6.15b, 6.17a and 6.17b, the base materials have different microstructures. The AA6056 alloy has larger

grains in the order of over 100 μ m, all elongated in the rolling direction. In the 4 mm thick AA7178 or in the 3 mm thick AA7075 alloy, the rolling direction can also be easily recognized, but the grains are smaller. The chemical etching used was more successful for the AA6056 alloy than for the AA7178 or for the AA7075 . In the nugget zone, the mixture of the two different alloys is easily identified due the etching applied, as can be seen in location D, see Figure 6.17d. The nugget zone, due the stirring effect, experiences high strains that associated to the temperature raises, lead to recryztallization in this zone. Smaller and regular grains are therefore found in this location with dimensions below 10 μ m. In the transition zone, the transformation of the large longitudinal grains into small grains can be recognized in the microstructure of Figures 6.15c and 6.17c. At the retreating side of the weld, see Figure 6.17e, the material flow inside the weld may be partially reconstructed by the shape of the elongated grains. Figures 6.15f and 6.16 suggests that vertical flow of the material seems to have taken place during welding, due to the appearance of the mixture of the two alloys. In the transition between the TMAZ and the heat affected zone (HAZ) is easily identified in Figures 6.15c and 6.17e. In the TMAZ, eutetic films are perceptible in the T-joint produced with AA7075-T6, which are associated with spontaneous local melting, as described by Gerlich *et. al* for the friction stir spot welding of AA7075-T6, [211].

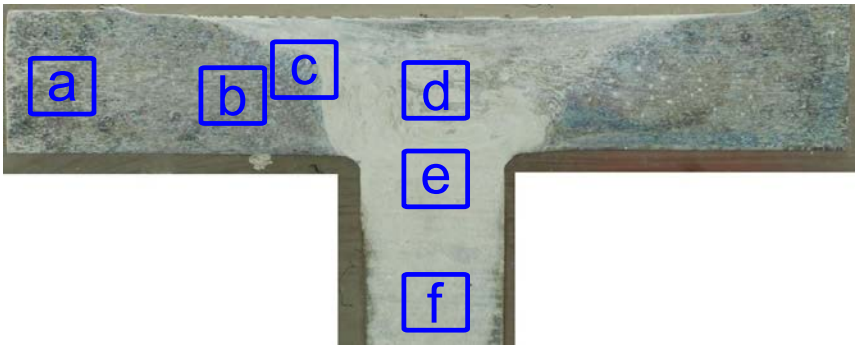

Figure 6.14: Macrostructure of the FSW T-joint AA6056-T6+AA7178-T6 and microstructure locations.

6.2 Tailored Welded Blanks

The optimization of the structural panels in aeronautics is also promoted with variations in the panel thickness, eliminating material where it is not required, reducing in this way the structural weight, [212]. Metallic panels, Tailor Made Blanks (TMB) with thickness variations can be produced with different manufacturing processes, mostly with conventional milling or chemical milling or adhesively bonded. However, with the emergence of welding processes in aeronautical structures, these processes can be an effective alternative.

(a) Base material AA6056-T4 **(b)** TMAZ **(c)** Transition TMAZ-SZ

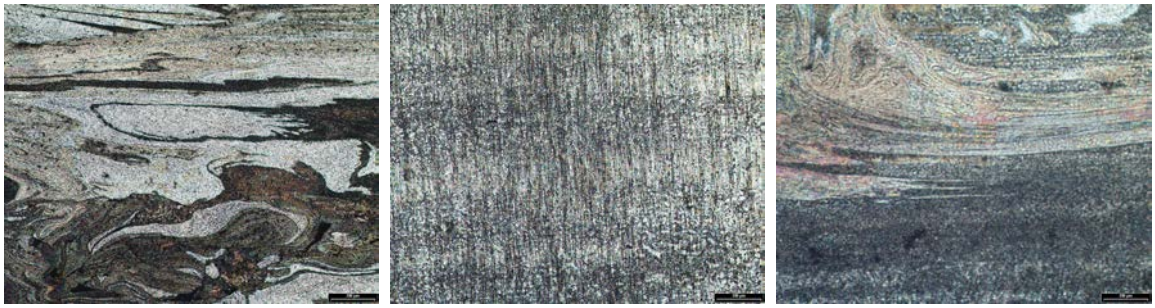

(d) Nugget, SZ **(e)** Base material AA7178-T6 **(f)** Transition TMAZ-SZ - bottom

Figure 6.15: Microstructures of the FSW T-joint AA6056-T6+7178-T6.

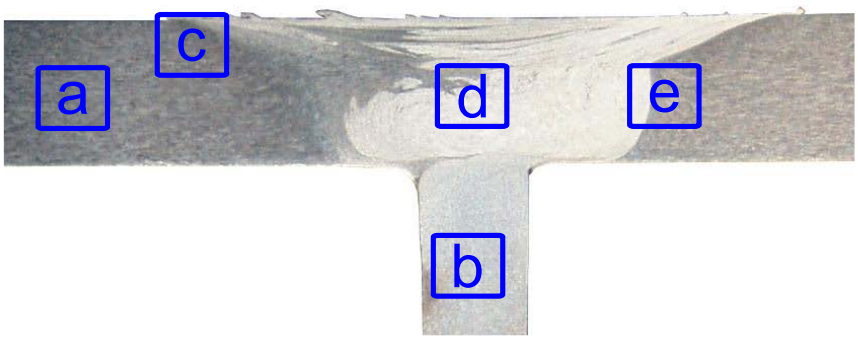

Figure 6.16: Macrostructure of the FSW T-joint AA6056-T6+AA7075-T6 and microstructure locations.

The automotive industry has been intensively applying TWB, a concept to produce blanks with different thicknesses and/or alloys that are laser welded into a single part, [213]. These parts are afterwards pressed to achieve the final shape with optimal material arrangement and weight reduction, increasing the manufacturing process efficiency. These TWB parts allow reduction of the number of parts, manufacturing costs reduction, enhanced crash energy absorption, higher stiffness/weight ratio and weight savings.

Due to the success in automotive industry, the introduction of the TWB concept in aeronautics has been investigated. Sinke *et al.*, [214] studied the application of this concept

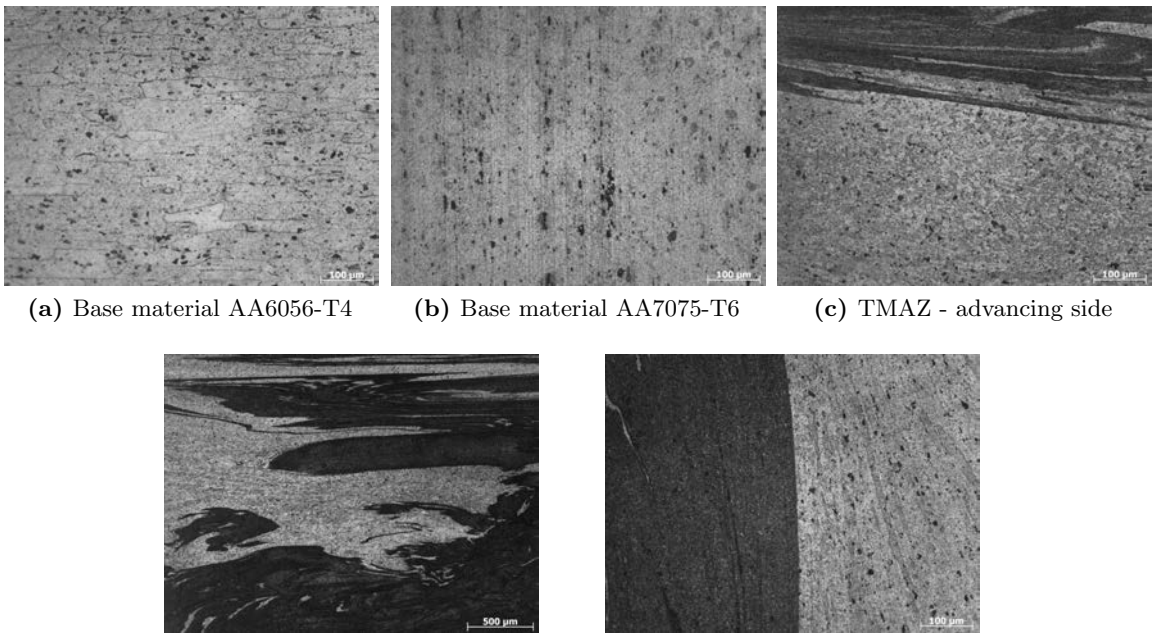

(a) Base material AA6056-T4 **(b)** Base material AA7075-T6 **(c)** TMAZ - advancing side

(d) Nugget, SZ **(e)** TMAZ - retreating side

Figure 6.17: Microstructures of the FSW T-joint AA6056-T6+7075-T6.

to produce a wing rib obtained through rubber forming of a tailor welded blank. They achieved a reduction in lead time of about 25% and a cost reduction of more than 50% compared to a wing rig conventionally machined. In addition, they noticed that if the weight becomes the prime target for the design, it is possible to reduce the weight in 25% or more. A characterization of TWB with FSW and with different aeronautical materials, AA2024-T3 and AA7075-T6, and different thicknesses, 1.2, 2 and 2.5 mm were studied by Zadpoor *et al.*, [215]. They concluded that the mechanical properties and microstructural features are different from those of the same thickness and same material due to the instability during the process.

In the scope of the COINS project, [151], and at HZG (former GKSS), two configurations of tailored welded blanks were characterized. This joint characterization was composed by the evaluation of static properties, fatigue behavior and crack growth behavior along the joint. Just one alloys was applied, the aluminium lithium alloy AA2198-T851, and two different configurations:

- 2.5 mm thick plates welded with 3.2 mm thick plates
- 2.5 mm thick plates welded with 4.5 mm thick plates

In addition to these two configurations, the application of a footstep with the welding tool in transition between the thin to the thicker plate was tested. This footstep is advantageous for fatigue crack retention since it reduces the stress intensity factor of a crack when the

crack tip approaches to this step, slowing down their growth, as demonstrated in the Chapter 5.

Due to the thickness differences between the two sheets, the welding tool is not positioned perpendicularly to the plates plane, requiring an additional axis to apply the forging force. Therefore TWB specimens were welded in a Tricept 805 robot with five axis and controlled with a Siemens 840D command, Figure 6.18.

Figure 6.18: Tricept 805 robot at GKSS, Germany.

6.2.1 Macrostructure Analysis

Figure 6.19 shows the macrostructure of three cross sections of TWB in AA2198-T851 with 2.5 mm and 3.2 mm. These cross sections were taken from the beginning, at the middle and at the end of the welded plate, Figures 6.19a, 6.19b and 6.19c respectively. The cross section at the beginning shows a tunnel defect that is not visible in the following sections, pointing out that this welding configuration is not as stable as the butt joints. It is also visible a line of oxides in the right plate that is a defect during the lamination. Although, in the Chapter 4 it was concluded that this defect does not affect substantially the joint performance.

(a) Beginning

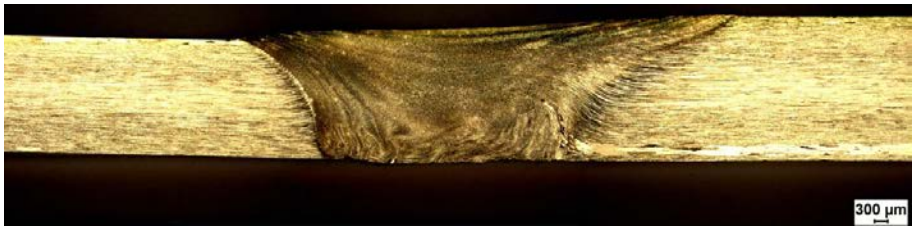

(b) Middle

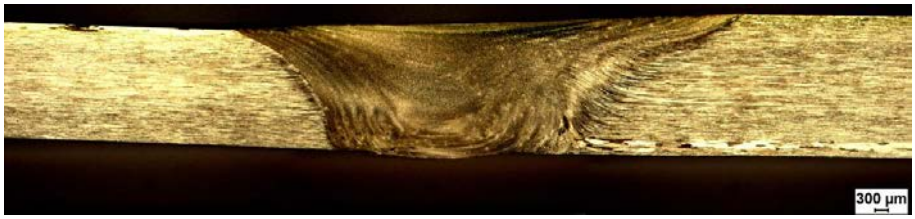

(c) End

Figure 6.19: Macrosections of TWB AA2198-T851, 2.5 mm with 3.2 mm thick.

Decreasing the tilt angle of the welding tool, a step in the thicker part of the joint was created. However, at the same time, some burr was produced worsening the surface finishing. Figure 6.20 shows two cross sections of TWB with different plates thicknesses. Besides the burr produced, the welds are sound. Nevertheless, in Figure 6.20a it is visible that the FSW tool reduced the cross section of the thinner plate, which should be avoided in order not to reduce the joint strength.

6.2.2 Mechanical Characterization

A mechanical characterization was performed with tensile strain tests, SN type fatigue tests and fatigue crack growth tests. The tensile test were performed in accordance to the European Standard EN 10002-1, [216], in a Zwick Roell static testing machine with a 100 kN load cell and with a laser extensometer. The tests were performed in displacement control with a speed of 0.5 mm/min. At least three tensile specimens were machined from each welded sample. Figure 6.21 shows some representative curves, where the stress is related to the thinner part of the TWB and the strain is related in a 30 mm distance

(a) TWB 3.2 mm with 4.5 mm

(b) TWB 2.5 mm with 3.2 mm

Figure 6.20: Macrosections of two TWB configurations.

centered in the welding line. Since this region does not have constant thickness, the real strain will be slightly different (higher in the thinner part and lower in the thicker part).

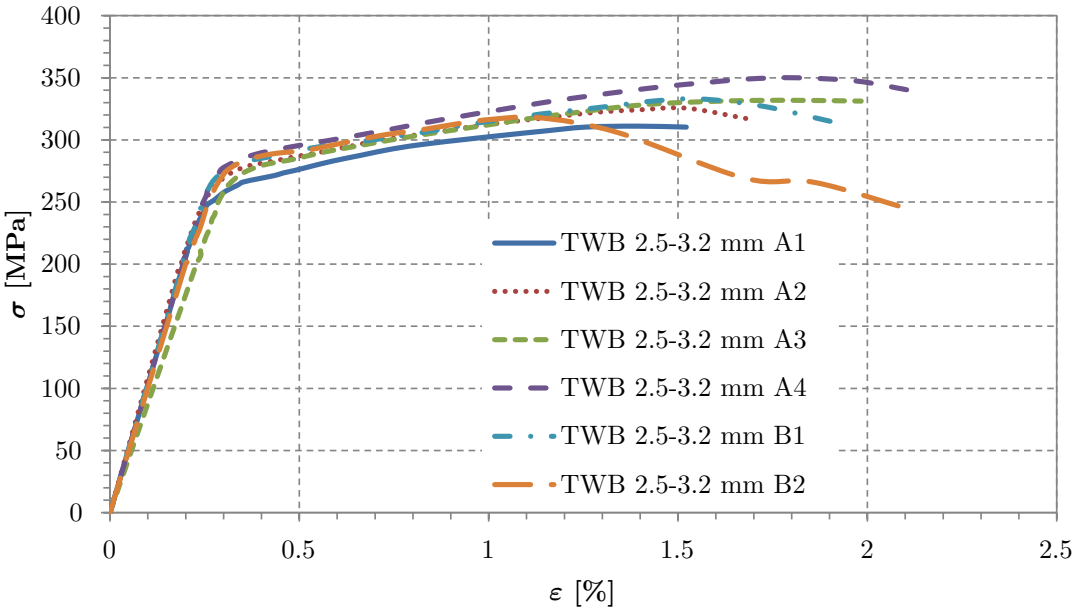

Figure 6.21: Stress strain curves of the TWB 2.5 - 3.2 mm thick.

Table 6.5 resumes the stress strain values obtained for different samples. The values of the Young's modulus presented in this table are indicative , since due to the variation of

thickness it is not possible to precisely determine the strain and stress in each point of the specimen giving a non correct estimation. Although, this modulus gives an overestimation for the thinner part, with the effect of lower strain at thicker part, increasing the Young's modulus.

Table 6.5: Tensile stress-strain properties of TWB in AA2198-T851.

	σ_{YTS} [Mpa]	σ_{UTS} [Mpa]	ε [%]	E [MPa] calculated
TWB 2.5-3.2 mm A	282.6	322.3	1.5	100.4
TWB 2.5-3.2 mm B	281.2	294.7	1.8	103.9
TWB 3.2-4.5 mm A	267.7	273.0	0.5	94.0
TWB 3.2-4.5 mm B	281.0	381.6	4.6	98.6

The fatigue characterization of these joints was performed with S-N curves (Wöhler curves). Specimens geometries were done in accordance to the prEN 6072 standard, [217], with the welds perpendicular to the load, with a stress concentration factor ($K_t = 1$) and with a curvilinear shape. In this way, the maximum stress is on the welded region ensuring that the specimen will rupture in this region and the measured fatigue strength is related to the welded material.

A total of 40 specimens 3.2-4.5 mm thick were produced. These specimens need to be tested with a constant thickness, because the bending moment originated a complex stress mode in the welded region. Due to this reason, the specimens were milled to a thickness around 3 mm to remove the thickness difference and the FSW striations. They were tested in force control mode and for two load ratios (R=0.1 and R=0.5). Just 26 specimens were validated, due to the errors in the machine control and ruptures in the grip zone. All tests were done at MTS servo hydraulic equipment at frequency of 10 Hz, under force control mode. Figures 6.22 and 6.23 shows the measured points for both load ratios and power trendlines to the measured points for a better comparison.

The crack propagation behavior along the welding line and along the transition of the panel thickness was analyzed with compact specimens, C(T), according to the ASTM standard E647, [218]. The C(T) specimen length was 50 mm, in order to comprise the thickness variations of the tailor welded blanks due to the standard limitations. Figure 6.24 shows the final geometry of the specimens that were used to measure the fatigue crack growth rates. The gray band represents the welded area when the crack is longitudinal to the welding line.

The crack propagation behavior was determined through the stress intensity factor vs. da/dN. The stress intensity factor as a function of the crack length for this configuration

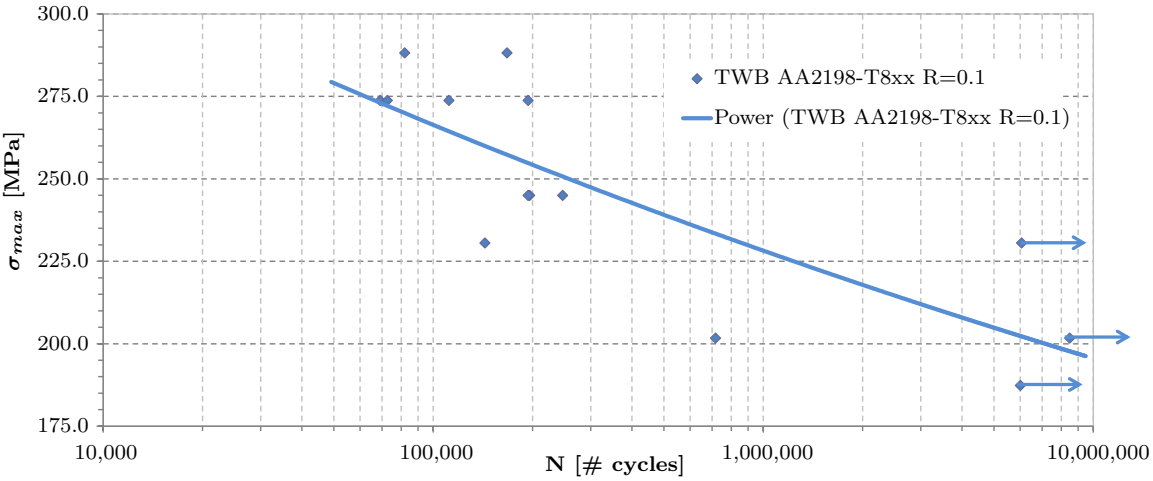

Figure 6.22: Fatigue SN curve, AA2198-T851 R=0.1.

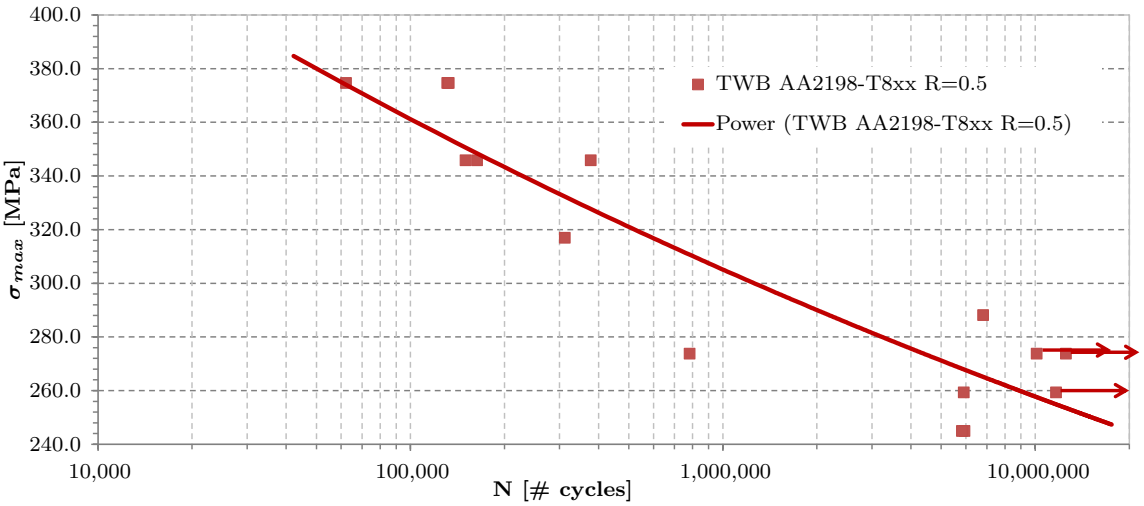

Figure 6.23: Fatigue SN curve, AA2198-T851 R=0.5.

is given by:

$$\Delta K = \frac{\Delta P}{B\sqrt{W}} \cdot \frac{(2+\lambda)}{(1-\lambda)^{1.5}} \cdot \left(0.886 + 4.64\lambda - 13.32\lambda^2 + 14.72\lambda^3 - 5.60\lambda^4\right) \tag{6.1}$$

where P is the applied load, $\Delta P = P_{max} - P_{min}$, B is the specimen thickness, W is the specimen width from the center of the grip hole and $\lambda = a/W$ valid for $a/W > 0.2$.

Given the relatively small difference between the original plates' thickness, the ΔK solution given by ASTM E647 was used as a first approximation, and the thickness of the thinner plate was used for the calculation, since when the crack are longitudinal to the weld, the crack converges to the thinner part. In the case of the crack perpendicular to the

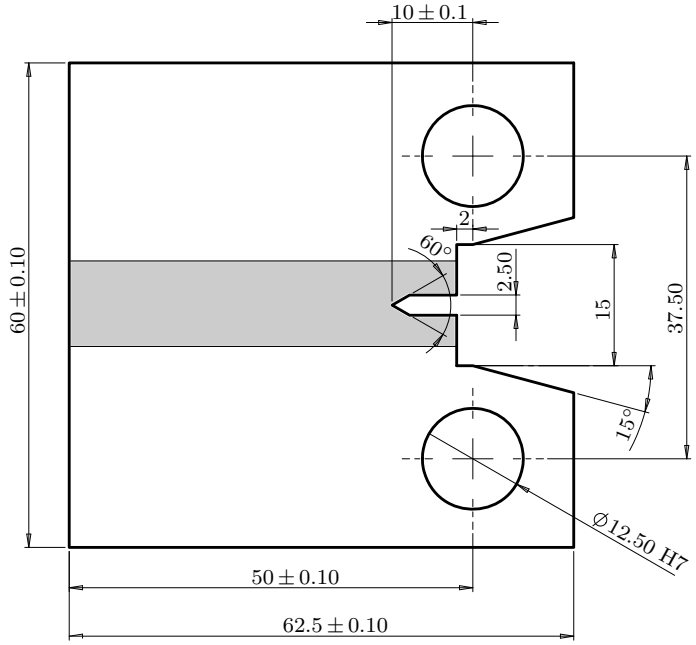

Figure 6.24: Base geometry of the compact deep edge-notched specimen, CT50.

weld, the thickness was estimated in function of the crack length a and taken into account in the equation 6.1.

The tests were performed in a servo hydraulic testing machine with Instron controls. The tests were ran under load control mode at frequency of 20 Hz in the pre-cracking and 15 Hz during the crack measurement and with a load ratio of R=0.1. Figure 6.25a shows the testing setup, with a optical microscope which was used to measure the crack length and a digital camera in the opposite side that was an attempt to measure the crack growth with the digital image correlation, [219]. Figure 6.25b shows one of the specimens after testing, with a crack along the welding line. Irregularities in the material structure induce a irregular crack path, which might be advantageous since the path length is larger than a straight crack path.

Figure 6.26 shows the measured results for four tested specimens. Figure 6.26a shows the crack growth rate in the base material along the lamination direction, since the welds were performed along this direction. Figure 6.26b shows the behavior of the crack along the welding line and Figures 6.26c and 6.26d perpendicular and along the welding line, respectively, for TWB specimens. In the case of crack growth along the welding line a large dispersion in the measured points, due to the instability of the crack propagation direction, was recorded. Nevertheless, a trend of the fatigue crack propagation was possible to obtain as a first indication of how the crack propagates along these type of joints.

Applying power trend lines to the acquired data, the different fatigue crack growth behaviors of these specimens were compared. This comparison is presented in Figure

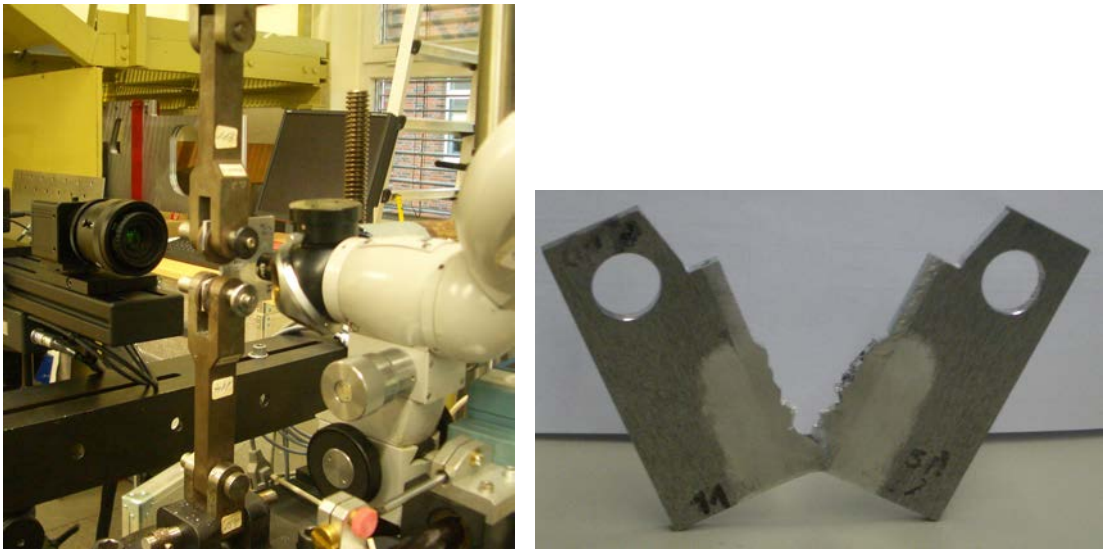

(a) Setup **(b)** Tested specimen

Figure 6.25: Fatigue crack growth characterization, setup and tested specimen.

6.27. Comparing with the base material, a small reduction of the fatigue crack growth rate is visible, as expected, possibly due to the recrystallization, which originates smaller grains and due to the residual stress. A similar fatigue crack growth behavior, as concerns differences between base material and FSW material was found by P. Moreira *et al.*, [220] for the aluminium lithium alloy AA2195- T8X. Nevertheless, the reduction in the fatigue crack growth is not substantial and is confined to the weld zone, which in large structures might be neglected.

6.3 Sliding Backing Bar

During an internship at Airbus Operations GmbH the applicability of the FSW to join large structures was analyzed. The joining of large panels can be mainly done in two configurations: butt-joint or overlap configuration. From the manufacturing point of view, the application of overlap geometry in FSW for aeronautical structures would be a more desirable replacement of the riveting process due to the similarity in tolerance management and use of less rigid grip systems, which makes its implementation more straightforward in comparison to butt welds. FSW butt joints in large structures require tight tolerances, since the gaps between the two plates will lead to the appearance of flaws in the welds.

Along this study, the performance of the overlap joints and their suitability for primary aeronautical structures was analyzed. This overlap configuration has been previously discussed, as in extensive work done by Cederqvist and Reynolds, [221]. They conclude that this FSW geometry has a weakness related to the unwelded interface of the lap sheets

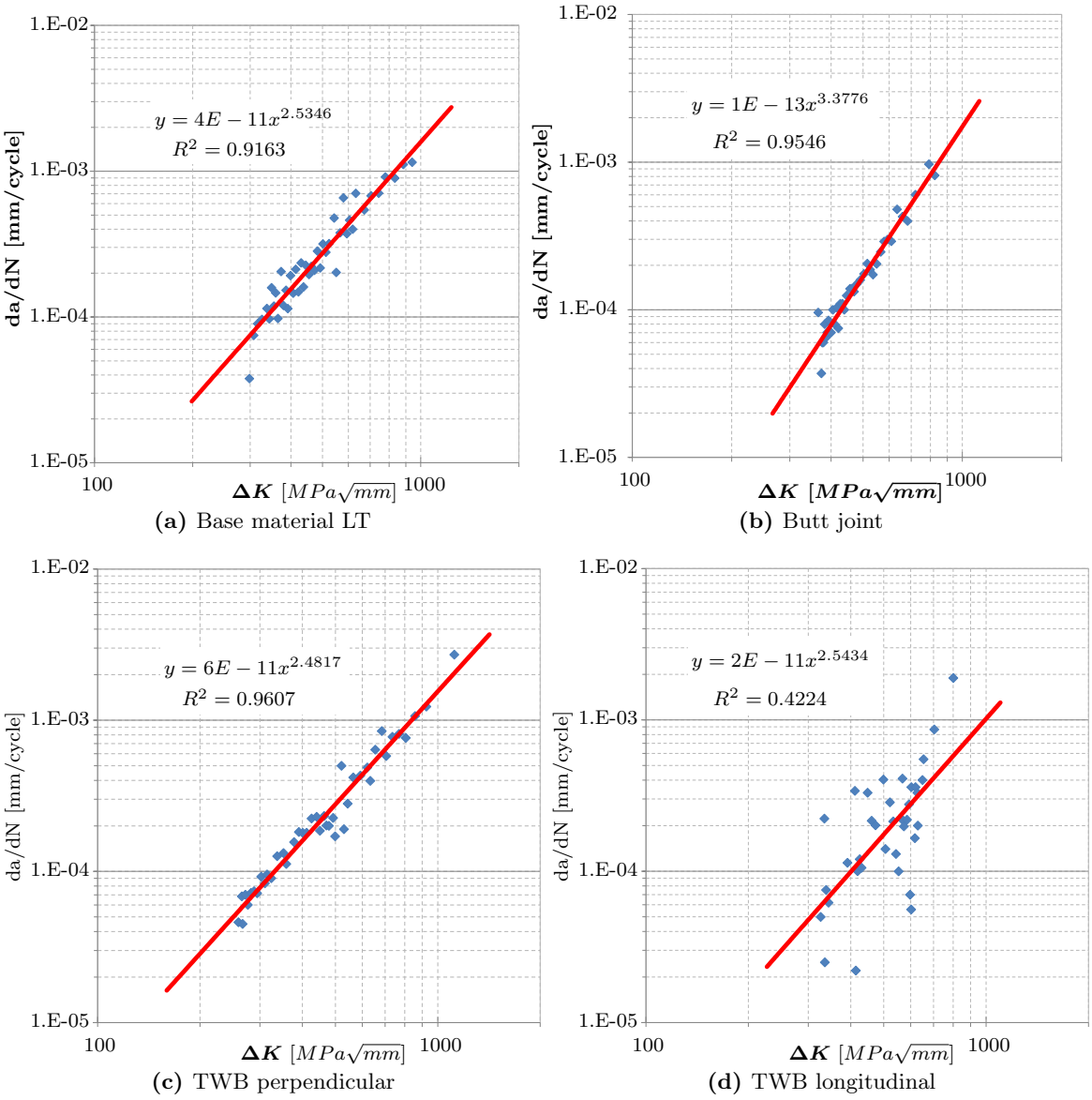

(a) Base material LT **(b)** Butt joint

(c) TWB perpendicular **(d)** TWB longitudinal

Figure 6.26: Fatigue crack growth, examples of the measurements .

that is upset by the vertical material flow during the process creating a reduction of the effective cross section as represented in Figure 6.28. In the advancing side, this interface effect takes the shape of a hook (due the pull up and pull down effect) and in the retreating side, a pull up effect takes place. These effects have repercussions in the static and fatigue strength performance of the joints. The static strength decrease is due to the reduction of reduction of sectional area, that usually is higher in the advancing side, Figure 6.28b. The stress intensity factors in the tip of these interface defects have also a substantially impact the fatigue strength reduction, as shown Ericsson *et al.*, [222]. Another weakness of the FSW overlap joint is the fact that during axial loading, a combination of shear forces and

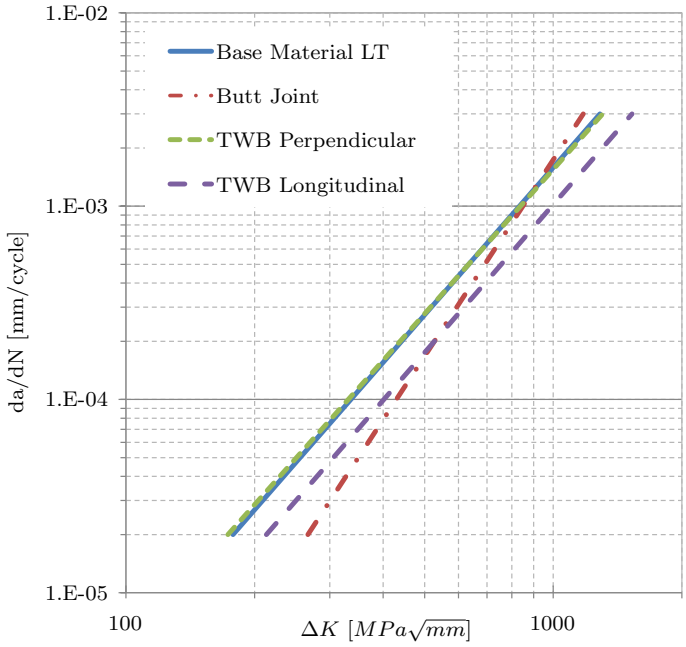

Figure 6.27: Fatigue crack growth comparison between different specimen types.

bending moments is created. This is caused by the eccentric loads in the joint area and can result in joint rotation.

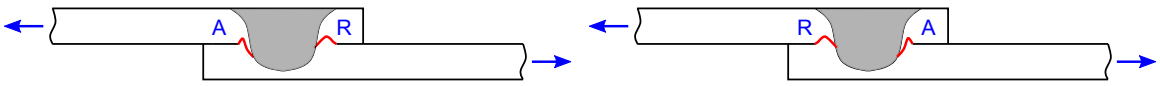

(a) Configuration A **(b)** Configuration B

Figure 6.28: FSW overlap joints, interface defects.

A research study about this configuration has been conducted by Airbus, where several overlap configurations, including double and triple FSW passes to reduce the interface defect in the advancing side and to increase the effective joined area were tested. The alloy used in this study was the classical AA2024-T3. Figure 6.29 presents schematically the FSW overlap weld with two passes. Overlap friction stir welds were performed with a standard tool and with a bobbin tool at EADS-IW in Ottobrunn and in EADS-IW Suresnes, respectively.

The results are detailed in [223] and [224], and summarized in Figure 6.30. With a bobbin tool it is possible to improve the static strength of an overlap joint up to close the base material strength. However, the fatigue strength of FSW overlap joints is very poor compared to the respective behavior of the base material. The welding defects combined with the load eccentricity caused by the overlap configuration, are very detrimental to the fatigue strength of these joints.

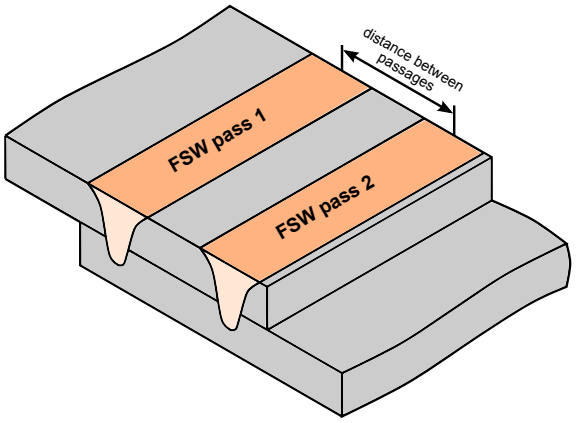

Figure 6.29: FSW overlap multipass configuration.

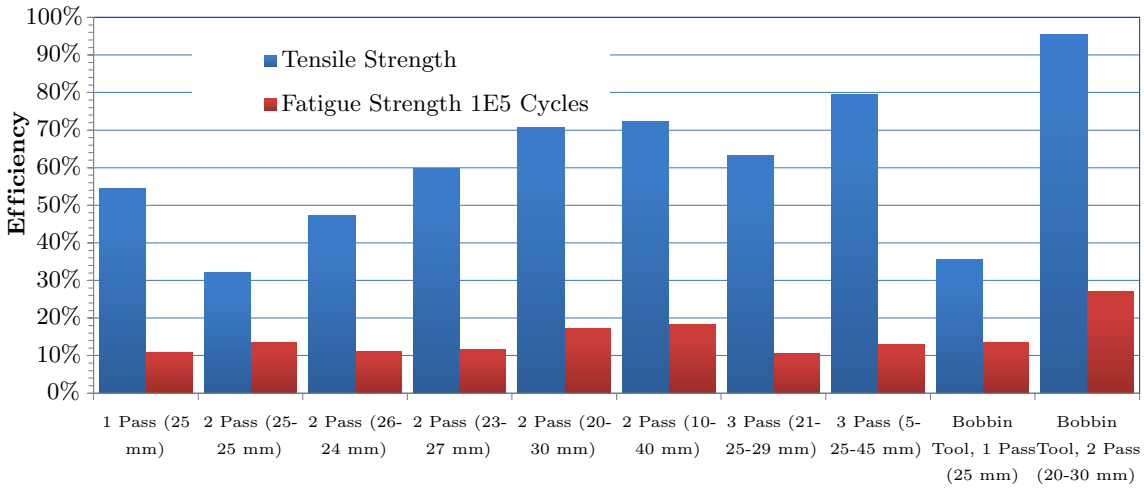

Figure 6.30: FSW overlap joint efficiency compared with the base material.

As a result of this study, it was inferred that this geometry is not a reasonable solution to replace the riveted joints in the large panels of primary structures. The butt joint should be more desirable, since it can simplify the joint and reduce the global weight because it does not require the overlap material. Figure 6.31 shows schematically the alternatives to apply FSW joints in these panels.

Inherent difficulties in the application of FSW to butt joints are, as mentioned above, tolerance management and the grip system to react to the forging loads. In addition, to apply the standard tool, a backing bar along the all welding extent to react the normal load applied by the tool is required. This standard backing bar is subjected to wear and damages during its service and it needs to be replaced sporadically. For large structures, the backing bar can be a problem due to the dimensional tolerances, different thermal expansion coefficients and the replacement of different parts when it is damaged. The

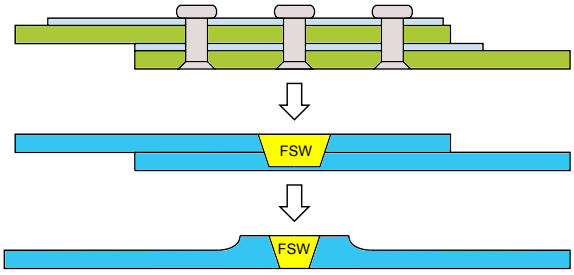

Figure 6.31: Replacement of overlap riveted joints by FSW.

tolerance of the distance between the pin tip and the backing bar is an important parameter since small variations can induce a lack of penetration in the weld, reducing the joint integrity. Bobbin tool can be a solution, since this tool is self reacting to the vertical loads. However, this tool is not as stable as the standard tool, it can originate defects with the plate waviness, and the final properties are better with the standard tool due to lower heat input during the process. Therefore, a concept that takes advantage of the standard tool and of the bobbin tool was developed. This new concept is a new backing method for FSW composed by a pad that follows the tool dragged by pin tip and that will react the normal load of the FSW tool. This pad is supported by the clamping system and can be guided by linear bearings or by low friction surfaces to make easy its drag. With this process it is possible to reduce and to solve several problems of the standard tool and of the bobbin tool, improving the weld quality and reducing operational costs related with the tool and backing bar damage. Comparing with the standard backing bar, this solution allows to avoid completely the lack of penetration, even compared with the adjustable pin tool. The FSW tool may be simplified since a fixed pin, Figure 6.32a, longer than the maximum material thickness is enough to provide sound welds. Anyhow, the concept can be used also in combination with a retractable pin tool, Figure 6.32b allowing higher pin length variations and therefore higher thickness variations.

This concept also requires tight tolerances, however it is not subject to damage and wear of the FSW tool being much easier to maintain the dimensional tolerances. This concept is also an enhanced alternative to the bobbin tool for long welds. The pin, in addition to the planar loads, needs to transmit the normal loads between the upper and bottom shoulder and the torque required to move the bottom shoulder. This combination of loads weakens the pin that can break during longer welds. In this invention the pin is just required to support the planar loads and a load to drag the pad, which can be very low if low friction coatings in the pad surface are used. This solution allows the process to be done with a single load control, permitting thickness variations. The bobbin tool requires a complex control system (sometimes with two load controls) in order to deal with thickness variations that for 3D welds paths could not be viable solution. In addition, the bobbin tool produces striations and flash in both sides of the weld. The moving pad does not

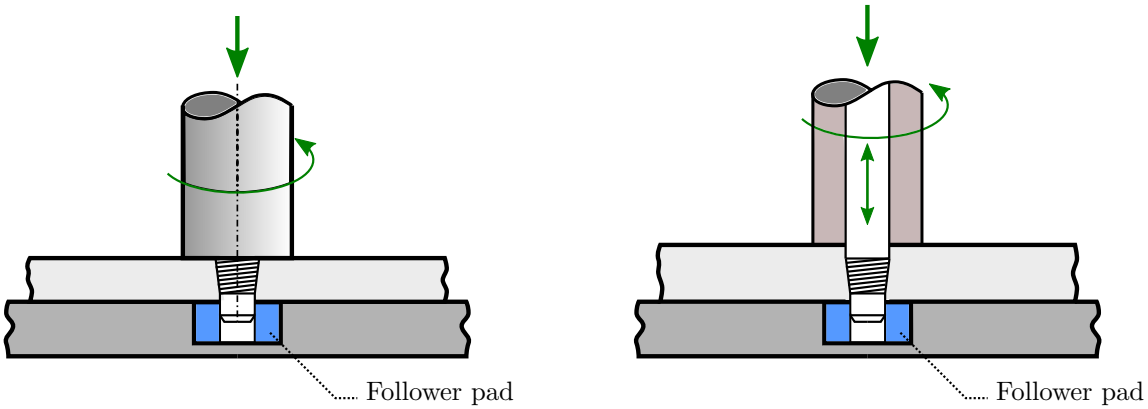

(a) Fixed pin **(b)** Retractable pin

Figure 6.32: Following backing bar concept.

produce striations and flash and if it is combined with a static shoulder can produce welds with good surface finish that do not require post machining operations on the backing-bar's side of the material.

With this concept, the welding can be done in force control mode or in position control mode. In force control mode is applied a constant forging force in the shoulder. With this load the face of the shoulder will keep up with the top surface of the plates, adapting to the thickness variations autonomously. In position control mode, the position of the shoulder may be controlled with a roller or other measuring system in front of the weld tool. Other alternatives can be used for the position control mode as prior mapping of the plates surfaces along the welding line. In some embodiments the pad may require a tracking system to guide the pad along the weld path. This tracking system can be done in multiples ways. Figure 6.33 illustrates a tracking system composed in two linear bearings which support the normal load and effortlessly moves the pad along the tracking system. Other solutions are also feasible since allows the pad motion along the welding line with low friction, including 2d movements with bearing tables. A patent application concerning this design and manufacturing concept was submitted to the *Deutsche Patent-und Markenamt* (German patent office).

6.4 FSW for Structural Repairs

Welding techniques are commonly used to repair damaged or cracked structure in many areas. However, in the aeronautical sector this is not a common procedure, possibly due to the difficulty to fusion weld aeronautical alloys and due to high requirements of structural integrity and high quality. Nevertheless, as FSW can weld with high efficiency aeronautical

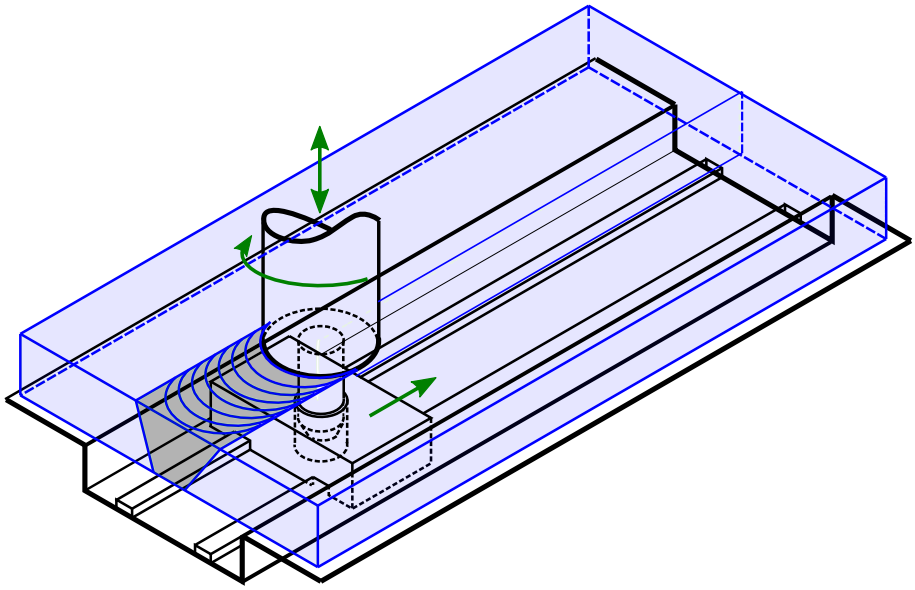

Figure 6.33: Follower backing above linear bearing and dragged by FSW pin.

alloys, such as AA2024, this process can be adopted for structural repairs in aeronautical structures.

The application of FSW for repairs was reported in Chapter 4, in Figure 4.7 with three examples: cracks and damages healing, reinforcement and casting porosity. At TAP Maintenance and Engineering, a Portuguese third party maintenance provider some potential applications with eventual interest for the use of FSW in maintenance and repair were examined. Two main potential areas were identified: *(i)* to replace the traditional processes or *(ii)* for recovery of damaged products that could not be repaired using conventional precesses.

In this company, it was noticed that most of structural maintenance operations in metallic parts are related with fractures and fatigue cracks in the components. Commonly, when the defect is within prescribed limits specified in the structural repair manuals, it is repaired using doublers. These doublers are riveted to the structure following the instructions given by the constructor. However, when the defect is out of limits, it is required to replace the complete part, involving large costs since most of parts are unique and due to the absence of local part stocks.

A typical repair in aircraft is the application of doublers to recover the structural integrity from cracks and damage in the skin panels. The application of these doublers is time consuming because it requires several tasks for their preparation as drilling, application of sealants and primary and riveting. The FSW process could be an interesting solution to be used in these cases, with the development of a portable machine easily manageable to weld thin plates. In the case of a crack, the tool could merge the material along the

crack and in this way the crack is removed using a bobbin tool. Nevertheless, it is required to take into account the decrease of mechanical properties as compared with the original component and in many situations the doubler will be required. Although, the doubler can be also welded with FSW, which takes less time when compared with the riveting.

Other aircraft components that are also frequently sent to the machining workshop to repair cracks or to be replaced are structural beams, as the ones used in the floors. Figure 6.34a shows an example of fracture found in a beam of the aircraft floor. This damage is outside of eligible limits for this component, therefore the beam is replaced by a new one. However, with the application of FSW, the mechanical properties and its integrity can be recovered to levels near those of the a new component. The forgings are components also widely applied in aeronautical structures. These components are expensive and can be damaged easily in overload conditions. Their replacement is also time consuming since heavy parts are attached to these components. In Figure 6.34b, a cracked forging component is presented , which due to a crack in the eyebar was replaced by a new forging. Some of the cracks in these components can be removed by machining the cracked zone until complete crack removal. A possible repair solution could consist of *(i)* before machining, the crack could be blended using FSW and thereafter, *(ii)* machined, minimizing the damage or loss of material caused by machining.

The application of these procedures can not be done by third party maintenance providers and only the aircraft manufactures can propose these solutions after a certification process for the validation of the repair procedure. Nevertheless, the application of this welding process can improve the maintenance operations, reducing the need of replacement of full parts and reducing the time required to repair an aircraft.

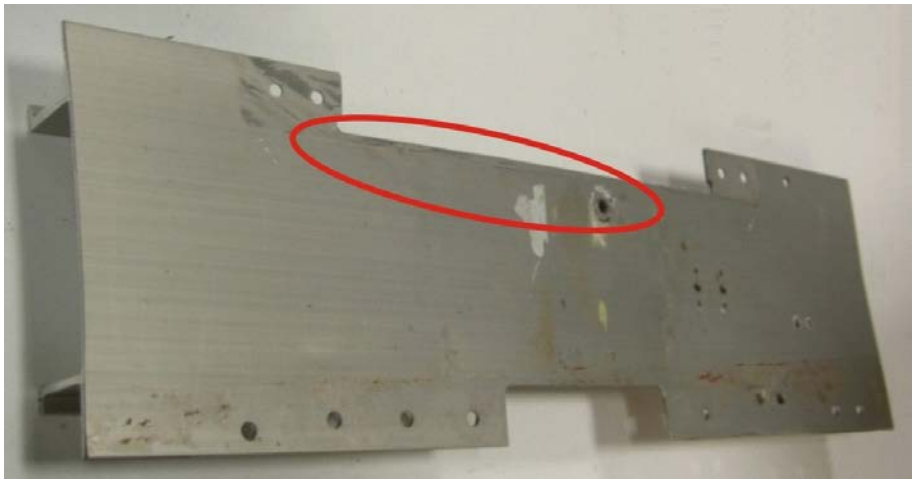

(a) Cracked beam

(b) Cracked forging

Figure 6.34: Cracked structural elements.

Chapter 7

Weight and Cost Assessment

As discussed in Chapter 2, the aeronautical sector has been driven by "Faster, Better and Cheaper" *motto*, progressively transitioning to "Quieter, Cleaner and Greener" goals. Nevertheless, the cost might be considered a transversal target since most of the drivers, as the environmental or performance, can be converted in costs. The cost reduction in aircraft may include optimization in development, manufacturing, operational and disposal costs. For instance, in the development of a new aircraft, it is a common option for the constructors to try to share the design and characteristics of parts in order to reduce development costs, [225]. One way to do this is to conceive a family of aircraft who share common parts and characteristics, such as platforms and systems, but each one satisfies a different mission requirement as the Boeing 757 and 767 or the Airbus A330 and A340 or the Embraer E170 and E190.

The cost of any product or component is significantly committed at the conceptual design stage. For more successful programs of new aircraft development or even new components development with infusion of new manufacturing processes, the cost evaluation is fundamental since the major fraction of the total life cycle cost for a product is committed in the early stages of design, see *e.g.* [226]. Notwithstanding the major drivers of aircraft industry mentioned above, aircraft manufacturing is a highly cost-driven sector. The tools used for multidisciplinary design cycle analysis have also taken into account the cost analysis, as in the tool proposed by van der Laan and van Tooren, [227]. These cost analyses can be done through different techniques, each one with its own specific characteristics, advantages and disadvantages. Curran *et al.* review these techniques in [228] based in four major groups:

Analogous cost estimation Product cost is estimated by comparing it with previously produced similar products. Taking into account technical differences between the product of which the cost is to be estimated and similar products that provide the analogous data can refine the cost estimation;

Parametric cost estimation Cost of a product is linked to technical parameters such as weight, size or part count. To link cost to the technical parameters, relations are developed based on historical data, using statistical techniques;

Bottom-up cost estimation In this approach, the cost of all entities in the work-breakdown structure of the product are determined; for instance, the cost of producing a joint based on all actions and materials involved in the process of producing the joint. The main disadvantage of this method is that it is very information intensive;

Genetic causal estimation The genetic causal cost modeling methodology imposes a breakdown of the cost into a number of cost elements, including material cost, fabrication cost and assembly cost, so that cost can be formulated into semi-empirical equations to be linked to the same design variables as considered in the structural analysis.

As concerns weight, it has a direct impact in most of the goals as it is detrimental to most of the variables in the aircraft design goals. For instance, Manufacturer's Empty Weight (MEW) reduction leads to improvements in the performance, reducing the fuel consumption and contributing to cleaner and greener aircraft. It is expected that a reduction of 1% in the MEW will reduce fuel consumption between 0.7% for larger aircraft and 0.75% for smaller aircraft, [229]. Figure 7.1 shows the trend proposed by Mendez and Eagar, [120], which correlates the vehicle speed with the transportation cost per pound, assuming the fuel cost between one to two dollars per gallon ($\sim$ 3.8 liters). This trend has been changed due to the increase of oil costs and increase of the transportation efficiency. Nevertheless, it is expected that this exponential trend keeps unaltered nowadays.

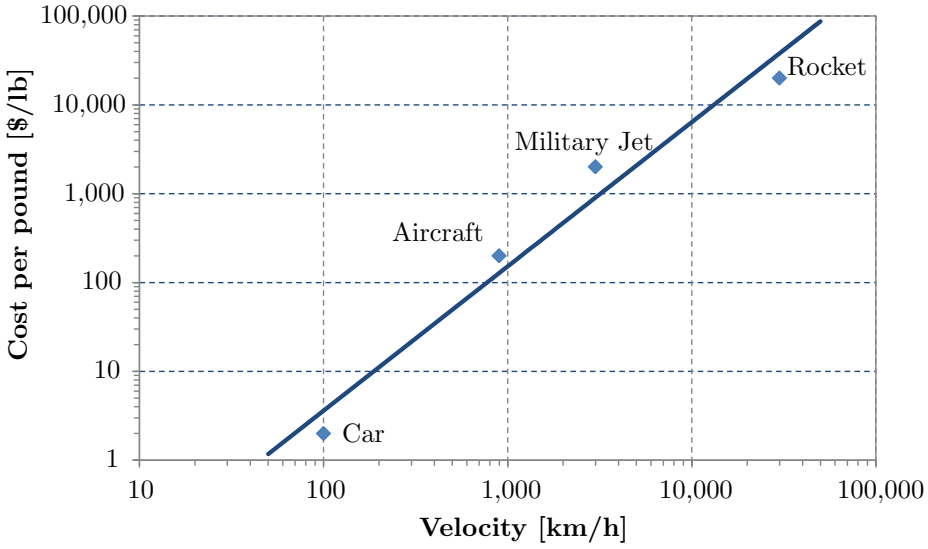

Figure 7.1: Costs per pound *vs.* transportation speed, illustrative trend.

Babikian *et al.*, [230] noticed that structural efficiency have decreased between 10% and 25% for regional and large aircraft between 1959 and 2000 even after all efforts to improve

this factor. The authors defend in this study that this efficiency reduction is related to the structural changes to improve aerodynamics, reinforcements to integrated new inflight systems and to accommodate increased engine weights.

This Chapter discusses and assesses the consequences of the adoption of FSW in the weight reduction and its cost compared with the riveting process. This assessment is based in generalist assumptions for medium and large civil aircraft in order to achieve preliminary comparisons and to determine some of the advantages and disadvantages of the application of FSW in this kind of structures. The long overlapped and riveted joints that are commonly found in aircraft structures will be the main focus of this analysis, since a simplification of the joint is straightforward, as documented in the previous chapter.

The importance of the structures' manufacturing costs in aircraft is illustrated in Figure 7.2[1]. The largest slice in the production costs of an aircraft, Figure 7.2a, corresponds to the structures, where in turn, the fuselage corresponds to about 55% of the total structure cost. Consequently, optimization in the structural manufacturing processes has large repercussions in the final aircraft cost and should be a main concern for the aircraft manufacturers. For instance, a huge amount of manual labor tasks are found in riveting structures due to the complexity involved in the automation of some of the procedures.

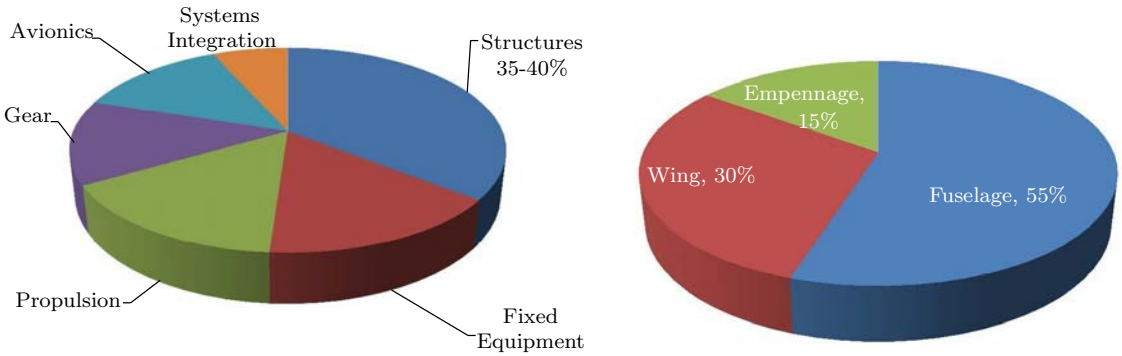

(a) Recurring production costs **(b)** Structures costs

Figure 7.2: Significance of fuselage costs, [175].

It is always a challenge to reduce simultaneously weight and costs, since new materials, adopted for weight reduction, are usually more expensive and require new design and manufacturing processes, increasing the final cost. The case of the adoption of carbon fiber reinforced polymers is an example where weight reductions are expected, although its price and manufacturing costs are greater than the aluminium solutions, [231]. Therefore, a tradeoff between these two variables is always required in order to achieve a good compromise. Figure 7.3 illustrates this trade-off that is usually associated to aeronautical components, requiring a compromise solution.

[1]These values are illustrative and dependent on the aircraft model.

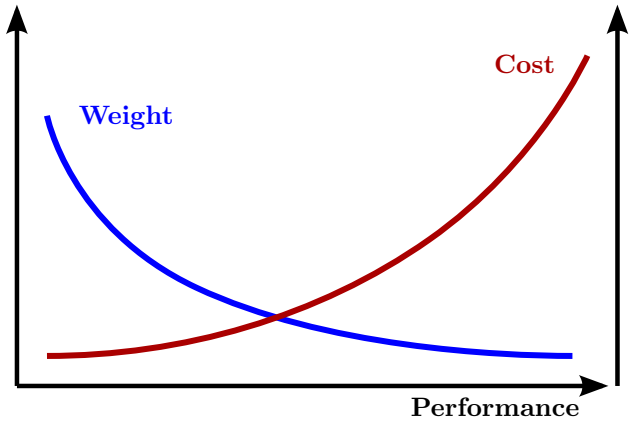

Figure 7.3: The variation of weight and cost in function of aircraft performance.

As the MEW has impact in the complete life cycle of the aircraft, relations between costs and weight are frequently used to optimize the structures. For instance, Kaufmann *et al.*, [232], proposed an objective function for Direct Operating Cost (DOC) based on the manufacturing and assembly costs - C_{man}, the costs of the lifetime fuel burnt per each kg of aircraft - p and the part weight - W:

$$DOC = C_{man} + pW \tag{7.1}$$

For a complete evaluation of the costs it is required to take into account, further to the manufacturing costs and fuel burnt costs, many other items of the life-cycle, as service, maintenance, repair and disposal. However, it is assumed that these (manufacturing and fuel burnt costs) are predominant for the design of new parts and can be used for structural optimization in order to find the best tradeoff between weight and cost, as in the example presented by Kaufmann *et al.*, [232] or by Hailian and Xiongqing for a composite structure, [233].

7.1 Weight Reduction

Several initiatives have been proposed to reduce the structural weight and improve the structural efficiency, mainly focused in two groups: *(i)* the application of new materials (as discussed in Chapter 3 with the new aluminium alloys or with carbon fiber reinforced polymers or even Glare) and *(ii)* new structural concepts as the integral panels produced by FSW.

The weight reduction using new materials was discussed in Section 3.2.4 considering the fatigue strength of the three major groups of materials presently applied in fuselages. The reduction of the weight through new design concepts is function of the material selected.

Concerning the aluminium alloys, the application of new design and manufacturing concepts has been done in different directions, with the new machining operations (as high speed machining) or with diverse treatments (as shot peening) or with new joining processes to create integral structures without fasteners.

An example of weight reduction using new design and manufacturing solutions is the case of adoption of LBW to join the stringers in the fuselage panels. The application of LBW to produce these panels has been adopted intensively by Airbus, mainly in three models of aircraft: A318 (2 panels, corresponding to more than 50 m of welds in each aircraft), A380 (8 panels, corresponding to more than 300 m of welds) and A340 (14 panels, corresponding to more than 400 m of welds in each aircraft), [234]. Rendigs and Knüwer in [122] pointed out that more than 1200 welded plates were produced until 2010 for Airbus aircraft.

The weight savings of applying LBW to join the stringers to the fuselage skin are significative compared with riveting. Pacchione and Telgkamp disclosed that the replacement of riveting stringer by welded stringers allows savings of 0.18 kg per meter of joint, [235]. This saving corresponds to savings of 9 kg in the A318, 54 kg in the A380 and 72 kg in the A340. These values are significant weight savings, since they corresponds to approximately 10% of weight savings just in those panels, [122].

The application of FSW can also be considered to produce these reinforced panels, with T-joint configuration as analyzed in the Section 6.1. Equivalent weight savings comparable to the LBW stiffened panels are expected, since the geometry of the joint is similar. The case of the small business jet Eclipse 500, which was the first aeronautical application where the FSW is the major joining process, approximately 7378 fasteners, corresponding to 65% of the riveted joint were replaced by FSW representing a weight saving of about 22 kg, [236]. The weight savings in this case are modest since the joint geometry was not adapted to this joining process. The joints skin-stringers are welded in the overlap positioning. As demonstrated in Section 6.3 this configuration has a weak fatigue strength due to the interface defects. However, these aircraft have lower number of fatigue loading cycles than the commercial aircraft and Eclipse reduced the interface defects with new tools, in order to not compromise the structural integrity, [237].

The replacement of longitudinal joints, as the ones applied to join fuselage panels has higher potential for weight savings, since these joints require 2 or 3 rows of rivets for the load distribution. Pacchione and Telgkamp in [235] indicate that for a joint with 3 rows of rivets requires 75 mm of overlap leads to up to 0.8 kg per meter of joint (for a plate thickness about 3.8 mm). Assuming that the Airbus A340 has at least 8 longitudinal joints along its 72 m length, about 450 kg could be saved just in these joints.

7.2 Manufacturing Costs

The major target of this section is the cost reduction concerning the manufacturing and assembly of aircraft structures. As mentioned above, these costs are an important part of the total aircraft costs. Due to the complexity of the automation of some tasks to manufacture these structures, as riveting, [238], their manufacturing still requires substantial amount of manual work. Nevertheless, several initiatives to develop new solutions to reduce the fabrication costs of metallic structures have been proposed. An example of the development of new manufacturing processes with the aim of cost reduction is disclosed by Pechiney Rhenalu, currently Rio Tinto, in [239]. These solutions comprise:

- Machining:
  - More near-to-the final shape products;
  - Low residual stress materials;
  - New machining sequences for reduced distortion;
- Forming:
  - Stretch forming with high formability qualities;
  - New age forming alloys and dedicated ageing practices;
  - Stringer alloys adapted to severe joggling.
- Heat treating:
  - Avoid heat treating due to high formability sheets;
  - Adapt aging treatments to the customer capabilities (shorter equivalent ageing practices).
- Assembly:
  - New solutions to reduce/suppress riveting, with weldable solutions as FSW; or integral machining of heavy gauge plates;
  - Improved alloys for increased stringer pitches;
  - New design alternatives (as cast doors).

The replacement or reduction of riveting has been a major goal in the aeronautical industry to reduce the manufacturing costs, since it presents several drawbacks from the manufacturing point of view such as being an expensive and time consuming process, still requiring hand intensive work because its automation is not always feasible. The adoption of integral structures to reduce the number of riveted joints has been the solution adopted for carbon fiber reinforced polymer fuselage panels, [240], and for the aluminium fuselages. In the case of aluminium fuselage, additionally to the weight reduction, also the manufacturing costs decrease since more automation is used. The fuselage panels where the stringers are welded with LBW or in the Eclipse 500 where FSW is adopted are examples where the manufacturing costs were substantially reduced. In the case of the Eclipse 500

this adoption allowed to produce a business jet with one quarter of the costs of comparable competitive aircraft, [241].

7.2.1 Main FSW Costs

A cost estimation comparing the FSW with the riveted joints based on deterministic and empirical assumptions was performed. Regarding FSW, the cost evaluation can be based in the methodology for cost evaluation of other welding processes. In this case, it is assumed that the major costs are the ones presented in Figure 7.4. For FSW process, equipment and labor (with considerable lead times) are the main costs. Although, when compared with other welding processes, as LBW, the major difference is in the consumables. In FSW the consumables costs do not contribute significantly to the manufacturing cost.

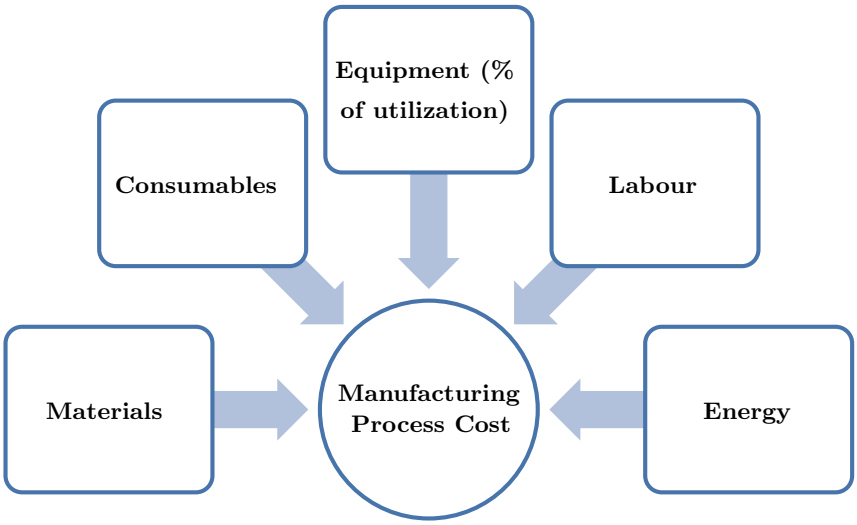

Figure 7.4: Major manufacturing costs of a joining process.

In the literature, an estimation cost tool for FSW is found. The E-Tool, developed by Tipaji, [242], estimates total manufacturing cost, C_T, based on:

$$C_T = C_L + C_M + C_P + C_{Tools} \tag{7.2}$$

where C_L is the cost related to weld preparation time plus the actual weld time, C_M is the machine cost, C_P is the power cost and C_{Tools} is the tooling cost. This study did not include the costs related to the fixture of the welding parts, which could be a substantial cost in large parts due to the tolerance management. For the detailed example in this study it was concluded that the machine cost represents 49% and labor cost 46% of the total costs.

Di Lorenzo and Fratini in [243] presented a cost model based on machine availability and maintenance, patent royalties, power supply, human resources, fixture and tooling and process set-up and tool change. From this study, it was observed that the multiple T-joints can decrease significantly the welding costs, i.e., the cost is reduced to half if the number of T-joint increases from 2 to 6 joints. Another conclusion is the cost reduction with the weld length increase and/or thickness decrease. The cost of a joint with 1 m is more than a double of a joint with 3m and the cost of a joint with 3 mm thick is nearly half of a joint with 25 mm thick.

Other cost model for estimation of manufacturing costs of FSW is proposed in [244]. In this study, a stiffened panel with 7 stringers with 2.05 m length joined by riveting and by FSW were modeled and compared. The authors of this study decomposed the riveting and the FSW process in three main phases, that in the case of FSW included: set-up and pre weld tasks, the welding and post welding operations. Figure 7.5 presents the comparison of the time and the cost required to manufacture this 7 stringer panels. They concluded that with FSW the manufacturing time is reduced by 60% and the cost is reduced in 18.5%.

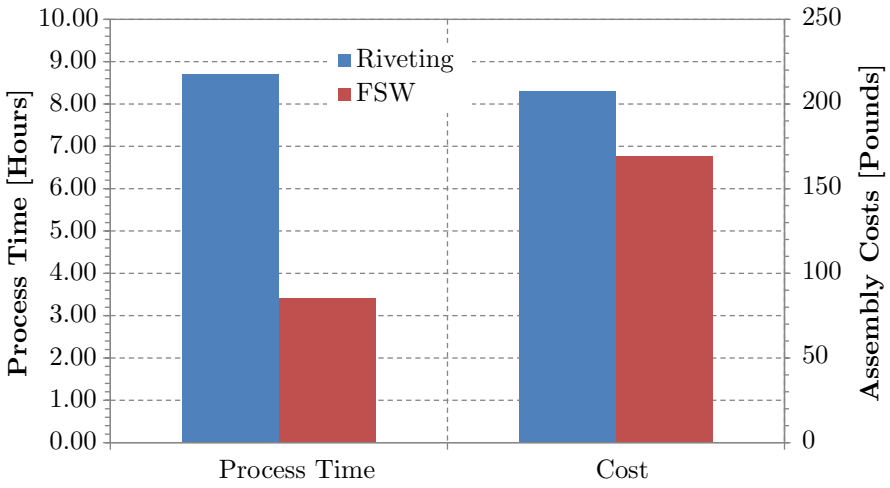

Figure 7.5: Process time and costs, comparison between riveting and FSW, [244].

The welding and setup equipment are the highest fixed costs for the adoption of FSW, and are a function of the application type, panels dimensions and geometries. Due to the specific requirements of aeronautics, the equipment for FSW should be multipurpose in order to be adaptable to different types of structures. For cost evaluation purposes, Table 7.1 shows three FSW machines for 2D welds, for welds about 1 to 2 m long, in force or displacement control mode and numerically controlled. Their prices are indicative and may present some variation due to other characteristics as the possible automatic variation of the tilt angle, refrigeration and other characteristics.

[1]Considering an exchange rate of 1 €= $1.42 U.S. dollars

Table 7.1: FSW example of equipment cost.

Company	Model	Price
Transformation Technologies	RM1	∼350,000 €
ESAB	LEGIO FSW 3UL	∼150,000 €
Nova-Tech Engineering (NTE)	V30K	∼300,000 €[1]

For the industrialization of the FSW to join large panels, as the reinforced fuselage panels with lengths higher than 5 m and sometimes with curvatures in two axis, larger machines with more than 3 axis are required. An example of a multipurpose FSW equipment is proposed by MTS Corporation, the I-STIR 10, Figure 7.6. This FSW has 5 degrees of freedom (3 linear and 2 angular) and can apply a maximum forging load of about 100 kN. Airbus in Bremen has been using this FSW model, [126] with retractable pin tool.

Figure 7.6: MTS I-STIR 10 friction stir welding equipment, (Courtesy of the I-STIR Technology Business), [245].

Comparisons between riveting and FSW costs can be done in a generic way considering illustrative costs. An illustrative comparison was done considering the replacement of riveting by FSW. For this purpose longitudinal joints were considered. With riveting, this joint has double rows of rivets and when welded has a single FSW pass. It is known that the manual riveting does not require heavy initial investments but is heavily labor consuming; on the opposite side, the automated riveting and the FSW process require significant initial investments but this is amortized along time with the low cost of operation. A base of 100 mm joint length was considered, that with a riveting pitch of 20 mm, [246], corresponds to 10 rivets. Considering the initial investment of $50,000 USD for the manual riveting equipment, $2,500,000 USD for automatic riveting and making an assumption of $2,000,000 USD for a multipurpose FSW grantry equipment, the break-even points was determined

for these processes considering a cost of \$0.04 USD per rivet with manual application, \$0.02 USD for automatic riveting and \$0.17 USD per 100 mm of FSW length, [247]. The cost per joint *vs.* the joint length for these three joining processes is presented in Figure 7.7. These results should be considered empirical since the cost data is highly variable in the joint types and length, although this can be used as a basis for comparison. In aeronautical applications the management of tolerances will have higher cost impact since with overlap joints is reasonably easy to manage the tolerances, but in the case of FSW butt joints, the required tolerances might be a manufacturing challenge.

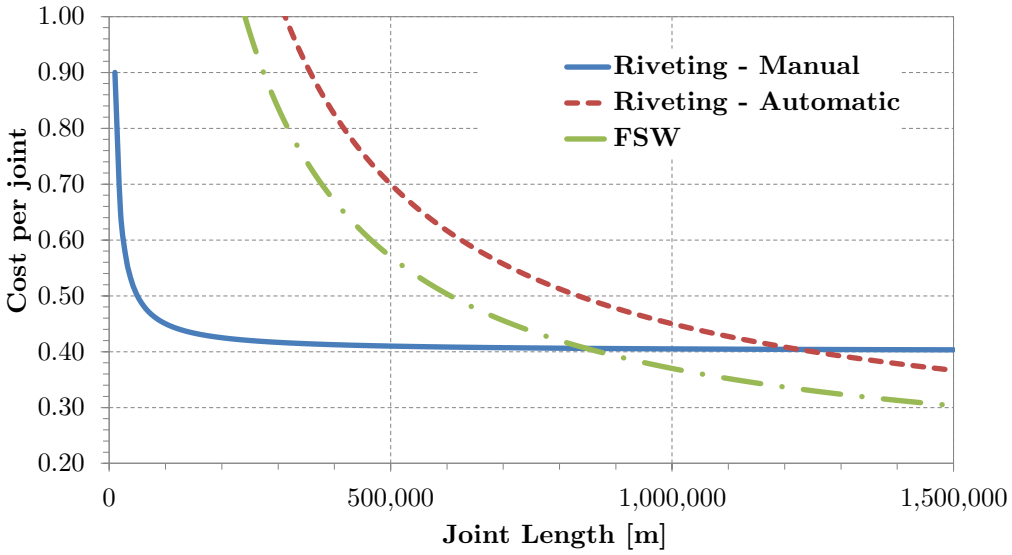

Figure 7.7: Cost analysis comparing FSW with riveting process.

Chapter 8

FSW Impact in the Design of Airframes

The systems engineering approach in the aeronautical and space industries has been moving from the traditional sequential or series approach to a parallel and iterative concurrent engineering paradigm, involving teams in several locations and sometimes different companies, [248]. Also, the traditional focus on performance and risk avoidance, paramount in that industry, is shifting towards the consideration of development lead time, life cycle cost, and risk management with product performance still meeting requirements. Tools involved include life cycle design, focusing on the complete life cycle of the product, from design through manufacture and service to final disposal, Design For Manufacture and Assembly (DFMA) to produce innovative, cost effective and easy to manufacture products with materials and technologies selected to maximize revenue while serving their purpose, design for quality, ensuring low failure rates and high performance levels, faster design cycles, and engineering without walls - a buzzword referring to a form of concurrent engineering where companies (not only suppliers, but also competitors) work together in certain problems, a fact known in the automotive and also aerospace industries. As stated by Marxt and Hacklin, [249] product innovation focus on creating new products or services, whilst generating an additional business for a company. Process innovation, on the other hand, refers to optimizing processes *e.g.* in manufacturing, to minimize costs or to increase quality, as in the case of the application of FSW to join aeronautical structures.

The introduction of new design concepts and solutions is tightly tapered by existing materials and manufacturing processes. In the case of aeronautical structures, this introduction is only done after deep analysis considering the different impacts during the all the product life cycle. In the context of the NPD, several tools have been developed to support the different development phases in order to achieve better product designs. Peters *et al.*, [250], discussed the use of some of these tools as Quality Function Deployment (QFD), Failure Mode and Effects Analysis (FMEA), Design for Assembly (DFA) or Design for Manufacturing (DFM), Concurrent Engineering (CE) or Design of Experiments (DOE), linked to the different phases of the NPD as represented in Figure 8.1. The authors stress that notwithstanding the linear simplification involved in this type of graphical

representation, the process is indeed iterative and within it there is an inherent amount of uncertainty and unpredictability. Notwithstanding those limitations, Figure 8.1 has the advantage of underlining the role of QFD in the early stages of the process, and of other tools in later stages. Nevertheless, these different tools might be applied along all the NPD improving the final outcome. Lockamy and Khurana discuss in [251] the application of the QFD from the product planing to the production, although the highest impact are in the first phases, considering and taking into account the right customers requisites in the concept development.

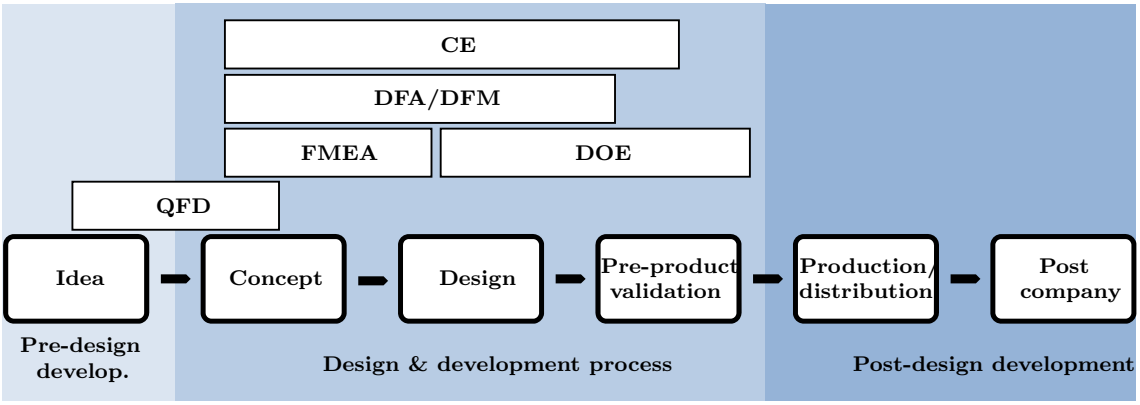

Figure 8.1: Design supporting tools in the product development.

8.1 Design for Manufacture, Design for Assembly, Design for Manufacture and Assembly

Design for manufacturing and for assembly are common tools which seek to promote efficiency. Aero-structural systems can be specified using systematic techniques such as the QFD to define functionality and key quality requirements, as described above and detailed by Curran *et al.*, [252].

These tools may be combined for a more comprehensive analysis. The Integrated Product and Process Design (IPPD) is an example of the combination which tries to embrace multiple design concepts during the product development and integrate the relevant processes in order to take into account their impact in the product lifecycle. IPPD decomposes the system in three levels: system level, component level and part level and based on the Georgia Tech (USA) approach, [253], four key elements exist to implement IPPD: quality engineering methods; computer integrated environment; top-down design decision support process and systems engineering methods.

IPPD needs to consider herewith the product design, assembly methods, manufacturing processes, tooling design and production costs, [254]. These analyses involve engineering

tools and models to predict engineering performance and characteristics such as acquisition costs, time to market, and life cycle performance. These models can be based on design rules and principles that can be used within the context of DFMA; the aims are the reduction of product complexity and cost, obviously without jeopardizing performance and safety. This involves the early integration of knowledge and analyses within a concurrent engineering environment as alternative design concepts are being considered, [252].

DFMA is applied by multidisciplinary teams in the aerospace sector to achieve more efficient product definitions at the concept design stage. Aero-structural systems are part- and labor-intensive, and costly to fabricate and assemble. The focus is on achieving the simplest structural configurations that meet the system requirements in terms of structural integrity, aerodynamic performance or any additional functionality. However, cost modeling tools are required to guide multidisciplinary teams in decision making, although it is widely acknowledged that it is extremely difficult to obtain fast and accurate cost estimates, as detailed by Curran, [228].

In particular, DFMA can be described as consisting of two stages as schematically presented in Figure 8.2 based on the methodology proposed by Knight, [255]. DFA is the first stage, aiming at product simplification and part count reduction, and involves a detailed analysis of the product for ease of assembly. The basic input for the DFA analysis is the product structure, *i.e.* a list of items and assembly order. Product simplification and part count reduction are performed in the course of interdisciplinary review exercises, applying criteria as the following, taken from Knight, [255]:

- In service, does the part moves relative to other parts already assembled?
- Must the part be of a different material, or be isolated from other parts already assembled?
- Must the part be separate from other parts assembled to make possible assembly or disassembly of other parts?

If an item fulfills none of these criteria, then it is theoretically unnecessary. This analysis leads to a theoretical minimum part count for the product. It does not imply that the product may practically or economically be built with this minimum of components, but gives a target to aim at. The result of the DFA analyses may be proposals for product simplification through elimination or integration of parts, including new combinations of materials and processes.

In the case of DFM, the objective is the development of the product aiming at the minimum manufacturing costs with high manufacture quality and an optimized life-cycle service (optimum reliability, maintainability and serviceability), [256]. In the case of joining processes, the minimization of tools, gigs, fasteners variety, and better tolerance management are the immediate analyses that can be done in the early stages of the concept

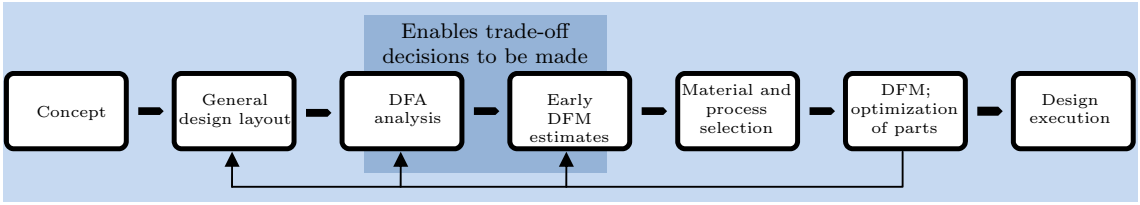

Figure 8.2: Sequence for design for manufacturability and assembly.

development, improving the final production lead times and product quality and the manufacturing cost.

The design for manufacturing and design for assembly were the first aspects analyzed in complex product development in order to achieve a more successful products. However, other variables have been also considered, originating the term Design for X (DFX) standing for design for a certain objective or multiple objectives, addressing the different needs of the customers and stakeholders. This DFX has been expanding to diverse areas, as environment, usability, testability, safety, serviceability and packaging [257, 258].

Civil aircraft are complex structures, including more than one million parts if fasteners are counted. Design is typically an iterative process of the concurrent engineering type due to this complexity, where issues of function, performance, manufacturing and cost are simultaneously dealt with for each component of the aircraft. The design process zooms in greater detail level as required, avoiding circular references. The digital mock-up is organized hierarchically, where each component can have multiple levels of sub-components. A whole aircraft consists of many components like wings, fuselage, horizontal and vertical stabilizers, and so on: *e.g.*, a fuselage contains frames, stringers, and windows. The same procedure can theoretically be continued down to the rivets, [259], see Figure 8.3.

The assembly of these structures is segmented in multiple levels for a better control and management. These assembly levels usually are distributed in different tiers with multiple specifications, as the tolerance management which is different for the diverse levels. Figure 8.4 details the different levels of the fuselage assembly. The generic product families used on a typical stringer-skin panel are the panel, which forms the skin of the aircraft, the stringers and the frames that support it in the longitudinal and lateral directions, the clips that are present at every stringer-frame junction and the rivets that fasten the assembly together. This design and the riveted aluminium alloy fuselage have been a dominant design, although it started to be replaced by other materials and integral joints.

Voland, [260] presents the engineering design process as a search for the best solution among several alternatives, involving *(i)* needs assessment - objectives to be achieved by a solution, *(ii)* problem formulation - defined in the form of prioritized design goals, specifications and explicit and implicit constraints, *(iii)* abstraction and synthesis - generating

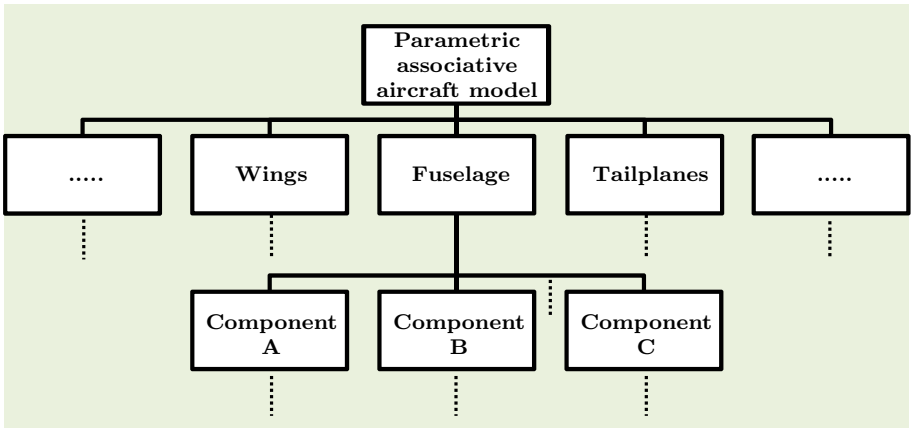

(a) Schematic representation of a parametric associative CAD assembly

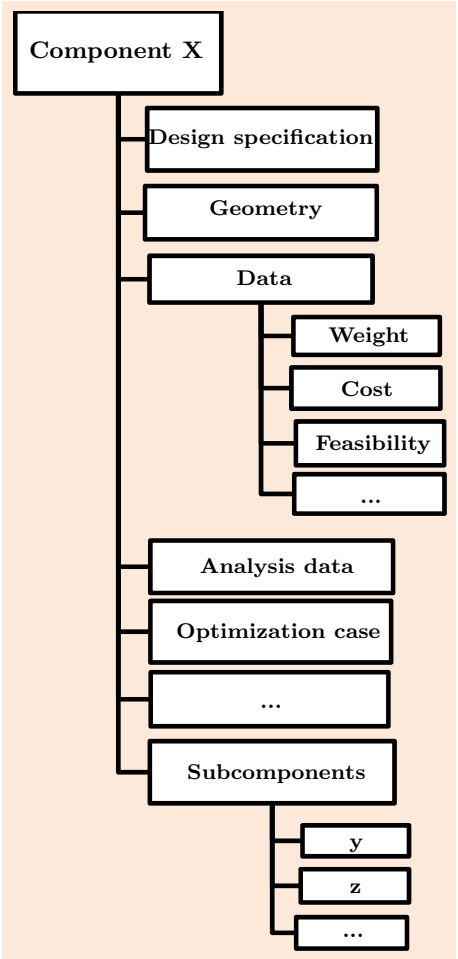

(b) Composition of a single component

Figure 8.3: Schematic representation of a parametric associative assembly of an airframe (adapted from [259]).

alternative solutions or designs, *(iv)* analysis - comparing and evaluating alternative designs, and *(v)* implementation. Constraints or specifications are associated with each design

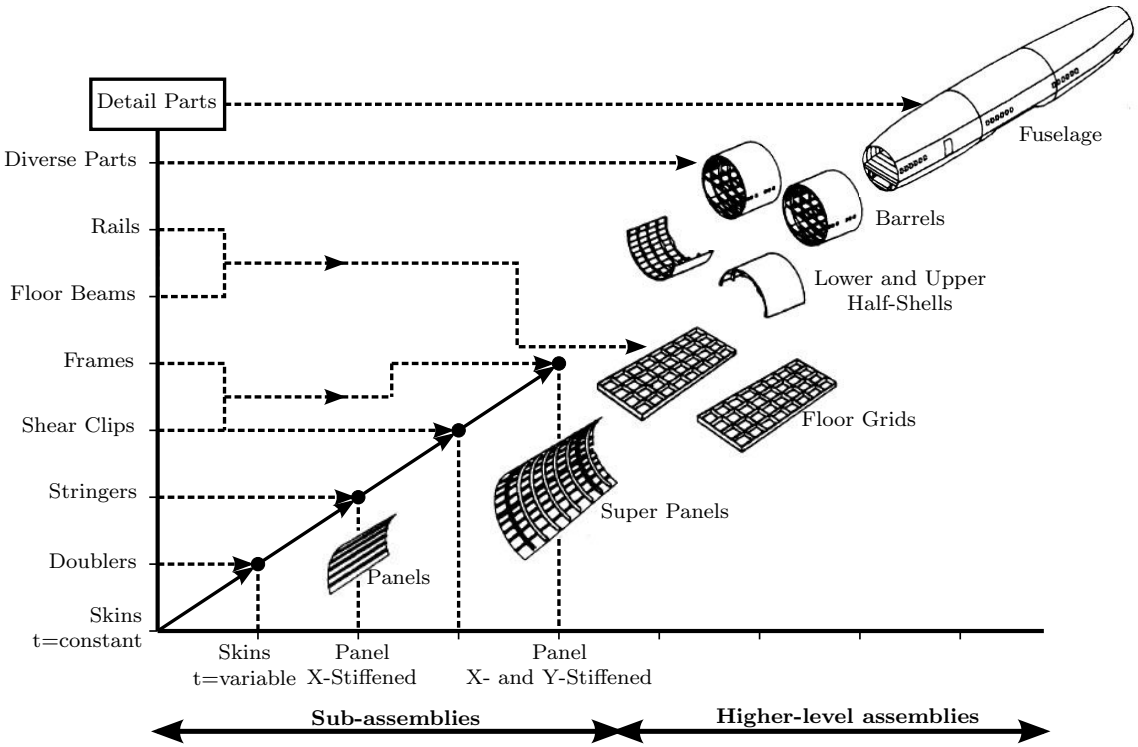

Figure 8.4: Aircraft fuselage assembly levels, [175].

goal. Some goals should be achieved completely, others *e.g.* lightweight or minimum cost should be defined quantitatively to give specific targets. In conceptual design, functional requirements are transformed into a physical configuration, [261]. If the desired function is to support an internal pressure with a lightweight stiff structure, then a thin thickness cylinder reinforced with ring frames and stringers comes to mind; that is precisely the concept of a traditional fuselage. The prioritization of these functional requirements is imperative in complex projects to focus efforts for design optimization in the most relevant parts. Afterwards, the quantification of the different design options to select the best configuration and options is done, supported by different tools, as the QFD, which will be analyzed in the following section. These analyses should be reinforced by economical, environmental and social considerations. In the present research, just the cost modeling was considered, with a bottom-up generative model, given the fact that FSW is an emergent technology.

During the design of aircraft structural components, predictions of the performance of the different design concepts are used to select the best design. This usually focuses on areas of weight, aerodynamics, manufacturability and costs, [227]. At the conceptual design stage, in-depth analyses using sophisticated computer tools are performed in the areas of aerodynamic and structural performance. Compared with these analyses the manufacturability and cost analysis may be rather unsophisticated [262], often consisting

of estimations based on cost per kilogram. Clearly, such weight based estimations do not incorporate important manufacturing factors to properly compare different design concepts.

The application of FSW in the fuselage requires multiple explorations of the impact in the design of theses structures and in the DFX of the most relevant dimensions. In the case of large civil aircraft the complexity of the assembly is substantial. Whitney presented in [263] a brief introduction to current practice for assembling the different fuselage parts of a large civil aircraft. Figure 8.5 shows schematically a simplified datum flow chain[1] of a fuselage, where three stakeholders have direct impact in the assembly: a first company that makes the frames and respective holes for fastners, a second supplier that supplies the skin with the stringers and attaches the frames to these panels and the final assembler that joins the different panels and adds the cargo and passenger floors. All these three companies have to follow a datum flow chain to control the final diameter and circumference of the barrel, Figure 8.5a. In the assembly of the fuselage barrels, several key characteristics are fundamental for a right design for assembly. Figure 8.5b presents some of these characteristics, as the minimum edge distance for rivet holes, the tolerance management of the seat tracks, the skin gap around the circumferential joint and the horizontal skin alignment.

Another advantage of the application of the FSW in the fuselage panels and assembly is the capability of the production larger panels for the final assembly of the fuselage reducing substantially the assembly lead times. The increase fuselage panels in order to create 'superpanels' has been investigated by several aircraft manufactures and is reported by Munroe *et al.* in [175], reducing the number of panels required to make a fuselage barrel, Figure 8.6. Other alternative is to increase the panel length, this option was adopted by Airbus for the fuselage panels in the A350 XWB, [264]. Some rough numbers of cost and weight reduction due to the reduction of the number of panels circumferentially required for the whole barrel are presented in Table 8.1. This table shows that a huge reduction of part fabrication costs and assembly costs can be achieved just increasing the size of fuselage panels.

A decomposition of the FSW process into sub-processes as schematically presented in Figure 8.7, followed by NDT since the inspection can have an important role in the manufacturing costs and time. A considerable part of these subtasks can be automated, even the non-destructive inspection using eddy currents detailed in Section 4.3.

[1] Graphical representation of assemblies, where the arcs represent matches between the parts and dots the parts and its manufacturer.

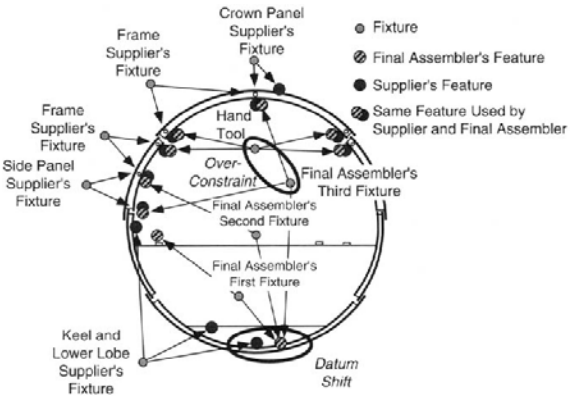

(a) Assembly features

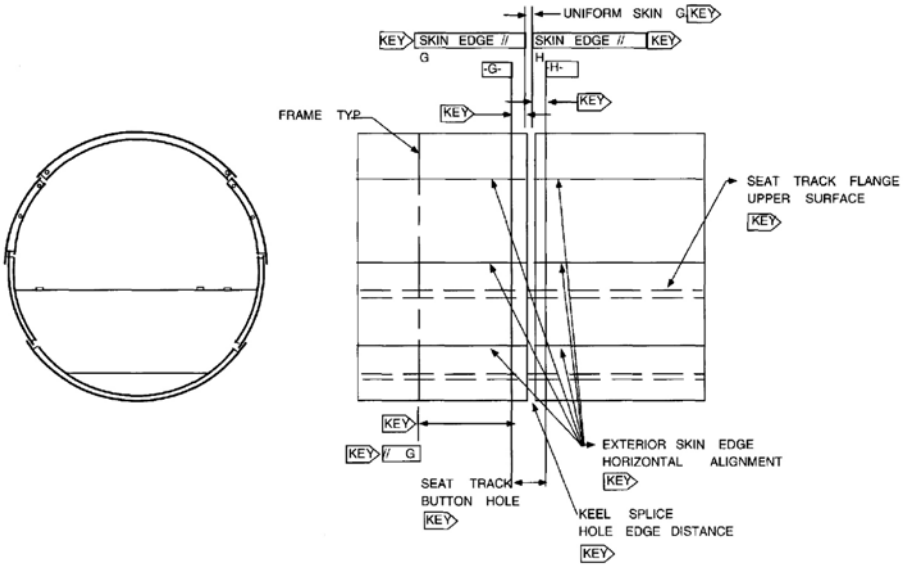

(b) Key characteristics

Figure 8.5: Fuselage assembly, different subassemblies and key characteristics, [263].

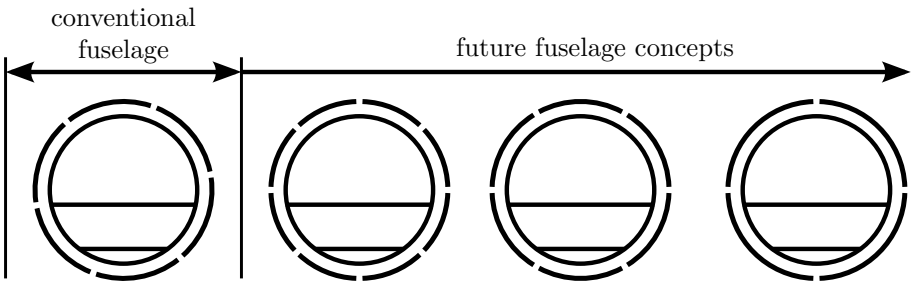

Figure 8.6: Reduction of the number of fuselage panels, [175].

Table 8.1: Cost reduction due the decrease the number of fuselage panels, [175].

No. of Panels/Superpanels	10 (Basis)	8	6	4
Engineering Cost	0	-10%	-20%	-30%
Material Cost	0	-5%	-10%	-15%
Part Fabrication Cost	0	-20%	-35%	-50%
Assembly Cost	0	-15%	-30%	-50%
Weight	0	-2%	-4%	-6%

8.2 Quality Function Deployment

As an exemplification of the tools that can support the development and the application of new manufacturing processes in aeronautics during the early stages, some of the QFD concepts were applied in order to have a more widespread comparison of the alternative joining processes for primary structures. Other tools are also feasible and perhaps with better characteristics, as the Theory of Inventive Problems Solving (TRIZ) and DSM reported by Tseng *et al.*, [265], due to the correlation between the different engineering characteristics of the different parts. Nevertheless, the QFD still was applied since it can give a fast assessment of the most important customer needs and an evaluation of how much a given concept meets the customers needs and targets [266].

This methodology, defining and prioritizing the customer's desires, translating them into engineering requirements and establishing targets for meeting those requirements, allows to obtain best design choices taking into account multidisciplinary aspects as the financial characteristics of determined solution, [267]. Customers have requirements and constraints; functional requirements are statements of the specific performance of the design, *i.e.* what the product should do; constraints are external factors that in some way limit the selection of system or subsystem characteristics. In general, the QFD method includes the following steps:

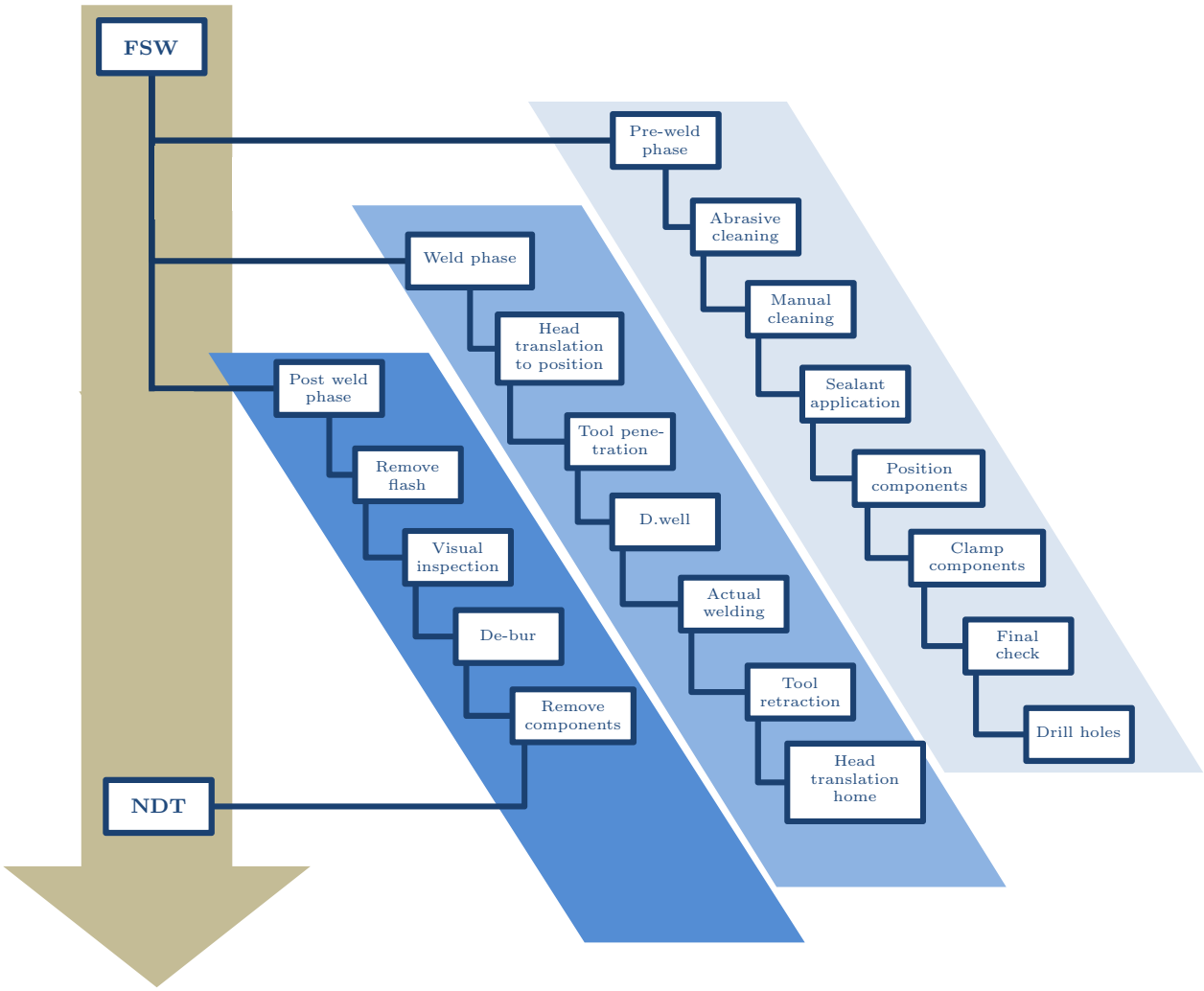

Figure 8.7: Phases and sub-processes of the friction FSW process.

1. Identification of the customer(s),
2. Identification of customer requirements /constraints,
3. Prioritization of requirements,
4. Benchmarking,
5. Translation of customer requirements into engineering specifications,
6. Setting targets,
7. Definition of the best design choice based on the above analysis.

The application of the QFD tools has been done successfully in new aircraft development projects, [268] as in the military aircraft Lockheed Martin F-22, [269]. Several advantages in the adoption of this methodology are listed by Bossert in [270]:

- **Customer driven**
  - Creates focus on customer requirements

  - Uses competitive information effectively
  - Prioritizes resources
  - Identifies items that can be acted upon
  - Structures resident experience/information
- **Reduces implementation time**
  - Decreases midstream design change
  - Limits post-introduction problems
  - Avoids future development redundancies
  - Identifies future application opportunities
  - Surfaces missing assumptions
- **Promotes teamwork**
  - Consensus based
  - Creates communication at interfaces
  - Identifies actions at interfaces
  - Creates global view out of details
- **Provides documentation**
  - Documents rationale for design
  - Is easy to assimilate
  - Adds structure to the information
  - Adapts to changes, a living document provides framework for sensitivity - analysis

The house of quality is the best known tool to apply the QFD concepts. This tool was developed at Mitsubishi's shipyard company, in 1972, with successful application in several other sectors, [271]. The house of quality is composed by multiple matrixes with correlations and quantifications of the customers needs and the design and engineering options and decisions. Figure 8.8 shows the structure of the house of quality based on the model presented by Bounds *et al.* [272]. Each one of these matrices is built with clearly defined measures of customers (in the left) that are matched with the design requirements in the top.

In complex and safety critical projects several house of qualities can be done at different levels of the project. In the base, as the case of aeronautical structures, the customer needs are more 'technical requirements' with several engineering variables. In the present work are considered, as the customer requirements several DFMA requirements in order to optimize the design as a function of the DFMA variables. This analysis allows the identification of the best solution among several alternatives, each of which with particular strengths and weaknesses. This assessment requires that goals to be achieved are explicit and subjected to ranking.

A ranking of the design goals was done applying the method of Cross, [273]. This method classifies the goals along rows, and for each goal is given a score of 1 if more

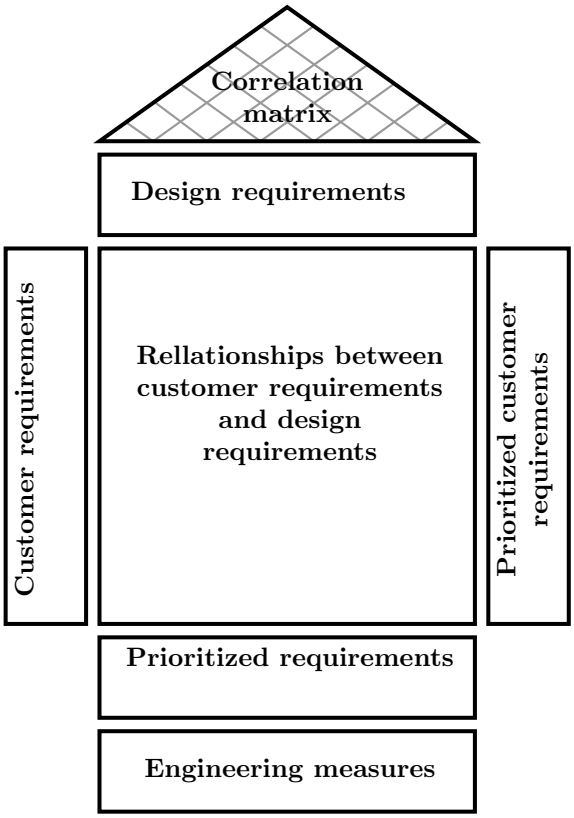

Figure 8.8: House of quality matrices.

important than the corresponding column goal. The goal along the row is given a score of 0 if perceived as less important than the corresponding column goal; where both column and row goals are perceived as of equal importance, they are given a value of 0.5. In Table 8.2 is presented the rank ordering of the some relevant design goals with this method and based upon the authors and experts engineering judgment and experience.

Considering this design goals, the following requirements, among others, were considered: minimization of the number of parts, designing parts to be functional, avoid separate fasteners, minimization of the number or need for assembly operations, maximization of the tolerances for easy assembly and minimization of the requirements of jigs and fixtures. A correlation of the goals initially presented which could be termed, in QFD terminology, 'customer requirements', with the engineering 'technical requirements' mentioned. Table 8.3 presents the correlation of these variables, where the strength of the correlation is graded according to a 4 level scale: S means strong relationship; M means medium relationship and L means low relationship and the sign "-" means no relationship. These correlations were obtained based upon engineering judgment and experience of experts in this field.

Table 8.2: Rank ordering the design goals using the method of Cross.

	Fatigue behavior	Minimum maintenance	Aerodynamic (& aesthetics)	Minimum fabrication cost	Availability of parts	Minimum weight	Minimum manufacturing time	**Total**
Fatigue behavior		1	1	1	1	1	1	6
Minimum maintenance	0		0	0	1	0	0	1
Aerodynamic (& aesthetics)	0	1		0	1	0	0	2
Minimum fabrication cost	0	1	1		1	0.5	1	4.5
Availability of parts	0	0	0	0		0	0	0
Minimum weight	0	1	1	0.5	1		1	4.5
Minimum manufacturing time	0	1	1	0	1	0		3

Tables 8.2 and 8.3 represent the initial stages of a QFD process based on the house of quality. In the present case the subsequent benchmark concerns a panel manufactured using the traditional riveting technique, or alternative solutions based on LBW or HSM, the other techniques that may be considered within the realm of fuselage metallic structures. It should be pointed out that HSM may be considered, at least theoretically, for panels, notwithstanding its huge waste of scrap (although aluminium is recyclable). Table 8.4 presents this benchmarking where '5' means the highest grade.

Cost but also manufacturing problems rule out HSM; indeed, many reinforcements used in fuselage panels (like frames or stringers with L, T or other cross sections) could not be practically machined using HSM, a technique that is geared towards pocketing. The above procedures are linked to the initial stages of a formal QFD exercise, although a more comprehensive assessment of different manufacturing processes was possible, pointing out the advantages of the panel design and manufactured with FSW. In industrial environment, other characteristics must be included for a more accurate assessment and applied to a different levels of the structure.

Table 8.3: Structural requirements and correlation with design goals.

	Damage tolerance	Minimize number of parts	Design parts to be functional	Avoid separate fasteners	Minimize the number or need for assembly operations	Maximize tolerances for easy assembly	Minimize requirements of jigs and fixtures
Fatigue behavior	S	M	S	M	-	-	-
Minimum maintenance	S	S	M	L	L	-	-
Aerodynamic (& aesthetics)	-	-	-	L	-	-	-
Minimum fabrication cost	-	S	L	S	S	S	S
Availability of parts	-	S	L	M	-	-	M
Minimum weight	-	S	S	S	M	-	-
Minimum manufacturing time	-	S	L	S	S	S	S

Table 8.4: Benchmarking between manufacturing processes.

	FSW panel	Riveted panel	LBW	HSM
Fatigue behavior	4	5	4	3
Minimum maintenance	5	3	5	5
Aerodynamic (& aesthetics)	5	3	3	5
Minimum fabrication cost	5	3	5	2
Availability of parts	4	3	4	5
Minimum weight	5	5	3	5
Minimum manufacturing time	5	3	5	5

8.3 Value Engineering

Value engineering is a generic methodology suitable for products, processes and projects where is assigned a fraction of the final cost to each function or impact in order to find where is feasible the reduction of the global cost (manufacturing or others). Mainly, the value engineering is decomposed in four activities, [274]:

- Identify the function of a product or service;
- Establish a worth for that function;
- Generate alternatives through the use of creative thinking;
- Provide the required functions to accomplish the original purpose of the project at the lowest life-cycle cost without sacrificing safety, necessary quality; and/or environmental attributes of the project.

The engineering value in aeronautical sector needs to address all costs during the life-cycle as discussed in previous Chapter. Nevertheless, Murman *et al.*, [14] reported a generic functional relationship for value as:

$$Value = \frac{f_p(performance)}{f_c(cost) \cdot f_t(time)} \tag{8.1}$$

This definition is based on the "Better, Cheaper and Faster" drivers which can be transposed into improved performance, lower cost and shorter times, respectively. With the tendency based on "More Affordable, Cleaner and Quieter" aircraft the value function needs to be changed taking into account the life-cycle cost, noise, and emissions. A functional relationship can be:

$$Value = \frac{1}{f_{lcc}(life-cycle\ costs) \cdot f_n(noise) \cdot f_n(emissions)} \tag{8.2}$$

These value functions can be considered in he value engineering analysis considering other aspects that are not only the cost. However, most of the value engineering still established on the cost. Most of these variables can be converted in cost (for instance environmental costs or social costs), although their quantification in complex and unobjective.

Based on the data and analyses acquired along this research, the replacement of riveted joints by FSW will add value to the aeronautical structures and subsequently to the aircraft, since it decreases the manufacturing costs, increases the performance due to the decrease of structural weight and decrease the lead time. The quantification of the value engineering added due to the FSW or other manufacturing processes can be estimated and assessed in the early phases of the product development resulting in a more successfully projects.

The International Air Transport Association (IATA) already identified the FSW as a technology ready and suitable to new aircraft designs prior to 2020, [275], concerning to short range aircraft. A technology readiness level of 7 (system prototype demonstrated in an operational environment) was pointed out by this association confirming the FSW applicability in aeronautical structures. In addition, a reduction of about 1% of fuel burn is reported, which means a considerable reduction of life-cycle costs.

From the value engineering point of view the replacement of riveting by FSW requires a considerable investment for equipment and resources although this investment is amortized

in a short period and allows several manufacturing improvements and reduction of the global lead times. This adoption is not absent of risk, since the structural integrity needs to be meticulously analysed in the product and process development and the joint quality needs to be completely ensured and inspected during all service life with non destructive techniques. The value added with this replacement is substantial considering the "Better, Cheaper and Faster" *motto*, nevertheless it also allows a more cleaner aircraft structure due to the weight reduction.

Chapter 9

Conclusions

A multi subject research was performed to investigate the replacement of the current joining process in aircraft primary structures, riveting, by a welding process, Friction Stir Welding (FSW). Due to the better joint efficiencies and capability to weld all aluminium aeronautical alloys, this process arouses interest by the major aircraft manufacturers. However, its application requires new design concepts and a full understanding of the joint behavior and requirements along the complete service life of these structures to ensure the structural integrity. In complex safety critical structures, this structural integrity is fundamental under the multiple environmental and service conditions. Structured product and process development is imperative for successful product design and complete fulfillment of all aeronautical requirements.

The adoption of new materials in aeronautical primary structures has been the major change in the last years in aircraft structures, which can lead to higher structural efficiency in terms of weight and cost reduction. The massive application of composite materials in the new generation of twin aisle long range aircraft is an example of this tendency. Nevertheless, the initial estimations of weight savings in these projects could be underestimated or overestimated since the behavior of new materials under aircraft service conditions are not fully investigated, namely from the environmental, scale and aging points of view. Beyond new materials in fuselage, other manufacturing processes have been emerging that can improve the structural efficiency. This research was focused in the replacement of the present joining process as a result of new manufacturing techniques that are emerging with overall better characteristics.

Riveting has been the preferred joining process for many years in fuselage structures since it is a very flexible joining process, allows easy repairs, is inexpensive and the riveted joints can be designed to be damage tolerant. However, on the other side, this process requires sealants, overlap areas and fasteners which are components that do not add value to the structure, the holes of riveting are stress concentration points or corrosion points where cracks usually initiate and the automation of the process is difficulty and costly.

Therefore, alternatives to replace this process may allow to produce more efficient structures from the manufacturing and service points of view.

FSW is a semi-solid state welding process, which is less aggressive when compared to fusion welding processes and produces joints with higher joint efficiency. Along this research, butt-joints welded by FSW for an aluminium lithium alloy, AA2198, were tested and their mechanical properties measured. The joint efficiency for this alloy is near to 100% of the static strength, demonstrating that this process has low impact in the mechanical properties. However, it is required to ensure that the welds are defect free. Although this process is not prone to defects, root flaws can occur due to the lack of penetration of the tool, reducing substantially the joint integrity. Three non destructive techniques were analyzed to detect these defects and it was demonstrated that defects up to 200 μm are detectable with Acoustic Micro Imaging. Defects with lower dimensions might possibly be detectable, developing and adapting the existing techniques to these defects.

Most of emerging joining processes suitable for fuselage structures, as FSW, introduce a new type of joint due to the joint continuity creating an integral structure. These integral structures are one of the design solutions to optimize lightweight structures, reducing the number of parts, simplifying the joints, reducing weight and costs. However, their behavior under the airframe stresses needs to be addressed very exhaustively to prevent unexpected behaviors. In addition, the FSW process promotes residual stresses that can be beneficial or detrimental for the fatigue life, depending on the location of the crack. Therefore, new approaches are required to design these structures concerning their fatigue life and integrity. A methodology to model and design structures joined by FSW is proposed, considering the behavior of a crack perpendicular to the stiffeners, allowing to predict the fatigue life when a crack or a damage arise in the structure. With the proposed methodology accurate fatigue life modeling is possible, if accurate residual stress measurements and fatigue material properties are available.

A few new design concepts to apply FSW in aeronautical structures were studied along this research. A new configuration to produce T-joints was developed and tested with dissimilar aluminium alloys. This configuration allows to produce reinforced panels where the skin is composed of a higher toughness alloy and the reinforcements are composed of higher strength alloys. Tensile-strain tests from of these welded dissimilar material T-joints showed that it is possible to achieve good weld efficiencies comparable to the base material strength and the fatigue behavior proved to be rather similar, although a light reduction in fatigue strength was found. Other concept analyzed was the tailor welded blanks joined by FSW, showing that it is also feasible to produce these panels with dissimilar alloys or with dissimilar thicknesses. The analyzes performed included fatigue crack growth characterization, showing some retardation in the welded zone. A new welding concept was also developed for large welds since the overlap welds joined by FSW were shown to

have low mechanical properties due to the interface defects. This new concept involves a sliding backing bar that holds the pin tip and follows it along all the weld. This concept, compared to the standard tool, avoids completely the lack of penetration defects and does not require a backing bar along the complete weld. Other potential application of FSW is the repair of damaged structures with cracks that can be healed recovering the structural integrity without the replacement of the all part.

The aeronautical sector is highly focused in cost and weight reduction. The weight reduction reduces the fuel burnt during the aircraft life-cycle, reducing operational costs and environmental impact. If FSW is used to join fuselage parts with a butt joint configuration the overlap material and fasteners are saved reducing substantially the joint weight. In terms of manufacturing costs, the initial investment of FSW is equivalent to the automatic riveting, however FSW is cheaper along the time and with lower lead times allowing significant cost savings. Nevertheless, the infusion of FSW requires a development and certification process which require additional investments that should be considered in the development of new components.

This development of new components and structures should be the most comprehensive possible considering the different impacts when a new technology is adopted, reducing in this way the risk. Multi tools are currently available to support the development and quantify the different design options, which are fundamental in complex product development. In this research, a preliminary quality function deployment analysis was performed to compare different manufacturing processes suitable to produce reinforced panels and using the information that was gathered along this research and from conversations with experts. The adoption of this process in future aircraft families is almost certain if the aluminium alloys will be used. The advantage of FSW is clear from the cost and weight point of views, and provided the structural integrity is ensured, the replacement of the riveting by FSW will add value to the final product.

9.1 Recommendations Concerning the Application of FSW

FSW is a highly reliable welding process suitable for all aluminium alloys. As a joining process, it can improve the efficiency of aeronautical and aerospace primary and secondary structures replacing the riveted joints simplifying the joint and making it more Lean, since it does not require hole drilling, application of fasteners and sealants and many other manufacturing tasks.

The mechanical performance of FSW joints is good since welding defects are avoided. The static strength in most aluminium alloys is higher than 90% of the base material and the fatigue strength is similar to base material. However, a considerable reduction of the

maximum elongation takes place in the welding zone, decreasing the maximum energy absorbed by the structure. In projects where this parameter is important, post welding heat treatments should by applied in order to recover this property. The quality control of the joints is imperative in order to avoid defects which can compromise the structural integrity. Non destructive techniques are available to detect the most critical defects in these welds, lack of penetration, detecting sizes up to 200 μm. When this defect size is not tolerable, the welding root should be machined or new FSW tool concepts as the bobbin tool or the sliding backing bar developed during this research should be applied.

This joining process can be applied to produce reinforced panels, welding the stiffeners to the skin with dissimilar aluminium alloys and can be applied to join the different panels that composed the fuselage, longitudinally or circumferentially, during the assembly of the fuselage improving the assembly process, increasing the joining automation and reducing the lead times.

Since overlap areas are not required, fasteners and sealants are not used, weight savings are obtained with the application of FSW in a butt joint configuration. The initial investment for the application of FSW in production is high, although it is comparable to automated riveting equipment and this initial cost is amortized at an higher rate than the automated riveting.

The butt-joint configuration to join large structures can be the biggest challenge in the application of this process, due to the tolerances management, since the gap between the parts should be very tight in order to not originate tunnel defects.

Innovation through new manufacturing process in aeronautical and aerospace structures has an important role, contributing to increase their efficiency and the final value of the product.

9.2 Future Works

Several topics concerning the adoption of a welding process for aeronautical structures and the replacement of the riveted joints was analyzed along this research, nevertheless it is not intended to produce detailed guidelines or a technology report for the application the FSW since this will be highly dependent on the application. The replacement of processes in aeronautics is very complex, requiring in-depth analysis of the impact in the complete product life-cycle in terms of technology performance, costs and social and/or environmental impacts.

From the FSW process point of view, further research can be done in specific applications analyzing the influence and the impact in the new product or part development. Case

studies can be performed for new products or their components, or for current products where the joining process is replaced. The reliability of the process and certification issues should be addressed case by case.

Regarding to the FSW process, research in the tolerance management, techniques to join large structures and development of portable FSW equipments are topics which require further development. Non destructive techniques to detect all kinds of root flaws also require further research and for the existing techniques the characterization of the probability of detection curves is needed in order to have a deeper information about the defect detection in the welds.

New methodologies to analyze and optimize new product and process development, considering different dimensions and drivers, constitute an important subject since the increasing complexity of aircraft requires a more parallel concurrent and systematic development to reduce development times, to reduce the risk and improve the final solution.

As the development of complex products is composed by the development of different sub-products, components and parts, integration tools for a successful interaction, should take into account not only geometrical, supply chain and manufacturing cost aspects but also the integrated global performance, risk analysis and life-cycle impact.

Bibliography

[1] I. Bordesoules, J. Ehrstrom, T. Warner, P. Lequeu, and F. Eberl, "Trends in Developments of Aluminum Solutions for Aerospace Applications Solutions Applications," in *European Work-shop on Short Distance Welding Concepts for Airframes - WELAIR*, (Geesthacht (Hamburg), Germany), June 13 -15 2007.

[2] Boeing Comercial Airplanes, "Boeing Current Market Outlook 2010 to 2029," November 2010.

[3] J. Leahy, "Airbus' Global Market Forecast for 2010-2029," Airbus, Toulouse, France, December 13th 2010.

[4] R. Martinez-Val and E. Perez, "Aeronautics and Astronautics: Recent Progress and Future Trends," *Proceedings of the Institution of Mechanical Engineers, Part C: Journal of Mechanical Engineering Science*, vol. 223, no. 12, pp. 2767–2820, 2009.

[5] M. Lehmann, "Clean Sky Initiative," *Aerospace Testing International*, vol. Swocase 2010, pp. 36–38, 2010.

[6] J. Hupe, "CAEP/8 - Delivering Substantial Proposals to Help Minimize Aviation's Effects on the Environment," *International Civil Aviation Organization (ICAO) Journal*, vol. 65, no. 3, pp. 6–12, 2010.

[7] F. De Florio, *Airworthiness: An Introduction to Aircraft Certification: A Guide to Understanding JAA, EASA, and FAA Standards*. Butterworth-Heinemann, 2006.

[8] ICAO, "International Civil Aviation Organization - ICAO, The Convention on International Civil Aviation - Annexes 1 to 18," 2009.

[9] A. Auer, "JAA-EASA Transition," *Aviation Safety World*, vol. July, pp. 24–25, 2006.

[10] K. Dalamagkidis, K. P. Valavanis, and L. A. Piegl, "Current Manned Aviation Regulation," in *On Integrating Unmanned Aircraft Systems into the National Airspace System* (K. Dalamagkidis, K. P. Valavanis, and L. A. Piegl, eds.), vol. 36 of *Intelligent Systems, Control and Automation: Science and Engineering*, pp. 29–42, Springer Netherlands, 2009.

[11] H. von Bose, *EU Aeronautics Research in FP6*. European Commission, Directorate-General for Research, 2002.

[12] Boeing, "Statistical Summary of Commercial Jet Airplane Accidents: Worldwide Operations 1959-2009," *Seattle, WA, July*, 2010.

[13] G. Schänzer, "Developments in Flight Guidance and Control," in *25th International Council of the Aeronautical Sciences (ICAS 2006)*, (Hamburg, Germany), September, 3-8 2006.

[14] E. Murman, M. Walton, and E. Rebentisch, "Challenges in the Better, Faster, Cheaper Era of Aeronautical Design, Engineering and Manufacturing," *Aeronautical Journal*, vol. 104, no. 1040, pp. 481–489, 2000.

[15] European Aviation Safety Agency - EASA, "CS-34 Certification Specifications for Aircraft Engine Emissions and Fuel Venting," October 17 2003.

[16] European Aviation Safety Agency - EASA, "CS-36 Certification Specifications for Aircraft Noise - Amendment 1," 3 April 2007.

[17] J. Utterback, *Mastering the Dynamics of Innovation*. Harvard Business Press, 1996.

[18] M. Swink, J. Sandvig, and V. Mabert, "Customizing Concurrent Engineering Processes: Five Case Studies," *Journal of Product Innovation Management*, vol. 13, no. 3, pp. 229–244, 1996.

[19] B. Oppenheim, E. Murman, and D. Secor, "Lean Enablers for Systems Engineering," *Systems Engineering*, vol. n/a, 2009.

[20] A. Karp and G. Thomas, "Countering the CSeries," *Air Transport World*, vol. 47, no. 4, pp. 27–30, 2010.

[21] C. Christensen and M. Raynor, *The Innovator's Solution: Creating and Sustaining Successful Growth*. Harvard Business Press, 2003.

[22] S. Tsach, O. Rix, and R. Bublitsky, "Innovative Approach For Future Aircraft Development At IAI," in *26th International Council of the Aeronautical Sciences (ICAS 2008)*, (Anchorage, Alaska, USA), September, 14-19 2008.

[23] G. Schmidt and C. Druehl, "When Is a Disruptive Innovation Disruptive?," *Journal of Product Innovation Management*, vol. 25, no. 4, pp. 347–369, 2008.

[24] I. Kroo, "Innovations in Aeronautics," in *42nd AIAA Aerospace Sciences Meeting*, vol. 4, pp. 1–11, Citeseer, January 5-8 2004.

[25] J. Leahy, "Airbus Commercial Update," in *Global Investor Forum*, (Toulouse, France), November 15-16 2010.

[26] E. Rogers, *Diffusion of Innovations*. Free Press, fourth ed., 1995.

[27] R. Foster, *Innovation: The Attacker's Advantage*. Summit Books New York, 1986.

[28] J. Robinson, D. Levack, R. Rhodes, and T. Chen, "The Need for Technology Maturity of Any Advanced Capability to Achieve Better Life Cycle Cost (LCC)," in *45th AIAA/ASME/SAE/ASEE Joint Propulsion Conference*, (Denver, Colorado, USA), 2-5 August 2009. AIAA 2009-5347.

[29] S. Sadin, F. Povinelli, and R. Rosen, "The NASA Technology Push Towards Future Space Mission Systems," *Acta Astronautica*, vol. 20, pp. 73–77, 1989.

[30] J. Mankins, "Technology Readiness Levels: A White Paper," *Office of Space Access and Technology, Advanced Concepts Office - NASA*, 1995.

[31] European Space Agency - ESA, "Technology Readiness Levels Handbook for Space Applications." Reference: TEC-SHS/5551/MG/ap, September 2008.

[32] The United States Department of Defense - DoD, "Defense Acquisition Guidebook." Defense Acquisition University, December 2010.

[33] K. G. Bowcutt, "Hypersonic Technology Status and Development Roadmap," in *AIAA - Hypersonic Technologies and Aerospace Planes (HyTASP) Program Committee*, December 18 2003.

[34] The United States Department of Defense - DoD, "Manufacturing Readiness Level Deskbook." OSD Manufacturing Technology Program and The Joint Service/Industry MRL Working Group, July 30 2010.

[35] B. Sauser, D. Verma, J. Ramirez-Marquez, and R. Gove, "From TRL to SRL: The Concept of Systems Readiness Levels," in *Conference on Systems Engineering Research, Los Angeles, CA*, April 7-8 2006.

[36] B. Sauser, R. Gove, E. Forbes, and J. Ramirez-Marquez, "Integration Maturity Metrics: Development of an Integration Readiness Level," *Information, Knowledge, Systems Management*, vol. 9, no. 1, pp. 17–46, 2010.

[37] B. Sauser, J. Ramirez-Marquez, D. Verma, and R. Gove, "Determining System Interoperability using an Integration Readiness Level," in *9th Annual Systems Engineering Conference "Focusing on Improving Performance of Defense Systems Programs", San Diego, CA*, National Defense Industrial Association, October 23-26 2006.

[38] W. Tan, J. Ramirez-Marquez, and B. Sauser, "A Probabilistic Approach to System Maturity Assessment," *Systems Engineering*, vol. n/a., pp. 1–15, 2010.

[39] J. Bilbro, "A Suite of Tools for Technology Assessment," in *AFRL Technology Maturity Conference, Virginia Beach, VA*, The United States Department of Defense, September 11-13 2007.

[40] D. Mavris, M. Kirby, and S. Qiu, "Technology Impact Forecasting for a High Speed Civil Transport," in *1998 World Aviation Conference, Anaheim, CA*, American Institute of Aeronautics and Astronautics (AIAA), September 28-30 1998. SAE Paper 985547.

[41] D. Mavris and M. Kirby, "Technology Identification, Evaluation, and Selection for Commercial Transport Aircraft," in *58th Annual Conference of Society of Allied Weight Engineers, San Jose, CA*, Society of Allied Weight Engineers, May 24-26 1999.

[42] M. Kirby and D. Mavris, "Forecasting Technology Uncertainty in Preliminary Aircraft Design," in *4th World Aviation Congress and Exposition, San Francisco, CA*, AIAA, October 19-21 1999.

[43] R. Smaling and O. de Weck, "Assessing Risks and Opportunities of Technology Infusion in System Design," *Systems Engineering*, vol. 10, no. 1, pp. 1–25, 2007.

[44] R. Shishko, D. Ebbeler, and G. Fox, "NASA Technology Assessment Using Real Options Valuation," *Systems Engineering*, vol. 7, no. 1, pp. 1–13, 2004.

[45] S. Dibb and L. Simkin, *The Marketing Casebook: Cases and Concepts*. Thomson Learning, 2nd ed., 2001.

[46] P. Kotler and G. Armstrong, *Princípios de Marketing.* Prentice-Hall do Brasil, 5th ed., 1993.

[47] K. Ulrich, S. Eppinger, *et al.*, *Product Design and Development.* McGraw-Hill International Edition, 8th ed., 2008.

[48] I. Kroo, "The Aircraft Design Process, Course Notes: Aircraft Design: Synthesis and Analysis." Stanford University's Department of Aeronautics and Astronautics, Course AA 241, `http://adg.stanford.edu/aa241/design/designprocess.html`, September 2006.

[49] F. Kafyeke, M. Abdo, F. Pépin, P. Piperni, and E. Laurendeau, "Challenges of Aircraft Design Integration." NATO - Research and Technology Organisation - Reduction of Military Vehicle Acquisition Time and Cost through Advanced Modelling and Virtual Simulation Project (RTO-MP-089), March 2003.

[50] T. Pardessus, "Concurrent Engineering Development and Practices for Aircraft Design at Airbus," in *Proceedings of the 24th International Congress of the Aeronautical Sciences (ICAS) Conference*, (Yokohama, Japan), August 29 - September 3 2004.

[51] Federal Aviation Administration - FAA, "Advisory Circular AC 25.1529-1: DInstructions for Continued Airworthiness of Structural Repairs on Transport Airplanes." United States Department of Transportation, September 1 1991.

[52] M. M. Ratwani, "Repair Types, Procedures - Part I." NATO - Research and Technology Organisation - Battle Damage Repair Techniques and Procedures on Air Vehicles - Lessons Learned and Prospects (RTO-EN-AVT-156), May 2010.

[53] M. T. A. Greenwell, "Design of Repair of Battle-Damaged Fixed-Wing Aircraft." NATO - Research and Technology Organisation - Battle Damage Repair Techniques and Procedures on Air Vehicles - Lessons Learned and Prospects (RTO-EN-AVT-156), May 2010.

[54] Federal Aviation Administration - FAA, "Advisory Circular AC 23-13A: Fatigue, Fail-Safe, and Damage Tolerance Evaluation of Metallic Structure For Part 23 Airplanes." United States Department of Transportation, 2005.

[55] Federal Aviation Administration - FAA, "Advisory Circular AC 25.571-1c: Damage Tolerance and Fatigue Evaluation of Structure." United States Department of Transportation, April 9 1998.

[56] T. Swift, "Fail-Safe Design Requirements and Features, Regulatory Requirements," in *2003 AIAA/ICAS International Air and Space Symposium and Exposition: The Next 100 Years*, (Dayton, Ohio, USA), July 14-17 2003.

[57] T. Swift, "Damage Tolerance in Pressurized Fuselages: 11th Plantema Memorial Lecture," in *14th Symposium of the International Committee on Aeronautical Fatigue (ICAF)*, (Ottawa, Canada), 1987.

[58] Federal Aviation Administration - FAA, "Damage Tolerance Assessment Handbook, Volume I: Introduction, Fracture Mechanics, Fatigue Crack Propagation." FAA Technical Report: DOT/FAA/CT-93/69. I, DOT-VNTSC-FAA-93-13. I, October 1993.

[59] Federal Aviation Administration - FAA, "Damage Tolerance Assessment Handbook, Volume II: Airframe Damage Tolerance Evaluation." FAA Technical Report: DOT/FAA/CT-93/69. II, DOT-VNTSC-FAA-93-13. II, October 1993.

[60] D. Gorinevsky, G. Gordon, S. Beard, A. Kumar, and F. Chang, "Design of Integrated SHM System for Commercial Aircraft Applications," in *Proceedings 5th International Workshop on Structural Health Monitor*, (Stanford, CA, USA), September 12-14 2005.

[61] H. Speckmann, "SHM: History and Future," in *International Workshop on Structural Heath Monitoring 2007*, (Stanford, CA, USA), September 11-13 2007.

[62] P. Katz, "Stresses and Strains on Aircraft," *Aviation Monthly*, September 1997.

[63] T. Megson, *Aircraft Structures for Engineering Students*. Butterworth Heinemann, 3rd ed., 1999.

[64] E. Starke *et al.*, "Application of Modern Aluminum Alloys to Aircraft," *Progress in Aerospace Sciences*, vol. 32, no. 2-3, pp. 131–172, 1996.

[65] Airbus, "Taking the Lead: the A350 XWB Xtra Wide Body (Airbus A350 XWB Presentation)," 2006.

[66] G. Tober and D. Schiller, "NDT in Aerospace - State of Art," in *15th World Conference on Nondestructive Testing*, October 15-21 2000.

[67] R. Wanhill, "Milestone Case Histories in Aircraft Structural Integrity," in *Comprehensive Structural Integrity* (I. Milne, R. O. Ritchie, and B. Karihaloo, eds.), pp. 61–72, Oxford: Pergamon, 2003.

[68] H. Rösner and K. Jockel-Miranda, "Airbus Airframe - New Technologies and Management Aspects," *Materialwissenschaft und Werkstofftechnik*, vol. 37, no. 9, pp. 768–772, 2006.

[69] B. Vermeulen and M. van Tooren, "Design Case Study for a Comparative Performance Analysis of Aerospace Materials," *Materials & Design*, vol. 27, no. 1, pp. 10–20, 2006.

[70] J. T. Staley and W. H. Hunt Jr, "Needs of the Aircraft Industry for Aluminum Products," in *12th Annual NCMS Technical Conference*, (Orlando, FL, USA), pp. 4–6, May 4-6 1998.

[71] F. Bickley and R. J. Schwinghamer, "NASA Experience with the Shuttle External Tank." National Manufacturing Week, NASA Marshall Space Flight Center, March 17 1999.

[72] B. Béral, "Airbus Composites Technologies & Structures," in *Colloque Composite - Toulouse*, (Toulouse, France), October 3, 2007.

[73] Z. Ahmad, "The Properties and Application of Scandium-Reinforced Aluminum," *JOM Journal of the Minerals, Metals and Materials Society*, vol. 55, no. 2, pp. 35–39, 2003.

[74] J. Lee and P. Chen, "Aluminum-Scandium Alloys: Material Characterization, Friction Stir Welding, and Compatibility With Hydrogen Peroxide," December 2004.

[75] J. Røyset and N. Ryum, "Scandium in Aluminium Alloys," *International Materials Reviews*, vol. 50, no. 1, pp. 19–44, 2005.

[76] J. Williams and E. Starke, "Progress in Structural Materials for Aerospace Systems," *Acta Materialia*, vol. 51, no. 19, pp. 5775–5799, 2003.

[77] J. Lin, R. Sawtell, G. Bray, C. Giummarra, A. Wilson, and G. Venema, "Aluminum-Copper Alloys Containing Vanadium." United States Patent and Trademark Office: Patent Application US 2010/0183474 A1, July 22 2010.

[78] M. S. Bhagyashekar and R. Rao, "Characterization of Mechanical Behavior of Metallic and Non-metallic Particulate Filled Epoxy Matrix Composites," *Journal of Reinforced Plastics and Composites*, vol. 29, no. 1, pp. 30–42, 2010.

[79] C. Soutis, "Carbon Fiber Reinforced Plastics in Aircraft Construction," *Materials Science and Engineering: A*, vol. 412, no. 1-2, pp. 171–176, 2005.

[80] B. Griffiths, "Boeing Sets Pace for Composite Usage in Large Civil Aircraft," *High Performance Composites*, pp. 68–71, 2005.

[81] H. Baldwin, "Boeing 787 Dreamliner: Unmatched Economics, Performance and Passenger Appeal," *Aviation Week & Space Technology Market Supplement*, pp. S1–S30, March 14 2005.

[82] Boeing, "Design Approaches: A Milestone for Composites in Aviation," *Journal of Failure Analysis and Prevention*, vol. 5, pp. 5–7, August 2005.

[83] A. Vlot, *Glare: History of the Development of a New Aircraft Material*. Springer Netherlands, 2001.

[84] J. Schijve, L. Vogelesang, and R. Marissen, "Laminate of Metal Sheet Material and Threads Bonded Thereto, as Well as Processes for the Manufacture Thereof." United States Patent and Trademark Office: US 4,489,123, December 18 1984.

[85] A. Vlot, L. B. Vogelesang, and T. J. De Vries, "Towards Application of Fibre Metal Laminates in Large Aircraft," *Aircraft Engineering and Aerospace Technology*, vol. 71, no. 6, pp. 558–570, 1999.

[86] L. Vogelesang and G. Roebroeks, "Metal-Resin Laminate Reinforced with S2-Glass Fibres." United States Patent and Trademark Office: US 5,039,571, August 13 1992.

[87] A. Vlot and R. C. Alderliesten, "Fiber Metal Laminates, Fatigue of," in *Encyclopedia of Materials: Science and Technology* (K. H. J. Buschow, R. W. Cahn, M. C. Flemings, B. Ilschner, E. J. Kramer, S. Mahajan, and P. Veyssière, eds.), pp. 3134–3237, Oxford: Elsevier, 2001.

[88] R. Alderliesten and J. Homan, "Fatigue and Damage Tolerance Issues of Glare in Aircraft Structures," *International Journal of Fatigue*, vol. 28, no. 10, pp. 1116–1123, 2006.

[89] G. Norris, M. Kingsley-Jones, D. Learmount, and M. Phelan, "Europe's Giant: A Special A380 Supplement," *Flight International Supplement*, vol. 20-26, pp. I–XVI, 2003.

[90] J. Patterson, "New Large Aircraft Composite Fire Fighting ." Federal Aviation Administration (FAA), Airport Technology Research And Development Branch, May 18 2009.

[91] A. Pun, "How to Predict Fatigue Life: Three Methods of Calculating Total Life, Crack Initiation, and Crack Growth ," *Design News*, vol. December, 2001.

[92] R. Alderliesten and R. Benedictus, "Fiber/Metal Composite Technology for Future Primary Aircraft Structures," *Journal of Aircraft*, vol. 45, no. 4, pp. 1182–1189, 2008.

[93] T. Lin and Y. Ito, "Fatigue Crack Nucleation in Metals," *Proceedings of the National Academy of Sciences of the United States of America*, vol. 62, no. 3, p. 631, 1969.

[94] United States Deptartment of Defense, *MIL-HDBK-5H: Military Standardization Handbook: Metallic Materials and Elements for Aerospace Vehicle Structures*. Knovel Interactive Editior, 2003.

[95] S. Sihn and S. Tsai, "Prediction of Fatigue SN curves of Composite Laminates by Super Mic-Mac," *Composites Part A: Applied Science and Manufacturing*, vol. 36, no. 10, pp. 1381–1388, 2005.

[96] J. Homan, "Fatigue Initiation in Fibre Metal Laminates," *International Journal of Fatigue*, vol. 28, no. 4, pp. 366–374, 2006.

[97] NASGRO, "Fracture Mechanics and Fatigue Crack Growth Analysis Software - Reference Manual, Version 4.02." Southwest Research Institute (SwRI), September 2002.

[98] A. Turon, J. Costa, P. Camanho, and C. Dávila, "Simulation of Delamination in Composites Under High-Cycle Fatigue," *Composites Part A: Applied Science and Manufacturing*, vol. 38, no. 11, pp. 2270–2282, 2007.

[99] D. Shim, R. Alderliesten, S. Spearing, and D. Burianek, "Fatigue Crack Growth Prediction in GLARE Hybrid Laminates," *Composites Science and Technology*, vol. 63, no. 12, pp. 1759–1767, 2003.

[100] K. Y. Lin, A. Styuart, and C. H. E. Cheung, "Development of Reliability-Based Damage Tolerant Structural Design Methodology," in *Advanced Materials in Transport Aircraft Structures (AMTAS), Spring 2007 Meeting*, April 12 2007.

[101] J. Ostrower, "Boeing 787-8 Weight Examined." Flight Blogger (Flightglobal Blogs), May 6 2009.

[102] J. Ostrower, "Boeing plans 787-9 horizontal stabiliser design change, explains -8 issues." Flight International, July 12 2010.

[103] D. N. Yates, "An Examination of Potential FST Hazards Regarding the Usage of CF/Epoxies for Fuselages in the New Generation Commercial Aircraft Such as the Boeing 787 and the Airbus 350," *Society for the Advancement of Material and Process Engineering Journal*, 2010 (to be submitted).

[104] C. Giummarra, B. Thomas, and R. Rioja, "New Aluminum Lithium Alloys for Aerospace Applications," in *Proceedings of the Light Metals Technology Conference*,

(Saint-Sauveur, Canada), September 24-26 2007.

[105] A. Noor, S. Venneri, D. Paul, and M. Hopkins, "Structures Technology for Future Aerospace Systems," *Computers & Structures*, vol. 74, no. 5, pp. 507–519, 2000.

[106] K.-H. Grote and E. Antonsson, eds., *Springer Handbook of Mechanical Engineering*, ch. Section 7.4 Assembly, Disassembly, Joining Techniques, pp. 656–732. Springer, 2009.

[107] E. Biel, J. Landy, G. Humrichouser, and B. Ervin, *Aviation Structural Mechanic (H & S) 3 & 2*. Naval Education and Training Professional Development and Technology Center, NAVEDTRA 14018, 1993.

[108] B. Rooks, "Automatic Wing Box Assembly Developments," *Industrial Robot: An International Journal*, vol. 28, no. 4, pp. 297–302, 2001.

[109] R. Holden, P. Haworth, I. Kendrick, and A. Smith, "Automated riveting cell for A320 wing panels with improved throughput and reliability (SA2)," in *AeroTech Congress & Exhibition*, (Los Angeles, CA, USA), SAE International, September 2007.

[110] P. Ponticel and C. Buchhei, "New Rivet Injector Design Used by Electroimpact for Airbus Wing Work," *SAE Aerospace Engineering & Manufacturing: Technology Update*, pp. 6–7, May 2008.

[111] N. de Bruyne, "Joint Design for Primary Structures," *Journal of Applied Polymer Science*, vol. 6, no. 20, pp. 122–129, 1962.

[112] A. Higgins, "Adhesive Bonding of Aircraft Structures," *International Journal of Adhesion and Adhesives*, vol. 20, no. 5, pp. 367–376, 2000.

[113] J. Schijve, *Fatigue of Structures and Materials*. Springer Netherlands, 2nd ed., 2001.

[114] E. Petrie, "Adhesives for the Assembly of Aircraft Structures and Components: Decades of Performance Improvement, With the New Applications of the Horizon," *Metal Finishing*, vol. 106, no. 2, pp. 26–31, 2008.

[115] A. Petrova and N. Lukina, "Adhesive Technologies in Aircraft Construction," *Polymer Science Series D*, vol. 1, no. 2, pp. 83–90, 2008.

[116] I. Ashcroft, D. Hughes, and S. Shaw, "Adhesive Bonding of Fibre Reinforced Polymer Composite Materials," *Assembly Automation*, vol. 20, no. 2, pp. 150–161, 2000.

[117] R. Messler, *Joining of Materials and Structures: From Pragmatic Process to Enabling Technology*. Elsevier Butterworth-Heinemann, 2004.

[118] Boeing, "Boeing To Deliver Major Section For First F-22 Fighter." `http://www.boeing.com/news/releases/1996/news.release.961015.html`, Seatle, WA, USA, October 15 1996.

[119] P. Mendez and T. Eagar, "Welding Processes for Aeronautics," *Advanced Materials and Processes*, vol. 159, no. 5, pp. 39–43, 2001.

[120] P. Mendez and T. Eagar, "New Trends in Welding in the Aeronautic Industry," in *2nd Conference "New Manufacturing Trends for Aeronautical Industries"*, (Bilbao,

Spain), HEGAN and INASMET, November 19-20 2002.

[121] R. Oldfield, "The Power to Perform, GKN Aerospace: Metallic Technology Briefing," in *Farnborough International Airshow 2010*, (Farnborough, UK), July 19-25 2010.

[122] K.-H. Rendigs and M. Knüwer, "Metal Materials in Airbus A380," in *2nd Izmir Global Aerospace and Offset Conference*, (Gaziemir-Izmir, Turkey), October 7-8 2010.

[123] W. Thomas, E. Nicholas, J. Needham, M. Murch, P. Temple-Smith, and C. Dawes, "Improvements Relating to Friction Welding." World Intellectual Property Organization Patent WO/1993/010,935 (Application: PCT/GB92/002203), June 10 1993.

[124] R. Nandan, T. DebRoy, and H. Bhadeshia, "Recent Advances in Friction-Stir Welding - Process, Weldment Structure and Properties," *Progress in Materials Science*, vol. 53, no. 6, pp. 980–1023, 2008.

[125] R. Mishra and M. Mahoney, *Friction Stir Welding and Processing*. ASM International, 2007.

[126] D. Lohwasser and Z. Chen, *Friction Stir Welding: From Basics to Applications*. Woodhead Publishing in Materials, CRC Press, 2010.

[127] TWI - The Welding Institute, "Known Friction Stir Welding Patents and Patent Applications." `http://www.twi.co.uk/content/fswpatents.html`, February 2011.

[128] C. Campbell, M. Fullen, and M. Skinner, "Welding Head." United States Patent and Trademark Office: US 6,199,745, March 13 2001.

[129] A. von Strombeck and J. Santos, "Device for Joining Workpieces by Friction Stir Welding." United States Patent and Trademark Office: US 6,799,708, October 5 2004.

[130] A. C. Nunes Jr., "Counterrotating-Shoulder Mechanism for Friction Stir Welding," *Marshall Space Flight Center, Alabama, NASA Tech Briefs*, pp. 21–22, April 2007.

[131] R. Carter and K. Lawless, "Gimballed Shoulders for Friction Stir Welding," *Marshall Space Flight Center, Alabama, NASA Tech Briefs*, pp. 27–28, January 2008.

[132] D. Burford and C. Widener, "Evaluation of Friction Stir Welding Process and Properties for Aerospace Application: Standards and Specifications Development," in *Federal Aviation Administration (FAA): Joint Advanced Materials and Structures (JAMS) CoE Technical Review Meeting*, Wichita State University, Wichita, KS (USA), July 21-22 2009.

[133] R. Mishra and Z. Ma, "Friction Stir Welding and Processing," *Materials Science and Engineering: R: Reports*, vol. 50, no. 1-2, pp. 1–78, 2005.

[134] T. Khaled, "An Outsider Looks at Friction Stir Welding." Federal Aviation Administration (FAA) Report: ANM-112N-05-06, 2005.

[135] R. Johnson and P. Threadgill, "Friction Stir Welding of Magnesium Alloys," *Materials Science Forum (Magnesium Alloys 2003)*, vol. 419, pp. 365–370, 2003.

[136] R. Zettler, A. da Silva, S. Rodrigues, A. Blanco, and J. dos Santos, "Dissimilar Al

to Mg Alloy Friction Stir Welds," *Advanced Engineering Materials*, vol. 8, no. 5, pp. 415–421, 2006.

[137] J. Defalco and S. R. Steel, "Friction Stir Process Now Welds Steel Pipe," *Welding Journal*, vol. 88, pp. 44–48, May 2009.

[138] T. Lienert, "Microstructure and Mechanical Properties of Friction Stir Welded Titanium Alloys," in *Friction Stir Welding and Processing* (R. Mishra and M. Mahoney, eds.), ASM, 2007.

[139] C. Rowe, J. Tuck, D. Staines, and W. Thomas, "Refractory Metal Tool for Friction Stir Welding Comprising a Shoulder Made of Tungsten, Molybdenum, Tantalum, Niobium Or Hafnium Alloy and a Coated or Treated Surface." World Intellectual Property Organization Patent WO/2008/102209, August 28 2008.

[140] C. Sorensen and T. W. Nelson, "Friction Stir Welding of Ferrous and Nickel Alloys," in *Friction Stir Welding and Processing* (R. Mishra and M. Mahoney, eds.), ASM International, 2007.

[141] F. Ye, H. Fujii, T. Tsumura, and K. Nakata, "Friction Stir Welding of Inconel Alloy 600," *Journal of Materials Science*, vol. 41, no. 16, pp. 5376–5379, 2006.

[142] B. Christner, "Enabling Technology for an Aircraft Alternative," *Mechanical Engineering Magazine (ASME)*, vol. 123, p. D14, March 2003.

[143] P. Condit, "Boeing Chairman Views 1999 as a Year Full of Outstanding Achievements and Significant Growth," in *Boeing News Releases*, (Seattle, WA, USA), December 20 1999.

[144] W. Polt, "A Little Friction at Boeing," *Boeing Frontiers*, vol. 3, September 2004.

[145] D. Bolse, "No Melt Miracle: Welding Industry Turns High-Tech," *ISO Focus*, pp. 21–22, November 2010.

[146] B. Bhat, R. Carter, R. Ding, K. Lawless, A. Nunes, C. Russell, and S. Shah, "Friction Stir Welding Development at NASA-Marshall Space Flight Center," in *TMS Special Publication on Friction Stir Welding,* `http://hdl.handle.net/2060/20020015869`, (Warrendale, PA, USA), 2001.

[147] S. Martel, "NASA Managers Meet to Set STS-130 Launch Date," *Marshall Star, Marshall Space Flight Center, NASA*, vol. 50, pp. 1, 5, January 28 2010.

[148] National Aeronautics and Space Administration - NASA, "Orion - America's Next Generation Spacecraft." NASA Publication NP-2010-10-025-JSC, 2010.

[149] D. Davis and J. McArthur, "NASA Ares I Crew Launch Vehicle Upper Stage Overview," in *44th AIAA/ASME/SAE/ASEE Joint Propulsion Conference & Exhibit*, (Connecticut, CT, USA), American Institute of Aeronautics and Astronautics - AIAA, July 21 - 23 2008.

[150] T. Heston, "Rocket Science, Entrepreneur-Style: SpaceX Takes a Fresh Approach to Rocket Fabrication," *The Fabricator,* `http://www.thefabricator.com/article/fabstories/rocket-science-entrepreneur-style`, November 11 2008.

[151] Cost Effective Integral Metallic Structure - COINS, "European Union, 6th Framework Programme: FP6-2005-Aero-1; Contract Number: AST5-CT-2006-03082," 2006.

[152] ASM International Handbook Committee, *ASM Handbook, Volume 02 - Properties and Selection: Nonferrous Alloys and Special-Purpose Materials*. ASM International, 1990.

[153] The Aluminum Association, "International Alloy Designations and Chemical Composition Limits for Wrought Aluminum and Wrought Aluminum Alloys," Revised in February 2009.

[154] R. Curtis, G. Narayanan, and W. Quist, "Low Temperature Underaging Process for Lithium Bearing Alloys." United States Patent and Trademark Office: US 4,840,682, June 20 1989.

[155] T. Warner, "Recently-Developed Aluminium Solutions for Aerospace Applications," *Materials Science Forum*, vol. 519-521, pp. 1271–1278, 2006.

[156] W. Johnston, W. Pollock, and D. Dawicke, "Biaxial Testing of 2195 Aluminum Lithium Alloy Using Cruciform Specimens." Analytical Services & Materials, Inc. and Langley Research Center - NASA, Technical Report: NASA/CR-2002-211942, October 2002.

[157] R. Leal and A. Loureiro, "Defects Formation in Friction Stir Welding of Aluminium Alloys," *Materials Science Forum*, vol. 455, pp. 299–302, 2004.

[158] H. Chen, K. Yan, T. Lin, S. Chen, C. Jiang, and Y. Zhao, "The Investigation of Typical Welding Defects for 5456 Aluminum Alloy Friction Stir Welds," *Materials Science and Engineering: A*, vol. 433, no. 1-2, pp. 64–69, 2006.

[159] Y. Kim, H. Fujii, T. Tsumura, T. Komazaki, and K. Nakata, "Three Defect Types in Friction Stir Welding of Aluminum Die Casting Alloy," *Materials Science and Engineering: A*, vol. 415, no. 1-2, pp. 250–254, 2006.

[160] C. Zhou, X. Yang, and G. Luan, "Effect of Root Flaws on the Fatigue Property of Friction Stir Welds in 2024-T3 Aluminum Alloys," *Materials Science and Engineering: A*, vol. 418, no. 1-2, pp. 155–160, 2006.

[161] C. Hellier, *Handbook of Nondestructive Evaluation*. McGraw-Hill Professional, 2001.

[162] D. E. Bray and R. K. Stanley, *Nondestructive Evaluation: A Tool in Design, Manufacturing, and Service*. Boca Raton: CRC Press, rev. ed., 1997.

[163] T. Santos, *Ensaios Não Destrutivos por Correntes Induzidas: Desenvolvimento e Aplicação à Soldadura por Fricção Linear*. PhD thesis, Universidade Técnica de Lisboa - Instituto Superior Técnico, Lisbon, Portugal, July 2009.

[164] H. Trétout, "Review of Advanced Ultrasonic Techniques for Aerospace Structures," in *7th European Conference on Non-destructive Testing - ECNDT '98*, (Copenhagen, Denmark), May 26-29 1998.

[165] ASM International Handbook Committee, *ASM Handbook, Volume 17 - Nondestructive Evaluation and Quality Control*. ASM International, 1989.

[166] N. Goldfine, T. Lovett, Y. Sheiretov, D. Grundy, T. Dunford, and V. Zilberstein, "Noncontact Torque Sensing for Performance Monitoring and Fault Detection," in *ASME 2009 Power Conference (POWER2009)*, (Albuquerque, NM, USA), ASME, July 21-23 2009.

[167] N. Goldfine, V. Zilberstein, D. Schlicker, D. Grundy, I. Shay, and A. Washabaugh, "High Resolution Inductive Sensor Arrays for Material and Defect Characterization of Welds." United States Patent and Trademark Office: US 6,995,557 B2, February 7 2006. US Patent App. 10/046,925.

[168] N. Goldfine, D. Grundy, V. Zilberstein, and D. Kinchen, "Friction Stir Weld Inspection Through Conductivity Imaging Using Shaped Field MWM (TM)-Arrays," in *Proceedings of the 6th International ASM Trends in Welding Research Conference*, (Pine Mountain, GA, USA), ASM International, April 15-19 2002.

[169] M. Grundy, V. Zilberstein, N. Goldfine, M. Green, and I. Stol, "MWM®-Array Inspection for Quality Control of Friction Stir Welded Extrusion," in *Proceedings of the ASM 7th International Conference on Trends in Welding Research Conference*, (Pine Mountain, GA, USA), ASM International, May 16-20 2005.

[170] USAF - United States Air Force, "Nondestructive Inspection Methods, Basic Theory." Technical Manual: T.O. 33B-1-1; NAVAIR 01-1A-16-1; TM 1-1500-335-23, September 15 2010.

[171] N. Goldfine, V. Zilberstein, J. Fisher, D. Grundy, D. Schlicker, V. Tsukernik, R. Lyons, I. Shay, and A. Washabaugh, "Applied and Residual Stress Measurements using Magnetic Field Sensors." United States Patent and Trademark Office: US 7,526,964 B2, May 5 2009.

[172] I. Sinka, S. Burch, J. Tweed, and J. Cunningham, "Measurement of Density Variations in Tablets using X-ray Computed Tomography," *International Journal of Pharmaceutics*, vol. 271, no. 1-2, pp. 215–224, 2004.

[173] DaToN - Innovative Fatigue and Damage Tolerance Methods for the Application of New Structural Concepts, "Annex I, - "Description of Work", Proposal/Contract no.: FP6-516053.2005." European Union, Sixth Framework Programme, 2005.

[174] M. Koçak, B. Petrovski, V. Uz, F. Palm, R. Kocik, and F. Syassenn, "Damage Tolerance Analysis of Laser Welded Short Distance Clip Welds using 4-Stringer Flat Panels," in *European Workshop on Short Distance Welding Concepts for Airframes, WEL-AIR*, (Geethacht (Hamburg), Germany), GKSS Research Center, June 13-15 2007.

[175] J. Munroe, K. Wilkins, and M. Gruber, "Integral Airframe Structures (IAS) - Validated Feasibility Study of Integrally Stiffened Metallic Fuselage Panels for Reducing Manufacturing Costs." Technical Report: NASA/CR-2000-209337, Prepared by Boeing for Langley Research Center under Contracts NAS1-20014 and NAS1-20267, May 2000.

[176] R. Pettit, J. Wang, and C. Toh, "Validated Feasibility Study of Integrally Stiffened Metallic Fuselage Panels for Reducing Manufacturing Costs." Technical Report: NASA/CR-2000-209342, Prepared by Boeing for Langley Research Center under

Contracts NAS1-20014, Task 34, May 2000.

[177] S. Häusler, P. Baiz, S. Tavares, A. Brot, P. Horst, M. Aliabadi, P. de Castro, and Y. Peleg-Wolfin, "Crack growth simulation in integrally stiffened structures including residual stress effects from manufacturing. part i: Model overview," *Structural Durability & Health Monitoring*, Submitted for Publication (2011).

[178] Femap, "UGS Femap: Finite Element Modeling and Postprocessing - Version 9.2." UGS Corporation, Exton, PA, 2006.

[179] ABAQUS, "ABAQUS v.6.8-1, User Documentation." Dassault Systems, 2008.

[180] A. Lanciotti, L. Lazzeri, and C. Polese, "DaToN Project - University of Pisa contributions to WP2 and WP3." Department of Aerospace Engineering, Pisa University, Presentation in Munich DaToN meeting, January 11 2007.

[181] MATLAB, "The MathWorks - MATLAB 2008b." Product Documentation, April 2008.

[182] S. Smith and I. Raju, "Evaluation of Stress-Intensity Factors Using General Finite-Element Models," in *Fatigue and Fracture Mechanics: Twenty-Ninth Volume*, ASM International, 1999.

[183] E. Rybicki and M. Kanninen, "A Finite Element Calculation of Stress Intensity Factors by a Modified Crack Closure Integral," *Engineering Fracture Mechanics*, vol. 9, no. 4, pp. 931–938, 1977.

[184] R. Krueger, "Virtual Crack Closure Technique: History, Approach, and Applications," *Applied Mechanics Reviews*, vol. 57, no. 2, pp. 109–143, 2004.

[185] R. Krueger, "The Virtual Crack Closure Technique: History, Approach and Applications." Technical Report: NASA/CR-2002-211628 and ICASE Report 2002-10, ICASE, Hampton, Virginia, USA, 2002.

[186] P. Paris and F. Erdogan, "A Critical Analysis of Crack Propagation Laws," *Journal of Basic Engineering*, vol. 85, no. 4, pp. 528–534, 1963.

[187] R. Forman, V. Kearney, and R. Engle, "Numerical Analysis of Crack Propagation in Cyclic-Loaded Structures," *Journal of Basic Engineering*, vol. 89, no. 3, pp. 459–464, 1967.

[188] K. Walker, "The Effect of Stress Ratio During Crack Propagation and Fatigue for 2024-T3 and 7075-T6 Aluminum," in *Effects of Environment and Complex Load History on Fatigue Life, ASTM STP 462*, pp. 1–14, American Society for Testing and Materials, 1970.

[189] D. Broek, *The Practical Use of Fracture Mechanics*. Kluwer Academic Publishers, 1988.

[190] P. Moreira, V. Richter-Trummer, S. Tavares, F. de Oliveira, and P. de Castro, "Characterization of Fatigue Crack Growth Rate of AA6056 T651 and T6: Application to DaToN Panels Life Prediction." Technical Report DaToN-WD5-WP2-WP3-1.0/IDMEC, December 21 2007.

[191] P. Moreira, V. Richter-Trummer, M. de Figueiredo, F. de Oliveira, and P. de Castro, "Stiffened Cracked Panel, DaToN Specimen: Fatigue Life and Experimental Measurements." Technical Report DaToN-WD7-WP3-1.0/IDMEC, July 2008.

[192] V. Ocenásek, M. Slámová, J. dos Santos, and P. Vilaça, "Microstructure and Properties of Friction Stir Welding Aluminium Alloys," in *METAL 2005, 14th International Metallurgical & Material Conference, Symposium E*, (Hradec nad Moravici, Czech Republic), May 24-26 2005.

[193] K. Erbslöh, C. Dalle Donne, and D. Lohwasser, "Friction Stir Welding of T-Joints," *THERMEC'2003, Materials Science Forum*, vol. 426-432, pp. 2965–2970, 2003.

[194] L. Fratini, G. Buffa, L. Filice, and F. Gagliardi, "Friction Stir Welding of AA6082-T6 T-Joints: Process Engineering and Performance Measurement," *Proceedings of the Institution of Mechanical Engineers, Part B: Journal of Engineering Manufacture*, vol. 220, no. 5, pp. 669–676, 2006.

[195] R. Steel, T. Nelson, C. Sorensen, and S. Packer, "Friction Stir Welding of Steel T-Joint Configurations," in *ISOPE-2005: 15th International Offshore and Offshore and Polar Engineering Conference*, (Seoul, Korea), June 19-24 2005.

[196] S. Tavares, P. Moreira, P. de Castro, and F. de Oliveira, "Soldadura por Fricção Linear de Chapas em Ligações de Juntas em T." Instituto Nacional de Propriedade Industrial, Portuguese Patent Number 103867 B, November 30 2009.

[197] S. Tavares, R. Castro, V. Richter-Trummer, P. Vilaca, P. Moreira, and P. de Castro, "Friction Stir Welding of T-joints with Dissimilar Aluminium Alloys: Mechanical Joint Characterisation," *Science and Technology of Welding & Joining*, vol. 15, no. 4, pp. 312–318, 2010.

[198] S. Tavares, P. Moreira, and P. de Castro, "Friction Stir Welding of T-joints Fabricated with Three Parts," in *DFE2008 Design, Fabrication and Economy*, (Miskolc, Hungary), pp. 519–526, April 24-26 2008.

[199] S. Tavares, P. Azevedo, B. Emílio, V. Richter-Trummer, M. Figueiredo, P. Vilaça, and P. de Castro, "Friction Stir Welding of T-Joints in Dissimilar Aluminium Alloys," in *2008 ASME International Mechanical Engineering Congress and Exposition*, (Boston, MA, USA), Nov. 2-6 2008.

[200] MatWeb, "Material Property Database, `www.matweb.com`." Automation Creations, Retrieved in 2008.

[201] ASTM International Standards, "ASTM E8 / E8M - 09 Standard Test Methods for Tension Testing of Metallic Materials." PA, USA, 2009.

[202] P. Cavaliere, R. Nobile, F. Panella, and A. Squillace, "Mechanical and Microstructural Properties of Al 6056 Friction Stir Welded Joints," in *Proceedings 11th International Conference on Fracture*, (Turin, Italy), March 20-25 2005.

[203] C. Gallais, A. Simar, D. Fabregue, A. Denquin, G. Lapasset, B. de Meester, Y. Brechet, and T. Pardoen, "Multiscale Analysis of the Strength and Ductility of AA 6056 Aluminum Friction Stir Welds," *Metallurgical and Materials Transactions A*, vol. 38, no. 5, pp. 964–981, 2007.

[204] ASME - American Society of Mechanical Engineers, "Boiler and Pressure Vessel Code - an Internationally Recognized Code: Qualification Standard for Welding and Brazing Procedures, Welders, Brazers, and Welding and Brazing Operators," 1998.

[205] ASTM International Standards, "ASTM E466 - 07 Standard Practice for Conducting Force Controlled Constant Amplitude Axial Fatigue Tests of Metallic Materials." PA, USA, 2007.

[206] ASTM International Standards, "ASTM E467 - 08 Standard Practice for Verification of Constant Amplitude Dynamic Forces in an Axial Fatigue Testing System." PA, USA, 2008.

[207] ASTM International Standards, "ASTM E468 - 90(2004)e1 Standard Practice for Presentation of Constant Amplitude Fatigue Test Results for Metallic Materials." PA, USA, 2004.

[208] S. Lomolino, J. dos Santos, and R. Tovo, "Fatigue Behaviour of Friction Stir Welded Butt Joints in AA6056 Alloy for Airframe Application," in *XXXII Convegno Nazionale dell'Associazione Italiana per l'Analisi delle Sollecitazioni (AIAS)*, (Salermo, Italy), September 3-6 2003.

[209] P. Colegrove and H. Shercliff, "Experimental and Numerical Analysis of Aluminium Alloy 7075-T7351 Friction Stir Welds," *Science and Technology of Welding & Joining*, vol. 8, no. 5, pp. 360–368, 2003.

[210] T. Nelson, R. Steel, and W. Arbegast, "In Situ Thermal Studies and Post-weld Mechanical Properties of Friction Stir Welds in Age Hardenable Aluminium Alloys," *Science and Technology of Welding & Joining*, vol. 8, no. 4, pp. 283–288, 2003.

[211] A. Gerlich, M. Yamamoto, and T. North, "Local Melting and Cracking in Al 7075-T6 and Al 2024-T3 Friction Stir Spot Welds," *Science and Technology of Welding & Joining*, vol. 12, no. 6, pp. 472–480, 2007.

[212] W. Saleem, F. Yuqing, and W. Yunqiao, "Application of Topology Optimization and Manufacturing Simulations - A New Trend in Design of Aircraft Components," *Proceedings of the International MultiConference of Engineers and Computer Scientists*, vol. 2, 2008.

[213] R. Trem, "The Future of Automaking: Tailor Welded Blanks," *Welding Design & Fabrication*, February 1 2004.

[214] J. Sinke, C. Iacono, and A. Zadpoor, "Tailor Made Blanks for the Aerospace Industry," *International Journal of Material Forming*, vol. 3, pp. 849–852, 2010.

[215] A. Zadpoor, J. Sinke, R. Benedictus, and R. Pieters, "Mechanical Properties and Microstructure of Friction Stir Welded Tailor-Made Blanks," *Materials Science and Engineering: A*, vol. 494, no. 1-2, pp. 281–290, 2008.

[216] European Standard, "EN 10002-1 Tensile Testing of Metallic Materials. Method of Test at Ambient Temperature." European Committee for Standardization (CEN), 2006.

[217] AECMA, "prEN 6072 Standard; Aerospace Series: Metallic materials: Test Methods:

Constant Amplitude Fatigue Testing." European Association of Aerospace Industries, January 2006.

[218] ASTM International Standards, "ASTM E647 - 08 Standard Test Method for Measurement of Fatigue Crack Growth Rates." PA, USA, 2008.

[219] T. Chu, W. Ranson, and M. Sutton, "Applications of Digital-Image-Correlation Techniques to Experimental Mechanics," *Experimental Mechanics*, vol. 25, no. 3, pp. 232–244, 1985. 10.1007/BF02325092.

[220] P. Moreira, A. de Jesus, M. de Figueiredo, M. Windisch, G. Sinnema, and P. de Castro, "Fatigue Crack Growth Behaviour of Friction Stir Welded Aluminium-Lithium Alloy 2195 T8X," in *Iberian Conference on Fracture and Structural Integrity*, (Porto, Portugal), March 17-19 2010.

[221] L. Cederqvist and A. Reynolds, "Factors Affecting the Properties of Friction Stir Welded Aluminum Lap Joints," *Welding Journal Research Supplement*, vol. 80, no. 12, pp. 281s–287s, 2001.

[222] M. Ericsson, L. Jin, and R. Sandström, "Fatigue Properties of Friction Stir Overlap Welds," *International journal of fatigue*, vol. 29, no. 1, pp. 57–68, 2007.

[223] S. Tavares, M. Papadopoulos, and M. Pacchione, "Mechanical Behaviour of Friction Stir Overlap Welds for Aeronautical Applications," in *1st Workshop on Aerostructures of the European Aeronautics Science Network*, (Suresnes, France), October 7-8 2010.

[224] M. Papadopoulos, S. Tavares, M. Pacchione, and S. Pantelakis, "Mechanical Behaviour of AA 2024 Friction Stir Overlap Welds," in *2nd International Conference of Engineering Against Fracture, ICEAF*, (Mykonos, Greece), June 22-24 2011.

[225] E. Murman, "A Value Perspective on Aerospace Innovation," in *24th Congress of International Council of the Aeronautical Sciences (ICAS 2004), Yokohama, Japan*, 2004.

[226] National Research Council (US). Committee on Engineering Design Theory, *Improving Engineering Design: Designing for Competitive Advantage*. National Academies Press, 1991.

[227] A. van der Laan and M. van Tooren, "Incorporating Cost Analysis in a Multi-Disciplinary Design Environment for Aircraft Movables," *Journal of Engineering Design*, vol. 19, no. 2, pp. 131–144, 2008.

[228] R. Curran, S. Raghunathan, and M. Price, "Review of Aerospace Engineering Cost Modelling: The Genetic Causal Approach," *Progress in Aerospace Sciences*, vol. 40, no. 8, pp. 487–534, 2004.

[229] J. Lee, S. Lukachko, I. Waitz, and A. Schafer, "Historical and Future Trends in Aircraft Performance, Cost, and Emissions," *Annual Review of Energy and the Environment*, vol. 26, pp. 167–200, 2001.

[230] R. Babikian, S. Lukachko, and I. Waitz, "The Historical Fuel Efficiency Characteristics of Regional Aircraft from Technological, Operational, and Cost Perspectives," *Journal of Air Transport Management*, vol. 8, no. 6, pp. 389–400, 2002.

[231] J. Hinrichsen and C. Bautista, "The Challenge of Reducing Both Airframe Weight and Manufacturing Cost," *Air & Space Europe*, vol. 3, no. 3-4, pp. 119–121, 2001.

[232] M. Kaufmann, T. Czumanski, and D. Zenkert, "Manufacturing Process Adaptation for Integrated Cost/Weight Optimisation of Aircraft Structures," *Plastics, Rubber and Composites, 38*, vol. 2, no. 4, pp. 162–166, 2009.

[233] Y. Hailian and Y. Xiongqing, "Integration of Manufacturing Cost into Structural Optimization of Composite Wings," *Chinese Journal of Aeronautics*, vol. 23, no. 6, pp. 670–676, 2010.

[234] J. Schumacher, "Laserstrahlschweißen im Flugzeugbau," in *Neueste Entwicklungen der Industriellen Lasertechnik*, (Wolfsburg, Germany), October, 20 2005.

[235] M. Pacchione and J. Telgkamp, "Challenges of the Metallic Fuselage," in *25th International Congress of Aeronautical Science (ICAS 2006)*, (Hamburg, Germany), September 3-8 2006.

[236] D. Harris and A. Norman, "Properties of Friction Stir Welded Joints: A Review of the Literature," in *TWI The Welding Institute; presented at EUROSTIR, Progress report presented at the 6th PSG Meeting*, June 17-18 2003.

[237] B. Christner, J. McCoury, and S. Higgins, "Development and Testing of Friction Stir Welding (FSW) as a Joining Method for Primary Aircraft Structure," in *23rd International Council of the Aeronautical Sciences (ICAS 2002)*, (Toronto, Canada), September 8-13 2002.

[238] P. Webb, S. Eastwood, N. Jayaweera, and Y. Chen, "Automated Aerostructure Assembly," *Industrial Robot: An International Journal*, vol. 32, no. 5, pp. 383–387, 2005.

[239] P. Lequeu, P. Lassince, T. Warner, and G. Raynaud, "Engineering for the Future: Weight Saving and Cost Reduction Initiatives," *Aircraft Engineering and Aerospace Technology*, vol. 73, no. 2, pp. 147–159, 2001.

[240] J. Rakow and A. Pettinger, "Failure Analysis of Composites: Laminate Behavior," *Advanced Materials & Processes*, vol. 167, no. 7, pp. 16–18, 2009.

[241] R. Aronson, "A New Look at Aircraft Assembly," *Manufacturing Engineering*, vol. 132, no. 3, pp. 101–108, 2004.

[242] P. Tipaji, "E-design Tools for Friction Stir Welding: Cost Estimation Tool," Master's thesis, Missouri University of Science and Technology, 2007.

[243] R. Di Lorenzo and L. Fratini, "A Cost Model for the Friction Stir Welding Process," in *Proceedings of ESAFORM 2005, 8th International. Conference of the European Scientific Association for Metal Forming*, (Cluj, Romania), pp. 1073–1076, April 27-29 2005.

[244] A. van der Laan, R. Curran, M. van Tooren, and C. van Ritchie, "Integration of Friction Stir Welding Into a Multi-Disciplinary Aerospace Design Framework," *Aeronautical Journal*, vol. 11, pp. 759–766, 2006.

[245] MTS Systems Corporation, "ISTIR^{TM}Friction Stir Welding Solutions." Eden Prairie, MN, USA, 2003.

[246] P. de Castro and F. Oliveira, "Advanced Design Concepts and Maintenance by Integrated Risk Evaluation for Aerostructures, WP3: Testing, Testing Programme of IDMEC, ADMIRE-TR-3-43-1.1/IDMEC," October 5 2001.

[247] J. Defalco, "Friction Stir Welding vs. Fusion Welding," *Welding Journal*, vol. 85, no. 3, pp. 42–44, 2006.

[248] G. Loureiro and P. Leaney, "A Systems and Concurrent Engineering Framework for the Integrated Development of Space Products," *Acta Astronautica*, vol. 53, no. 12, pp. 945–961, 2003.

[249] C. Marxt and F. Hacklin, "Design, Product Development, Innovation: All The Same in the End? A Short Discussion on Terminology," *Journal of Engineering Design*, vol. 16, no. 4, pp. 413–421, 2005.

[250] A. Peters, E. Rooney, J. Rogerson, R. McQuater, M. Spring, and B. Dale, "New Product Design and Development: a Generic Model," *The TQM Magazine*, vol. 11, no. 3, pp. 172–179, 1999.

[251] A. Lockamy and A. Khurana, "Quality Function Deployment: Total Quality Management for New Product Design," *International Journal of Quality & Reliability Management*, vol. 12, no. 6, pp. 73–84, 1995.

[252] R. Curran, M. Price, S. Raghunathan, E. Benard, S. Crosby, S. Castagne, and P. Mawhinney, "Integrating Aircraft Cost Modeling into Conceptual Design," *Concurrent Engineering*, vol. 13, no. 4, pp. 321–330, 2005.

[253] W. Marx, D. Mavris, and D. Schrage, "Effects of Alternative Wing Structural Concepts on High Speed Civil Transport Life Cycle Costs," in *Conference proceedings of 37th AIAA/ASME/AHS/ASC Structures, Structural Dynamics, and Materials Conference, Salt Lake City, UT USA*, vol. 15, p. 17, Citeseer, April 1996.

[254] J. Harrison, B. Christensen, J. Bianco, and M. Gulli, "Virtual Collaborative Simulation Environment for Integrated Product and Process Development," in *High Performance Distributed Computing: Proceedings of the 5th IEEE International Symposium on High Performance Distributed Computing*, (Broadway, NY, USA), Association for Computing Machinery, 1996.

[255] W. Knight, *Advances in Integrated Design and Manufacturing in Mechanical Engineering*, ch. Integrated Design for Manufacture, Service and Environment, pp. 17–30. Editors: A.N. Bramley, D. Brissaud, D. Coutellier, C. McMahon, Springer, 2005.

[256] P. Selvaraj, P. Radhakrishnan, and M. Adithan, "An Integrated Approach to Design for Manufacturing and Assembly Based on Reduction of Product Development Time and Cost," *The International Journal of Advanced Manufacturing Technology*, vol. 42, no. 1, pp. 13–29, 2009.

[257] M. Mottonen, J. Harkonen, P. Belt, H. Haapasalo, and J. Simila, "Managerial View on Design for Manufacturing," *Industrial Management & Data Systems*, vol. 109, no. 6, pp. 859–872, 2009.

[258] G. Huang, *Design for X: Concurrent Engineering Imperatives*. Springer, 1996.

[259] C. Ledermann, C. Hanske, J. Wenzel, P. Ermanni, and R. Kelm, "Associative parametric cae methods in the aircraft pre-design," *Aerospace Science and Technology*, vol. 9, no. 7, pp. 641–651, 2005.

[260] G. Voland, *Engineering by Design*. Addison-Wesley, 1999.

[261] S. Finger and J. Dixon, "A Review of Research in Mechanical Engineering Design. Part I: Descriptive, Prescriptive, and Computer-based Models of Design Processes," *Research in Engineering Design*, vol. 1, no. 1, pp. 51–67, 1989.

[262] C. Rush and R. Roy, "Capturing quantitative & qualitative knowledge for cost modelling within a ce environment," in *8th ISPE International Conference on Concurrent Engineering: Research and Applications*, (Anaheim, Los Angeles, USA), pp. 209–218, Citeseer, July 29-August 1 2001.

[263] D. Whitney, *Mechanical Assemblies: Their Design, Manufacture, and Role in Product Development*. Oxford University Press, 2004.

[264] D. Kaminski-Morrow, "German plant produces largest a350 panel," *Flightglogal,* `http://www.flightglobal.com/articles/2011/03/18/354540/picture-german-plant-produces-largest-a350-panel.html`, March 18 2011.

[265] C. Tseng, C. Torng, and S. Lin, "Prioritization of Product Design Tasks using QFD, TRIZ and DSM," in *IEEE 17th International Conference on Industrial Engineering and Engineering Management (IE&EM)*, (Xiamen, China), pp. 871–875, IEEE, October 29 - 31 2010.

[266] L. Cohen, *Quality Function Deployment: How to Make QFD Work for You*. Addison-Wesley, 1995.

[267] J. Tang, R. Fung, B. Xu, and D. Wang, "A New Approach to Quality Function Deployment Planning with Financial Consideration," *Computers & Operations Research*, vol. 29, no. 11, pp. 1447–1463, 2002.

[268] G. Delano, G. Parnell, C. Smith, and M. Vance, "Quality function deployment and decision analysis: a R&D case study," *International Journal of Operations & Production Management*, vol. 20, no. 5, pp. 591–609, 2000.

[269] C. Fink, "An Introduction to Manufacturing," *Advanced Materials, Manufacturing and Testing Information Analysis (AMMTIAC) Quarterly, Techsolutions 9*, vol. 3, no. 3, pp. 9–15, 2008.

[270] J. Bossert, *Quality Function Deployment: a Practitioner's Approach*. ASQC Quality Press, 1991.

[271] J. Hauser and D. Clausing, "The House of Quality," *Harvard Business Review*, vol. 66, no. 3, pp. 63–73, 1988.

[272] G. Bounds, L. Yorks, and M. Adams, *Beyond Total Quality Management: Toward the Emerging Paradigm*. McGraw-Hill, McGraw-Hill, 1994.

[273] N. Cross, *Engineering Design Methods: Strategies for Product Design*. Jonh Wiley &

Sons Ltd., 4th. ed., 2008.

[274] KPIT Cummins, "Value Engineering, White Paper." http://www.kpitcummins.com/downloads/value-engineering-whitepaper.pdf, 2011.

[275] International Air Transport Association (IATA), "The IATA Technology Roadmap Report, 3rd Edition," June 2009.